Cosmological Probes of Modified Gravity

Hans Arnold Winther

Thesis submitted for the degree of
Philosophiæ Doctor

Institute of Theoretical Astrophysics
Faculty of Mathematics and Natural Sciences
University of Oslo

2013

Series of dissertations submitted to the
Faculty of Mathematics and Natural Sciences, University of Oslo
No. 1383

ISSN 1501-7710

Cover: Inger Sandved Anfinsen.
Printed in Norway: AIT Oslo AS.

Produced in co-operation with Akademika Publishing.
The thesis is produced by Akademika Publishing merely in connection with the thesis defence. Kindly direct all inquiries regarding the thesis to the copyright holder or the unit which grants the doctorate.

Acknowledgements

I wish to thank a number of people who have meant a lot to me during the last few years.

The biggest thanks goes to my supervisor David Mota. I cannot thank David enough for what he has done for me throughout these four years I have spent at ITA. David has given me the freedom to work with what I enjoy, putting me in contact with researchers around the world and encouraging me every step of the way. I'm very grateful for this.

Next, I want to thank all the people I have had projects with during my Ph.D: Anne-Christine Davis, Baojiu Li, Bruno Moraes, Carlos Martins, Carsten van de Bruck, Claudio Llinares, David Mota, David Polarski, Gong-Bo Zhao, Ilia Musco, Joe Silk, Marvin Silva, Philippe Brax, Radouane Gannouji and Shinji Tsujikawa. A special thanks to Anne-Christine Davis at DAMPT Cambridge, Phillippe Brax at IPTh Saclay and Baojiu Li at Durham University for the hospitality shown when visiting their institutions and for involving me in interesting projects.

I would like to thank all my fellow colleagues at ITA for thought-provoking discussions and a good social environment. Two people that deserves special mention are Sigurd Ness and Mikjel Thorsrud. Sigurd has been like a mentor to me when it comes to numerics and has always taken time from his own work to answer my questions. Mikjel has been my office mate for over five years and has, for most parts, been a great guy to have around.

The administration at ITA also deserves a thanks for always being very helpful. Lastly I want to apologize to Hans Kristian Eriksen for beating him in chess so many times.

This thesis was founded by the Research Council of Norway FRINAT grant 197251/V30.

Contents

Part I

Introduction

Chapter 1

Cosmology and Modified Gravity

1.1 Introduction

Within cosmology, the study of the overall composition and history of the universe, we are today in the position of having a well-tested standard model that agrees with all observations while at the same time relying only a few adjustable parameters. In this model the universe started out in an extremely hot and dense state called the Big Bang some 14 billion years ago. This was followed by a phase of extremely rapid expansion, called inflation.

During inflation, the size of the universe increased exponentially by at least a factor of 10^{25}, leaving an almost perfectly flat and smooth universe, but which contained small fluctuations which were generated by the magnification of quantum fluctuations of the inflaton field(s).

After inflation had ended the universe continued expanding, but much more slowly, and eventually cooling down enough so that neutral atoms could form. The latter happened about 370 000 years after the Big Bang, when the temperature of the universe had fallen to about 3000 K. Formation of atoms turned the baryon-photon plasma that had filled the universe until then into a neutral gas, making the universe transparent for the first time.

From the formation of atoms and until today, the small fluctuations in the matter fluid grew over time by gravitational collapse to form all the complex hierarchical system of stars, galaxies, groups of galaxies and galaxy clusters we today see as a cosmic web of structures.

Over the last century, astrophysical and cosmological observations of these structures has revealed a lot of what the universe is made of, what the laws governing its evolution is, revealing many surprises along the way.

The first big discovery came when Edwin Hubble in 1923 discovered

that the recessional velocity of galaxies increases with distance from the earth [1], implying the expansion of the universe.

Next came the discovery, by Jan Oort and later by Fritz Zwicky in the 1930s [2], that galaxy clusters contains more material than that could be seen. Later, studies of galaxy rotation curves [3] and velocity dispersions of galaxies [4] revealed that this missing matter could not be purely baryonic (atoms, photons, etc.). There have to be an unknown substance, now called dark matter, which behaves just like normal baryonic matter under gravity, but which interacts very weakly with photons so that we cannot see it directly. Today we believe that around 80% of the matter content of the universe is in the form of dark matter [5].

In 1964 American radio astronomers Arno Penzias and Robert Wilson discovered [6], by accident, the cosmological microwave radiation. This was the first major discovery that was predicted in advance and provided proof for the Big Bang model. Almost immediately after this discovery, searches began for anisotropies in the CMB - the signatures of the primordial fluctuations that grew to form the structures that we see today. Convincing evidence for a dipole anisotropy was reported in [7], and the detection of higher-order anisotropies came with the COBE satellite [8] in 1992. The COBE results established the existence of a nearly scale-invariant spectrum of primordial fluctuations, consistent with the predictions of inflationary cosmology. These predictions have later been confirmed by the much more accurate observations made by the WMAP [9] and Planck [5] missions.

The last major discovery came in 1997 when studies of supernovae [10, 11] revealed that the universe was not just expanding, but that the expansion was speeding up. Since gravity is attractive we would expect the expansion to be slowing down and in order to have accelerated expansion within general relativity we need something new. The simplest candidate which can produce accelerated expansion is vacuum energy and the so-called cosmological constant: a free parameter in general relativity which is not fixed by requiring the theory to reduce to newtonian gravity in the weak field regime. This unknown substance is refereed to as dark energy [12].

When adding dark matter and dark energy (in the form of a cosmological constant) together with inflation into the theory of general relativity we obtain the standard model of cosmology, the ΛCDM model. This model in its minimal form has only six free parameters: physical baryon density, physical dark matter density, dark energy density, scalar spectral index, curvature fluctuation amplitude and reionization optical depth. ΛCDM is in excellent agreement with all observations we have made so far, and the error-bars on the parameters have now become so small that we can talk about being in the era of precision cosmology.

We know a lot more about the universe today than we did a century

ago, but the process that has lead us here have revealed many new and greater challenges like the questions what dark matter, dark energy and inflaton really is. It could still be that these unknown ingredients reflect our lack of understanding of the universe and that the seemingly perfect ΛCDM model needs revision.

In this thesis our focus is on the way gravity works on large distance scales. By considering modifications of gravity we aim to find novel ways to test the theory of general relativity on cosmological scales and see if these new models can share any insight for the challenges we face in cosmology today. Such studies are important both to strengthen the case for the standard model or more interestingly to perhaps discover evidence for new physics.

1.2 Modified Gravity

The first mathematical model for how gravity works, the inverse square law, was proposed by Issac Newton in 1687. Newton's law of gravity stood for over 200 years until Einstein improved upon it by formulating his general theory of relativity in 1916. In Einstein's theory, gravity is no longer a force, but spacetime is instead curved and matter (energy) acts as the source for this curvature.

General relativity (GR) was able to explain effects like for example the bending of light rays around the sun and the perihelion problem of mercury [13], something Newtonian gravity was unable to account for.

For objects like planets and stars, GR basically reduces to Newtonian gravity and for example in the solar-system the deviation is typically a very small (of order $\frac{v^2}{c^2} \sim \frac{\Phi_N}{c^2} \sim 10^{-8}$) correction [14]. Thus Newtonian gravity is an excellent approximation to GR in most situations, the exceptions being strongly gravitational systems and gravitational lensing.

Since the invention of GR, the theory has been thoroughly tested on Earth and in the solar-system [14]. Several high precision experiments have over the last century been able to probe the small post-Newtonian corrections predicted by GR and the theory has been in agreement with all experiments performed so far.

For theories that aim to modify GR at large scales this is a severe challenge and the result is often that when the theory agrees with solar-system tests then there is not much left of the theory: it behaves very much like GR in most situations. If this is the case, then this would imply no modifications at all for the process of structure formation.

This view has changed over the last decade. It turns out it is possible for a modified gravity theory to remain hidden in the solar-system, where most experiments of GR have been performed, while at the same time give rise to large deviations from GR at cosmological scales. If this is the case

for a theory we say it possesses a screening mechanism [15].

A screening mechanism is a way of utilizing non-linear effects to hide the modifications of gravity in regions of high matter density (relative to the cosmological mean density) like on the Earth and in the solar-system[1].

Such a mechanism works by explicitly breaking the super-position principle of Newtonian gravity. As this principle follows from linearity of the field equation, a screening mechanism is necessarily a highly non-linear phenomenon which makes studies of such theories a challenging topic to work with.

1.3 Why Modify Gravity?

GR is the simplest theory of a massless spin two field one can construct. It agrees perfectly with all experiments so far. One might ask why bother with looking at alternative gravity theories? This is a question that deserves an answer and I will try to summarize the main motivations we have for looking at modifications of GR.

First of all, we know from quantum field theory that physics change with energy (and therefore with distance). GR is only well tested on distance scales ranging from a few millimeters up to the size of the solar-system. On cosmological scales, the order of mega parsecs, we don't yet know if gravity operates precisely like GR predicts.

Then there are all these open questions in cosmology. As all these problems are found within the framework of GR it is a real possibility that some of them can be evaded if a different theory of gravity operates on large scales.

Next there is the problem of quantum gravity. As today we don't have a theory of quantum gravity that works for the energy scales in the early universe. This is a hint that GR might not be the full story.

On the other side, modified gravity theories can often bring with them new problems like fine-tuning of parameters, ghosts, tachyons and superluminality [16, 17]. For example, the theories we will discuss later on will in some form or another have fine-tuned parameters. This makes this last point perhaps the most important one.

Alternative theories can help us find new ways of testing the current paradigm. When gravity was tested in the solar system, several models (see e.g. [14] for a comprehensive list) was constructed that were competitors to GR. As time went on and most of them became ruled out or rendered irrelevant, but they served a purpose nonetheless. Instead of testing a theory as it is, it is often useful to expand the theory space and look at other models.

[1]The solar-system might seem like an empty space, but it is contained in our galactic halo which contains dark matter. The average dark matter density in our solar-system is about a million times the mean density in our universe today.

These alternative theories will often have distinct signatures, which are not found in the current theory, and these signatures serves as a smoking gun for new physics. Therefore studying other candidate theories might help us find new ways of testing and thereby either strengthening the case for the current paradigm or finding evidence for new physics.

When it comes to how gravity operates on large distance scales, current observations leave a lot of room for deviations from GR. The study of modified gravity can be seen as a way of expanding the parameter space around GR, finding observable signatures, and then use observational data to look for these.

Future large scale structure surveys which will culminate in the Euclid mission [18] aims to test gravity to percent accuracy on large scales. These results will largely settle the case for how gravity works on cosmological scales.

1.4 Modifying Gravity with a scalar field

There are several ways of modifying gravity. The simplest cases involving a single scalar field and the most general gravitational sector for a scalar-tensor theory (with second order field equations) was first derived by Horndeski [19]. It is given by the Horndeski action

$$\begin{aligned} S = \int \sqrt{-g} dx^4 \, & [G_2(X,\phi) - G_3(X,\phi)\Box\phi + G_4(X,\phi)R \\ & + G_{4,X}(\Box\phi)^2 - \phi_{;\mu\nu}\phi^{;\mu\nu} + G_5(X,\phi)G_{\mu\nu}\phi^{;\mu\nu} \\ & - \frac{1}{6}G_{5,X}\Big[(\Box\phi)^3 - 3(\Box\phi)\phi_{;\mu\nu}\phi^{;\mu\nu} + 2\phi^{;\nu}_{;\mu}\phi^{;\lambda}_{;\nu}\phi^{;\mu}_{;\lambda}\Big]\Big] \\ & + S_m(g_{\mu\nu}, \psi_m) \end{aligned} \tag{1.1}$$

where S_m is the matter action, ψ_m represents the different matter-fields, G_i are free functions of the scalar field and $X = \frac{1}{2}(\partial\phi)^2$.

I will in this thesis only consider a sub-class of this action which takes the simple form

$$S = \int d^4x\sqrt{-g}\left(\frac{R}{2}M_{\rm Pl}^2 - \frac{1}{2}(\partial\phi)^2 - V(\phi)\right) + S_m(\psi_m, \tilde{g}(\phi)_{\mu\nu}) \tag{1.2}$$

namely a canonical scalar field with some self-interacting potential and where the dependence of the scalar field on the Ricci scalar have been removed by a conformal transformation so that the metric felt by the matter fields, $\tilde{g}_{\mu\nu}$, is given by

$$\tilde{g}_{\mu\nu} = A^2(\phi)g_{\mu\nu} \tag{1.3}$$

for some function $A(\phi)$. Known examples of theories of this class are the so-called chameleon/$f(R)$ gravity [20, 21, 22, 23, 24], symmetron [25] and the environmental dependent dilaton [26].

We also have the possibility of formulating the theory in terms of the metric $\tilde{g}_{\mu\nu}$. In this formulation, the so-called Jordan frame, one can easily see that gravity is modified directly from the action: we will no longer have a Einstein-Hilbert term describing usual gravity and consequently the Einstein-equation is explicitly modified.

In the Einstein-frame formulation Eq. (1.2) we have that the Einstein-equation looks very similar to those in pure GR

$$G_{\mu\nu} = \frac{8\pi G}{3}\left[A(\phi)T_{\mu\nu} + T^{\phi}_{\mu\nu}\right] \tag{1.4}$$

The exception is that we now have an explicit coupling between the matter-fields and the scalar field on the right hand side.

In the Einstein frame matter no longer moves on geodesics of the metric $g_{\mu\nu}$ (for which the Einstein equations are formulated in terms of) and the geodesics equation instead reads

$$\ddot{x}^{\mu} + \Gamma^{\mu}_{\alpha\beta}\dot{x}^{\alpha}\dot{x}^{\beta} = -\frac{d\log A}{d\phi}\left(\nabla^{\mu}\phi - \dot{x}^{\mu}\dot{x}^{\alpha}\nabla_{\alpha}\phi\right) \tag{1.5}$$

In the non-relativistic limit the right hand side corresponds to a fifth-force:

$$\vec{F}_{\phi} = -\frac{d\log A}{d\phi}\vec{\nabla}\phi. \tag{1.6}$$

This picture of the theory as GR supplemented by a fifth-force is intuitively and mathematically much easier to work with than the Jordan-frame formulation and is the chosen formulation in this thesis.

All the particular studies presented in this thesis are of models in the class Eq. (1.2) discussed above.

1.5 Screening mechanisms

As I mention above, a screening mechanism is crucial to have a modified gravity theory that agree with local experiments and at the same time produce deviations from GR on cosmological scales. Too see in more detail how a screening mechanism might work, I will give a simple example.

We start with the action Eq. (1.2) and take $A(\phi) = e^{\frac{\beta\phi}{M_{\rm Pl}}}$ where β is a dimensionless parameter. The potential does not need to be specified at the present, but we assume that it is decreasing with ϕ and that $\lim_{\phi\to 0} V(\phi) = \infty$ so that the effective potential (defined below) has a minimum for any given density ρ_m.

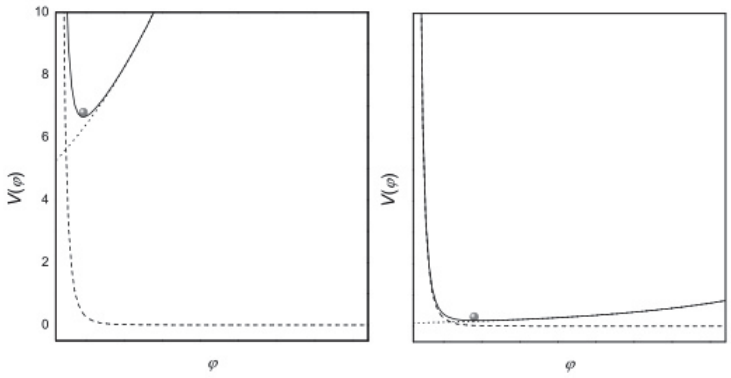

Figure 1.1: Illustration of the effective potential. The dashed, dotted and solid curves are respectively the bare potential $V(\phi)$ of the scalar field, the coupling $\rho_m A(\phi)$ and the total effective potential $V_{\rm eff}(\phi)$. Left panel: Large ambient matter density. Right panel: Small ambient matter density.

The equation of motion for the scalar field is determined by the Klein-Gordon equation

$$\Box\phi = V_{,\phi} - A_{,\phi} T_m \tag{1.7}$$

where T_m is the trace of the energy momentum tensor for matter. For non relativistic matter (dust) we have $T_m = -\rho_m$: the matter density. The dynamics of ϕ is thus determined by an effective potential

$$V_{\rm eff} = V(\phi) + A(\phi)\rho_m \tag{1.8}$$

which depends on the local matter density, see Fig. (1.1).

Lets consider a static spherical massive object of density ρ_c and radius R embedded in a background of homogenous density ρ_∞ and look at solutions to the field equation Eq. (1.7). The minimum of the effective potential inside (outside) the object is denoted ϕ_c (ϕ_∞).

If we are in a regime where the field equation can be linearized we easily obtain the solution[2]

$$\phi(r) = \phi_\infty - \frac{\beta\rho_c R^2}{2M_{\rm Pl}}\frac{1}{r}e^{-m_\infty r}, \qquad r > R \tag{1.9}$$

[2]We assume $m_\infty^{-1} \gg R$ and $\frac{\beta\phi}{M_{\rm Pl}} \ll 1$. Thus the scalar field force is assumed to be long ranged compared to the object in question.

where $m_\infty \equiv \sqrt{V_{\text{eff},\phi\phi}(\phi_\infty)}$ is the mass of the scalar field in the background. The fifth-force, Eq. (1.6), on a test-mass outside the object (with $r \ll m_\infty^{-1}$) becomes

$$\vec{F}_\phi = 2\beta^2 \vec{F}_{\text{Gravity}} \tag{1.10}$$

Thus for $\beta = \mathcal{O}(1)$ the fifth-force is comparable in strength to ordinary gravity. For large separations, $r \gtrsim m_\infty^{-1}$, the force will be exponentially suppressed.

The linearization done above is only valid for sufficiently small (mass and size) objects. For very large objects the linearization breaks down and one must solve the highly non-linear ODE Eq. (1.7) to find the solution. If a few constraints are placed on the form of the potential and the coupling we can show that quite generally [27, 23] there exists a critical solution given approximately by

$$\phi(r) = \begin{cases} \phi_c, & r < R \\ \phi_\infty - (\phi_\infty - \phi_c)\frac{R}{r} e^{-m_\infty r}, & r > R \end{cases} \tag{1.11}$$

Defining

$$\frac{\Delta R}{R} = \frac{|\phi_\infty - \phi_c|}{2\beta M_{\text{Pl}} \Phi_N} \tag{1.12}$$

where Φ_N is the Newtonian potential for the massive object, we find that the fifth-force on a test mass outside our massive object is now

$$\vec{F}_\phi = 2\beta^2 \left(\frac{\Delta R}{R}\right) \vec{F}_{\text{Gravity}} \tag{1.13}$$

It is thus suppressed by a factor $\frac{\Delta R}{R} \propto \frac{1}{\Phi_N}$ compared to the linear, unscreened, case. The more massive the object, the greater the gravitational potential Φ_N is and the more screened it becomes. The critical solution is valid as long as the suppression factor $\frac{\Delta R}{R} \ll 1$.

Physically one can explain this effect by looking at perturbations to the exterior field when we increase the mass of our object. The contribution to the exterior field from a mass perturbation in the interior of the object is found to be exponentially suppressed. It's only a fraction $\sim \frac{\Delta R}{R}\delta M$, namely the mass of a small shell of size ΔR close to the surface, of the added mass which contributes to pushing up the exterior field and thereby the fifth-force. When the critical solution is reached the exterior solution and therefore the force field becomes independent of the mass of the object exerting this force; a complete breakdown of the superposition principle.

This example is the so-called chameleon mechanism [20]. There exist several examples of screening mechanisms in the literature and we can classify modified gravity theories by which screening mechanism they use to screen the fifth-force in high density regions.

For theories which have a conformal coupling to matter these different screening mechanism roughly match the symmetries of the theory:

- Models with no apparent symmetry (apart from a trivial mirror symmetry) can screen via a chameleon-like mechanism [20, 25] (like the one described in the example above). The screening condition is roughly $|A(\phi) - 1| \ll \Phi_N$, i.e. the local fifth-force potential must be much smaller than the gravitational potential. This is the type of screening we look at in this thesis.

- Models with a shift-symmetry, $\phi \to \phi + c$, can screen by having $\partial\phi$ becoming large close to massive sources [28].

- Models with a derivative shift-symmetry, $\phi \to \phi + c_\mu x^\mu + d$, can screen by having $\partial\partial\phi$ becoming large close to massive sources. This is the so-called Vainshtein mechanism [29, 30] and is the reason Galileon models [31, 32] can evade local constrains.

On top of this we have models that employs a disformal coupling,

$$\tilde{g}_{\mu\nu} = A^2(\phi) g_{\mu\nu} + B(\phi)\phi_{,\mu}\phi_{,\nu} \tag{1.14}$$

to the matter fields which can screen the fifth-force by making the field static and smooth locally, for which the coupling becomes invisible in the Solar System. This is the so-called disformal screening mechanism [33].

In summary, a screening mechanism allows for a fifth-force which can be stronger than gravity in some regimes, while at the same time being hidden in the solar system where most gravity experiments are performed. The regimes for which the fifth-force is in full effect are regions with very low matter density, like in the cosmological background. This makes the cosmological study of these theories even more interesting.

1.6 The Cosmology of modified gravity

I will give a brief summary of the cosmology we get from the modified gravity models we have focused on. A more complete discussion can be found in the attached papers.

In a flat, homogenous and isotropic universe the metric is on the FRLW form

$$ds^2 = -dt^2 + a^2(t)(dx^2 + dy^2 + dz^2) \tag{1.15}$$

where a is the scale-factor. In this metric, the late time background cosmology of the models given by the action Eq. (1.2) is determined by the

Friedmann equation [34]

$$3H^2M_{\rm Pl}^2 = \rho_m A(\phi) + V(\phi) + \frac{1}{2}\dot{\phi}^2 \tag{1.16}$$

and the Klein Gordon equation for the scalar field

$$\ddot{\phi} + 3H\dot{\phi} = -V_{{\rm eff},\phi} = -\left(V_{,\phi} + \frac{\beta(\phi)}{M_{\rm Pl}}\rho_m A(\phi)\right) \tag{1.17}$$

where $H(t) = \dot{a}/a$ is the expansion rate of the Universe. The minimum of the effective potential acts as an attractor as the universe evolves. The field adiabatically tracks this attractor from the early universe until the present. By calculating the equation of state ω along this attractor we find that the dark energy needs to be very close to that of a cosmological constant [27, 35] and this means that these models are not novel dark energy candidates[3] in the sense that it's usually very hard to distinguish the background evolution from that of ΛCDM.

However, at the level of perturbations we start to see clear signatures. The equation describing the growth of the matter perturbations are modified relative to ΛCDM. For sub-horizon modes, and in Fourier-space, we have [34] that the matter perturbations satisfy the equation

$$\ddot{\delta}_m + 2H\dot{\delta}_m = \frac{3}{2}H(a)^2\Omega_m(a)\frac{G_{\rm eff}(a,k)}{G} \tag{1.18}$$

which is similar to that in ΛCDM except we now have an effective gravitational constant given by

$$\frac{G_{\rm eff}}{G} = 1 + \frac{2\beta(\phi)^2}{1 + \frac{m_\phi^2 a^2}{k^2}} \tag{1.19}$$

On length scales smaller than the Compton wavelength of the scalar-field, $\lambda_\phi = 1/m_\phi$, we have

$$\frac{G_{\rm eff}}{G} \simeq 1 + 2\beta(\phi)^2 \tag{1.20}$$

an enhancement of the strength of gravity while for larger length scales $\frac{G_{\rm eff}}{G} \simeq 1$ and we recover the ΛCDM result.

This scale-dependence of the effective gravitational constant means that the growth rate of perturbations,

$$f \equiv \frac{d\log\delta_m}{d\log a}, \tag{1.21}$$

[3] There do exist some particular models that can have observable signatures on the background expansion, but this is the exception not the rule.

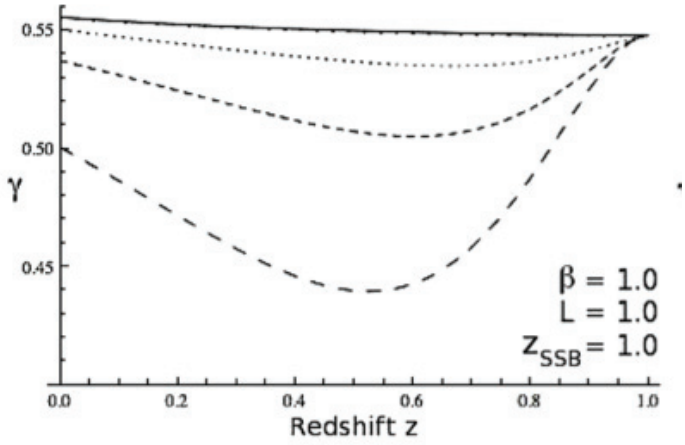

Figure 1.2: The evolution of the growth index $\gamma(z,k)$ for four different wavenumbers k = 0.01, 0.05, 0.1, 0.2 h/Mpc (from top to bottom) for a particular modified gravity model known as the symmetron model [25]. The solid line shows the prediction of ΛCDM.

will also be scale-dependent. In ΛCDM we have $f = \Omega_m(a)^\gamma$ where $\gamma \simeq 0.55$ almost constant in time and constant in scale.

In Fig. (1.2) we show the growth-index γ as function of scale and time for a particular modified gravity model known as the the symmetron model [25, 36]. The model parameters used here are in agreement with local constraints and indicate that quite large deviations are allowed. Current constraints on the growth index (see e.g. results from the WiggleZ survey [37]), agree with the GR prediction, but cannot yet rule out a $5-10\%$ deviation. The Euclid mission [18] promises a 1% determination of γ and will be able to settle the case of modified gravity on linear scales.

The scale where the growth rate of the perturbations start to deviate from ΛCDM depends on the value λ_ϕ has in a particular model. This value is indirectly dictated by local gravity constraints. For concrete models (and one can make arguments why this holds for most models [27]) within the class Eq. (1.2) one can show that local gravity experiments forces the Compton wavelength of the scalar field in the cosmological background to be less then the order of mega parsecs [27, 35], putting the modifications in the mildly to fully non-linear regime of structure formation. This is in the regime where perturbation theory starts to break down and other methods beyond perturbation theory is needed to obtain accurate predictions. One such method is N-body simulations and is one of the main tools we have

used in this thesis.

Chapter 2

N-body Simulations

2.1 Introduction

For studies of the early universe, like inflation and the CMB, the physics is linear to a good approximation [38]. This is due to the fluctuations being much less than unity. Linear theory is very well understood and the beauty in study linear matter clustering for example is that when put in Fourier space, all the different modes of the density field decouples and one can solve them one by one.

However, the structures we see around us today have density contrasts which are much larger than unity. The average density of our galaxy is around a million times the average density of the universe today. In order to study the formation of structures beyond the linear level one must rely on other methods.

There exists semi-analytical models, like spherical collapse and the halo model [39, 40], which can be used to obtain quantitative predictions in the mildly non-linear regime, but the only known method of going far into the non-linear regime and obtaining accurate trustworthy predictions is by using N-body simulations.

In N-body simulations the matter density field is approximated with particles and put in a periodic box. The particles are then evolved by calculating the gravitational force from all the other particles and using this to move them forward in time.

The initial conditions are found by calculating predications from linear theory and using (for example) the Zeldovich approximation [41] to produce a realisation of particles that gives the desired linear matter power-spectrum. The simulation is started sufficiently early so that the modes we are interested in are indeed in the linear regime.

The equations used to evolve the system comes from perturbing GR [42]. The end result are equations that are very similar to that of Newtonian gravity, but in an expanding Universe.

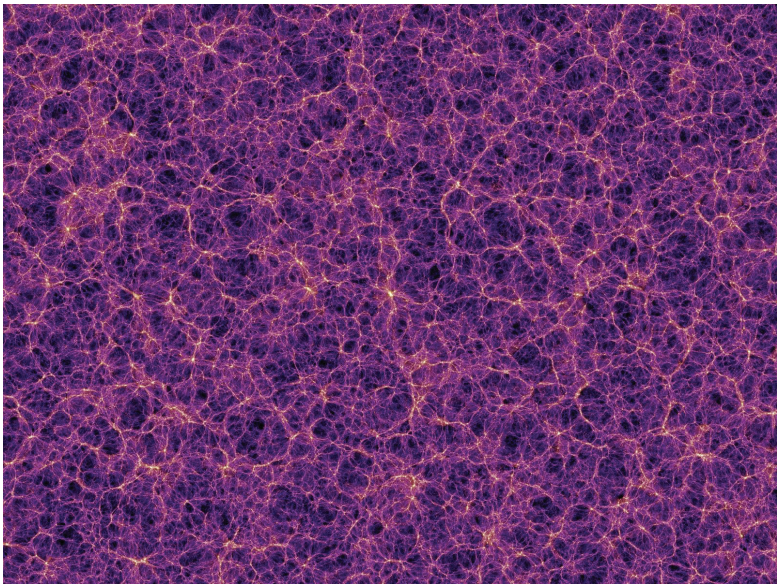

Figure 2.1: A snapshot from an N-body simulation showing the cosmic web at the present time. Dark colors indicate underdense regions (voids) while bright colors indicate overdense regions (halos). Image credit Volker Springel, "The Millennium Simulation".

There are only two equations that form the basic for any N-body simulation of dark matter. One first finds the gravitational potential from using the Poisson equation

$$\frac{1}{a^2}\nabla^2\Phi_N = 4\pi G(\rho_m - \overline{\rho}_m) \tag{2.1}$$

and then move the particles using the geodesics equation

$$\ddot{\vec{x}} + 2H\dot{\vec{x}} = -\frac{1}{a^2}\vec{\nabla}\Phi_N \tag{2.2}$$

In Fig. (2.1) we show the dark matter densify field at the present time taken from an N-body simulation. The figure shows the complex structures of dark matter halos, filaments and voids that make up the cosmic web.

From the output of a simulation one can study a wide range of observables [43], the simplest one being matter power spectrum and the halo mass-function. See the appendix for a definition of these observables.

2.2 N-body simulations of modified gravity

In order to do N-body simulations for our modified gravity theories the most challenging part is to solve for the scalar field in the N-body code.

The scalar field is determined by the Klein-Gordon equation, which reads

$$\ddot{\phi} + 3H\dot{\phi} - \frac{1}{a^2}\nabla^2\phi + V_{,\phi} + \frac{\beta(\phi)}{M_{\rm Pl}}\rho_m = 0 \tag{2.3}$$

This is a very complicated equation to solve numerically as it depends on both space and time and is usually highly non-linear. A simplification that is often done is to neglect the time-derivatives[1]. This is called the quasi-static approximations and the field equation reads [44]

$$\frac{1}{a^2}\nabla^2\phi = V_{,\phi} - V_{,\overline{\phi}} + \frac{\beta(\phi)}{M_{\rm Pl}}\rho_m - \frac{\beta(\overline{\phi})}{M_{\rm Pl}}\overline{\rho}_m \tag{2.4}$$

When the scalar field solution is known the geodesic equation is as simple as before. It reads

$$\ddot{\vec{x}} + 2H\dot{\vec{x}} = -\frac{1}{a^2}\left(\vec{\nabla}\Phi_N + \frac{\beta(\phi)}{M_{\rm Pl}}\vec{\nabla}\phi\right) \tag{2.5}$$

and the new term on the right hand side is the scalar fifth-force.

Eq. (2.4) is similar to the Poisson equation for gravity Eq. (2.1), but there are some important differences. First the source (right hand side) of the field depends on the field itself. This means we cannot use an explicit method to solve the equation. Secondly, as the equation is non-linear we cannot use Fourier methods. Thirdly, the field ϕ might vary over several orders of magnitude going from clusters to voids. This can pose a problem for the accuracy of the numerical solver and one might need to redefine the field ϕ to avoid this problem, but this creates a non-canonical kinetic term which again complicates.

The main method we have used to solve for the scalar field is an implicit Newton-Gauss-Seidel relaxation method with multi-grid acceleration. The method is described in full in Paper VII, but I will give a short review here.

The equation we want to solve, $\mathcal{L} = \nabla^2\phi - V_{{\rm eff},\phi} = 0$, is discretisized on a regular grid. For the differential operator (here in 1D) we use a second order Taylor expansion

$$\nabla^2\phi \rightarrow \frac{\phi_{i+1} + \phi_{i-1} - 2\phi_i}{dx^2} \tag{2.6}$$

Then we loop over the grid changing the value of the field in each cell according to the Newton-Gauss-Seidel algorithm

$$\phi^{\rm new}_{i,j,k} = \phi_{i,j,k} - \frac{\mathcal{L}(\phi_{i,j,k})}{\partial\mathcal{L}/\partial\phi_{i,j,k}} \tag{2.7}$$

[1] Or more correctly, neglect them for the perturbations around the background field $\overline{\phi}$.

After doing N sweeps through the grid we have a tentative solution ϕ on the grid. Denoting the true solution (the one which have $\mathcal{L} = 0$) by ϕ^{true} we define the residual as

$$r = \mathcal{L}(\phi) - \mathcal{L}(\phi^{\text{true}}) = \mathcal{L}(\phi) \tag{2.8}$$

We expect that the relaxation on the fine grid has removed most small-scale error modes, so the error mainly consists of longer wavelength modes. To remove the error in the larger wavelength modes we use the multigrid approach: we will solve for the error $\phi - \phi^{\text{true}}$ on coarser grids and then use this solution to correct ϕ on the finer grid. On the coarser grids the residual equation reads

$$\mathcal{L}(\phi) = \mathcal{L}(\mathcal{R}\phi) - \mathcal{R}r \tag{2.9}$$

where $\mathcal{R}$ is a restriction operator (averages the finer grid solution down to the coarser grid). We solve this equation in the same way as we did on the finest grid and this procedure is done iteratively down to the coarsest grid. We now take the solution on the coarsest grid and use it to correct the solution on the finer grid above using

$$\phi^{\text{fine new}} = \phi^{\text{fine}} + \mathcal{P}(\phi^{\text{coarse}} - \mathcal{R}\phi^{\text{fine}}) \tag{2.10}$$

where $\mathcal{P}$ is a prolongation operator (interpolates the coarse solution up to the fine grid). Again we do this iteratively all the way up to the finest grid. One such cycle going down and up again is called a V-cycle. After each V-cycle we check for convergence by calculating the RMS value of the residual. If convergence is not found we repeat the process again. The advantage of the multigrid approach is that the number of operations needed to sweep though the finest grid is comparable to the number of operations done on all the coarser grids put together. Also the coarser grids can much more easily solve for the longer wavelength modes of the solution and thereby speed up the convergence.

2.3 Parameterisation of modified gravity

The theories we are concerned with in this thesis are highly non-linear and how each model works in detail depend sensitively on the exact form of the potential and coupling. We are therefore often forced to choose a particular model, work out local constraints for this particular model and then go look for cosmological signatures within the viable parameterspace. When comparing observations with theory it is a cumbersome process to do this model by model. This is where a parameterisation comes in handy.

There do exist useful parameterisations in the linear regime, see e.g. [45] and references within. However, for us a linear parametrisation is of little

use. Modifications of gravity are often found in the non-linear regime and the most important ingredient of our models, the screening mechanism, is absent in a linear parametrisation.

We shall show how we can build up a parametrisation that can be used to study a large part of the whole class of models contained in Eq. (1.2). This parametrisation is built upon physically intuitive quantities instead of the more abstract potential V and coupling function A.

Scalar tensor theories given by the action Eq. (1.2) are uniquely defined once we choose the coupling function $A(\phi)$ and the self-interaction potential $V(\phi)$. Another way to define the theory is to specify the two functions $\beta(a)$ and $m(a)$, namely the coupling and the mass of the field at the minimum of the effective potential $V_{\rm eff}$ at time a in the cosmological background. As shown in [27], the minimum of the effective potential in the cosmological evolution can be found from

$$\phi(a) = \frac{3}{M_{\rm Pl}} \int_{a_{\rm ini}}^{a} \frac{\beta(a)}{am^2(a)} \overline{\rho}_m(a) da + \phi_{\rm ini} \tag{2.11}$$

and the potential at the minimum can be found from

$$V(a) = V_0 - \frac{3}{M_{\rm Pl}^2} \int_{a_{\rm ini}}^{a} \frac{\beta^2(a)}{am^2(a)} \overline{\rho}_m^2(a) da \tag{2.12}$$

From these two relations one can reconstruct the potential $V(\phi) = V(a(\phi))$. Likewise, from the relation $\beta(\phi) \equiv M_{Pl} \frac{dA(\phi)}{d\phi}$, we can reconstruct $A(\phi)$. This demonstrates the equivalence of the two formulations $[V(\phi), A(\phi)]$ and $[m(a), \beta(a)]$. Explicit examples of such reconstructions can be found in [27].

The minimum of the effective potential $\phi(a)$ is an attractor which the field oscillates around as the Universe expands. Because of the large mass of the field the oscillations are heavily damped and the field adiabatically tracks the minimum since before BBN until the present. This implies that $m(a)$ and $\beta(a)$ turns out to be very close to the true mass and coupling of the field in the cosmological background for viable models in this class.

The advantage of this novel formulation is that the functions $m(a)$ and $\beta(a)$ are more directly related to physical observables than $V(\phi)$ and $A(\phi)$. For instance, we have that the linear perturbations in the sub-horizon limit are determined by

$$\ddot{\delta}_m + 2H\dot{\delta}_m = \frac{3}{2}\Omega_m(a)H^2(a)\delta_m \left(1 + \frac{2\beta^2(a)}{1 + \frac{m^2(a)a^2}{k^2}}\right) \tag{2.13}$$

and this formulation can for example be used to directly engineer models directly from their linear perturbations properties. Within this formulation

we are not limited to study just simple background and linear perturbations properties, but since we can reconstruct (analytically or numerically) the exact form of the potential and coupling we can also use it to study, among many things, non-linear clustering with N-body simulations. Another advantage is that we can usually calculate local constraints directly from the functions $\beta(a), m(a)$ [27].

In most known and viable scalar tensor theories of modified gravity the mass $m(a)$ and coupling $\beta(a)$ turns out to be nice monotonic functions (power-laws and exponentials) of time. Using this we can, by choosing a convenient parameterisation for these two functions, parametrize a large range of models in this entire model class.

It turns out that generalizing the well known chameleon, dilation and symmetron models by using the mapping above gives rise to most of the different situations (monotonic $m(a)$ and $\beta(a)$) that can be viable. These functions are given by

$$m(a) = m_0 a^{-r}, \tag{2.14}$$
$$\beta(a) = \beta_0 a^{-s}, \tag{2.15}$$

for the generalized chameleon model,

$$m(a) = m_0 a^{-r}, \tag{2.16}$$
$$\beta(a) = \beta_0 \exp\left(\frac{s}{2r-3}(a^{2r-3}-1)\right) \tag{2.17}$$

for the generalized dilaton model and

$$m(a) = m_0 \left(1 - \left(\frac{a_*}{a}\right)^3\right)^m, \tag{2.18}$$
$$\beta(a) = \beta_0 \left(1 - \left(\frac{a_*}{a}\right)^3\right)^n, \tag{2.19}$$

for the generalized symmetron model.

β_0 and m_0 are common parameters for all models that describe the value of the mass and coupling at the present. On top of that comes two-three parameters, r, s, n, m, a_*, to describe the shape of the two functions.

These generalized models can be looked upon as a first try for making a parametrisation of the whole class of viable modified gravity models given by Eq. (1.2). In Paper IV and V we have performed systematic N-body simulations of these models.

2.4 Cosmological Probes of modified gravity

One of the main objectives of this thesis was to find novel ways to probe modified gravity via cosmological observations of the non-linear regime.

We will go through some of the probes that we have looked at which can be used to test for these theories from observations in current and future surveys.

2.4.1 The matter density field

The main observable of modified gravity is the matter power-spectrum or, in the linear regime, the so-called growth factor. The matter power spectrum describes the matter fluctuations in our Universe as a function of scale. If gravity departs from GR on some scales at some time then this will be imprinted on the matter power-spectrum. Studies have showed that a modified gravity model of the type Eq. (1.2) will produce a bump in the power-spectrum relative to ΛCDM, see Fig. (2.3). The location of the bump depends on the Compton wavelength of the scalar field and the amplitude depends on the coupling strength β. On large scales the results converge to ΛCDM due to the limited range of the fifth-force.

An important lesson learned from N-body simulations of modified gravity theories of the class Eq. (1.2) is that predictions made from linear theory cannot be quantitatively trusted even in the linear regime. This seems counterintuitive, but it is easy to understand. For GR, because of the super position principle, the large scales do not feel what is going on small scales. If the the mass contained in small scale halos were compressed into tiny regions then the gravitational force this mass would exert on other far away objects would remain the same. For modified gravity theories this is not the case. If small scale halos are screened then they would not contribute to the fifth-force on far away objects at all. This effect is shown in Fig. (2.2). The same goes for small halos inside or close to very massive halos due to the environmental screening effect.

Thus to obtain trustable, accurate, predictions for the matter power spectrum in modified gravity theories simulations seems to be required at least to check, and tune, semi-analytical approaches [46, 47].

2.4.2 The velocity field

Studies of simulations have showed that the velocity field might be the best way, in terms of the signatures found in N-body simulations, to probe the modifications of gravity.

One way to study this is to look at the velocity divergence field. Even for models that produce a very small enhancement in the matter power-spectrum the enhancement in the velocity divergence spectra can be many times larger [48]. This is illustrated in Fig. (2.4) where we show the fractional difference in the matter and velocity divergence power-spectra with respect to ΛCDM for the chameleon simulation presented in Paper V. We see that even when the matter-power spectra deviates less than $\sim 1\%$ from

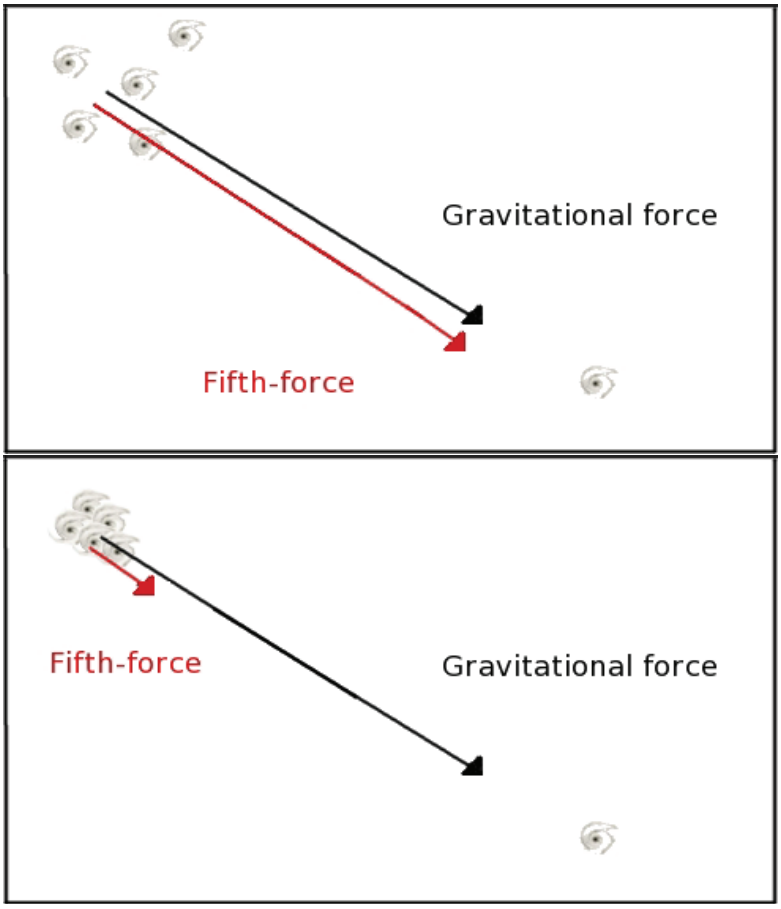

Figure 2.2: This figure illustrates how large-scale clustering in modified gravity, apposed to GR, depends on the small scale clustering. Above we show the forces from five galaxies, spread out in one region of space, on a single galaxy far away. Below we have the same situation, but we have placed the same five galaxies on top of each other. The gravitational force in the figure above is the same as that in the figure below (the superposition principle). However, due to the screening mechanism, the fifth-force in the situation below is suppressed.

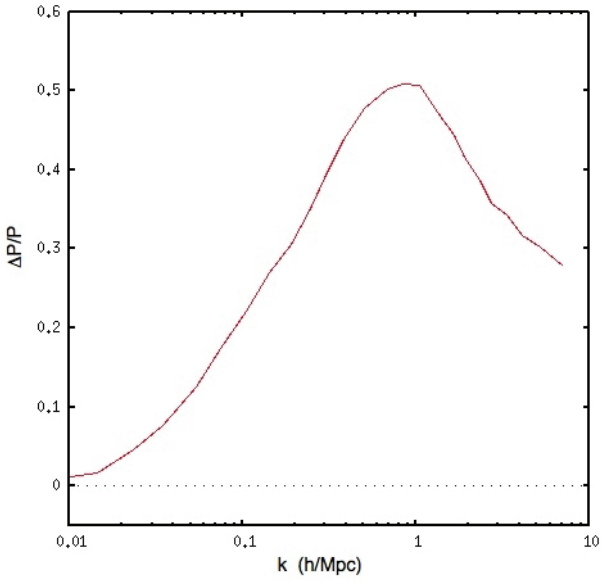

Figure 2.3: The fraction difference in the matter power spectra with respect to ΛCDM for a $f(R)$ gravity simulation taken from Paper VII.

ΛCDM for scales $k \lesssim 10\ h/\mathrm{Mpc}$ the deviation in the velocity divergence spectra can be as large as 20%.

In GR, the average velocity field of the dark matter around galaxy clusters is uniquely determined by the mass profile. This is not the case for modified gravity theories. By comparing the measured mass density and velocity profiles of galaxy clusters allows for a model-independent test of Einstein gravity. One way this can be tested in future observations is to combine lensing (to get the matter field) with stacking of redshifts (to get velocities) of the surrounding galaxies of a cluster in a spectroscopic sample [49].

2.4.3 The mass function

The halo mass-function $n(M, z)$ is defined as the number density of halos of mass M at redshift z. It is observationally, at least in principle, relatively easy to obtain. We just have to go out and count clusters of galaxies and measure their mass. To observationally determine the mass-function one can use optical galaxy surveys, weak lensing, X-ray measurements of hot gas in clusters and inverse Compton scattering of CMB photons (the Sunyaev-Zeldovich effect [50]).

Modified gravity tends to increase clustering and thereby increasing the number density of intermediate sized halos. The largest halos in our Universe are formed over a very long time and because of their large mass is very likely to be screened. This means that the modified gravity predictions usually converge to ΛCDM for large halo masses.

One can already use such observations to make constraints on modified gravity as was done in [51] for the Hu-Sawicky $f(R)$ model.

2.4.4 Shapes of clusters

If we have a non-spherical object then the fifth-force need not be pointing in the same direction as gravity. As first shown in [52], the isocontours for the scalar field, because of the short range compared to gravity, follows more closely the shape of the object than does the gravitational potential. Due to this and the fact that clustering is stronger in modified gravity models we expect signatures on the shapes of clusters and voids.

An analysis of the shapes of dark matter halos in modified gravity was performed in Paper VII. The results we found was that low-mass dark matter halos are more elongated than in ΛCDM while the most massive halos on the other hand give similar results. Present observations show some tension between the shape of real clusters [53] and the predictions obtained from simulations. Our results indicate that if scalar fields make any difference, it is in the right direction to correct the apparent discrepancy.

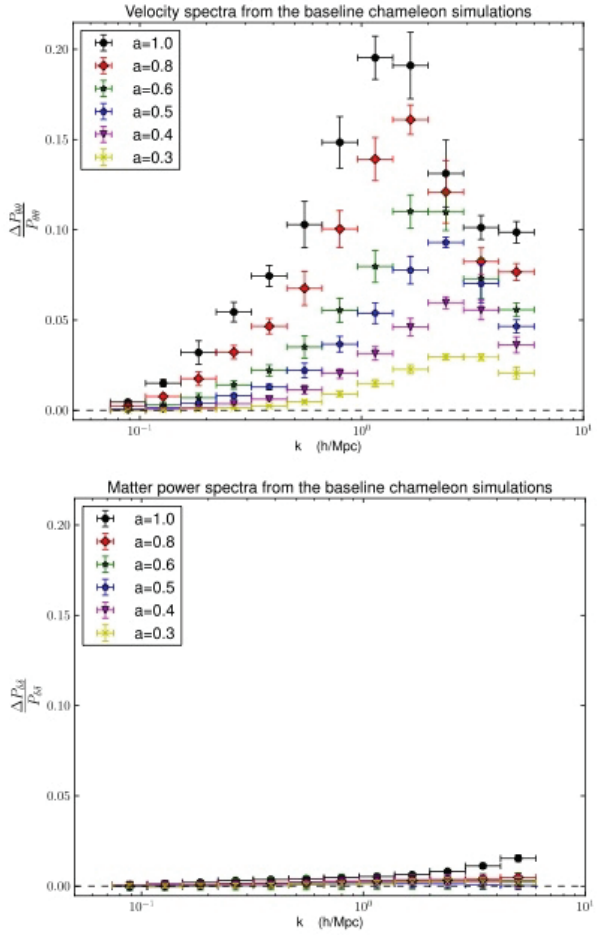

Figure 2.4: The fraction difference in the matter and velocity divergence spectra with respect to ΛCDM for a chameleon simulation taken from Paper V.

2.4.5 Voids

The screening mechanism of modified gravity depends on having a large ambient matter density to be effective. In regions where the density is low, the screening is expected to be weak and the fifth-force will be in full operation. Voids are regions of the Universe where the average matter density is lower than mean density which makes them very interesting for probing modified gravity.

In a void, matter is being pulled out towards massive halos in the surrounding clusters and filaments. Since the fifth-force is expected to play a big role in voids, we expect larger and emptier voids in modified gravity than we find in ΛCDM. This have been investigated in [54] and in our upcoming paper [55] and the results confirm the intuitive predictions.

A problem with voids in observations is that results (like for example the density profile of a void) depend sensitively on missing tracers. If for some reason our observations don't see some galaxies then this can bias the results significantly. A way around this problem is to stack many voids of a certain size on top of each other [56]. If we have enough voids this should give us a spherical symmetric void (assuming homogenity and isotropy). This procedure can be applied to observations as well as in simulations.

We have investigated stacked voids for $f(R)$ gravity in our upcoming paper [55]. The stacked voids in modified gravity have shallower density profiles and a larger compensating profile outside the void than what we find in ΛCDM. See Fig. (2.5) for an example.

Another interesting effect that can strengthen the modified gravity signal is redshift-space distortions [57] due to the streaming motions of halos in and on the boundary of voids. Modified gravity gives rise to (on average) larger peculiar velocities which leads to a stronger redshift-space distortion. Voids in redshift-space therefore appear more squeezed along the line-of-sight than we find in ΛCDM.

2.4.6 Dynamical masses

Mass estimates obtained through observations can be grouped into two categories: lensing and dynamical masses. The lensing mass is determined by the lensing potential $\Phi_L = \frac{\Phi+\Psi}{2}$ which for our class of models give the same prediction as GR. The dynamical mass on the other hand is defined as the mass contained within a radius r, inferred from the gravitational force felt by a test particle at r. Since the dynamical mass probes forces it is sensitive to the presence of a fifth-force and the prediction in modified gravity theories will differ from GR.

The lensing mass and the dynamical mass can observationally be measured using strong lensing and the peculiar velocity dispersion respectively.

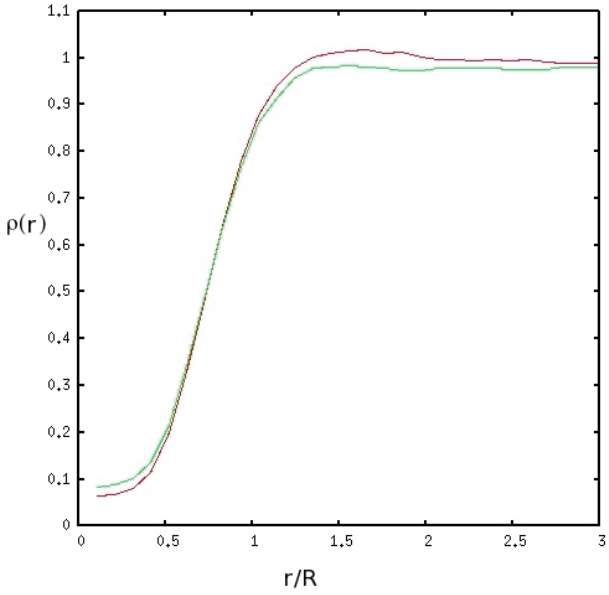

Figure 2.5: The density profile, in terms of the mean density of the Universe, of a stacked void of size $R = 8$ Mpc/h for a $f(R)$ gravity model (red) and ΛCDM (green).

This effect have, using results from N-body simulations, been studied in [58], [59] and [60]. The results show that the difference can be significant. However, measurements of the difference between the two mass estimates are likely to be contaminated by systematical effects.

2.4.7 Environmental dependence

The most intriguing signature of modified gravity is an environmental dependence of observables as such environmental effects are something we don't expect to find within GR.

A galaxy which is not screened if put by itself in a region of space, might indeed by screened if its located in a region of space with large ambient density. This can be seen from the expression of the screening factor

$$\frac{\Delta R}{R} = \frac{|\phi_\infty - \phi_c|}{2\beta M_{\rm Pl}\Phi_N} \tag{2.20}$$

Here ϕ_∞ is the scalar field value in the environment the object in question lies in[2]. If the environment is very dense then ϕ_∞ can be small enough so that $\frac{\Delta R}{R} \ll 1$ and the fifth-force is screened. If the environment is sparse then ϕ_∞ will be larger and we can have $\frac{\Delta R}{R} \sim 1$ which means no screening and a fifth-force in full operation.

For measurements of dynamical masses for example, a strong environmental dependence of the dynamical mass may provide a way to get around the problem of large systematical effects in the observations [59]. Observationally, one could divide galaxy samples into subgroups according to the environment each galaxy lies in and measure the difference of the two mass-measurements among those subsamples. If a correlation is found, then it will be a smoking gun of a modified gravity signal.

[2]When solving for the scalar field of a spherical object, ϕ_∞ comes in as the boundary condition.

Chapter 3

Summary

This thesis represents an effort to try to gain more knowledge of a, so far, largely undiscovered part of structure formation in models beyond ΛCDM, namely the non-linear regime. These studies can serve to provide novel ways to test gravity on large scales and to constrain models beyond ΛCDM. With new satellite and ground based mission planned in the upcoming years we will hopefully come closer to confirming GR or more excitingly find evidence of new physics beyond the standard model.

Below I will give a short summary of the papers that I have produced during my Ph.D studies and which are attached to this thesis.

Paper I

In this paper we studied structure formation in the symmetron model. We looked at predictions from linear perturbation theory, we implemented the model in the N-body code MLAPM, tested it and ran simulations. From the simulations we looked at signatures in the non-linear matter power-spectrum and the halo mass function.

Paper II

We used the results from the simulation in Paper I to look at a particularly interesting signature of modified gravity effect namely the environmental dependence of dark matter halos. By comparing the lensing mass with the dynamical mass for dark matter halos found in the simulation we quantified the ratio between these two masses and we also looked at the environmental dependence of this quantity.

Paper III

We showed that all scalar-tensor theories within a certain class can be unified within a simple and intuitive formalism. From this formalism we constructed generalisations of the chameleon, symmetron and dilaton scenarios.

Paper IV and V

We took the generalized models we constructed in Paper III and performed systematic N-body simulations of these models. From these simulations we studied the effects of modified gravity on the matter power-spectrum and the halo mass-function.

Paper VI

In this paper we investigate the cosmological evolution of a particular modified gravity model inspired by supersymmetry.

Paper VII

In this paper we presented a code which can be used to perform N-body simulations for a large class of modified theories of gravity. In this same paper we also studied the signatures of modified gravity on the shapes of dark matter halos. The main result we find is that halos tends to be more elongated in modified gravity than the ΛCDM counterpart.

Paper VIII

In this paper I derived the Layzer-Irvine equation for scalar tensor theories and showed how this equation can be used as a test of N-body codes.

Appendix

The matter power spectrum

In this appendix we give the definition of the matter power-spectrum which measures the density contrast of the universe as a function of scale.

The matter density field in the Universe can be composed in a homogenous part and a perturbation: $\rho(r,t) = \overline{\rho}(t)\,(1+\delta_m(r,t))$.

The two-point correlation function of the matter field is defined as

$$\xi(r) = \langle \delta_m(\mathbf{x})\delta_m(\mathbf{x}+\mathbf{r})\rangle \tag{3.1}$$

and measures the excess probability above the Poisson distribution of finding a pair of objects with separation r.

The Fourier transform of $\xi(r)$ is called the matter power-spectrum

$$P(k) = \int d^3r\xi(r)e^{-i\mathbf{k}\cdot\mathbf{x}} \tag{3.2}$$

which is related to the density field in k-space via

$$\langle \delta_m(\mathbf{k_1})\delta_m(\mathbf{k_2})\rangle = (2\pi)^3 P(k)\delta_D^{(3)}(\mathbf{k_1}+\mathbf{k_2}) \tag{3.3}$$

where δ_D is the Dirac delta-function.

Chapter 4

Bibliography

[1] E. Hubble. A Relation between Distance and Radial Velocity among Extra-Galactic Nebulae. *Proceedings of the National Academy of Science*, 15:168–173, March 1929. doi: 10.1073/pnas.15.3.168.

[2] F. Zwicky. On the Masses of Nebulae and of Clusters of Nebulae. *ApJ*, 86:217, October 1937. doi: 10.1086/143864.

[3] V. C. Rubin and W. K. Ford, Jr. Rotation of the Andromeda Nebula from a Spectroscopic Survey of Emission Regions. *ApJ*, 159:379, February 1970. doi: 10.1086/150317.

[4] S. M. Faber and R. E. Jackson. Velocity dispersions and mass-to-light ratios for elliptical galaxies. *ApJ*, 204:668–683, March 1976. doi: 10.1086/154215.

[5] Planck Collaboration, P. A. R. Ade, N. Aghanim, C. Armitage-Caplan, M. Arnaud, M. Ashdown, F. Atrio-Barandela, J. Aumont, C. Baccigalupi, A. J. Banday, and et al. Planck 2013 results. XVI. Cosmological parameters. *ArXiv e-prints*, March 2013.

[6] A. A. Penzias and R. W. Wilson. A Measurement of Excess Antenna Temperature at 4080 Mc/s. *ApJ*, 142:419–421, July 1965. doi: 10.1086/148307.

[7] G. F. Smoot, M. V. Gorenstein, and R. A. Muller. Detection of anisotropy in the cosmic blackbody radiation. *Physical Review Letters*, 39:898–901, October 1977. doi: 10.1103/PhysRevLett.39.898.

[8] G. F. Smoot, C. L. Bennett, A. Kogut, E. L. Wright, J. Aymon, N. W. Boggess, E. S. Cheng, G. de Amici, S. Gulkis, M. G. Hauser, G. Hinshaw, P. D. Jackson, M. Janssen, E. Kaita, T. Kelsall, P. Keegstra, C. Lineweaver, K. Loewenstein, P. Lubin, J. Mather, S. S. Meyer, S. H. Moseley, T. Murdock, L. Rokke, R. F. Silverberg, L. Tenorio, R. Weiss,

and D. T. Wilkinson. Structure in the COBE differential microwave radiometer first-year maps. *ApJL*, 396:L1–L5, September 1992. doi: 10.1086/186504.

[9] G. Hinshaw, D. Larson, E. Komatsu, D. N. Spergel, C. L. Bennett, J. Dunkley, M. R. Nolta, M. Halpern, R. S. Hill, N. Odegard, L. Page, K. M. Smith, J. L. Weiland, B. Gold, N. Jarosik, A. Kogut, M. Limon, S. S. Meyer, G. S. Tucker, E. Wollack, and E. L. Wright. Nine-Year Wilkinson Microwave Anisotropy Probe (WMAP) Observations: Cosmological Parameter Results. *ArXiv e-prints*, December 2012.

[10] A. G. Riess, A. V. Filippenko, P. Challis, A. Clocchiatti, A. Diercks, P. M. Garnavich, R. L. Gilliland, C. J. Hogan, S. Jha, R. P. Kirshner, B. Leibundgut, M. M. Phillips, D. Reiss, B. P. Schmidt, R. A. Schommer, R. C. Smith, J. Spyromilio, C. Stubbs, N. B. Suntzeff, and J. Tonry. Observational Evidence from Supernovae for an Accelerating Universe and a Cosmological Constant. *AJ*, 116:1009–1038, September 1998. doi: 10.1086/300499.

[11] S. Perlmutter, G. Aldering, G. Goldhaber, R. A. Knop, P. Nugent, P. G. Castro, S. Deustua, S. Fabbro, A. Goobar, D. E. Groom, I. M. Hook, A. G. Kim, M. Y. Kim, J. C. Lee, N. J. Nunes, R. Pain, C. R. Pennypacker, R. Quimby, C. Lidman, R. S. Ellis, M. Irwin, R. G. McMahon, P. Ruiz-Lapuente, N. Walton, B. Schaefer, B. J. Boyle, A. V. Filippenko, T. Matheson, A. S. Fruchter, N. Panagia, H. J. M. Newberg, W. J. Couch, and Supernova Cosmology Project. Measurements of Omega and Lambda from 42 High-Redshift Supernovae. *ApJ*, 517:565–586, June 1999. doi: 10.1086/307221.

[12] E. J. Copeland, M. Sami, and S. Tsujikawa. Dynamics of Dark Energy. *International Journal of Modern Physics D*, 15:1753–1935, 2006. doi: 10.1142/S021827180600942X.

[13] G. M. Clemence. The Relativity Effect in Planetary Motions. *Reviews of Modern Physics*, 19:361–364, October 1947. doi: 10.1103/RevModPhys.19.361.

[14] C. M. Will. Theory and experiment in gravitational physics. *Cambridge University Press*, 1981.

[15] J. Khoury. Theories of Dark Energy with Screening Mechanisms. *ArXiv e-prints*, November 2010.

[16] R. Durrer and R. Maartens. Dark energy and dark gravity: theory overview. *General Relativity and Gravitation*, 40:301–328, February 2008. doi: 10.1007/s10714-007-0549-5.

[17] R. Durrer and R. Maartens. Dark Energy and Modified Gravity. *ArXiv e-prints*, November 2008.

[18] R. Laureijs, J. Amiaux, S. Arduini, J. . Augueres, J. Brinchmann, R. Cole, M. Cropper, C. Dabin, L. Duvet, A. Ealet, and et al. Euclid Definition Study Report. *ArXiv e-prints*, October 2011.

[19] G. W. Horndeski. Second-Order Scalar-Tensor Field Equations in a Four-Dimensional Space. *International Journal of Theoretical Physics*, 10: 363–384, September 1974. doi: 10.1007/BF01807638.

[20] J. Khoury and A. Weltman. Chameleon Fields: Awaiting Surprises for Tests of Gravity in Space. *Physical Review Letters*, 93(17):171104, October 2004. doi: 10.1103/PhysRevLett.93.171104.

[21] J. Khoury and A. Weltman. Chameleon cosmology. *PRD*, 69(4):044026, February 2004. doi: 10.1103/PhysRevD.69.044026.

[22] D. F. Mota and D. J. Shaw. Strongly Coupled Chameleon Fields: New Horizons in Scalar Field Theory. *Physical Review Letters*, 97(15):151102, October 2006. doi: 10.1103/PhysRevLett.97.151102.

[23] D. F. Mota and D. J. Shaw. Evading equivalence principle violations, cosmological, and other experimental constraints in scalar field theories with a strong coupling to matter. *PRD*, 75(6):063501, March 2007. doi: 10.1103/PhysRevD.75.063501.

[24] A. de Felice and S. Tsujikawa. f(R) Theories. *Living Reviews in Relativity*, 13:3, June 2010. doi: 10.12942/lrr-2010-3.

[25] K. Hinterbichler and J. Khoury. Screening Long-Range Forces through Local Symmetry Restoration. *Physical Review Letters*, 104(23):231301, June 2010. doi: 10.1103/PhysRevLett.104.231301.

[26] P. Brax, C. van de Bruck, A.-C. Davis, and D. Shaw. Dilaton and modified gravity. *PRD*, 82(6):063519, September 2010. doi: 10.1103/PhysRevD.82.063519.

[27] P. Brax, A.-C. Davis, B. Li, and H. A. Winther. Unified description of screened modified gravity. *PRD*, 86(4):044015, August 2012. doi: 10.1103/PhysRevD.86.044015.

[28] P. Brax, C. Burrage, and A.-C. Davis. Screening fifth forces in k-essence and DBI models. *JCAP*, 1:020, January 2013. doi: 10.1088/1475-7516/2013/01/020.

[29] A. I. Vainshtein. To the problem of nonvanishing gravitation mass. *Physics Letters B*, 39:393–394, May 1972. doi: 10.1016/0370-2693(72)90147-5.

[30] E. Babichev, C. Deffayet, and R. Ziour. k-MOUFLAGE Gravity. *International Journal of Modern Physics D*, 18:2147–2154, 2009. doi: 10.1142/S0218271809016107.

[31] A. Nicolis, R. Rattazzi, and E. Trincherini. Galileon as a local modification of gravity. *PRD*, 79(6):064036, March 2009. doi: 10.1103/PhysRevD.79.064036.

[32] C. Deffayet, G. Esposito-Farèse, and A. Vikman. Covariant Galileon. *PRD*, 79(8):084003, April 2009. doi: 10.1103/PhysRevD.79.084003.

[33] M. Zumalacárregui, T. S. Koivisto, and D. F. Mota. DBI Galileons in the Einstein frame: Local gravity and cosmology. *PRD*, 87(8):083010, April 2013. doi: 10.1103/PhysRevD.87.083010.

[34] P. Brax, C. van de Bruck, A.-C. Davis, J. Khoury, and A. Weltman. Detecting dark energy in orbit: The cosmological chameleon. *PRD*, 70 (12):123518, December 2004. doi: 10.1103/PhysRevD.70.123518.

[35] J. Wang, L. Hui, and J. Khoury. No-Go Theorems for Generalized Chameleon Field Theories. *Physical Review Letters*, 109(24):241301, December 2012. doi: 10.1103/PhysRevLett.109.241301.

[36] A.-C. Davis, B. Li, D. F. Mota, and H. A. Winther. Structure Formation in the Symmetron Model. *ApJ*, 748:61, March 2012. doi: 10.1088/0004-637X/748/1/61.

[37] C. Contreras, C. Blake, G. B. Poole, F. Marin, S. Brough, M. Colless, W. Couch, S. Croom, D. Croton, T. M. Davis, M. J. Drinkwater, K. Forster, D. Gilbank, M. Gladders, K. Glazebrook, B. Jelliffe, R. J. Jurek, I.-h. Li, B. Madore, D. C. Martin, K. Pimbblet, M. Pracy, R. Sharp, E. Wisnioski, D. Woods, T. K. Wyder, and H. K. C. Yee. The WiggleZ Dark Energy Survey: measuring the cosmic growth rate with the two-point galaxy correlation function. *MNRAS*, 430:924–933, April 2013. doi: 10.1093/mnras/sts608.

[38] Ruth Durrer. Gauge invariant cosmological perturbation theory: A General study and its application to the texture scenario of structure formation. *Fund.Cosmic Phys.*, 15:209, 1994.

[39] P. J. E. Peebles. The large-scale structure of the universe. *Princeton University Press*, 1980.

[40] O. Lahav, P. B. Lilje, J. R. Primack, and M. J. Rees. Dynamical effects of the cosmological constant. *MNRAS*, 251:128–136, July 1991.

[41] J. Betancort-Rijo and M. López-Corredoira. The Complete Zeldovich Approximation. *ApJL*, 534:L117–L121, May 2000. doi: 10.1086/312679.

[42] J. S. Bagla and T. Padmanabhan. Cosmological N-body simulations. *Pramana*, 49:161, August 1997. doi: 10.1007/BF02845853.

[43] E. Bertschinger. Simulations of Structure Formation in the Universe. *ARAA*, 36:599–654, 1998. doi: 10.1146/annurev.astro.36.1.599.

[44] P. Brax, A.-C. Davis, B. Li, H. A. Winther, and G.-B. Zhao. Systematic simulations of modified gravity: chameleon models. *JCAP*, 4:029, April 2013. doi: 10.1088/1475-7516/2013/04/029.

[45] T. Baker, P. G. Ferreira, and C. Skordis. The parameterized post-Friedmann framework for theories of modified gravity: Concepts, formalism, and examples. *PRD*, 87(2):024015, January 2013. doi: 10.1103/PhysRevD.87.024015.

[46] B. Li and G. Efstathiou. An extended excursion set approach to structure formation in chameleon models. *MNRAS*, 421:1431–1442, April 2012. doi: 10.1111/j.1365-2966.2011.20404.x.

[47] P. Brax and P. Valageas. Impact on the power spectrum of Screening in Modified Gravity Scenarios. *ArXiv e-prints*, May 2013.

[48] B. Li, W. A. Hellwing, K. Koyama, G.-B. Zhao, E. Jennings, and C. M. Baugh. The non-linear matter and velocity power spectra in f(R) gravity. *MNRAS*, 428:743–755, January 2013. doi: 10.1093/mnras/sts072.

[49] T. Y. Lam, T. Nishimichi, F. Schmidt, and M. Takada. Testing Gravity with the Stacked Phase Space around Galaxy Clusters. *Physical Review Letters*, 109(5):051301, August 2012. doi: 10.1103/PhysRevLett.109.051301.

[50] R. A. Sunyaev and I. B. Zeldovich. Microwave background radiation as a probe of the contemporary structure and history of the universe. *ARAA*, 18:537–560, 1980. doi: 10.1146/annurev.aa.18.090180.002541.

[51] F. Schmidt, A. Vikhlinin, and W. Hu. Cluster constraints on f(R) gravity. *PRD*, 80(8):083505, October 2009. doi: 10.1103/PhysRevD.80.083505.

[52] C. Llinares and D. F. Mota. Shape of Clusters of Galaxies as a Probe of Screening Mechanisms in Modified Gravity. *Physical Review Letters*, 110(15):151104, April 2013. doi: 10.1103/PhysRevLett.110.151104.

[53] E. T. Lau, D. Nagai, A. V. Kravtsov, A. Vikhlinin, and A. R. Zentner. Constraining Cluster Physics with the Shape of X-Ray Clusters: Comparison of Local X-Ray Clusters Versus ΛCDM Clusters. *ApJ*, 755:116, August 2012. doi: 10.1088/0004-637X/755/2/116.

[54] B. Li, G.-B. Zhao, and K. Koyama. Haloes and voids in f(R) gravity. *MNRAS*, 421:3481–3487, April 2012. doi: 10.1111/j.1365-2966.2012.20573.x.

[55] H. A. Winther, D. Mota, and J. Silk. Stacked voids in modified gravity. *To appear*, 2013.

[56] G. Lavaux and B. D. Wandelt. Precision Cosmography with Stacked Voids. *ApJ*, 754:109, August 2012. doi: 10.1088/0004-637X/754/2/109.

[57] E. Jennings, C. M. Baugh, B. Li, G.-B. Zhao, and K. Koyama. Redshift-space distortions in f(R) gravity. *MNRAS*, 425:2128–2143, September 2012. doi: 10.1111/j.1365-2966.2012.21567.x.

[58] F. Schmidt. Dynamical masses in modified gravity. *PRD*, 81(10): 103002, May 2010. doi: 10.1103/PhysRevD.81.103002.

[59] G.-B. Zhao, B. Li, and K. Koyama. Testing Gravity Using the Environmental Dependence of Dark Matter Halos. *Physical Review Letters*, 107 (7):071303, August 2011. doi: 10.1103/PhysRevLett.107.071303.

[60] H. A. Winther, D. F. Mota, and B. Li. Environment Dependence of Dark Matter Halos in Symmetron Modified Gravity. *ApJ*, 756:166, September 2012. doi: 10.1088/0004-637X/756/2/166.

Part II

Papers

Paper I

Structure Formation in The Symmetron Model
Anne-Christine Davis, Baojiu Li, David F. Mota, Hans A. Winther
The Astrophysical Journal, Volume 748, Issue 1, (2012).

The Astrophysical Journal, 748:61 (18pp), 2012 March 20 doi:10.1088/0004-637X/748/1/61

STRUCTURE FORMATION IN THE SYMMETRON MODEL

Anne-Christine Davis[1], Baojiu Li[1,2], David F. Mota[3], and Hans A. Winther[3]
[1] DAMTP, Centre for Mathematical Sciences, University of Cambridge, Wilberforce Road, Cambridge CB3 0WA, UK
[2] Kavli Institute for Cosmology Cambridge, Madingley Road, Cambridge CB3 0HA, UK
[3] Institute of Theoretical Astrophysics, University of Oslo, 0315 Oslo, Norway
Received 2011 August 18; accepted 2012 January 12; published 2012 March 6

ABSTRACT

Scalar fields, strongly coupled to matter, can be present in nature and still be invisible to local experiments if they are subject to a screening mechanism. The symmetron is one such mechanism that relies on restoration of a spontaneously broken symmetry in regions of high density to shield the scalar fifth force. We have investigated structure formation in the symmetron model by using *N*-body simulations and find observable signatures in both the linear and nonlinear matter power spectrum and on the halo mass function. The mechanism for suppressing the scalar fifth force in high-density regions is also found to work very well.

Key words: cosmology: miscellaneous – cosmology: theory – large-scale structure of Universe

Online-only material: color figures

1. INTRODUCTION

Our current standard model of cosmology, ΛCDM, has been very successful in explaining a large range of observations probing a vast range of length scales. We should nevertheless be open to the possibility that ΛCDM is just a first-order approximation of some more fundamental theory. Many theories of high-energy physics, like string theory and supergravity, predict light gravitationally coupled scalar fields (see, e.g., Binetruy 2006; Linde 2008, and references therein). These scalars may play the role of dark energy (quintessence). If these scalar fields have non-minimal coupling to matter fields, then they could mediate extra forces that are potentially detectable in local experiments.

Over the past few decades, several laboratory and solar system experiments have tried to detect a sign of such fundamental coupled scalar fields (Adelberger 2002; Hoskins et al. 1985; Decca et al. 2007; Bertotti et al. 2003), but the results so far have been negative. Naively, the results of these experiments have ruled out any such scalar fields. However, one should bear in mind that a coupled scalar field might exist but is undetected because of some sort of screening mechanism.

To date we know three types of theoretical mechanisms (see Khoury 2010 for a review) that can explain why such light scalars, if they exist, may not be visible to experiments performed near the Earth. One such class, the chameleon mechanism (Khoury & Weltman 2004; Brax et al. 2004; Clifton et al. 2005; Mota & Barrow 2004a, 2004b), operates when the scalars are coupled to matter in such a way that their effective mass depends on the local matter density. In space, where the local mass density is low, the scalars would be light and deviations from general relativity (GR) would be observed. But near the Earth, where experiments are performed, the local mass density is high and the scalar field would acquire a heavy mass, making the interactions short range and therefore unobservable.

The second mechanism, the Vainshtein mechanism (Vainshtein 1972; Deffayet et al. 2002; Arkani-Hamed et al. 2003), operates when the scalar has derivative self-couplings that become important near matter sources such as the Earth. The strong coupling near sources essentially cranks up the kinetic terms, which translates into a weakened matter coupling. Thus, the scalar screens itself and becomes invisible to experiments. This mechanism is central to the phenomenological viability of braneworld modifications of gravity and galileon scalar theories (Dvali et al. 2000; de Rham et al. 2008; Nicolis et al. 2009; Hinterbichler et al. 2010; Mota et al. 2010; Gabadadze 2009; de Rham 2010; Brax et al. 2011a).

The last mechanism, the one explored in this paper, is the symmetron mechanism (Hinterbichler & Khoury 2010; Hinterbichler et al. 2011; Olive & Pospelov 2008; Brax et al. 2011b; Clampitt et al. 2012). In this mechanism, the vacuum expectation value (VEV) of the scalar depends on the local mass density, becoming large in regions of low mass density and small in regions of high mass density. By taking the coupling of the scalar to matter to be proportional to the VEV, we can have a viable theory where the scalar couples with gravitational strength in regions of low density but is decoupled and screened in regions of high density. This is achieved through the interplay of a symmetry breaking potential and a universal quadratic coupling to matter. A similar screening mechanism applies in the case of the environmentally dependent dilaton model (Brax et al. 2010a).

In vacuum, the scalar field acquires a VEV that spontaneously breaks the $\mathbb{Z}_2$ symmetry $\phi \rightarrow -\phi$. In the regions of sufficiently high matter density, the field is confined near $\phi = 0$, and the symmetry is restored. The fifth force arising from the matter coupling is proportional to ϕ making the effects of the scalar small in high-density regions.

In contrast to chameleons, where the strongest constraints (Mota & Shaw 2006, 2007; Brax et al. 2007a, 2007b, 2008, 2010c; Gannouji et al. 2010; Gies et al. 2008) come from laboratory experiments that in effect wash out any observable effects in the solar system, the symmetron predicts a host of observational signatures in experiments designed to look for deviations from GR, which are just below the current bounds and within reach of the next-generation experiments.

In the simplest formulation (Hinterbichler & Khoury 2010), which is the one studied here, the symmetron cannot account for dark energy (Hinterbichler et al. 2011). To have a successful cosmology, a cosmological constant must be added to the model. The model is nevertheless a concrete example of a viable modification of gravity that can leave observable imprints

on cosmological scales. Indeed, the symmetron model was constructed as a scalar-tensor theory with a screening mechanism to suppress fifth forces in solar system tests of GR. Whilst fifth forces are screened in the solar system they could still have observable effects cosmologically. In this paper we address this issue. In particular we investigate the effect the symmetron has on structure formation in order to obtain results that can be compared with observation.

The cosmology of coupled scalar field models is usually strongly constrained by local gravity experiments, which could put limits on the range and the coupling strength of the scalar field. There do exist several cases in which signatures on the linear perturbations are found, but in most cases the range of the field is well below linear scales. To proceed into the region of nonlinear structure formation, one can use the spherical collapse model to obtain the qualitative behavior, but in order to obtain accurate quantitative results deep into the nonlinear regime, one is almost required to perform *N*-body simulations.

Studies of coupled scalar field models, and other models where a fifth-force is present, using *N*-body simulations (Zhao et al. 2010, 2011; Brax et al. 2011c; Li & Barrow 2011a, 2011b; Li et al. 2011a; Li & Zhao 2010; Ferraro et al. 2011; Oyaizu et al. 2008; Schmidt et al. 2009; Schmidt 2009; Baldi et al. 2010; Baldi 2009; Hellwing & Juszkiewicz 2009; Hellwing et al. 2010) have revealed several interesting signatures that can in principle be detected by observations in the near future. For example, in Zhao et al. (2011) and Schmidt (2010) it was found that $f(R)$ theories can give rise to a dependence on the environment of the dynamical to lensing mass ratio of halos; an observable feature that is not found in ΛCDM. This signature is also present in the symmetron model (Winther et al. 2011).

In this article we will study the effects a symmetron field has on structure formation. By performing high-resolution *N*-body simulations, we demonstrate explicitly how the symmetron mechanism works in screening the fifth force and obtain observables such as the matter power spectrum and the mass function.

2. THE SYMMETRON MODEL

In this section we review the symmetron model, explaining the screening mechanism, and discuss the local constraints on the model parameters. At the end of this section we reparameterize the model parameters by introducing more physically intuitive parameters that will help us discuss the results in the following sections more clearly.

The action governing the dynamics of the symmetron model is given by

$$S = \int dx^4\sqrt{-g}\left[\frac{R}{2}M_{\rm pl}^2 - \frac{1}{2}(\partial\phi)^2 - V(\phi)\right] + S_m(\tilde{g}_{\mu\nu}, \psi_i), \quad (1)$$

where g is the determinant of the metric $g_{\mu\nu}$, R is the Ricci scalar, ψ_i are the different matter fields, and $M_{\rm pl} \equiv 1/\sqrt{8\pi G}$, where G is the bare gravitational constant. The matter fields couple to the Jordan frame metric $\tilde{g}_{\mu\nu}$ via a conformal rescaling of the Einstein frame metric $g_{\mu\nu}$ given by

$$\tilde{g}_{\mu\nu} = A^2(\phi)g_{\mu\nu}. \quad (2)$$

The coupling function $A(\phi)$ is chosen to be an even polynomial in ϕ (to be compatible with the $\phi \to -\phi$ symmetry)

$$A(\phi) = 1 + \frac{1}{2}\left(\frac{\phi}{M}\right)^2 + \mathcal{O}\left(\frac{\phi^4}{M^4}\right) \quad (3)$$

described by a single mass scale M. For the range of parameters we are interested in we have $(\phi/M)^2 \ll 1$. Thus, we can neglect the higher order correction terms. The potential is chosen to be of the symmetry breaking form

$$V(\phi) = V_0 - \frac{1}{2}\mu^2\phi^2 + \frac{1}{4}\lambda\phi^4, \quad (4)$$

where V_0 is a cosmological constant (CC). We will for simplicity absorb all contributions to the CC into V_0 by simply putting $V_0 \equiv \Lambda$. We will later see that Λ must be taken to be the usual CC to obtain late time acceleration of the universe. Thus, the symmetron model considered here cannot account for dark energy. It will be interesting to see if a more complicated setup, e.g., extensions of the proposals discussed in Hinterbichler et al. (2011), can lead to dark energy. This is, however, beyond the scope of this work.

The field equation for ϕ follows from the variation of the action Equation (1) with respect to ϕ and reads

$$\Box\phi = V_{{\rm eff},\,\phi}. \quad (5)$$

The effective potential is given in terms of the trace, T_m, of the matter energy-momentum tensor by

$$V_{\rm eff}(\phi) = \frac{1}{2}\left(-\frac{T_m}{M^2} - \mu^2\right)\phi^2 + \frac{1}{4}\lambda\phi^4 \quad (6)$$

$$= \frac{1}{2}\left(\frac{\rho_m}{M^2} - \mu^2\right)\phi^2 + \frac{1}{4}\lambda\phi^4 \quad (7)$$

depending on the two mass scales μ, M and the dimensionless coupling constant λ. It is convenient to define the critical matter density (and the critical redshift) as

$$\rho_{\rm SSB} \equiv \mu^2 M^2 = 3H_0^2 M_{\rm pl}^2 \Omega_m (1 + z_{\rm SSB})^3, \quad (8)$$

where SSB stands for spontaneous symmetry breaking, Ω_m is the matter density parameter in the universe today, and H_0 is the Hubble parameter. In regions where $\rho_m > \rho_{\rm SSB}$ (where ρ_m is the local matter density) the symmetry $\phi \to -\phi$ is upheld and the effective potential has a minimum at $\phi_{\rm min} = 0$, whereas in regions where $\rho_m < \rho_{\rm SSB}$ the symmetry is spontaneously broken and the field acquires a VEV

$$\phi_{\rm min} = \pm\phi_0\sqrt{1 - \frac{\rho_m}{\rho_{\rm SSB}}}, \quad (9)$$

where $\phi_0 \equiv \mu/\sqrt{\lambda}$ is the symmetry breaking VEV for $\rho_m \to 0$. The mass of small fluctuations around the minimum of the effective potential is given by

$$m_\phi^2 \equiv V_{{\rm eff},\,\phi\phi} = \left(\frac{\rho_m}{\rho_{\rm SSB}} - 1\right)\mu^2 + 3\lambda\phi_{\rm min}^2 = \begin{cases} \mu^2\left(\frac{\rho_m}{\rho_{\rm SSB}} - 1\right), & \rho_m > \rho_{\rm SSB} \\ 2\mu^2\left(1 - \frac{\rho_m}{\rho_{\rm SSB}}\right), & \rho_m < \rho_{\rm SSB}. \end{cases} \quad (10)$$

The symmetron field acquires the longest range, $\lambda_\phi \equiv 1/m_\phi$, in low-density regions where

$$\lambda_\phi = \lambda_0 \equiv \frac{1}{\sqrt{2}\mu}. \quad (11)$$

For future convenience we introduce the dimensionless quantity $L \equiv \lambda_0/(\text{Mpc } h^{-1})$, which is the maximum range of the force mediated by the symmetron in units of Mpc h^{-1}.

The gravitational field equation for $g_{\mu\nu}$ is given by

$$G_{\mu\nu} = 8\pi G T_{\mu\nu} \quad (12)$$

where the total energy-momentum tensor $T_{\mu\nu}$ is the sum of the matter and scalar field parts:

$$T_{\mu\nu} = A(\phi)T^m_{\mu\nu} + \phi_{,\mu}\phi_{,\nu} - g_{\mu\nu}\left(\frac{1}{2}(\partial\phi)^2 + V(\phi)\right). \quad (13)$$

Note that the matter part itself is not conserved, but instead satisfies

$$\nabla_\nu T^{\mu\nu}_m = \frac{d\log A(\phi)}{d\phi}\left(T_m\nabla^\mu\phi - T^{\mu\nu}_m\nabla_\nu\phi\right). \quad (14)$$

In N-body simulations we are interested in describing the matter sector by particles. The energy-momentum tensor of an individual particle with mass m_0 at position $\mathbf{r_0}$ is given by

$$T^{\mu\nu}_m(\mathbf{r}) = \frac{m_0}{\sqrt{-g}}\delta(\mathbf{r} - \mathbf{r}_0)\dot{r}^\mu_0\dot{r}^\nu_0, \quad (15)$$

where $\mathbf{r}$ is the general spatial coordinate. Taking the divergence of Equation (12) and using the Bianchi identity, we get the geodesic equation for the matter particles

$$\ddot{r}^\mu_0 + \Gamma^\mu_{\alpha\gamma}r^\alpha_0 r^\gamma_0 = -\frac{d\log A(\phi)}{d\phi}\left(\nabla^\mu\phi + \dot{\phi}\dot{r}^\mu_0\right) \quad (16)$$

which for $A \equiv 1$ reduces to the standard geodesic equation in GR.

From Equation (16) we see that the symmetron field gives rise to a fifth force on the matter fields that, in the nonrelativistic limit, is given by

$$\vec{F}_\phi = \frac{\phi}{M^2}\vec{\nabla}\phi = \frac{\beta}{M_{\rm pl}}\left(\frac{\phi}{\phi_0}\right)\vec{\nabla}\phi, \quad (17)$$

where we have introduced the coupling constant $\beta \equiv \phi_0 M_{\rm pl}/M^2$.

The static, spherically symmetric solutions of the field equations were found in Hinterbichler & Khoury (2010). For two test masses in a region where $\phi = \phi_B$ it was shown that the fifth force is simply

$$\frac{F_\phi}{F_N} = 2\beta^2\left(\frac{\phi_B}{\phi_0}\right)^2. \quad (18)$$

In a low-density region ($\rho \ll \rho_{\rm SSB}$) we have $\phi_B = \phi_0$ and the fifth force is comparable with gravity for $\beta = \mathcal{O}(1)$.

For very large bodies, the situation is quite different. The symmetry is restored in the interior of the body and the fifth force on a test mass outside becomes

$$\frac{F_\phi}{F_N} = 2\beta^2\left(\frac{\phi_B}{\phi_0}\right)^2\frac{1}{\alpha},\ \alpha^{-1} = 2\frac{\rho_{\rm SSB}}{\rho_{\rm body}}\left(\frac{\lambda_0}{R_{\rm body}}\right)^2. \quad (19)$$

The fifth force is suppressed by a factor $\alpha^{-1} \ll 1$ – similar to the thin shell factor found in chameleon theories (Khoury & Weltman 2004).

We also see that if the test masses are inside a screened region ($\phi_B/\phi_0 \ll 1$) the force will be further suppressed.

Since the field is long ranged (and universally coupled) in almost all situations today, the theory is best constrained by solar system experiments that have been performed with high precision.

It turns out that as long as our Galaxy is sufficiently screened ($10 \lesssim \alpha_G$), our Sun will also be screened and the combined effects discussed above are enough to evade the current parameterized post-Newtonian (PPN) constraints.

By assuming that $\phi \to \phi_0$ outside our Galaxy, i.e., that our galactic neighborhood is not screened, these constraints were derived in Hinterbichler & Khoury (2010) and Brax et al. (2011b) and require

$$M \lesssim 10^{-3}M_{\rm pl}. \quad (20)$$

If the assumption about the value of ϕ outside our Galaxy, which is very likely to be true, can be relaxed, then the bound above can be relaxed somewhat as well. The constraint on M turns into a constraint on the range of the field and the redshift in which the SSB takes place:

$$\lambda_0 \lesssim 2.3\sqrt{\frac{0.3}{\Omega_m}}(1 + z_{\rm SSB})^{-3/2}\ \text{Mpc } h^{-1}. \quad (21)$$

Thus, for transitions that take place close to the present time, the fifth force can have a range of at most a few Mpc h^{-1}.

In the rest of this article, instead of working with the parameters $\{\mu, M, \lambda\}$, we will instead choose to work with the more physically intuitive quantities $\{L, \beta, z_{\rm SSB}\}$: the cosmological range of the fifth force in Mpc h^{-1}, the strength of the fifth force relative to gravity, and the redshift at which the SSB takes place in the cosmological background, respectively.

The transformation between the two sets of parameters is given by

$$\frac{\mu}{H_0} = \frac{2998}{\sqrt{2}L} \quad (22)$$

$$\frac{M}{M_{\rm pl}} = 10^{-3}\sqrt{\frac{\Omega_m}{0.27}}\left(\frac{L}{2.36}\right)(1 + z_{\rm SSB})^{3/2} \quad (23)$$

$$\lambda = \left(\frac{10^{60}H_0}{M_{\rm pl}}\cdot\frac{0.27}{\Omega_m}\right)^2\frac{1.38\times10^{-100}}{\beta^2L^6(1 + z_{\rm SSB})^6}. \quad (24)$$

For typical parameters $L \sim \beta \sim 1$ and $z_{\rm SSB} \sim 0$ we have $\mu \sim 10^3H_0$, $M \sim 10^{-3}M_{\rm pl}$, and $\lambda \sim 10^{-100}$. Thus, the symmetron is very weakly self-coupled. As with other models with screening mechanisms, our parameters require a certain degree of fine-tuning. This means that SSB is a rather late-time phenomenon.

We will choose to work with values of the parameters that are close to the local constraints and in which the symmetron can produce observable cosmological effects. This means we will be most interested in the parameter space $L = \mathcal{O}(1)$, $\beta = \mathcal{O}(1)$, and $0 \lesssim z_{\rm SSB} \lesssim 2$.

3. SYMMETRON COSMOLOGY

In this section we discuss the cosmological evolution of the symmetron field from the background evolution to linear perturbations and derive the nonrelativistic limits of the field equations to be implemented in the *N*-body code. The analysis in this section is mainly for comparison with the *N*-body simulations. For a more thorough discussion regarding the background cosmology and linear perturbations in the symmetron, see Hinterbichler et al. (2011) and Brax et al. (2011b), respectively.

3.1. Background Cosmology

The background evolution of the symmetron in a flat Friedmann–Lemaitre–Robertson–Walker (FLRW) metric

$$ds^2 = -dt^2 + a^2(t)(dx^2 + dy^2 + dz^2) \tag{25}$$

is determined by the field equation

$$\ddot{\phi} + 3H\dot{\phi} + V_{\mathrm{eff},\,\phi} = 0 \tag{26}$$

together with the Friedman equations

$$3H^2 M_{\mathrm{pl}}^2 = \rho_m A(\phi) + \rho_\phi \tag{27}$$

$$\dot{\rho}_m + 3H\rho_m = 0 \tag{28}$$

where

$$\rho_\phi = \Lambda - \frac{1}{2}\mu^2\phi^2 + \lambda\phi^4 + \frac{1}{2}\dot{\phi}^2. \tag{29}$$

When the field follows the minimum of the effective potential, we have

$$\left|\frac{\rho_\phi - \Lambda}{\Lambda}\right| \lesssim \frac{\mu^4}{\lambda\Lambda} = \beta^2 \frac{\rho_{\mathrm{SSB}}}{\Lambda}\left(\frac{M}{M_{\mathrm{pl}}}\right)^2 \tag{30}$$

$$\lesssim 10^{-6}\beta^2(1 + z_{\mathrm{SSB}})^3. \tag{31}$$

Thus, for $\beta, z_{\mathrm{SSB}} \sim \mathcal{O}(1)$ the dynamical part of the potential is too small to contribute significantly to the energy density of the universe and we are left with the cosmological constant to account for dark energy.

In the same regime, the coupling function $A(\phi)$ satisfies

$$|A(\phi) - 1| = \frac{1}{2}\left(\frac{\phi}{M}\right)^2 \lesssim \beta^2\left(\frac{M}{M_{\mathrm{pl}}}\right)^2 \lesssim 10^{-6}\beta^2 \tag{32}$$

which is also too small to produce an observable effect on the background expansion. This implies that the symmetron evades Big Bang Nucleosynthesis (BBN) bounds on the variation of masses of the standard model particles (see Section 3.5). It might be possible to make the symmetron responsible for dark energy by changing the form of the potential and coupling. One such modification was proposed in Hinterbichler et al. (2011); however, it was shown that additional fine-tuning of the parameters was required to yield the desired late-time cosmology.

In Figure 1 we see the background evolution $\phi(z)$ for $z_{\mathrm{SSB}} = 2$ together with the analytical minimum. Note that the field does not start to follow the minimum immediately after SSB. This has important consequences for the evolution of the perturbations, which will be discussed in Section 3.4.

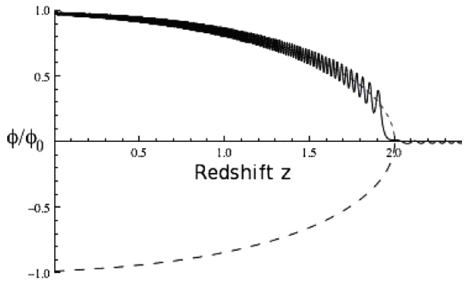

Figure 1. Background evolution of the symmetron for $\beta = 1$, $L = 1$, and $z_{\mathrm{SSB}} = 2$ together with the analytical background (dashed lines). The symmetry is broken at $z = 2$ and the field settles at one of the two branches.

3.2. Linear Perturbations

The most general metric in a perturbed FLRW space-time is given by

$$\begin{aligned} ds^2 = &-(1+2\alpha)dt^2 - 2aB_{,i}dtdx^i \\ &+ a^2((1+2\psi)\delta_{ij} + 2\gamma_{,i;j})dx^i dx^j, \end{aligned} \tag{33}$$

where the covariant derivative is given in terms of the spatial metric, which in the case of our flat background reduces to δ_{ij}. We decompose the field ϕ into the background and perturbated parts: $\phi(\mathbf{x}, t) = \overline{\phi}(t) + \delta\phi(\mathbf{x}, t)$. The energy-momentum tensor of nonrelativistic matter can be decomposed as

$$T_0^0 = -\rho_m(1 + \delta_m), \;\; T_i^0 = -\rho_m v_i, \tag{34}$$

where v is the peculiar velocity of nonrelativistic matter and δ_m is the matter density perturbation defined by

$$\delta_m \equiv \frac{\delta\rho_m}{\rho_m} - \frac{\dot{\rho}_m}{\rho_m}v \equiv \frac{\delta\rho_m}{\rho_m} \;\text{ in the comoving gauge.} \tag{35}$$

The equation determining the evolution of the perturbations, neglecting anisotropic stresses, follows from the Einstein equations. The scalar perturbations can be read off from the formulation of Hwang & Noh (2002), which is independent of gauge. In the following we use units of $M_{\mathrm{pl}} \equiv 1$. After solving for the different metric potentials, we find that the scalar perturbations, in the comoving gauge ($v = 0$), are determined by

$$\begin{aligned} &\ddot{\delta}_m + 2H\dot{\delta}_m - \frac{1}{2}\rho_m\delta_m \\ &- \frac{\phi\delta\phi}{M^2}\left(6H^2 + 6\dot{H} + \Omega_m H^2 - \frac{k^2}{a^2} + 2\dot{\phi}^2\right) \\ &- \frac{\phi}{M^2}(\ddot{\delta\phi} + 5H\dot{\delta\phi}) - \frac{2\dot{\phi}}{M^2}(\dot{\delta\phi} + H\delta\phi) \\ &+ V_{\mathrm{eff},\,\phi}\left(1 + \frac{1}{M^2}\right)\delta\phi - 2\dot{\phi}\dot{\delta\phi} = 0 \end{aligned} \tag{36}$$

$$\begin{aligned} &\ddot{\delta\phi} + \left(3H + \frac{2\phi\dot{\phi}}{M^2}\right)\dot{\delta\phi} + \frac{\phi\rho_m\delta_m}{M^2} - \dot{\phi}\dot{\delta}_m \\ &+ \left(m_\phi^2 + \frac{k^2}{a^2} - \frac{2\phi}{M^2}V_{\mathrm{eff},\,\phi} + \frac{2\dot{\phi}^2}{M^2}\right)\delta\phi = 0. \end{aligned} \tag{37}$$

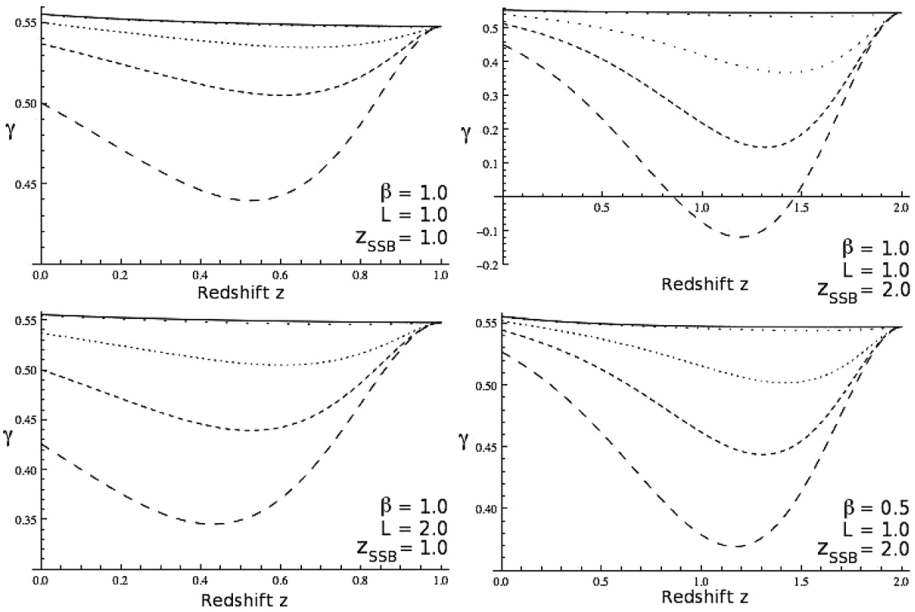

Figure 2. Evolution of the growth index $\gamma(z)$ when $z_{\rm SSB} = 1$ (left) and $z_{\rm SSB} = 2$ (right) for four different wavenumbers $k = \{0.01, 0.05, 0.1, 0.2\}$ Mpc h^{-1} (from top to bottom in each figure). The solid line shows the prediction of ΛCDM.

In studying the perturbations it is convenient to introduce the growth index

$$\gamma(z, k) = \frac{\log\left(\frac{d\log\delta_m}{d\log a}\right)}{\log(\Omega_m(z))}. \tag{38}$$

In ΛCDM we have $\gamma \approx 0.55$ (for $0.2 \lesssim \Omega_m \lesssim 0.3$), which is scale and almost redshift independent. In modified theories, however, γ can have significant scale and redshift dependence as shown in Gannouji et al. (2010) and Mota & Winther (2011) for the case of chameleon models, Tsujikawa et al. (2009), Brax et al. (2008, 2010b), Motohashi et al. (2010), Narikawa & Yamamoto (2010), and Appleby & Weller (2010) for $f(R)$ modified gravity, and Baldi (2011) for interacting dark energy.

If we assume that the field is rolling slowly along the minimum, we can neglect all terms proportional to $\dot\phi$ and the oscillating term $V_{{\rm eff},\phi}$. The perturbations in ϕ will evolve more slowly than the perturbations in δ_m for scales deep inside the Hubble radius. Thus, the terms $\rho_m\beta_{,\phi}\,\delta_m$ and $(m_\phi^2 + (k^2/a^2))\delta\phi$ will dominate over the $\delta\phi$ time derivatives in Equation (37). Under these assumptions, we can simplify Equation (36) to

$$\ddot\delta_m + 2H\dot\delta_m = \frac{3}{2}\Omega_m H^2 \frac{G_{\rm eff}}{G}\delta_m \tag{39}$$

$$\frac{G_{\rm eff}}{G} = 1 + \frac{2\beta^2\phi^2/\phi_0^2}{1 + \frac{a^2}{\lambda_\phi^2 k^2}} \tag{40}$$

which are the equations we use to integrate the perturbations.

At times before SSB we have $\phi \approx 0$ and therefore $G_{\rm eff} \approx G$. After SSB the field approaches the minimum $\phi = \phi_0$, in this regime we have

$$\frac{G_{\rm eff}}{G} = \begin{cases} 1 & \frac{a}{k} \gg \lambda_\phi \\ 1 + 2\beta^2 & \frac{a}{k} \ll \lambda_\phi. \end{cases} \tag{41}$$

Thus, small scales will feel a stronger gravitational constant.

In Figure 2 we show the redshift evolution of γ for several different wavenumbers, and in Figure 3 we show contour plots for $\gamma(k, z = 0)$ for two comoving wavenumbers. The evolution of the growth index is very similar, with a minimum at some redshift $z > 0$, to the behavior found in other coupled scalar field models in the literature (see the references below Equation (38)).

The growth rate on really large scales ($k \lesssim 0.01\ h$ Mpc^{-1}) is not affected by the symmetron fifth force unless $L, \beta \gg 1$. However, on the smallest, linear scales we can still have a deviation from the predictions of GR. Note that we have integrated the perturbations using the approximation Equation (39) instead of the full equations (36) and (37). The explanation for this is given in Section 3.4.

3.3. Linear Power Spectrum and the CMB

In Figure 4 we show the factional difference of the linear power spectrum of the symmetron to that of ΛCDM, defined as $\Delta P(k)/P(k) \equiv (P(k) - P_{\Lambda{\rm CDM}}(k))/P_{\Lambda{\rm CDM}}(k)$. Note that on linear scales ($k \lesssim 0.1\ h$ Mpc^{-1}) the power spectrum is very close to ΛCDM. Going down to scales comparable to the length scale of the symmetron ($k \sim L^{-1}\ h$ Mpc^{-1}) the power spectrum starts to deviate significantly. However, in this regime the perturbations are already nonlinear and we cannot trust the results of the linear perturbation theory. Once we discuss the *N*-body results, we will see that the symmetron mechanism is at work in this regime, thereby suppressing the fractional difference from ΛCDM in the power spectrum predicted by linear perturbation theory.

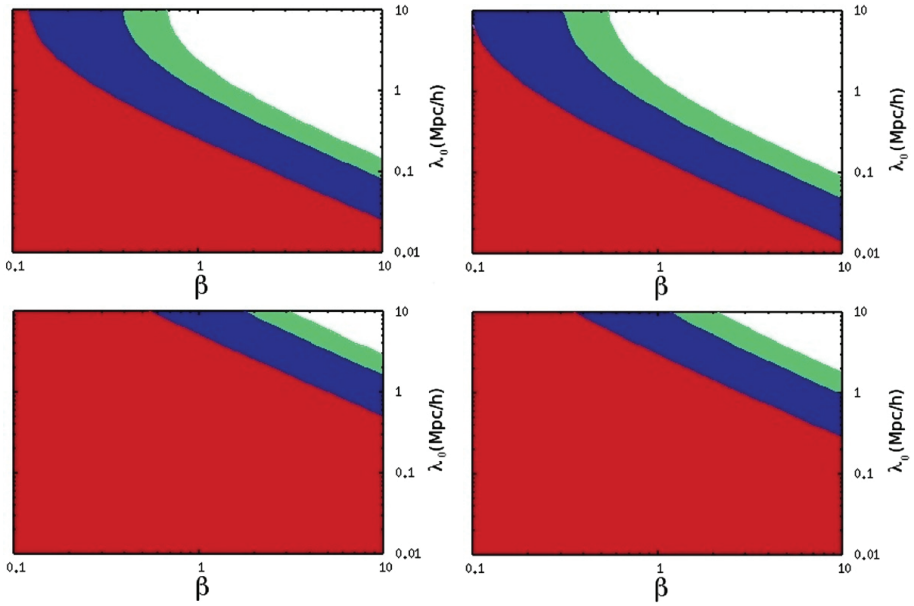

Figure 3. Growth index $\gamma(z=0)$ for $z_{\rm SSB}=1.0$ (left) and $z_{\rm SSB}=2.0$ (right) for two comoving wavenumbers: $k=0.2$ Mpc h^{-1} (above) and $k=0.01$ Mpc h^{-1} (below). The red region shows the GR regime $\gamma\simeq 0.555$, the blue region shows the regime where $0.5<\gamma<0.55$, the green region shows $0.4<\gamma<0.5$, and the white region shows $\gamma<0.4$.

(A color version of this figure is available in the online journal.)

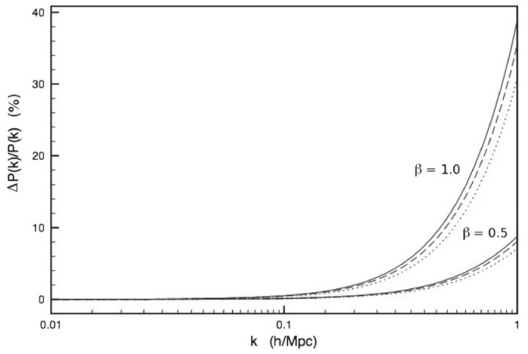

Figure 4. Linear power spectrum relative to that of ΛCDM for three different SSB redshifts: $z_{\rm SSB}=0.5$ (dotted), $z_{\rm SSB}=1.0$ (dashed), and $z_{\rm SSB}=2.0$ (solid). We have fixed $L=1$ and shown the results for the two values $\beta=0.5$ and $\beta=1.0$.

The short range ($\lesssim$Mpc) of the fifth force means that it will not affect the cosmic microwave background (CMB) unless $L,\beta\gg 1$. Take $L=1$ and $\beta=2$ as an example: we find a maximal increase in power (due to the integrated Sacks–Wolfe effect) of $\sim 0.25\%$ for multipoles around $l\sim 100$. One needs a much larger β and/or L to have a detectable signature in the CMB. The second case is not allowed by local experiments, while the first case implies a growth rate of the linear perturbations that should have difficulty satisfying constraints coming from large-scale structure surveys.

A more thorough analysis of the linear perturbations in the symmetron model can be found in Brax et al. (2011b). There it was shown that strong signatures appear in other interesting linear observables such as the weak-lensing slip parameter and the modified gravity parameter.

3.4. Tachyonic Instability in the Perturbations

The perturbations in Section 3.2 were integrated using the approximate Equation (39), which is equivalent to using the analytical minimum as the background field. The reason we did not use the full equations is because perturbation theory breaks down close to $z_{\rm SSB}$.

Immediately before $z_{\rm SSB}$ the field is still close to $\phi=0$; as $z\to z_{\rm SSB}$ the mass of the field vanishes. This means that the field cannot follow the minimum and starts to lag behind as seen in Figure 1. The global minimum of the effective potential $\phi=0$ now becomes a local maximum, and the mass squared of the field becomes negative, leading to an exponential growth in the perturbations.

To see what happens, we can simplify Equation (37) by discarding all but the most important terms:

$$\ddot{\delta\phi}+\left(m_\phi^2+\frac{k^2}{a^2}\right)\delta\phi\simeq 0. \tag{42}$$

If $m_\phi^2+k^2/a^2<0$, then the solution to the above equation reads $\delta\phi\propto\exp(t\sqrt{|m_\phi^2+k^2/a^2|})$, which is exponentially growing.

In a realistic situation the field would roll very quickly down from the false minimum $\phi=0$, making m_ϕ^2 positive and thereby stabilizing the field close to the symmetry breaking minimum (Felder et al. 2001). Since perturbation theory is only valid as

long as the perturbations $\delta\phi$ are small, we get a breakdown of the perturbation theory when using the true background solution. The blowup in $\delta\phi$, in turn, leads to a blowup in the matter perturbations, and the numerical results cannot be trusted.

We have investigated this further by using N-body simulations. In Figure 10 we see a snapshot of the ϕ-distribution both before and after $z = z_{\rm SSB} = 2.0$. There we see the same sort of behavior as is familiar from symmetry breaking in condensed matter physics: symmetry breaking takes place at different places at different times according to the local matter density. This type of dynamics is not taken care of in the standard perturbation theory approach, which leads to the apparent instability.

Note that by using the analytical minimum when integrating the perturbations we do not have control over the accuracy of our results. A full analysis of this phenomenon could be handled with N-body simulations, but in our simulations we have not explicitly taken into account the time variation of the scalar field (we work in the quasi-static limit), and our simulation box is also too small to reach far enough into the linear regime. We leave this study for future work.

3.5. Varying Constants

One important constraint on coupled scalar field theories comes from the time variation of the gravitational constant G in the Jordan frame, or equivalently in the masses of the standard model particles in the Einstein frame. *Wilkinson Microwave Anisotropy Probe* (*WMAP*) constrains any such variation to be less than about 5% since recombination (Nagata et al. 2004). Light-element abundances provide similar constraints between the time of nucleosynthesis and today (Accetta et al. 1990).

Due to the conformal coupling to matter, $A(\phi)$, a constant mass scale in the Jordan frame becomes time and space varying in the Einstein frame. The mass variation between today and recombination is given by

$$\frac{\Delta m}{m} = \frac{A(\phi_{\rm rec}) - A(\phi_{\rm today})}{A(\phi_{\rm rec})} \simeq \frac{1}{2}\left(\frac{\phi_{\rm today}}{M}\right)^2, \qquad (43)$$

where we have put $\phi_{\rm rec} \simeq 0$ since $z_{\rm rec} \gg z_{\rm SSB}$ in all interesting cases. If we further assume $\phi_{\rm today} = \phi_0$, we get the conservative constraint

$$\frac{\Delta m}{m} \simeq \frac{1}{2}\left(\frac{\phi_0}{M}\right)^2 = \beta^2\left(\frac{M}{M_{\rm pl}}\right)^2 < 10^{-6}\beta^2. \qquad (44)$$

The *WMAP* constraint $|\Delta m/m| \lesssim 0.05$ is satisfied for all $\beta \lesssim 100$.

Analysis of absorption spectra of quasars has led some to claim that the fine structure constant α might have evolved by approximately one part in 10^5 over the redshift range $0.2 < z < 3.7$. If this turns out to be true, then general covariance would imply that α can vary both in space and in time, that is, it must be a function of a field.

Since we have so far assumed that the symmetron couples conformally to matter fields, and since the Maxwell action is conformally invariant, at tree level the symmetron does not lead to a time-varying α. By considering a coupling of the symmetron to photons of the form

$$S_\gamma = -\frac{1}{4}\int d^4x\sqrt{-g}A_\gamma(\phi)F_{\mu\nu}F^{\mu\nu} \qquad (45)$$

where

$$A_\gamma(\phi) = 1 + \frac{\zeta_\gamma}{2}\left(\frac{\phi}{M}\right)^2 \qquad (46)$$

then variations in ϕ will lead to variations in α. Here ζ_γ is the symmetron-photon coupling relative to the symmetron-matter coupling. The variation in the fine-structure constant between Earth (E) and another place (S) in the universe is given by

$$\left|\frac{\Delta\alpha}{\alpha}\right| = \frac{A_\gamma(\phi_E) - A_\gamma(\phi_S)}{A_\gamma(\phi_E)} \simeq \frac{\zeta_\gamma}{2}\left(\frac{\phi_S}{M}\right)^2. \qquad (47)$$

If S is a very low density environment where $\phi_S \approx \phi_0$, then

$$\left|\frac{\Delta\alpha}{\alpha}\right| \simeq \zeta_\gamma 10^{-6}\beta^2 \qquad (48)$$

which for $\mathcal{O}(1) \lesssim \beta, \zeta_\gamma$ is close to the reported detection.

However, the local density in most Lyα-emitting systems is usually much larger than the cosmological background density today (see, e.g., Brax et al. 2004 and references therein), which implies $\phi_S \ll \phi_0$ and the above estimate becomes even smaller.

To be able to account for the reported claims, we need $z_{\rm SSB}$ to be well before the observed redshift of these systems and/or these systems to be located in voids to produce the desired 10^{-5} effect. This makes it possible that the symmetron is responsible for the claimed variations, but will probably require a fine-tuning $\zeta_\gamma \gg 1$. A more detailed analysis, as done in Li et al. (2011b), is required to see if this is the case. This is beyond the scope of this paper.

3.6. N-body Equations

To implement the general relativistic Equations (5), (12), (13), and (16) in N-body simulations, it suffices to work in the nonrelativistic limits, since the simulations only probe the weak gravity regime and small volumes compared with the cosmos. We write the perturbed metric in the (flat) conformal Newtonian gauge as

$$ds^2 = -a^2(1+2\Xi)d\tau^2 + a^2(1-2\Psi)dx^\mu dx_\mu, \qquad (49)$$

where τ is the conformal time and x^μ is the comoving coordinate. In Appendix A we list the expressions for the Christoffel symbols, the Ricci tensor, and the Ricci scalar for the metric Equation (49), which are used in deriving the equations below.

The scalar field equation of motion in terms of the perturbed quantities becomes

$$\begin{aligned} &-(1-2\Xi)\phi'' + \nabla^2_{\mathbf{x}}\phi - \phi'(2H(1-2\Xi) - \Xi' - 3\Psi') \\ &= a^2\left(\phi\left(\frac{\rho_m}{M^2} - \mu^2\right) + \lambda\phi^3\right). \end{aligned} \qquad (50)$$

Taking the quasi-static limit of this equation, in which we can neglect terms such as Ξ', Ψ', and $H\phi'$ since the time derivative of a quantity is much smaller than its spatial gradient, and removing the background part, we obtain

$$\begin{aligned} \nabla^2_{\mathbf{x}}\phi \approx{}& \frac{a^2}{M^2}(\rho_m\phi - \overline{\rho}_m\overline{\phi}) \\ &+ a^2(\mu^2(\overline{\phi} - \phi) + \lambda(\phi^3 - \overline{\phi}^3)), \end{aligned} \qquad (51)$$

where we have also used the approximation $A(\phi) \approx 1$ to simplify the equation further.

The $(0, 0)$-component of the Ricci tensor and the trace of the total energy-momentum tensor in the perturbed quantities become

$$a^2 R_0^0 \approx -\nabla_{\mathbf{x}}^2 \Xi + 3\left(\frac{a''}{a} - H^2\right)(1 - 2\Xi) - 3\Psi'' - 3H(\Xi' + \Psi') \quad (52)$$

$$T \approx -A(\phi)\rho_m - 4V(\phi) + \frac{1}{a^2}(1 - 2\Psi)\phi'^2. \quad (53)$$

The $(0, 0)$-component of the Einstein equation with the background part removed gives the nonrelativistic Poisson equation

$$\nabla_{\mathbf{x}}^2 \Phi \approx 4\pi G\left(\rho_m - \overline{\rho}_m\right) a^3, \quad (54)$$

where we have neglected the contribution from the potential $(V(\phi) - V(\overline{\phi}))$, put $A(\phi) \approx 1$, and taken $\Phi = a\Xi$ for convenience.

The equation of motion for the N-body particles follows from the geodesic equation and reads

$$\ddot{\mathbf{x}} + 2H\dot{\mathbf{x}} = -\frac{1}{a^3}\nabla_{\mathbf{x}}\Phi - \frac{1}{a^2}\frac{\phi}{M^2}\nabla_{\mathbf{x}}\phi - \frac{\phi\dot{\phi}}{M^2}\dot{\mathbf{x}}. \quad (55)$$

By rewriting this equation in terms of the conjugate momentum to $\mathbf{x}$, $\mathbf{p} = a^2\dot{\mathbf{x}}$, we have

$$\frac{d\mathbf{x}}{dt} = \frac{\mathbf{p}}{a^2} \quad (56)$$

$$\frac{d\mathbf{p}}{dt} = -\frac{1}{a}\nabla_{\mathbf{x}}\Phi - \frac{\phi}{M^2}(\nabla_{\mathbf{x}}\phi + \dot{\phi}\mathbf{p}). \quad (57)$$

Equations (51), (54), and (56) are all we need to put into the N-body simulation code in order to study structure formation in the nonlinear regime. The discretization of these equations, as implemented in the N-body code, is shown in Appendix B.

4. N-BODY SIMULATIONS

Below we describe the algorithm and model specifications of the N-body simulations we have performed. We also give results from tests of the code to show that the scalar field solver works accurately.

4.1. Outline

For our simulations we have used a modified version of the publicly available N-body code MLAPM (Knebe et al. 2001). The modifications we have made follow the detailed prescription of Li & Barrow (2011a), and here we only give a brief description. The MLAPM code has two sets of meshes: the first includes a series of increasingly refined regular meshes covering the whole cubic simulation box, with, respectively, 4, 8, 16,..., N_d cells on each side, where N_d is the size of the domain grid, which is the most refined of these regular meshes. This set of meshes is needed to solve the Poisson equation using the multigrid method or fast Fourier transform (for the latter only the domain grid is necessary). When the particle density in a cell exceeds a pre-defined threshold, the cell is further refined into eight equally sized cubic cells; the refinement is done on a cell-by-cell basis, and the resulting refinement could have arbitrary shape, which matches the true equal density contours of the matter distribution. This second set of meshes is used to solve the Poisson equation using the linear Gauss–Seidel relaxation scheme.

Table 1
The Symmetron Parameters Used in Our Simulations

Model	A	B	C	D	E	F	G	H	ΛCDM
$z_{\rm SSB}$	0.5	0.5	1.0	1.0	2.0	2.0	1.0	1.0	0.0
β	0.5	1.0	0.5	1.0	0.5	1.0	0.5	1.0	0.0
L	1.0	1.0	1.0	1.0	1.0	1.0	2.0	2.0	0.0

The symmetron field is the most important ingredient in the model studied here, and we have to solve for it to obtain detailed information about the fifth force. In our N-body code, we have added a new scalar field solver. It uses a nonlinear Gauss–Seidel scheme for the relaxation iteration and the same criterion for convergence as the default Poisson solver in MLAPM. However, it uses V-cycle instead of the self-adaptive scheme in arranging the Gauss–Seidel iterations.

The modified Poisson equation is then solved using nonlinear Gauss–Seidel relaxation on both the domain grid and the refinements. With the gravitational potential Φ and the scalar field ϕ at hand, we can evaluate the total force on the particles and update their momenta (velocities), which are used to advance the particles in space.

4.2. Simulation Details

The physical parameters we use in the simulations are as follows: the present dark-energy energy density $\Omega_\Lambda = 0.733$, total matter density $\Omega_m = \Omega_b + \Omega_c = 0.267$, baryon density $\Omega_b = 0.045$, CDM density $\Omega_c = 0.222$, $H_0 = 71.9$ km s^{-1} Mpc^{-1}, $n_s = 0.963$, and $\sigma_8 = 0.801$. We use a simulation box with size 64 Mpc h^{-1}, in which $h = H_0/(100$ km s^{-1} Mpc$^{-1})$. We simulate nine different models; see Table 1 for the symmetron parameter values.

These parameters are chosen so that they predict local fifth forces that are of the same order of magnitude as allowed by current experiments and observations and are such that we can see the effect of the different parameters. In this way the results from our N-body simulations will show the maximum allowed deviation from ΛCDM. Note that the energy density in the symmetron is always much less than that of dark energy and therefore does not alter the background cosmology, which in all runs will be that of ΛCDM.

In all those simulations, the particle number is 256^3, so that the mass resolution is 1.114×10^9 Mpc h^{-1}. The domain grid is a $128 \times 128 \times 128$ cubic and the finest refined grids have 16,384 cells on each side, corresponding to a force resolution of about 12 kpc h^{-1}. The force resolution determines the smallest scale on which the numerical results are reliable. Our simulations are purely N-body, and baryons are treated as CDM, which means that no baryonic physics has been included in the numerical code.

The simulation box used, $B = 64$ Mpc h^{-1}, is small compared to linear scales, and we are therefore possibly neglecting effects of mode coupling between linear and nonlinear scales. This will have to be checked by simulations with a larger box size. However, since the fifth force has a short range ($\lesssim$ Mpc), it does not reach far into the linear regime (see Figure 11), and therefore we expect the accuracy on large scales to be the same as for the ΛCDM simulations.

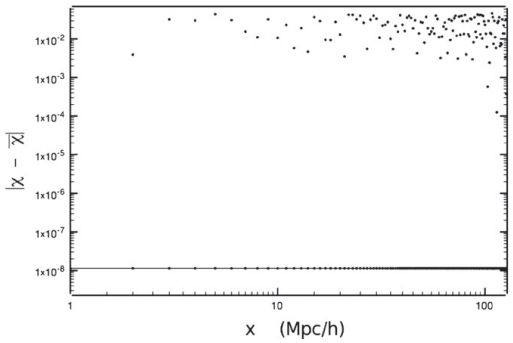

Figure 5. Scalar field relative to the analytical solution before (random initial values above) and after (below) the Newton–Gauss–Seidel relaxation.

4.3. Initial Conditions

Initial conditions for the simulation were generated using GRAFIC2 (Bertschinger 2001; Prunet et al. 2008) by using the parameters described above. The same initial conditions were used for all the simulations in order to see clearly the effect of the symmetron compared with ΛCDM.

This choice needs some justification. First of all, we start the simulation at $z = 49$, a time in which the symmetron has no effect on the growth of the perturbations. This means that the only change the symmetron will have on the initial conditions is on the value of σ_8 today, which is used to normalize the perturbations. Since the symmetron field has a rather short range compared to the linear regime, we do not expect a large effect on σ_8 for the range $L \lesssim \mathcal{O}(1)$ we are considering.

To check this assumption, we integrated the perturbations and calculated the value of σ_8 (by normalizing to the CMB) for our simulation models and found that the model with $L = 1$ that is furthest away from ΛCDM, namely, F in which $z_{\rm SSB} = 2.0$, $L = 1$, and $\beta = 1$, only has $\sigma_8 \simeq 1.01\sigma_8^{\rm LCDM}$, justifying the use of ΛCDM initial conditions.

If one is to consider models in which L is much larger than 1, then this becomes an issue that should be dealt with properly.

4.4. Code Tests

Before we run simulations, we have to make sure that the scalar field solver, which is the main modification to the MLAPM code, works accurately by performing code tests for situations where the outcome is known from analytical solutions.

The scalar field solver uses the nonlinear Newton–Gauss–Seidel relaxation scheme to compute $\chi \equiv \phi/\phi_0$, and an indicator that it works is to show that, given the initial guess of the solution that is very different from the true solution, the relaxation could produce the latter within a reasonable number of iterations. We consider a simulation box with homogeneous density (obtained by putting particles on a regular grid inside the simulation box); then the true solution is given by $\chi = \overline{\chi}$: the background solution. We therefore make an initial guess for χ that is randomly scattered around $\overline{\chi}$ and let the scalar field solver solve for χ. The results for $|\chi - \overline{\chi}|$ before and after the relaxation scheme are shown in Figure 5. The difference between the initial guess and the true solution varies between 0.001 and 0.1, while after the relaxation the difference is of order 10^{-8}. By using double-precision numbers in all the calculations, we obtained exactly the analytical solution (to double precision $\approx 10^{-15}$), while using only floating point numbers the accuracy dropped to 10^{-6}, which is exactly the accuracy in floats. This shows that the scalar field solver works accurately.

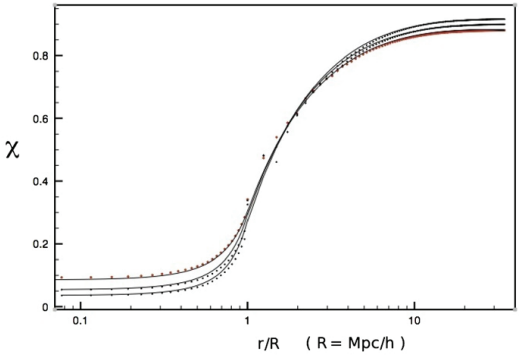

Figure 6. Scalar field value as a function of distance from the center for a spherical overdensity embedded in a background of homogenous density ρ_b together with the analytical solution for $\rho_c = 4000$, 6000, and 8000 times ρ_b. The points shown here are calculated by binning the scalar field value using a bin width $\Delta(r/R) = 0.01$ and taking the average. We used the same amount of particles, 128^3, in each run so that the background density ρ_b differs for the three cases shown above.

The most important effect of the symmetron is the screening mechanism, in which the local value of the field should be pushed down toward $\chi = 0$ in high-density environments. We therefore consider a spherical overdensity, located at the center of the box, with a given radius R, homogeneous density ρ_c inside R, and embedded in a background of homogenous density ρ_b. The analytical solution reads

$$\chi(r) = \chi(0)\frac{\sinh[m_c r]}{m_c r}, \quad r < R \tag{58}$$

$$\chi(r) = \chi_b + \frac{(\chi(R) - \chi_b)R}{r} e^{-m_b(r-R)}, \quad r > R \tag{59}$$

where

$$m_c^2 \simeq \left(\frac{\rho_c}{M^2}\right), \quad m_b^2 \simeq \left(\frac{\rho_b}{M^2} + \mu^2\left(3\chi_b^2 - 1\right)\right)$$
$$\chi_b \simeq \sqrt{1 - \frac{\rho_b}{\rho_{\rm SSB}}}, \quad \chi(R) = \chi_b\left(\frac{1 + m_b R}{\frac{m_c R}{\tanh(m_c R)} + m_b R}\right)$$
$$\chi(0) = \chi(R)\frac{m_c R}{\sinh(m_c R)}. \tag{60}$$

For the trial solution on the grid we use the background value χ_b and perform the test for a range of densities ρ_c. The results after relaxation for the most massive cases are shown in Figure 6. There are some small discrepancies from the analytical solution in the region $R < r < 2R$ for the most extreme cases $\rho_c > 10^3\rho_b$. This is not a surprise as the density suddenly drops over 3 orders of magnitude at $r = R$, meaning that we need a lot of particles in this region in order to get accurate results. In the region $r < R$ and $r > 2R$ the scalar field solver produces the analytical solution to high accuracy.

5. NUMERICAL RESULTS

In this section we present the results from the simulations, including the snapshots, the matter power spectrum, and the halo mass function.

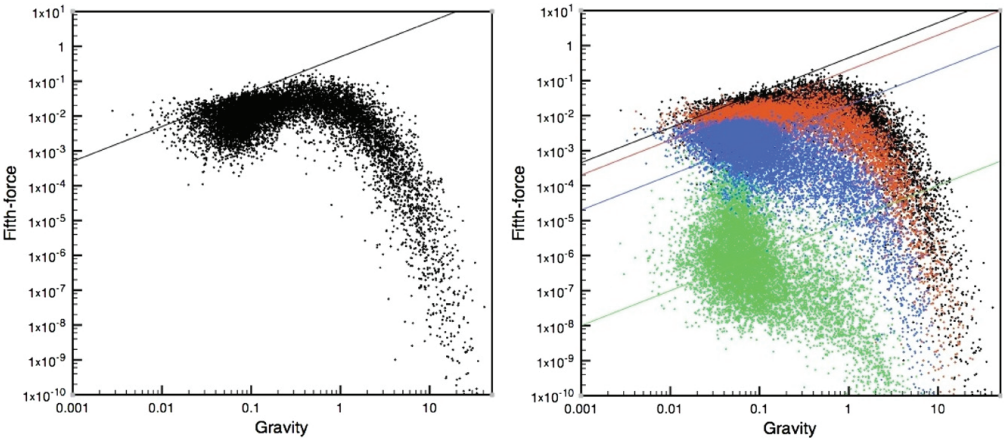

Figure 7. Fifth force to gravity in a slice of the simulation box at $z = 0$ (left) and the comparison between four different redshifts (right) for a run with $z_{\rm SSB} = 0.5$, $\beta = 1$, and $L = 1$. Black shows $z = 0$, red $z = 0.25$, blue $z = 0.65$, and green $z = 1$. The solid lines show $(F_\phi/F_{\rm gravity}) = 2\beta^2\chi_b^2(z)$, which is the prediction for the (short-range) forces at the perturbation level (see Equation (39)). Note that the force will be dispersed around this prediction because we already have significant over- and underdensities in which $\chi \neq \chi_b$. At $z = 1$ the background field is close to $\chi_b = 0$ and the force is small everywhere in space. As we move closer to $z = 0$, the symmetry breaks, and the background value moves toward $\chi_b = 1$. This means that the force in low-density regions (small gravitational force) will increase whereas in high-density regions (strong gravitational force) the screening kicks in and the force becomes suppressed just as seen above. The numerical size of the forces is given in terms of code units, which are H_0^2/B times the physical force unit.

(A color version of this figure is available in the online journal.)

5.1. Snapshots

In the symmetron model $\chi \equiv \phi/\phi_0$, and thereby the fifth force, is suppressed in high-density regions. In this subsection we demonstrate these qualitative features using some snapshots.

Figure 7 shows the ratio of the fifth force to gravity today and for redshifts both before and after $z_{\rm SSB}$.

At early times, the density is high everywhere and we expect the fifth force on all particles to be strongly suppressed. At later times we expect a screening in regions of high matter density. These predictions are confirmed in Figure 7. We see that fifth force on the particles that feel a strong gravitational force (i.e., particles in a high-density environment) is highly suppressed whereas the fifth force on particles that feel a weak gravitational force (i.e., particles in a low-density environment) follows the unscreened theoretical prediction $F_\phi \simeq 2\beta^2\chi_b^2(z)F_{\rm gravity}$ (see Equation (39)).

Figures 8–10 show the density and scalar field distribution in a slice of the simulation box at different redshifts for the three cases $z_{\rm SSB} = 0.5$, 1.0, and 2.0 with $\beta = L = 1.0$ fixed.

For redshifts $z > z_{\rm SSB}$, χ is very close to the minimum $\chi = 0$ almost everywhere in space except in voids where the symmetry has already been (weakly) broken. When we go down to redshifts $z < z_{\rm SSB}$, the symmetry is broken in most parts of the box, except in the high-density regions where we still have $\chi \sim 0$. Comparing the scalar field distribution today for runs with different $z_{\rm SSB}$, we see that the earlier the symmetry breaking takes place, the part of the box that is unscreened ($\chi \sim 1$) today becomes larger. This is because the critical density for the symmetry breaking is larger for larger $z_{\rm SSB}$ and therefore the halos have to be more massive in order to be effectively screened.

5.2. Matter Power Spectrum

The nonlinear matter power spectrum is an important observable and could be used to distinguish between different models of structure formation. As we have seen above, the symmetron can have a strong effect on the growth rate of the linear perturbations for parameters that are allowed by local experiments. We expect these signatures to show up in the nonlinear matter power spectrum.

Figure 12 displays the fractional difference in the matter power spectrum from that of ΛCDM, defined as $(P(k) - P_{\Lambda{\rm CDM}}(k))/P(k)$, and in Figure 11 we show the actual power spectra for the symmetron and ΛCDM together with the corresponding predictions from linear perturbation theory.

Generally, the power spectrum is expected to be reliable up to the scale

$$k_{\rm max} = N_{\rm eff} k_{N/2}, \tag{61}$$

where $k_{N/2} = \pi N_p^{1/3}/(4B)$ is half the particle Nyquist scale, N_p is the total number of particles, B is the box size, and $N_{\rm eff}$ is a factor determined by the adaptive nature of the code. For non-adaptive simulations $N_{\rm eff} = 1$ and it was shown in Stabenau & Jain (2006) that the power spectra cannot be trusted for wavenumbers much larger than $k_{N/2}$.

The MLAPM code, on the other hand, is adaptive, meaning that $N_{\rm eff} > 1$, and allows us to go beyond the half Nyquist scale. The exact value of $N_{\rm eff}$ depends on the number of refinements triggered in the whole simulation process, and for our simulations we estimate $N_{\rm eff} = 8$–10. To be conservative, we follow Zhao et al. (2011), which uses the same simulation details as us but for the case of $f(R)$ gravity, and take $N_{\rm eff} = 7$. This translates into an estimate $k_{\rm max} \simeq 22\ h\ {\rm Mpc}^{-1}$ for the validity of our results.

This estimate can be invalidated by the contribution from shot noise due to limited resolution at small scales. In Figure 13 we show the expected shot-noise contribution in one of our simulations together with the statistical error in the power spectrum estimation computed by POWMES. We define $k_{\rm SN}$ to be the wavenumber such that the expected shot-noise contribution is

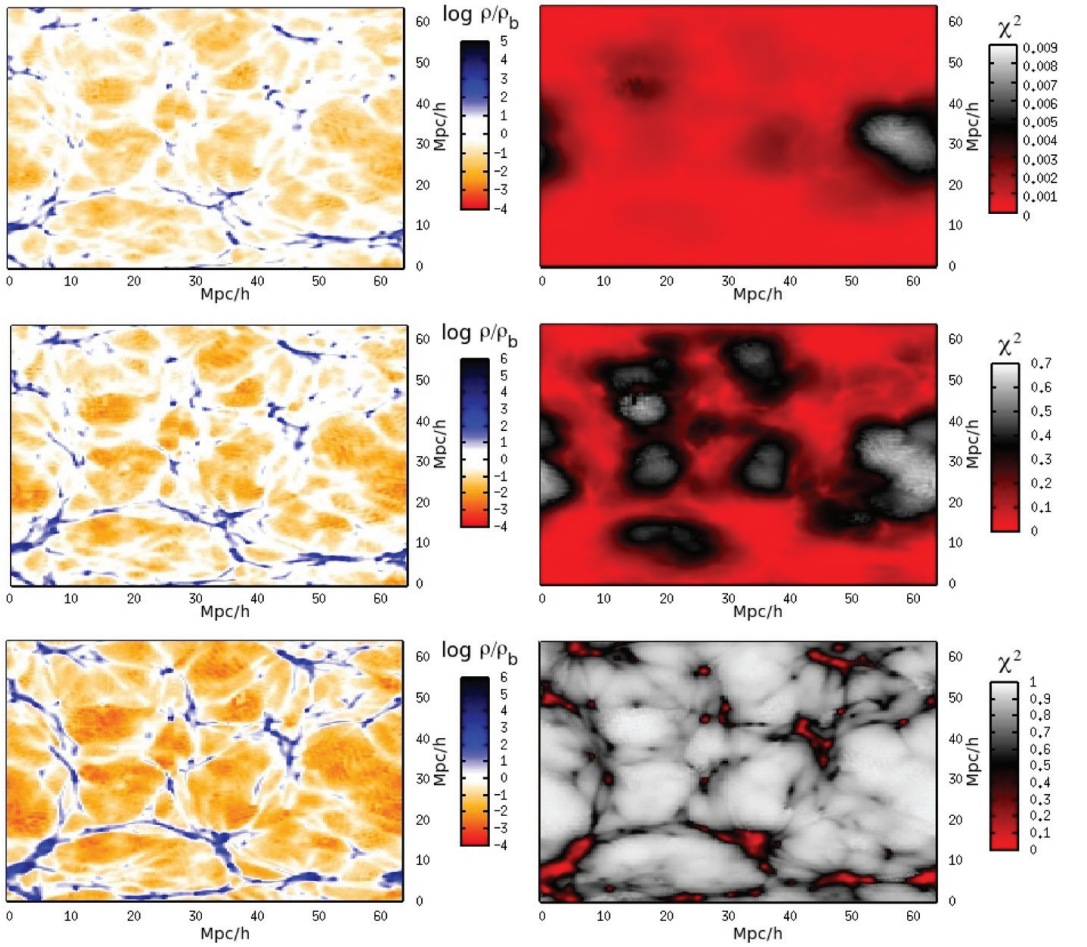

Figure 8. Density distribution (left) and scalar-field distribution (right) for a run with $z_{SSB} = 0.5$, $\beta = 1$, and $L = 1$. From top to bottom $z = 1$, $z = 0.66$, and $z = 0$. (A color version of this figure is available in the online journal.)

below 5% for all $k < k_{SN}$ up to $z = z_{SSB}$, which is the redshift for which the symmetron power spectrum starts deviating from ΛCDM, and overplot the scale $k = \min(k_{max}, k_{SN})$ in Figures 12 and 14. For all of our simulations we find $k_{SN} \gtrsim k_{max}$ except when $z_{SSB} = 2.0$, where $k_{SN} \simeq 12\,h$ Mpc^{-1}.

The power spectrum agrees with the predictions of linear perturbation theory on large scales ($k \lesssim 0.1$ Mpc h^{-1}), but on smaller scales the results found here are weaker than the prediction of linear perturbation theory seen in Figure 4. This is because when linearizing the field equation we are basically using the background matter density everywhere and therefore preventing the symmetron mechanism from taking effect in suppressing the fifth force when matter perturbations become large. In contrast, the *N*-body simulation avoids this approximation by taking full account of the suppression of the fifth force.

The fractional difference relative to ΛCDM is growing with z_{SSB} and β as the fifth force has more time to operate and is stronger. Comparing runs with the same β, we see an important effect if the symmetry breaking is earlier. When $z_{SSB} = 2.0$, the fractional power is increasing until we reach a scale where the screening mechanism becomes stronger and then starts to decrease again toward ΛCDM, only to start growing again at even smaller scales. This is because the critical density for having screening is much higher for larger z_{SSB} so that most halos (which are on small scales and of low mass) are unscreened.

In Figure 14 we show the redshift evolution of the power spectrum. The power spectrum is found to be practically identical to that of ΛCDM for redshifts $z > z_{SSB}$, but as soon as the symmetry breaks at the background level, the symmetron fifth force can kick in and enhance the clustering of matter.

It is clear from Figure 12 that there exist a large range of parameters in which the symmetron model can be distinguished from ΛCDM easily.

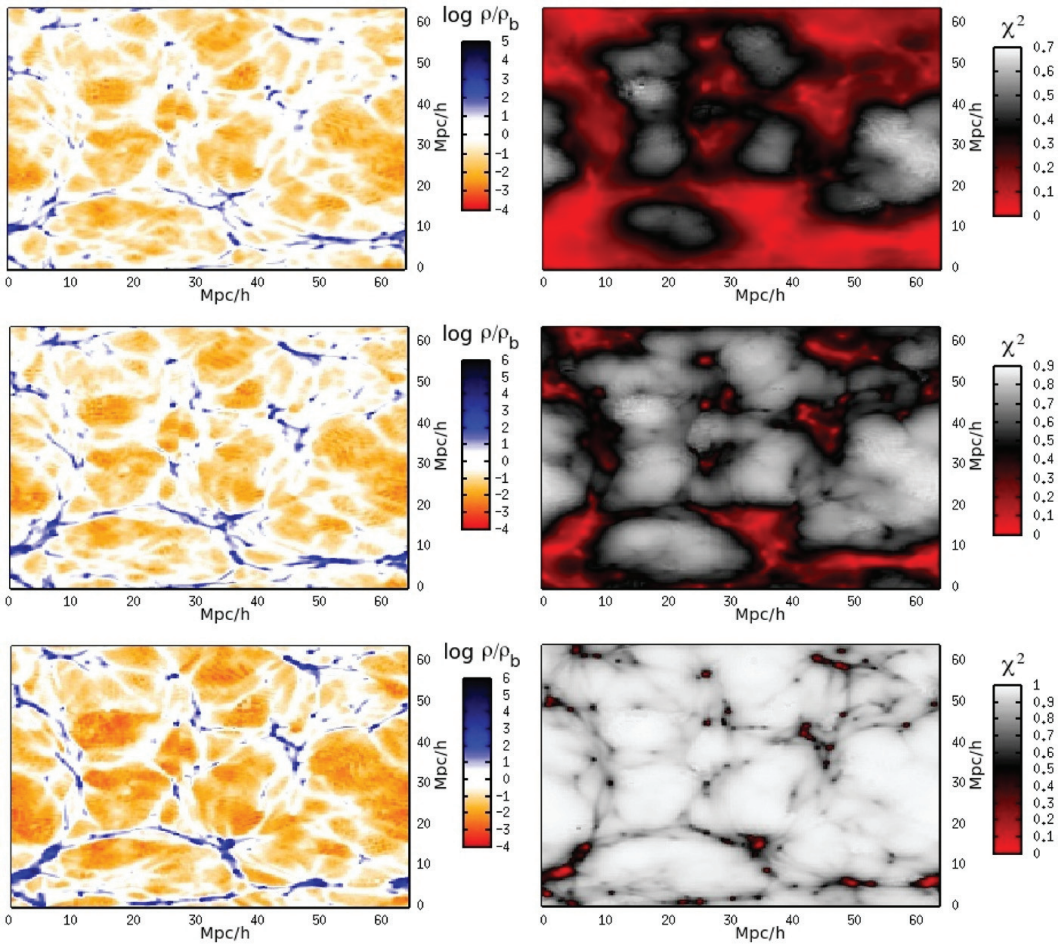

Figure 9. Density distribution (left) and scalar-field distribution (right) for a run with $z_{SSB} = 1$, $\beta = 1$, and $L = 1$. From top to bottom $z = 1$, $z = 0.66$, and $z = 0$. (A color version of this figure is available in the online journal.)

5.3. Halo Profiles for χ

In Figure 15 we show the profile of χ inside the most massive halos found in the simulation. Since the fifth force is proportional to χ, this figure also provides information about the fifth force in halos.

The field profile of χ is seen to increase from the inner to the outer regions of the halos and shows that the fifth force is most suppressed in the central region as expected.

The fifth force is stronger for smaller halos, because those generally reside in low-density regions where the fifth force is less suppressed. We see that the closer the symmetry breaking redshift is to zero, the smaller χ becomes inside the halo and the more suppressed the fifth force is. Again this is because early symmetry breaking means a higher critical density and the halo needs to be more massive to be effectively screened. This effect is also seen in Figures 8–10 (note the difference in distribution of χ at $z = 0$ between the different runs) and also on the matter power spectrum in Figure 12.

This has some important consequences for the local constraints. We mentioned in Section 2 that the local constraints were derived by assuming that our galactic neighborhood was not screened today, and lead to the constraint

$$L(1 + z_{SSB})^{3/2} \lesssim 2.3. \quad (62)$$

From our numerical results we see that when $z_{SSB} = 2.0$, only the most massive halos are screened. This means that the assumption that went into the constraint above is very likely to be true. On the other hand, for SSB that happens very close to today, halos of much smaller mass are in fact screened and it might be possible to have a range L that exceeds Equation (62) and still be in agreement with experiments.

We note that we have not seen any significant effect on the halo density profiles. For a given mass range, the halo profiles seem to have approximately the same distribution. There should be some important differences for low-mass halos, but the resolution in our simulation is too low to study this.

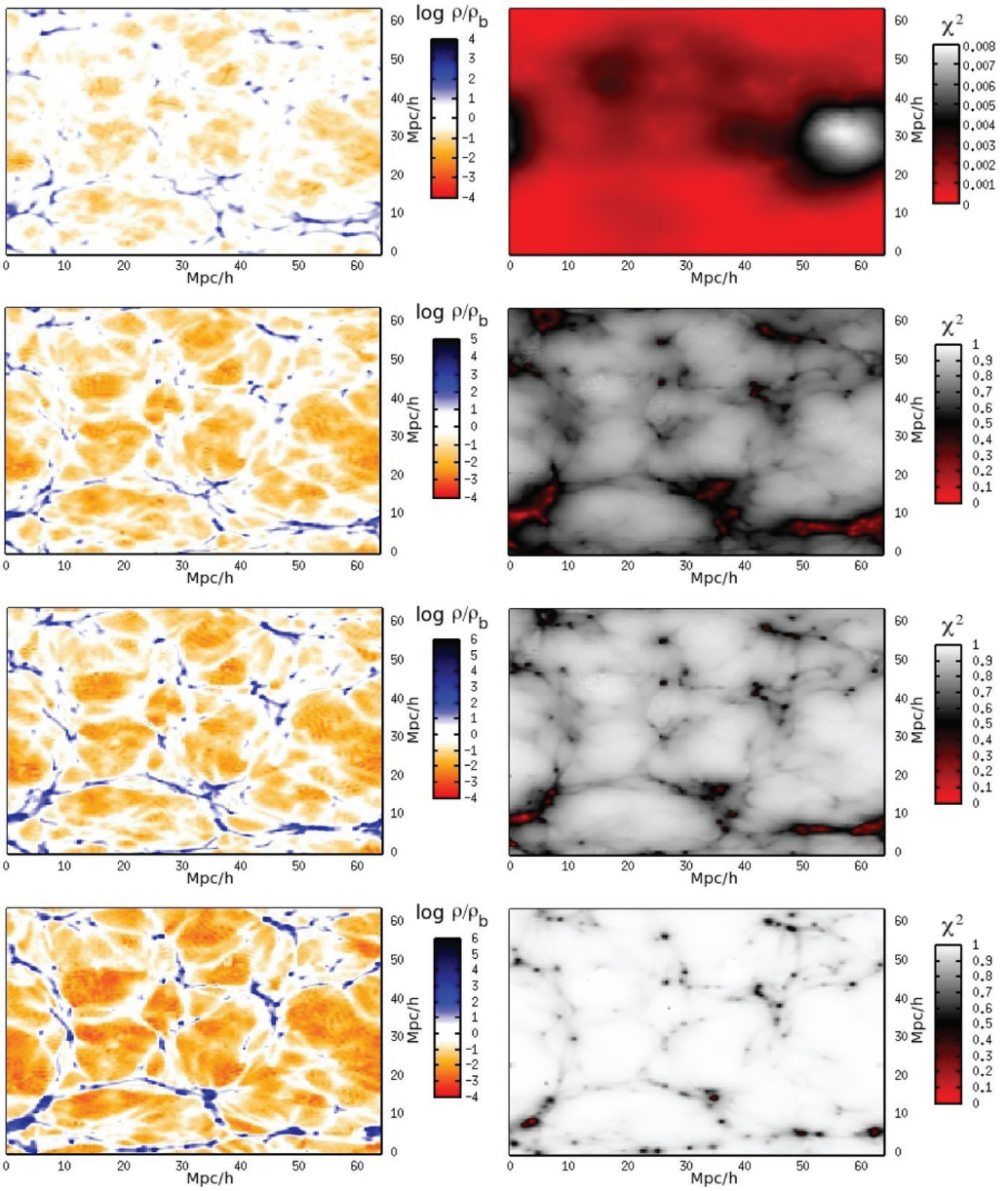

Figure 10. Density distribution (left) and scalar-field distribution (right) for a run with $z_{SSB} = 2$, $\beta = 1$, and $L = 1$. From top to bottom $z = 2.33$, $z = 1$, $z = 0.66$, and $z = 0$.

(A color version of this figure is available in the online journal.)

However, the halo number counts were significantly different as we shall see in the next section.

5.4. Halo Mass Function

The halo mass function n is another key structure formation observable. It is defined to be the number density of dark matter halos within a given mass range. Because of the symmetron fifth force, we expect more halos to be formed relative to the standard ΛCDM scenario.

We first look at the total number of halos (the integrated mass function) with more than 100 particles, which clearly shows the effect of the fifth force (see Table 2).

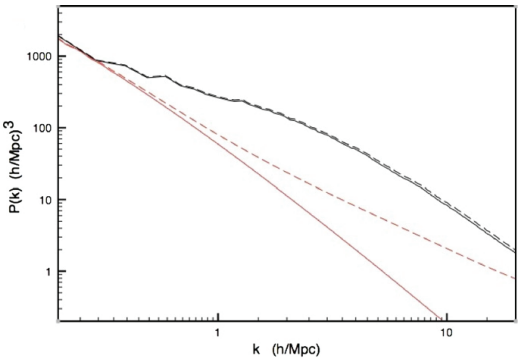

Figure 11. Full nonlinear power spectrum for a run with $z_{SSB} = L = \beta = 1.0$ (dashed black) and ΛCDM (solid black). For comparison we also show the corresponding predictions from linear perturbation theory in red. We clearly see the effectiveness of the screening mechanism. The linear predictions do not take the symmetron mechanism into account and are hugely overestimating the power on small scales relative to ΛCDM.

(A color version of this figure is available in the online journal.)

In Figure 16 we have shown the mass function of the symmetron compared to ΛCDM at $z = 0$. We see a significantly higher mass function, especially for low-mass halos, which are generally found in low-density regions where the fifth force is unscreened. The earlier symmetry breaking occurs and the stronger the coupling strength β, the more halos are formed in agreement to what we would naively expect.

Table 2
The Total Halo Count for Our Nine Simulations at $z = 0.0$

Simulation	A	B	C	D	E	F	G	H	ΛCDM
Total halo count	1634	1694	1678	1871	1758	2051	1671	1788	1607

Note. The corresponding symmetron parameters for the runs A–H can be found in Table 1.

The mass function converges to that of ΛCDM at very large halo masses for most parameters we have looked at. This is because the most massive halos have taken a very long time to form, and therefore when the symmetron kicks in at some low redshift, the halo is already massive enough to be screened. However, for the largest $z_{SSB} = 2.0$ we do have small increases in both the halo number density and the mass of the most massive halos. There have been reports of some tension between observations and ΛCDM predictions with regard to very massive halos. Unfortunately, for the symmetron model to be able to elevate this tension significantly we would need values of the parameters that are in conflict with local experiments.

On the other hand, the symmetron seems to produce a large excess of low-mass halos for some values of the parameters. These are many times the satellite structures of main galactic or

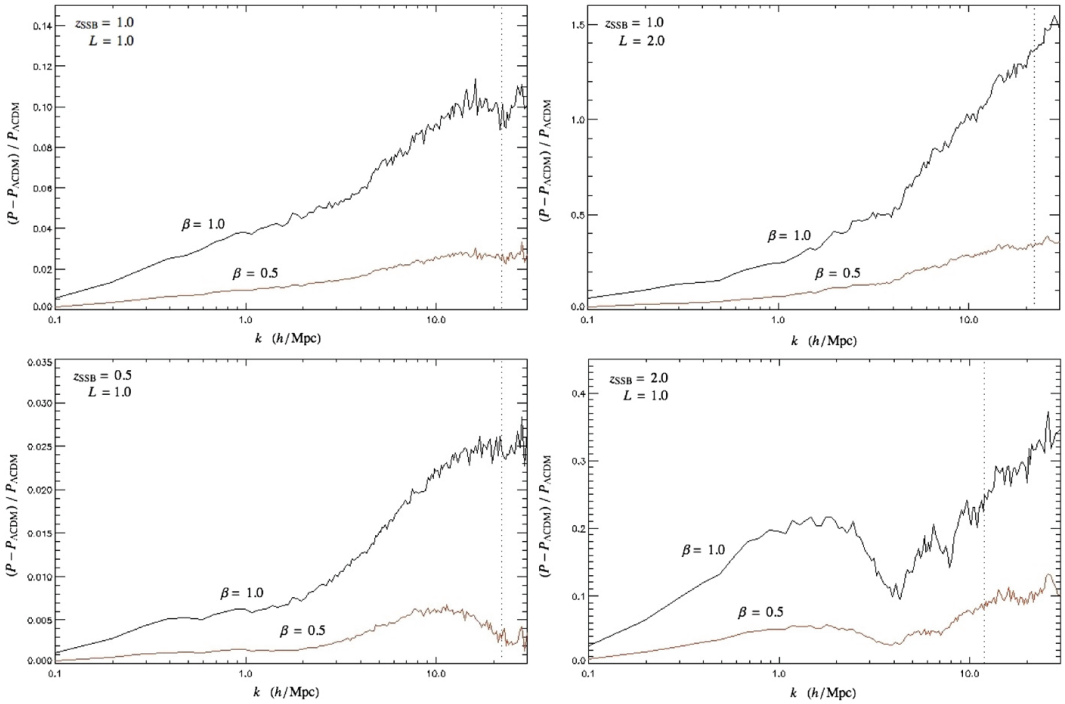

Figure 12. Fractional difference in the nonlinear power spectrum relative to ΛCDM for $\{z_{SSB} = 1.0, L = 1.0\}$ (top left), $\{z_{SSB} = 1.0, L = 2.0\}$ (top right), $\{z_{SSB} = 0.5, L = 1.0\}$ (bottom left), and $\{z_{SSB} = 2.0, L = 1.0\}$ (bottom right). For each case we show the results for the two values $\beta = 0.5$ and $\beta = 1.0$. The vertical dotted line shows the scale $\min(k_{max}, k_{SN})$ (see Equation (61)), for which we expect our results to be reliable.

(A color version of this figure is available in the online journal.)

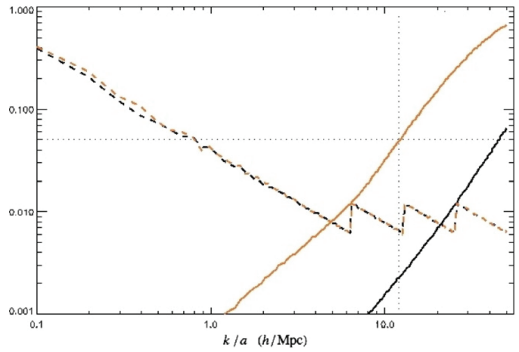

Figure 13. Expected $1/N_{\rm particles}$ shot-noise contribution to the power spectrum, $P_{\rm shot-noise}/P$ (solid), together with the statistical error $\Delta P/P$ in the power spectrum estimation (dashed) for the two redshifts $z = 0.0$ (black) and $z = 2.0$ (orange) for a simulation with $\{z_{\rm SSB} = 2.0, L = 1.0, \beta = 1.0\}$. See Colombi et al. (2009) for details about how the statistical error is computed. The vertical dotted line shows the scale $k_{\rm SN} \simeq 12\,h\,{\rm Mpc}^{-1}$ for which the expected shot-noise contribution is 5% at $z = z_{\rm SSB} = 2.0$.

(A color version of this figure is available in the online journal.)

cluster-sized halos. This increases the long-standing satellite problem of ΛCDM, i.e., the lower abundance of satellite structures seen in observations compared to *N*-body simulations. We do not draw any conclusions about this at the present as the resolution for the low-mass halos is relatively low plus baryonic physics has not yet been included in our simulations. This point might prove to be a useful constraint on the symmetron model and more general models with a fifth force in the future.

There is a large range of viable parameters for the symmetron where the mass function deviates significantly from ΛCDM.

6. SUMMARY AND CONCLUSIONS

The symmetron mechanism is a modification of gravity in which a scalar field is non-minimally coupled to matter, but the screening mechanisms result in potential fifth forces evading local gravity tests. Despite this, the symmetron does affect structure formation. We have investigated this with *N*-body simulations, finding observable signatures in the matter power spectrum and the halo mass function. Whilst the symmetron suffers from the same fine-tuning problems as chameleon models, it has the advantage of looking like a more natural effective theory.

The energy density of the symmetron is too low to contribute to the dark energy, and we must therefore add a cosmological constant to get accelerated expansion of the universe. The background evolution of the symmetron model is simply indistinguishable from that of the ΛCDM model.

This degeneracy is broken by the linear perturbations. In particular, we have shown that the linear growth index $\gamma(z, k)$ can have a significant scale and redshift dependence together with a value today that can be distinguished from the ΛCDM prediction for a large part of the parameter space.

The structure formation in the nonlinear regime was investigated by using *N*-body simulations. *N*-body simulations have the advantage over linear theory in its ability of fully capturing the nonlinear environmental dependence of the symmetron field. Our results confirm the expectation that in high-density environments the fifth force becomes screened. Consequently, the key observables such as the nonlinear matter power spectrum are closer to the ΛCDM predictions than expected from a linear analysis.

We found that the symmetron can still produce large observable signatures in both the nonlinear matter power spectrum and the halo mass function, which could in principle be detected by current and near-future cosmological observations such as Euclid.

Note that in the simulations performed in this work, we have treated baryons as dark matter. However, since the symmetron field has a uniform coupling to all matter fields, we expect that all the results will qualitatively remain even after baryons are included. This has to be explicitly checked from simulations. Baryons are known to have a significant effect on small-scale structures, and a natural extension of our work is to study the effects of baryons when a fifth force is present. This is much more computationally expensive and is left for future work.

In conclusion, the symmetron model has been found to have a wide range of observable cosmological effects on both linear and nonlinear scales. This adds to the list of observational signatures like making galaxies brighter (Davis et al. 2011), environment dependence of dark matter halos (Winther et al. 2011), and the possibility of being detected in near-future local gravity experiments (Hinterbichler & Khoury 2010), to mention some.

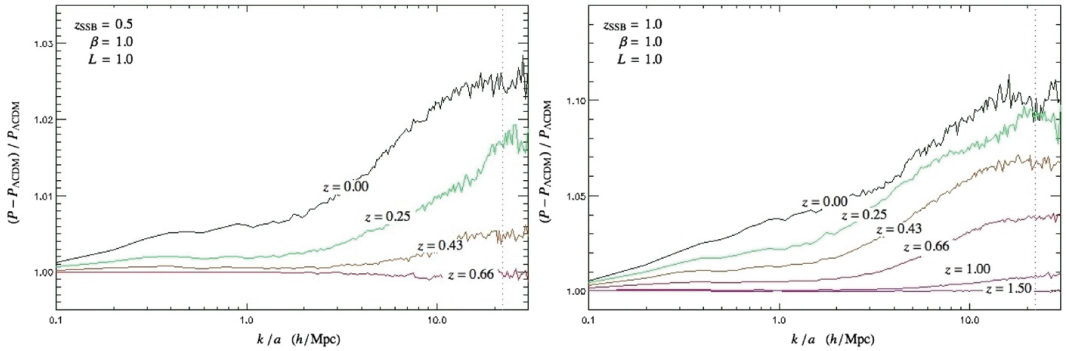

Figure 14. Fractional difference in the nonlinear power spectrum relative to ΛCDM for $\{z_{\rm SSB} = 0.5, L = 1.0, \beta = 1.0\}$ (left) and $\{z_{\rm SSB} = 1.0, L = 1.0, \beta = 1.0\}$ (right) as a function of redshifts. The vertical dotted line shows the scale $\min(k_{\rm max}, k_{\rm SN})$ (see Equation (61)), for which we expect our results to be reliable.

(A color version of this figure is available in the online journal.)

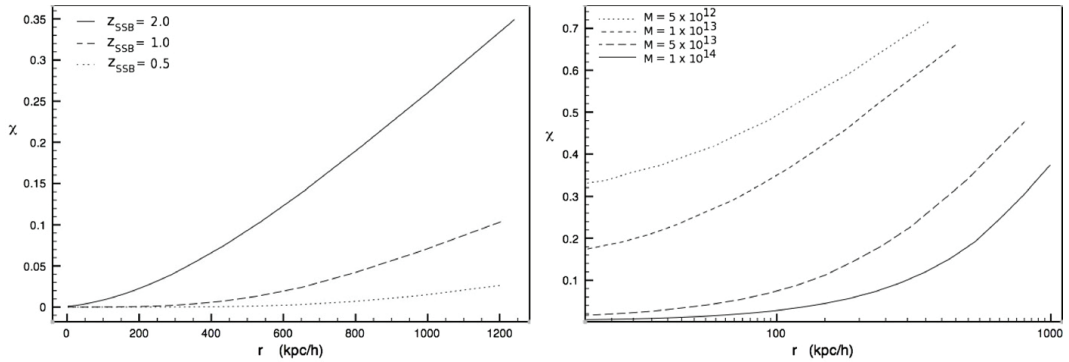

Figure 15. Left: the halo profile of χ in the most massive halo of the simulation for three different symmetry breaking redshifts. Right: the halo profile of χ for four halos of mass (from top to bottom) $M = \{5 \times 10^{12}, 10^{13}, 5 \times 10^{13}, 10^{14}\} M_{\rm sun}/h$ in the same simulation where $z_{\rm SSB} = 2.0$. In both cases we have fixed $\beta = L = 1$.

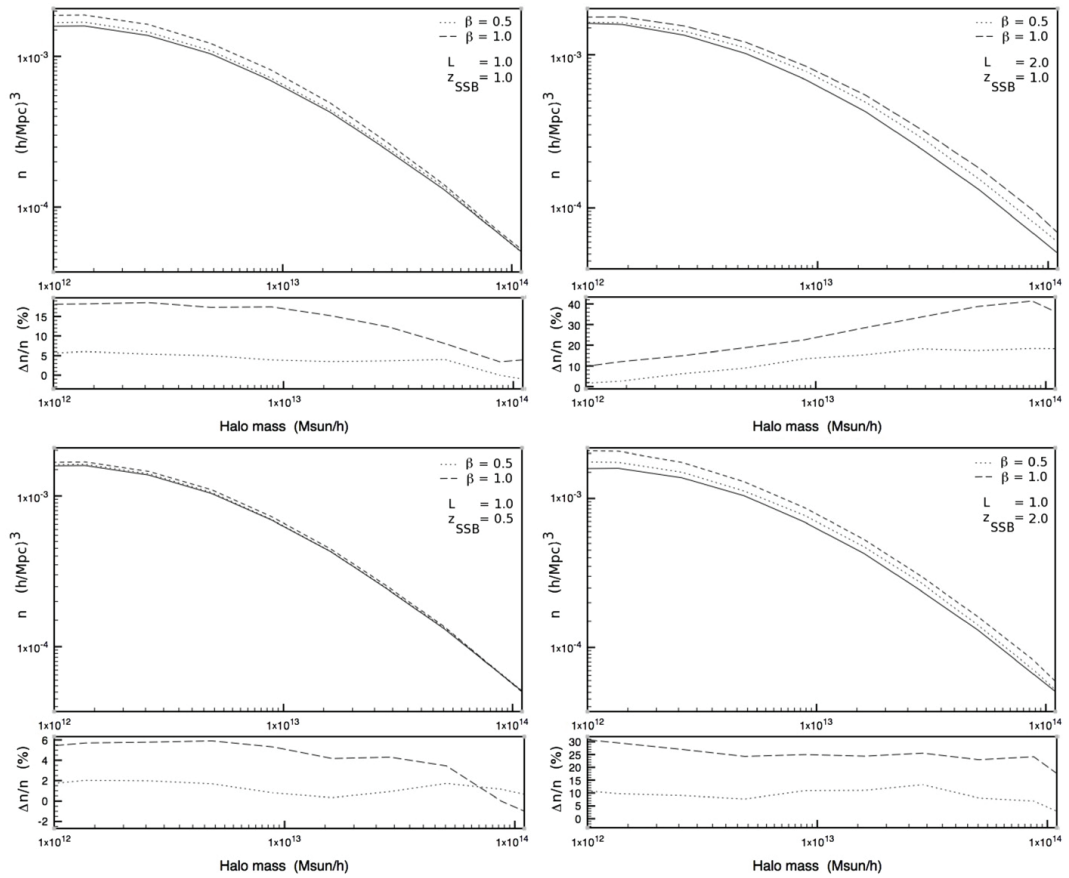

Figure 16. Halo mass function for $\{z_{\rm SSB} = 1.0, L = 1.0\}$ (top left), $\{z_{\rm SSB} = 1.0, L = 2.0\}$ (top right), $\{z_{\rm SSB} = 0.5, L = 1.0\}$ (bottom left), and $\{z_{\rm SSB} = 2.0, L = 1.0\}$ (bottom right). The solid black line shows the prediction of ΛCDM ($\beta = 0$), and the dotted and dashes lines are for the two values $\beta = 0.5$ and $\beta = 1.0$, respectively. We also show the fractional difference from ΛCDM. Note that we have smoothed the mass function over neighboring bins to remove noise arising from the binning to show the trends more clearly.

The symmetron is therefore a good candidate for the detection of new physics beyond the standard model.

The work described in this paper has been performed on TITAN, the computing facilities at the University of Oslo in Norway. The matter power spectrum was computed using POWMES (Colombi et al. 2009) and the halo properties using MHF (Gill et al. 2004). D.F.M. and H.A.W. thank the Research Council of Norway FRINAT grant 197251/V30. D.F.M. is also partially supported by project PTDC/FIS/111725/2009 and CERN/FP/116398/2010. H.A.W. thanks DAMPT at Cambridge University for the hospitality where a part of this work was carried out. B.L. is supported by Queens' College and the Department of Applied Maths and Theoretical Physics of University of Cambridge. B.L. and A.C.D. thank STFC for partial support. We also thank Douglas Shaw for useful discussions and the anonymous referee for many useful comments that have improved this work.

APPENDIX A

USEFUL EXPRESSIONS

Up to first order in the perturbed metric variables Ξ, Ψ the non-zero components of the symmetric Levi-Civita connection are

$$\Gamma^0_{00} = \frac{a'}{a} + \Xi' \tag{A1}$$

$$\Gamma^0_{0k} = \Xi_{,k} \tag{A2}$$

$$\Gamma^i_{00} = \Xi^{,i} \tag{A3}$$

$$\Gamma^i_{0k} = \left(\frac{a'}{a} - \Psi'\right)\delta^i_k \tag{A4}$$

$$\Gamma^0_{jk} = \delta_{jk}\left(\frac{a'}{a}(1 - 2\Xi - 2\Psi) - \Psi'\right) \tag{A5}$$

$$\Gamma^i_{jk} = -\Psi_{,k}\delta^i_j - \Psi_{,j}\delta^i_k + \Psi^{,i}\delta_{jk}. \tag{A6}$$

From these expressions we find that the components of the Ricci tensor and Ricci scalar are found to be

$$R_{00} = \Xi^{,i}_{,i} - 3\left(\frac{a''}{a} - \left(\frac{a'}{a}\right)^2\right) + 3\Psi'' + 3\frac{a'}{a}(\Psi' + \Xi') \tag{A7}$$

$$R_{0j} = 2\Psi'_{,j} + 2\frac{a'}{a}\Xi_{,j} \tag{A8}$$

$$R_{ij} = -\Psi''\delta_{ij} - \frac{a'}{a}(\Xi' + 5\Psi')\delta_{ij} - \Psi^{,k}_{,k}\delta_{ij} + \left(\frac{a''}{a} + \left(\frac{a'}{a}\right)^2\right)(1 - 2\Psi - 2\Xi)\delta_{ij} - (\Xi - \Psi)_{,ij} \tag{A9}$$

$$R = 6\frac{a''}{a^3}(1 - 2\Xi) + \frac{1}{a^2}\left(4\Psi^{,k}_{,k} - \Xi^{,k}_{,k}\right) - \frac{6}{a^2}\left(\Psi'' + \frac{a'}{a}(\Xi' + 3\Psi')\right). \tag{A10}$$

APPENDIX B

DISCRETIZATION OF EQUATIONS

To implement the nonrelativistic equations into our numerical code, we have to rewrite them using code units, which are given by

$$\mathbf{x_c} = \frac{\mathbf{x}}{B}, \mathbf{p_c} = \frac{\mathbf{p}}{H_0 B}, t_c = tH_0, \chi = \frac{\phi}{\phi_0}$$
$$\mathbf{\Phi_c} = \frac{\mathbf{\Phi}}{(H_0 B)^2}, \rho_c = \frac{\rho_\mathbf{m}}{\overline{\rho_\mathbf{m}}}, \nabla = \mathbf{B}\nabla_\mathbf{x}, \tag{B1}$$

where subscript c stands for code units, B is the box size, $H_0 = 100\ \mathrm{km\ s^{-1}\ Mpc^{-1}}$, and an overline denotes background quantities. In what follows we shall write $\nabla = \nabla_c$ for simplicity.

B.1. Scalar Field Equation of Motion

The equation of motion for χ in code units becomes

$$\frac{ac^2}{(BH_0)^2}\nabla^2\chi \simeq a^3\left(\overline{\chi} - \chi + \chi^3 - \overline{\chi}^3\right)\left(\frac{\mu}{H_0}\right)^2 + 3\Omega_m\left(\frac{M_{\rm pl}}{M}\right)^2(\rho_c\chi - \overline{\chi}), \tag{B2}$$

where $\overline{\chi}$ is the background solutions and we have used $\phi_0^2 = \mu^2/\lambda$ to simplify. Note that χ varies in the region $0 \leqslant \chi^2 \leqslant 1$. Discretized this equation becomes $L^h(\chi_{i,j,k}) = 0$, where

$$\begin{aligned} L^h(\chi_{i,j,k}) = {} & \frac{1}{h^2}\frac{ac^2}{(BH_0)^2}(\chi_{i+1,j,k} - 2\chi_{i,j,k} + \chi_{i-1,j,k}) \\ & + \frac{1}{h^2}\frac{ac^2}{(BH_0)^2}(\chi_{i,j+1,k} - 2\chi_{i,j,k} + \chi_{i,j-1,k}) \\ & + \frac{1}{h^2}\frac{ac^2}{(BH_0)^2}(\chi_{i,j,k+1} - 2\chi_{i,j,k} + \chi_{i,j,k-1}) \\ & - a^3\left(\frac{\mu}{H_0}\right)^2(\overline{\chi} - \chi_{i,j,k}) \times \\ & \times \left(1 - \chi^2_{i,j,k} - \overline{\chi}\chi_{i,j,k} - \overline{\chi}^2\right) \\ & - 3\Omega_m\left(\frac{M_{\rm pl}}{M}\right)^2(\rho_c\chi_{i,j,k} - \overline{\chi}). \end{aligned} \tag{B3}$$

The Newton–Gauss–Seidel iteration says that we can obtain a new and more accurate solution of $\chi^{\rm new}_{i,j,k}$ using our knowledge about the old solution $\chi^{\rm old}_{i,j,k}$ as

$$\chi^{\rm new}_{i,j,k} = \chi^{\rm old}_{i,j,k} - \frac{L^h\left(\chi^{\rm old}_{i,j,k}\right)}{\partial L^h\left(\chi^{\rm old}_{i,j,k}\right)/\partial\chi^{\rm old}_{i,j,k}} \tag{B4}$$

where

$$\frac{\partial L^h(\chi_{i,j,k})}{\partial\chi_{i,j,k}} = -\frac{6}{h^2}\frac{ac^2}{(BH_0)^2} + a^3\left(\frac{\mu}{H_0}\right)^2\left(1 - 3\chi^2_{i,j,k}\right) - 3\Omega_m\left(\frac{M_{\rm pl}}{M}\right)^2\rho_c. \tag{B5}$$

B.2. Poisson Equation

Since we can neglect the scalar field contribution to the Poisson equation, it remains unmodified from that of ΛCDM and reads (in code units)

$$\nabla^2\Phi_c = \frac{3}{2}\Omega_m(\rho_{c,i,j,k} - 1). \tag{B6}$$

B.3. Particle Equation of Motion

Using the code units, Equation (56) can be rewritten as

$$\frac{d\mathbf{x_c}}{dt_c} = \frac{\mathbf{p_c}}{a^2} \tag{B7}$$

$$\frac{d\mathbf{p_c}}{dt_c} = -\frac{1}{a}\nabla\Phi_c - \chi\left(\frac{\beta M}{M_{\rm pl}}\right)^2\left(\frac{c^2\nabla\chi}{(BH_0)^2} + \frac{d\chi}{dt_c}\mathbf{p_c}\right). \tag{B8}$$

The factor $(M/M_{\rm pl})^2$ can be also rewritten in terms of L, β, and $z_{\rm SSB}$ by using Equation (22).

REFERENCES

Accetta, F. S., Krauss, L. M., & Romanelli, P. 1990, Phys. Lett. B, 248, 146
Adelberger, E. G. 2002, in CPT and Lorentz Symmetry, ed. V. A. Kostelecký (Singapore: World Scientific), 9
Appleby, S. A., & Weller, J. 2010, J. Cosmol. Astropart. Phys., JCAP12(2010)006
Arkani-Hamed, N., Georgi, H., & Schwartz, M. D. 2003, Ann. Phys., 305, 96
Baldi, M. 2009, Nucl. Phys. B, 194, 178
Baldi, M. 2011, MNRAS, 411, 1077
Baldi, M., Pettorino, V., Robbers, G., & Springel, V. 2010, MNRAS, 403, 1684
Bertotti, B., Iess, L., & Tortora, P. 2003, Nature, 425, 374
Bertschinger, E. 2001, ApJS, 137, 1
Binétruy, P. 2006, Supersymmetry: Theory, Experiment, and Cosmology (Oxford, UK: Oxford Univ. Press), 520
Brax, P., Burrage, C., & Davis, A.-C. 2011a, J. Cosmol. Astropart. Phys., JCAP09(2011)020
Brax, P., van de Bruck, C., Davis, A.-C., et al. 2011b, Phys. Rev. D, 84, 123524
Brax, P., van de Bruck, C., Davis, A.-C., Khoury, J., & Weltman, A. 2004, Phys. Rev. D, 70, 123518
Brax, P., van de Bruck, C., Davis, A.-C., Li, B., & Shaw, D. J. 2011c, Phys. Rev. D, 83, 104026
Brax, P., van de Bruck, C., Davis, A.-C., Mota, D. F., & Shaw, D. J. 2007a, Phys. Rev. D, 76, 124034
Brax, P., van de Bruck, C., Davis, A.-C., Mota, D. F., & Shaw, D. J. 2007b, Phys. Rev. D, 76, 085010
Brax, P., van de Bruck, C., Davis, A.-C., & Shaw, D. J. 2008, Phys. Rev. D, 78, 104021
Brax, P., van de Bruck, C., Davis, A.-C., & Shaw, D. 2010a, Phys. Rev. D, 82, 063519
Brax, P., van de Bruck, C., Davis, A.-C., & Shaw, D. 2010b, J. Cosmol. Astropart. Phys., JCAP04(2010)032
Brax, P., van de Bruck, C., Mota, D. F., Nunes, N. J., & Winther, H. A. 2010c, Phys. Rev. D, 82, 083503
Clampitt, J., Jain, B., & Khoury, J. 2012, J. Cosmol. Astropart. Phys., JCAP01(2012)030
Clifton, T., Mota, D. F., & Barrow, J. D. 2005, MNRAS, 358, 601
Colombi, S., Jaffe, A., Novikov, D., & Pichon, C. 2009, MNRAS, 393, 511
Davis, A.-C., Lim, E. A., Sakstein, J., & Shaw, D. 2011, arXiv:1102.5278
de Rham, C. 2010, Phys. Lett. B, 688, 137
de Rham, C., Dvali, G., Hofmann, S., et al. 2008, Phys. Rev. Lett., 100, 251603
Decca, R. S., López, D., Fischbach, E., et al. 2007, Phys. Rev. D, 75, 077101
Deffayet, C., Dvali, G., Gabadadze, G., & Vainshtein, A. 2002, Phys. Rev. D, 65, 044026
Dvali, G., Gabadadze, G., & Porrati, M. 2000, Phys. Lett. B, 485, 208
Felder, G., Kofman, L., & Linde, A. 2001, Phys. Rev. D, 64, 123517
Ferraro, S., Schmidt, F., & Hu, W. 2011, Phys. Rev. D, 83, 063503
Gabadadze, G. 2009, Phys. Lett. B, 681, 89
Gannouji, R., Moraes, B., Mota, D. F., et al. 2010, Phys. Rev. D, 82, 124006
Gies, H., Mota, D. F., & Shaw, D. J. 2008, Phys. Rev. D, 77, 025016
Gill, S. P. D., Knebe, A., & Gibson, B. K. 2004, MNRAS, 351, 399
Hellwing, W. A., & Juszkiewicz, R. 2009, Phys. Rev. D, 80, 083522
Hellwing, W. A., Juszkiewicz, R., & van de Weygaert, R. 2010, Phys. Rev. D, 82, 103536
Hinterbichler, K., & Khoury, J. 2010, Phys. Rev. Lett., 104, 231301
Hinterbichler, K., Khoury, J., Levy, A., & Matas, A. 2011, Phys. Rev. D, 84, 103521
Hinterbichler, K., Trodden, M., & Wesley, D. 2010, Phys. Rev. D, 82, 124018
Hoskins, J. K., Newman, R. D., Spero, R., & Schultz, J. 1985, Phys. Rev. D, 32, 3084
Hwang, J.-C., & Noh, H. 2002, Phys. Rev. D, 65, 023512
Khoury, J. 2010, arXiv:1011.5909
Khoury, J., & Weltman, A. 2004, Phys. Rev. D, 69, 044026
Knebe, A., Green, A., & Binney, J. 2001, MNRAS, 325, 845
Li, B., & Barrow, J. D. 2011a, Phys. Rev. D, 83, 024007
Li, B., & Barrow, J. D. 2011b, MNRAS, 413, 262
Li, B., Mota, D. F., & Barrow, J. D. 2011a, ApJ, 728, 109
Li, B., Mota, D. F., & Barrow, J. D. 2011b, ApJ, 728, 108
Li, B., & Zhao, H. 2010, Phys. Rev. D, 81, 104047
Linde, A. 2008, in Inflationary Cosmology, ed. M. Lemoine, J. Martin, & P. Peter (Lecture Notes in Physics, Vol. 738; Berlin: Springer), 1
Mota, D. F., & Barrow, J. D. 2004a, MNRAS, 349, 291
Mota, D. F., & Barrow, J. D. 2004b, Phys. Lett. B, 581, 141
Mota, D. F., Sandstad, M., & Zlosnik, T. 2010, J. High Energy Phys., JHEP12(2010)051
Mota, D. F., & Shaw, D. J. 2006, Phys. Rev. Lett., 97, 151102
Mota, D. F., & Shaw, D. J. 2007, Phys. Rev. D, 75, 063501
Mota, D. F., & Winther, H. A. 2011, ApJ, 733, 7
Motohashi, H., Starobinsky, A. A., & Yokoyama, J. 2010, Prog. Theor. Phys., 123, 887
Nagata, R., Chiba, T., & Sugiyama, N. 2004, Phys. Rev. D, 69, 083512
Narikawa, T., & Yamamoto, K. 2010, Phys. Rev. D, 81, 043528
Nicolis, A., Rattazzi, R., & Trincherini, E. 2009, Phys. Rev. D, 79, 064036
Olive, K. A., & Pospelov, M. 2008, Phys. Rev. D, 77, 043524
Oyaizu, H., Lima, M., & Hu, W. 2008, Phys. Rev. D, 78, 123524
Prunet, S., Pichon, C., Aubert, D., et al. 2008, ApJS, 178, 179
Schmidt, F. 2009, Phys. Rev. D, 80, 043001
Schmidt, F. 2010, Phys. Rev. D, 81, 103002
Schmidt, F., Lima, M., Oyaizu, H., & Hu, W. 2009, Phys. Rev. D, 79, 083518
Stabenau, H. F., & Jain, B. 2006, Phys. Rev. D, 74, 084007
Tsujikawa, S., Gannouji, R., Moraes, B., & Polarski, D. 2009, Phys. Rev. D, 80, 084044
Vainshtein, A. I. 1972, Phys. Lett. B, 39, 393
Winther, H. A., Mota, D. F., & Li, B. 2011, arXiv:1110.6438
Zhao, G.-B., Li, B., & Koyama, K. 2011, Phys. Rev. D, 83, 044007
Zhao, H., Macciò, A. V., Li, B., Hoekstra, H., & Feix, M. 2010, ApJ, 712, L179

Paper II

Environment Dependence of Dark Matter Halos in Symmetron Modified Gravity
Hans A. Winther, David F. Mota, Baojiu Li
The Astrophysical Journal, Volume 756, Issue 2, (2012)

The Astrophysical Journal, 756:166 (10pp), 2012 September 10 doi:10.1088/0004-637X/756/2/166

ENVIRONMENT DEPENDENCE OF DARK MATTER HALOS IN SYMMETRON MODIFIED GRAVITY

Hans A. Winther[1], David F. Mota[1], and Baojiu Li[2,3,4,5]
[1] Institute of Theoretical Astrophysics, University of Oslo, NO-0315 Oslo, Norway
[2] ICC, Department of Physics, University of Durham, South Road, Durham DH1 3LE, UK
[3] DAMTP, Centre for Mathematical Sciences, University of Cambridge, Wilberforce Road, Cambridge CB3 0WA, UK
[4] Kavli Institute for Cosmology Cambridge, Madingley Road, Cambridge CB3 0HA, UK
[5] Institute of Astronomy, Madingley Road, Cambridge CB3 0HA, UK
Received 2011 December 16; accepted 2012 July 17; published 2012 August 24

ABSTRACT

We investigate the environment dependence of dark matter halos in the symmetron modified gravity scenario. The symmetron is one of three known mechanisms for screening a fifth force and thereby recovering general relativity in dense environments. The effectiveness of the screening depends on both the mass of the object and the environment it lies in. Using high-resolution *N*-body simulations we find a significant difference, which depends on the halo's mass and environment, between the lensing and dynamical masses of dark matter halos similar to the $f(R)$ modified gravity. The symmetron can however yield stronger signatures due to a freedom in the strength of coupling to matter.

Key words: cosmology: miscellaneous – cosmology: theory – large-scale structure of universe

Online-only material: color figures

1. INTRODUCTION

Many theories of high-energy physics, such as string theory and supergravity, predict light gravitationally coupled scalar fields (see, e.g., Binetruy 2006; Linde 2008, and references therein). These scalars may play the role of dark energy (quintessence). If these scalar fields have non-minimal coupling to matter fields, then they could mediate extra forces and are potentially detectable in local experiments and from observations on cosmological scales.

Several laboratory and solar system experiments over the last decades have tried to detect a sign of such fundamental coupled scalar fields (Adelberger 2002; Hoskins et al. 1985; Decca et al. 2007; Bertotti et al. 2003), but the results so far show no signature of them. Naively, the results of these experiments have ruled out any such scalar fields, which also can have an effect on the large-scale structure of the universe, unless there is some mechanism which suppresses the scalar fifth force on small scales where the experiments are performed. One should keep in mind that general relativity (GR) is only well tested on length scales ranging from millimeters to the size of the solar system. Comparing this to the size of the horizon, this leaves a wide range of scales where there could be deviations from GR.

To this day we know three such types of theoretical mechanisms (see Khoury 2010 for a review) that can explain why light scalars, if they exist, may not be visible in experiments performed near the Earth. One such class, the chameleon mechanism (Khoury & Weltman 2004; Brax et al. 2004, 2010b; Clifton et al. 2005; Mota & Barrow 2004a, 2004b; Mota & Shaw 2007), operates when the scalars are coupled to matter in such a way that their effective mass depends on the local matter density. In regions where the local mass density is low, the scalars would be light and deviations from GR would be observed. But near the Earth, where experiments are performed, the local mass density is high and the scalar field would acquire a heavy mass making the interactions short range and therefore unobservable. This mechanism is the reason why $f(R)$ modified gravity can lead to viable cosmologies and still evade local gravity constraints.

The second mechanism, the Vainshtein mechanism (Vainshtein 1972; Deffayet et al. 2002; Arkani-Hamed et al. 2003), operates when the scalar has derivative self-couplings which become important near matter sources such as the Earth. The strong coupling near sources essentially cranks up the kinetic terms, which translates into a weakened matter coupling. Thus, the scalar screens itself and becomes invisible to experiments. This mechanism is central to the phenomenological viability of braneworld modifications of gravity and galileon scalar theories (Dvali et al. 2000; de Rham et al. 2008; Nicolis et al. 2008; Hinterbichler et al. 2010; Mota et al. 2010; Gabadadze 2009; de Rham 2010; Brax et al. 2011a).

The last mechanism, the one explored in this paper, is the symmetron mechanism (Hinterbichler & Khoury 2010; Hinterbichler et al. 2011; Olive & Pospelov 2008; Brax et al. 2011c; Gannouji et al. 2010). In this mechanism, the vacuum expectation value (VEV) of the scalar depends on the local matter density, becoming large in regions of low mass density, and small in regions of high mass density. The scalar couples with gravitational strength in regions of low density, but is decoupled and screened in regions of high density. This is achieved through the interplay of a symmetry-breaking potential and a universal quadratic coupling to matter. A similar screening mechanism applies for the environmentally dependent dilaton model (Brax et al. 2010a).

In vacuum, the scalar acquires a nonzero VEV which spontaneously breaks the $\mathbb{Z}_2$ symmetry $\phi \rightarrow -\phi$. In regions of sufficiently high matter density, the field is confined near $\phi = 0$, and the symmetry is restored. The fifth force arising from the matter coupling is proportional to ϕ, making the effects of the scalar small in high-density regions. Because of this effect, dark matter halos in high-density regions will produce different scalar fifth forces compared to those in low-density regions.

This effect has been studied for the case of $f(R)$ gravity (chameleon mechanism) in Zhao et al. (2011b), Schmidt (2010), and the Dvali–Gabadadze–Porratti (DGP) model (Vainshtein mechanism) in Schmidt (2010). It was found that in the DGP model the screening of halos is almost independent of environment while in $f(R)$ gravity there can be a significant environmental dependence. Another signature that has been

found recently in $f(R)$ and symmetron models is that the luminosity of galaxies (Davis et al. 2011b) might also depend on the environment.

Recent work on the symmetron has focused on background cosmology, linear (Brax et al. 2011c) and nonlinear structure formation (Davis et al. 2011a), and also made halo scale predictions (Clampitt et al. 2012). In this paper, we use the high-resolution N-body simulations of Davis et al. (2011a) to study the environment dependence of dark matter halos in the symmetron modified gravity scenario (see, for instance, Zhao et al. 2011a; Li & Zhao 2009, 2010; Li et al. 2011; Ferraro et al. 2011; Oyaizu et al. 2008; Schmidt 2009; Hellwing & Juszkiewicz 2009; Brax et al. 2011b for N-body simulations within other scenarios of modified gravity).

This paper is organized as follows. In Section 2, we recall the main properties of the symmetron model which are relevant for our analysis. Then, in Section 3, we introduce the dynamical and lensing masses of a halo and explain how these are obtained from the N-body simulations. In Section 4, we explain how we define the environment of a halo in our analysis. The main results are shown and discussed in Section 5, and we also compare our simulation results to semianalytical predictions in Section 6. Finally, we summarize and give our conclusions in Section 7.

2. SYMMETRON REVIEW

The symmetron modified gravity is a scalar field theory specified by the following action:

$$S = \int dx^4\sqrt{-g}\left[\frac{R}{2}M_{\rm pl}^2 - \frac{1}{2}(\partial\phi)^2 - V(\phi)\right] + S_m(\tilde{g}_{\mu\nu}, \psi_i), \tag{1}$$

where g is the determinant of the metric $g_{\mu\nu}$, R is the Ricci scalar, ψ_i are the different matter fields, and $M_{\rm pl} \equiv 1/\sqrt{8\pi G}$, where G is the bare gravitational constant. The matter fields couple universally to the Jordan frame metric $\tilde{g}_{\mu\nu}$, which is a conformal rescaling of the Einstein frame metric $g_{\mu\nu}$ given by

$$\tilde{g}_{\mu\nu} = A^2(\phi)g_{\mu\nu}. \tag{2}$$

The equation of motion for the symmetron field ϕ following from the action Equation (1) reads

$$\Box\phi = V_{,\phi} + A_{,\phi}\rho_m \equiv V_{{\rm eff},\phi}, \tag{3}$$

where the potential is chosen to be of the symmetry-breaking form

$$V(\phi) = -\frac{1}{2}\mu^2\phi^2 + \frac{1}{4}\lambda\phi^4 \tag{4}$$

and the coupling is quadratic in ϕ to be compatible with the $\phi \to -\phi$ symmetry

$$A(\phi) = 1 + \frac{1}{2}\left(\frac{\phi}{M}\right)^2. \tag{5}$$

The effective potential can then be written as

$$V_{\rm eff}(\phi) = \frac{1}{2}\left(\frac{\rho_m}{M^2} - \mu^2\right)\phi^2 + \frac{1}{4}\lambda\phi^4, \tag{6}$$

from which the range of the scalar field (i.e., the range of the resulting fifth force) can be found as

$$\lambda_\phi \equiv \frac{1}{\sqrt{V_{{\rm eff},\phi\phi}}}. \tag{7}$$

The range of the field in vacuum, denoted λ_0, is given by $\lambda_0 = 1/\sqrt{2}\mu$.

In high-density regions where $\rho_m > \mu^2M^2$, the effective potential has a minimum at $\phi = 0$. The fifth force, given by

$$\boldsymbol{F}_\phi = \boldsymbol{\nabla}A(\phi) = \frac{\phi}{M^2}\boldsymbol{\nabla}\phi, \tag{8}$$

is proportional to ϕ and will be suppressed. In vacuum, or in large underdensities, where $\rho_m \ll \mu^2M^2$, the $\phi \to -\phi$ symmetry is broken and the field settles at one of the two minima $\phi = \phi_0 \equiv \pm\mu/\sqrt{\lambda}$. The fifth force between two small test masses in such a region will achieve its maximum value compared to gravity,

$$\frac{F_\phi}{F_N} = 2M_{\rm pl}^2\left(\frac{d\ln A}{d\phi}\right)^2_{\phi=\phi_0} = 2\beta^2. \tag{9}$$

For very large bodies in the sense that

$$\alpha^{-1} \equiv 2\frac{\rho_{\rm SSB}}{\rho_{\rm body}}\left(\frac{\lambda_0}{R_{\rm body}}\right)^2 \ll 1, \tag{10}$$

the situation is quite different (Hinterbichler & Khoury 2010). Here, the symmetry is restored in the interior of the body and the fifth force on a test mass outside becomes suppressed by a factor α^{-1}:

$$\frac{F_\phi}{F_N} = 2\beta^2\frac{1}{\alpha}. \tag{11}$$

If the body lies in a high-density environment, where $\phi = \phi_{\rm env} < \phi_0$, the fifth force will be further suppressed by a factor $(\phi_{\rm env}/\phi_0)^2$. Thus, there are two ways a body can be screened: it can be large enough so as to make $\alpha^{-1} \ll 1$ or it can be located in a high-density region where $\phi_{\rm env} \ll \phi_0$. The latter in particular leads to an environment dependence of the fifth force in a dark matter halo which we will investigate in the next section.

Instead of working with μ, M, and λ we chose to define three more physically intuitive parameters L, β, and $z_{\rm SSB}$ which are the (vacuum) range of the field in Mpc h^{-1}, the coupling strength to matter, and the cosmological redshift where symmetry breaking takes place on the background level, respectively. The conversion to the original model parameters is given by

$$L = \frac{\lambda_0}{{\rm Mpc}\ h^{-1}} = \frac{3000H_0}{\sqrt{2}\mu}, \tag{12}$$

$$\beta = \frac{\phi_0 M_{\rm pl}}{M^2} = \frac{\mu M_{\rm pl}}{\sqrt{\lambda}M^2}, \tag{13}$$

$$(1+z_{\rm SSB})^3 = \frac{\mu^2M^2}{\rho_{m0}}. \tag{14}$$

3. THE DYNAMICAL AND LENSING MASSES

In any universally coupled scalar-field theory, like the symmetron, we have the choice of describing the dynamics of the model in two mathematically equivalent frames defined by choosing either $g_{\mu\nu}$ or $\tilde{g}_{\mu\nu}$ in Equation (2) as the space–time metric. In the *Einstein frame*, the one described by Equation (1), gravity is described by standard GR, but the geodesic equation

is modified compared to GR:

$$\ddot{x}^\mu + \Gamma^\mu_{\alpha\beta}\dot{x}^\alpha\dot{x}^\beta = -\frac{d\log A(\phi)}{d\phi}(\phi^{,\mu} + 2\phi_{,\beta}\dot{x}^\beta\dot{x}^\mu). \quad (15)$$

In the *Jordan frame* gravity is described by a scalar–tensor-like modified gravity theory, but the matter particles follow the geodesics of the space–time metric $\tilde{g}_{\mu\nu}$:

$$\ddot{x}^\mu + \tilde{\Gamma}^\mu_{\alpha\beta}\dot{x}^\alpha\dot{x}^\beta = 0, \quad (16)$$

where $\tilde{\Gamma}$ is the Levi-Civita connection of $\tilde{g}_{\mu\nu}$. The prediction of the theory is usually easier to derive in the Einstein frame and the corresponding quantities can be found in the Jordan frame by performing the transformation Equation (2).

Working in the Einstein frame and the conformal Newtonian gauge, the line element can be written as

$$ds^2 = a^2(\eta)[-d\eta^2(1+2\Phi_N) + (1-2\Phi_N)d\boldsymbol{x}^2], \quad (17)$$

where Φ_N is the usual Newtonian potential. Transforming to the Jordan frame using Equation (2) we find

$$ds^2 = a^2(\eta)[-d\eta^2(1+2\Phi) + (1-2\Psi)d\boldsymbol{x}^2], \quad (18)$$

where

$$\Phi \simeq \Phi_N + \delta A(\phi), \quad (19)$$

$$\Psi \simeq \Phi_N - \delta A(\phi), \quad (20)$$

with

$$\delta A(\phi) \equiv A(\phi) - 1 = \frac{1}{2}\left(\frac{\phi}{M}\right)^2. \quad (21)$$

Note that we have neglected a term[6] $2\Phi_N\delta A(\phi) \ll \Phi_N$ in the equations above. In the solar system deviations from GR are often phrased in terms of the so-called parameterized post-Newtonian (PPN) parameter γ. In the case of the symmetron, we have

$$\gamma = \frac{\Psi}{\Phi} = \frac{\Phi_N - \delta A(\phi)}{\Phi_N + \delta A\phi)} = 1 - \frac{2\delta A(\phi)}{\Phi_N + \delta A(\phi)}. \quad (22)$$

The solar system constraints for the symmetron were derived in Hinterbichler & Khoury (2010) and give a constraint on the range of the field and the symmetry-breaking redshift: $L(1+z_{\rm SSB})^3 \lesssim 2.3$ (Davis et al. 2011a).

Typically observations of, e.g., clusters probe forces (gradients of the potentials) instead of the potentials themselves and different observables are related to different combinations of the potentials. The fifth-force potential is given by the difference in the above two potentials:

$$\Phi_- = \frac{\Phi - \Psi}{2} = \delta A(\phi). \quad (23)$$

Lensing, on the other hand, is affected by the lensing potential

$$\Phi_+ = \frac{\Phi + \Psi}{2} = \Phi_N, \quad (24)$$

which satisfies the Poisson equation

$$\nabla^2\Phi_+ = 4\pi G a^2\delta\rho_m. \quad (25)$$

This is the same equation as in GR since the action of the electromagnetic field is conformally invariant and thus photons do not feel the scalar fifth force. In general, there will also be a contribution from the clustering of the scalar field $4\pi G a^2\delta V(\phi)$, but in our case this term is negligible as the difference in the clustered and unclustered energy density of the scalar field is always much less than the energy density of matter in a halo.[7] We define the lensing mass as

$$M_L = \frac{1}{4\pi G a^2}\int \nabla^2\Phi_+ dV, \quad (26)$$

which is the actual mass of the halo. It is determined from the N-body simulations by counting the number of particles within a given radius. For spherical symmetry we can use Stokes' theorem, $\int \nabla^2\Phi_+ dV = \int \nabla\Phi_+ \cdot d\boldsymbol{S} = 4\pi r^2(d\Phi_+/dr)$, which gives

$$M_L(r) \propto r^2\frac{d\Phi_+}{dr}. \quad (27)$$

The dynamical mass $M_D(r)$ of a halo is defined as the mass contained within a radius r as inferred from the gravitational potential Φ, i.e.,

$$M_D(r) = \frac{1}{4\pi G a^2}\int \nabla^2\Phi dV, \quad (28)$$

where the integration is over the volume of the body out to radius r. For spherical symmetry, we can again use Stokes' theorem on the right-hand side to find

$$M_D(r) \propto \int r^2\frac{d\Phi(r)}{dr} = r^2\left(\frac{d\Phi_N}{dr} + \frac{\phi}{M^2}\frac{d\phi}{dr}\right). \quad (29)$$

The terms in the brackets are recognized as the sum of the gravitational force and the fifth force. In our N-body simulations, we measure M_D of a halo by first using a halo finder to locate the particles which make up the halo and binning them according to radius. Then, we calculate the average total force in each radial bin by summing over all the particles in the bin. Note that the force obtained in this way can have a contribution from the particles outside the halo. For spherical symmetry, this contribution largely cancels out and we are left with the total force produced by the halo itself. Observationally, M_D can be determined from measurements of, e.g., the velocity dispersion of galaxies in halos (Schmidt 2010).

In GR, the lensing mass is the same as the dynamical mass, but they can be significantly different in modified gravity. We follow Zhao et al. (2011b) and define the relative difference

$$\Delta_M(r) = \frac{M_D}{M_L} - 1 = \frac{d\Phi_-/dr}{d\Phi_+/dr}. \quad (30)$$

This allows us to quantity the difference between the two masses in the simulations. In GR, we have $\Delta_M \equiv 0$ while in the symmetron model Δ_M will vary depending on the mass of the

[6] For the symmetron, it was shown in Davis et al. (2011a) that $\delta A(\phi) \leqslant \delta A(\phi_0) \sim \beta^2 \times 10^{-6}$ which for the values of $\beta \lesssim \mathcal{O}(1)$ we are interested in is much less than one.

[7] The potential energy of the scalar field satisfies $|\delta V(\phi)| \leqslant |V(\phi_0) - V(0)| = \mu^4/4\lambda \sim \rho_{\rm SSB}\beta^2\left(M/M_{\rm pl}\right)^2 \lesssim \overline{\rho}_{m0}\beta^2(1+z_{\rm SSB})^3 \times 10^{-6}$. For β, $z_{\rm SSB} \lesssim \mathcal{O}(1)$ this term is negligible compared to the energy density of matter in a halo.

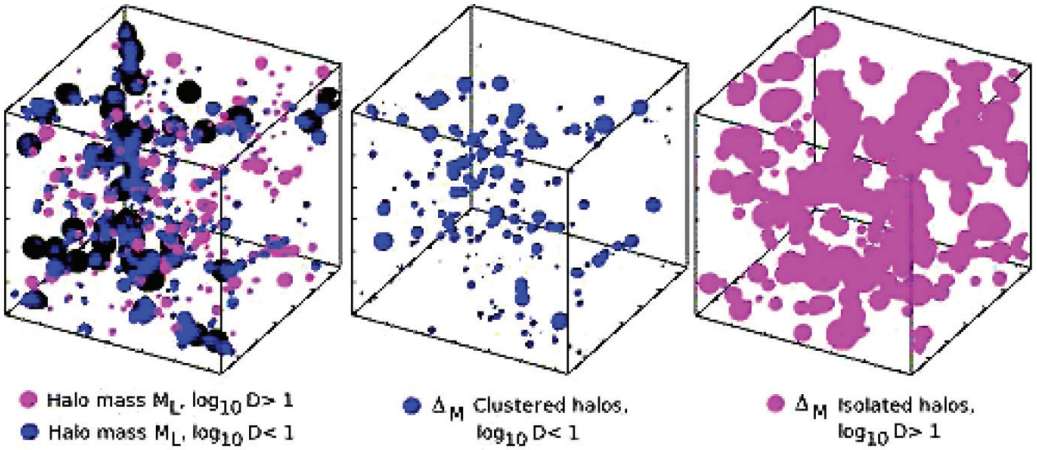

Figure 1. Three-dimensional distribution of the halos in the simulation box for a simulation with $z_{\rm SSB} = 0.5$ and $\beta = L = 1.0$. Left: the blue ($D < 10$) and purple ($D > 10$) spheres are 500 randomly selected halos in the mass range $11.5 < \log_{10}(M_L/M_{\rm sun}\,h^{-1}) < 12.5$. Because of the definition of the environment equation (32) the largest halos in the simulation will almost always be in a low-density environment and we therefore separate out the 50 most massive halos and show these separately in black with a fixed size for the spheres. Middle and right: the value of Δ_M for the clustered halos ($\log_{10} D < 1$) and the isolated halos ($\log_{10} D > 1$), respectively.

(A color version of this figure is available in the online journal.)

halo and the environment it lies in. The theoretical maximum is achieved for small objects in a low-density environment where the screening is negligible and reads (see Equation (9))

$$\Delta_M^{\rm Max}(r) = 2\beta^2. \tag{31}$$

In the next section, we will apply these to the *N*-body simulation results.

4. DEFINING THE ENVIRONMENT

The environment a halo lies in can have large effects on the fifth force that operates by the halo since the fifth force is directly proportional to the spatial gradient of the square of the local field value (see Equation (29)). This value is small in high-density regions and this will provide the halo with an additional screening to the self-screening due to its size or mass.

As a result, when looking for an environmental dependence it is crucial to choose a definition of the environment that does not correlate heavily with the halo mass. The quantity one chooses should also allow for an easy determination both in our simulations and in observations. Such a quantity was found in Haas et al. (2011) and used in the same analysis as we have done, but for the case of $f(R)$ gravity (Zhao et al. 2011b). This quantity,

$$D_{N,f} \equiv \frac{d_{N,M_{\rm NB}/M_L \geqslant f}}{r_{\rm NB}}, \tag{32}$$

is defined as the distance to the *N*th nearest neighbor whose mass exceeds *f* times the halo under consideration divided by the virial radius of the neighboring halo. A large value of *D* indicates that the halo lives in a low-density environment in the sense that it has no larger halos close by. It was shown in Haas et al. (2011; see also Fakhouri & Ma 2009, 2010) that the quantity $D \equiv D_{1,1}$ represents the local density well and is almost uncorrelated with the halo mass. We have explicitly checked that this is also the case for our simulations.

We follow Zhao et al. (2011b) and define a *high-density environment* as $\log_{10} D < 1$ and a *low-density environment* as $\log_{10} D > 1$. Halos in low- and high-density environments will be called *isolated halos* and *clustered halos*, respectively. In order to study the variation of Δ_M with halo mass we will say that a halo with $M_L/(M_{\rm sun}\,h^{-1}) > 5 \times 10^{12}$ is a *large halo*, while a halo with $5 \times 10^{11} < M_L/(M_{\rm sun}\,h^{-1}) < 2 \times 10^{12}$ is a *small halo*. The lower limit comes from the fact that smaller halos in our simulations are not well resolved (less than ∼500 particles per halo) and will therefore not be used in this analysis. This choice, arbitrary as it might seem, is made so that we have approximately equal numbers of halos in each of the two categories.

In Figure 1, we show the three-dimensional halo lensing mass distribution together with the corresponding value of Δ_M in the simulation box for one of the simulations. Each sphere represents a halo; in the left panel the size of the spheres is proportional to the halo lensing mass M_L and in the other two panels it is proportional to Δ_M; the color indicates the environment of the halos as illustrated by the legend. This plot shows the environmental dependence clearly: in high-density environments the value of Δ_M is generally smaller than in low-density environments, and the definition of the environment used here is capable of capturing this behavior fairly well.

5. RESULTS

We use the *N*-body simulations of Davis et al. (2011a) which have been performed using a modified version (Li & Barrow 2011) of the publicly available *N*-body code MLAPM (Knebe et al. 2001). The simulation suite consists of six simulations with different model parameters $\{\beta, L, z_{\rm SSB}\}$ shown in Table 1, and we have calculated Δ_M for the halos found in these simulations. The initial conditions for the symmetron models are the same for each simulation and allow for a direct comparison of the effects of the different parameters in the theory. The halos in the simulation have been found with the halo finder MHF (Gill et al. 2004) using the definition $M_{\rm vir} = M(r_{340}) \equiv M_{340}$ for the halo mass, where r_{340} is the radius of the halo where the local density is $\rho = 340\overline{\rho}$.

Table 1
The Symmetron Parameters for Each of the *N*-body Simulations A–F Together with Some Relevant Cosmological and *N*-body Parameters (Same for All Simulations)

							Parameter	Value
							Ω_m	0.267
Simulation	A	B	C	D	E	F	Ω_Λ	0.733
$z_{\rm SSB}$	0.5	0.5	1.0	1.0	2.0	2.0	h	0.719
β	0.5	1.0	0.5	1.0	0.5	1.0	σ_8	0.801
L	1.0	1.0	1.0	1.0	1.0	1.0	n_s	0.963
							$N_{\rm particles}$	256^3
							B_0	64 Mpc h^{-1}

Note. For a complete list of parameters see Davis et al. (2011a).

The condition for screening of an isolated halo (i.e., not taking the environment into account) can be found theoretically. For a spherical top-hat overdensity with radius r_{340} and density $\rho = 340\overline{\rho}_{m0}$, we have

$$\frac{\Delta_M(r_{340})}{\Delta_M^{\rm Max}} \simeq \begin{cases} \alpha^{-1} & \alpha \gtrsim 1, \\ 1 & \alpha \lesssim 1, \end{cases} \quad (33)$$

where α is given in Equation (10). The condition for screening, $\alpha \gtrsim 1$, can be written as

$$\frac{M_{340}}{10^{12}\, M_{\rm sun}\ h^{-1}} \gtrsim 0.6(1+z_{\rm SSB})^3 L^2 \left(\frac{r_{340}}{\rm Mpc\ h^{-1}}\right), \quad (34)$$

where $M_{340} = (4\pi/3)\rho r_{340}^3$ is the halo mass. This condition is not accurate for real halos as the top-hat approximation is very crude (Clampitt et al. 2012), but it nevertheless is able to capture the essence of the screening mechanism. In Table 2, we show the ratio of halos more massive than $5 \times 10^{11}\, M_{\rm sun}\ h^{-1}$ which are expected to be screened in the different simulations based on this simple approximation. The effectiveness of the symmetron screening mechanism increases with increasing halo mass M_{340} and decreasing symmetry-breaking redshift $z_{\rm SSB}$. This is because a larger value of $z_{\rm SSB}$ means the symmetry is broken at higher matter densities and consequently a larger halo mass is required to restore the symmetry.

In Figure 2, we show $\Delta_M(r_{340})$ for our simulations as a function of the environment for both large (blue circles) and small (purple circles) halos. First, we note that the predictions from simulations with different β are very similar and the only real effect of changing β is to change the normalization factor $\Delta_M^{\rm Max} = 2\beta^2$. This can be understood from noting that changing β only affects the geodesic equation (15) and not the Klein–Gordon equation[8] (3). However, for simulations with larger β we will on average have more massive halos because the fifth force, and therefore the matter clustering, is stronger. This effect, which for our simulations is very small, can also be seen in Table 2. Second, we note that the predictions of $\Delta_M(r_{340})$ for high-mass and low-mass halos in low-density environments are easy to separate at 1σ for all our simulations. The small dispersion about the solid curves (which represent the average values in the two mass bands) seen in Figure 2 is due to the difference in the halo masses within each mass band.

Table 2
The Percentage of Halos More Massive than $5 \times 10^{11}\, M_{\rm sun}\ h^{-1}$ Which are Expected to be Screened (to Some Degree) in the Different Simulations Based on the Approximation Equation (34)

Simulation	A	B	C	D	E	F
Screened	99.82%	99.83%	64.38%	65.27%	13.91%	14.12%

Notes. There is a very small difference between the simulations where $\beta = 0.5$ (A, C, E) compared to $\beta = 1.0$ (B, D, F) even though the screening is only sensitive to L and $z_{\rm SSB}$. This small difference comes from the fact that simulations with stronger β will in general have more massive halos.

To see this more closely, we have used the size of the circles (which represent halos) to denote their masses: bigger circles are more massive halos. We can see the clear trend that Δ_M decreases with increasing circle size (or halo mass), and this confirms that in a given environment the screening of a halo, or equivalently Δ_M, depends very sensitively on the mass of that halo. Third, for very high density environments $D \to 0$ we recover GR independent of the halo mass for all of our simulations, which is because the local value of ϕ in a very high density environment (which is often a part of or very close to a very massive halo) is small and so the fifth force is suppressed.

In Figure 3, we show $\Delta_M(r_{340})$ for our simulations as a function of the halo mass in both high-density (purple circles) and low-density (blue circles) environments. This figure shows that GR is recovered for larger halos, independent of the environment, as expected from Equation (34). For low-mass halos we see a significant dispersion of Δ_M from 0 to the maximum value obtained in low-density environments for the same mass ranges. This is because low-mass halos cannot efficiently screen themselves and must rely on the environment to get the screening. The environment, defined by D, ranges from $D = 0$ up to $D = 10$ for these halos, and the lower the value of D the better screened the halo will be. To observe this point more clearly, in the figure we have also used the size of the circles to denote the value of D: the bigger circles are halos in environments with larger D (or lower density) and vice versa. As expected, we see a clear trend that the small halos which are efficiently screened generally reside in high-density environments, while those which are less screened lie in low-density environments.

Massive halos, on the other hand, can screen themselves efficiently and the environment only plays a small role in their total screening.

In Figure 4, we show $\Delta_M(r)$ as a function of the distance r from the halo center, for small and large halos in high- and low-density environments respectively. Again we see a large difference between large halos in dense environments and small halos in low-density environments. The r dependence of $\Delta_M(r)$ is seen to be rather weak in high-density environments since the value of the scalar field inside the halo is mainly determined by the environment, while in low-density environments the value of the scalar field mainly depends on the mass of the halo, which leads to a stronger r dependence. Note also that in all the figures above the deviation from GR is stronger for higher symmetry-breaking redshift $z_{\rm SSB}$, as expected from Equation (34), and for larger values of the coupling β, which implies a stronger fifth force and therefore a stronger effect.

It should be emphasized that the environment dependences that are seen in the figures above will depend on the way the halos are binned, i.e., our definitions in Section 4.

[8] The Klein–Gordon equation (3) can be written as $\Box\psi = (1/2\lambda_0^2)[(\rho/\overline{\rho}_{m0}(1+z_{\rm SSB})^3) - 1 + \psi^2]\psi$ where $\psi = \phi/\phi_0$. Using this variable the fifth force can be written $F = \beta^2(M/M_{\rm pl})^2\psi\nabla\psi$. Thus, the solution ψ is independent of β and its only the geodesic equation, through the fifth force, which has a β dependence.

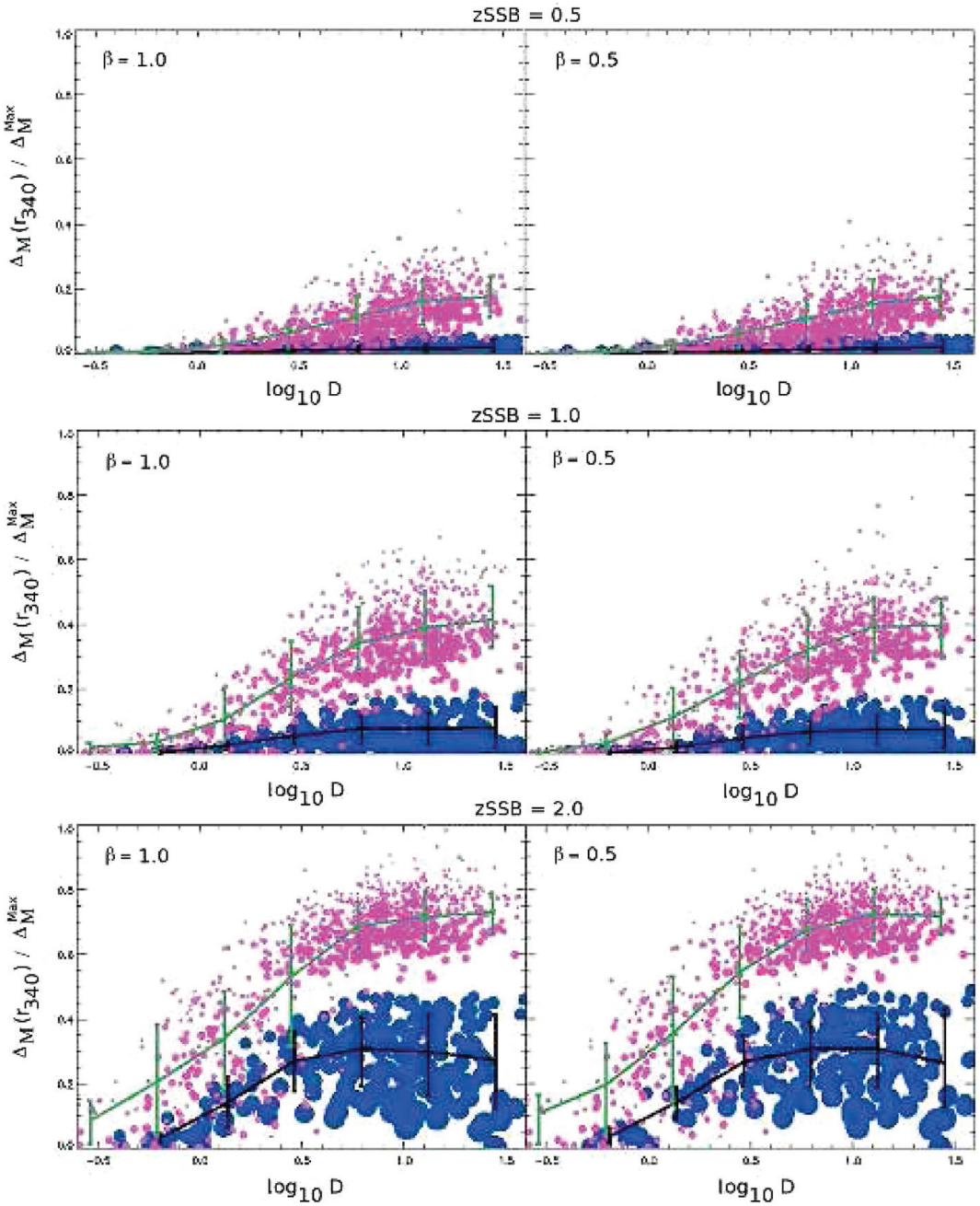

Figure 2. $\Delta_M(r_{340})/\Delta_M^{\rm Max}$ as a function of the environment for large halos ($(M_L/M_{\rm sun}\,h^{-1}) > 5 \times 10^{12}$, blue) and small halos ($(M_L/M_{\rm sun}\,h^{-1}) < 2 \times 10^{12}$, purple) where $\Delta_M^{\rm Max} = 2\beta^2$ and where the size of the circles increases with the mass of the halos. The error bars are 1σ. We see a clear difference between the values of Δ_M for what we have defined as high-mass and low-mass halos.

(A color version of this figure is available in the online journal.)

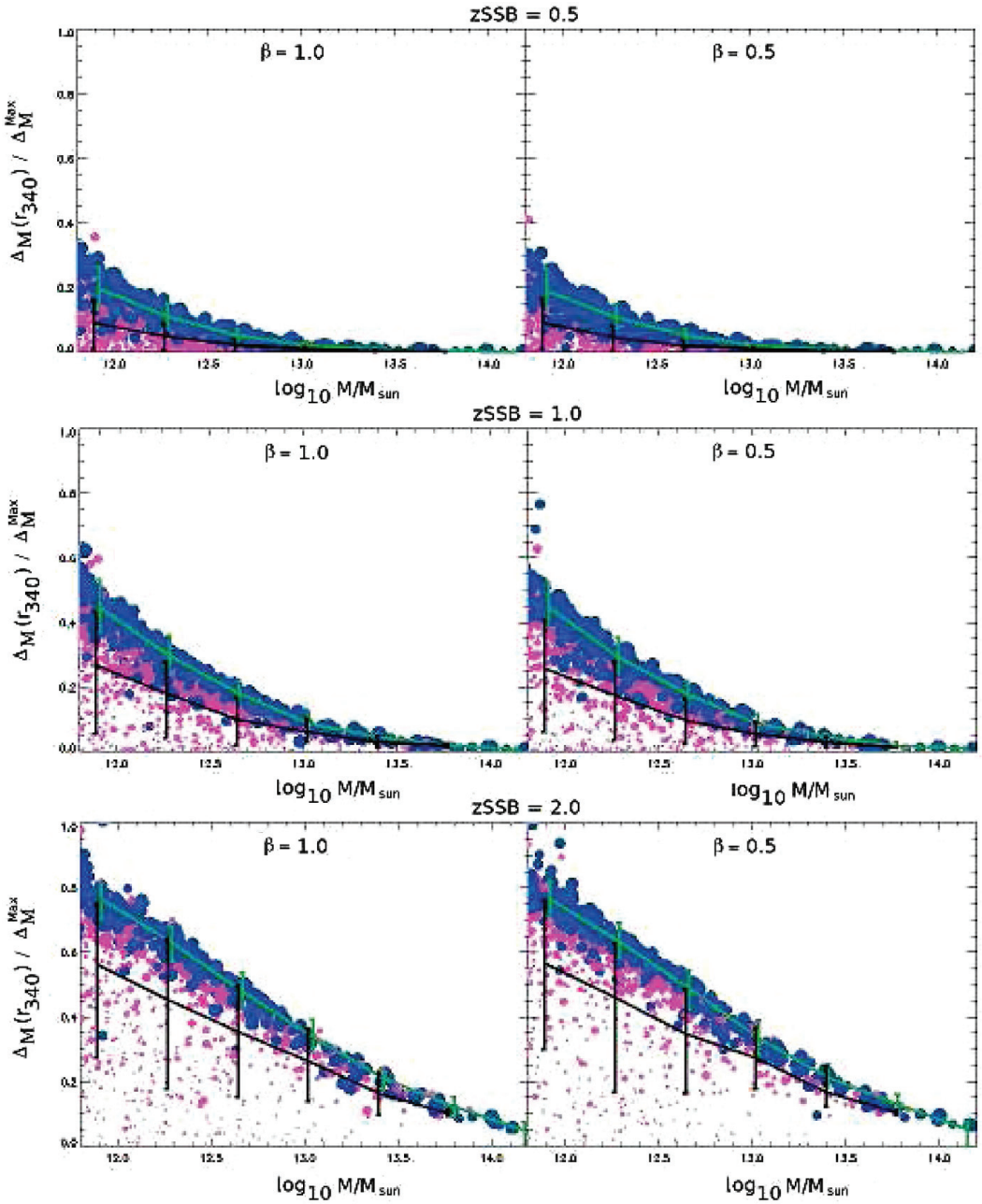

Figure 3. $\Delta_M(r_{340})/\Delta_M^{\rm Max}$ as a function of the halo lensing mass M_L for high-density environments ($D < 10$, purple) and low-density environments ($D > 10$, blue) where $\Delta_M^{\rm Max} = 2\beta^2$ and where the size of the circles increases with D (i.e., a smaller circle indicates a denser environment). The error bars are 1σ. For the high-mass halos we recover GR independent of the environment as the effectiveness of the screening increases with mass.

(A color version of this figure is available in the online journal.)

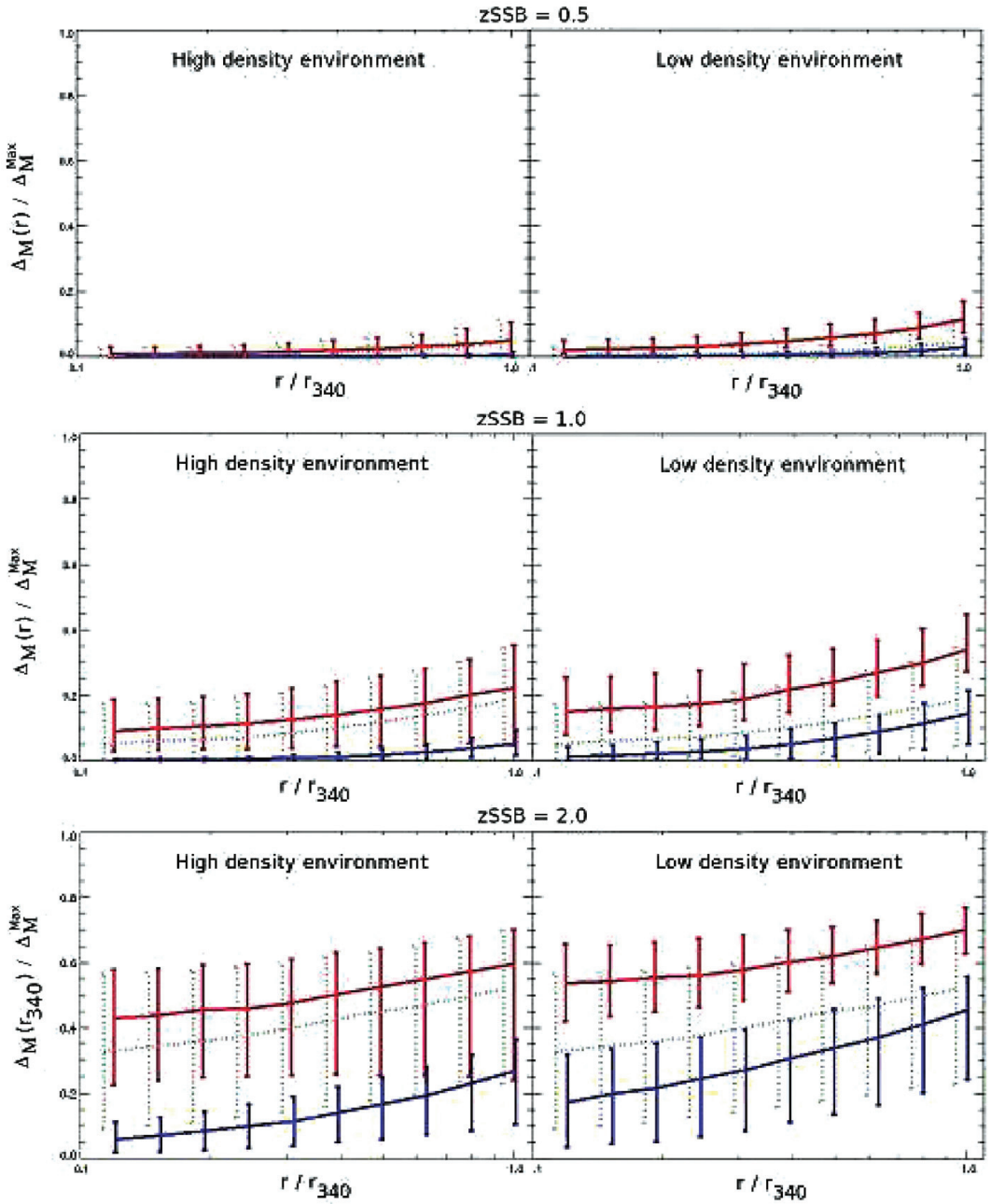

Figure 4. $\Delta_M(r)/\Delta_M^{\rm Max}$ as a function of the rescaled halo radius r/r_{340}, where $\Delta_M^{\rm Max} = 2\beta^2$, for high- ($D < 10$) and low- ($D > 10$) density environments and small (red) and large (blue) halos. The error bars are 1σ. For comparison, we show the profile for all halos in the simulation (dashed green) in each plot and this curve has been displaced -5% in the r-direction to more clearly see the error bars.

(A color version of this figure is available in the online journal.)

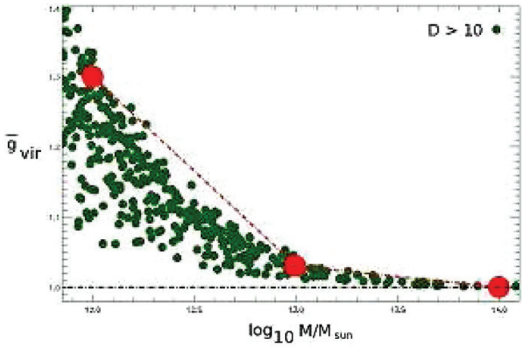

Figure 5. $\overline{g}_{\rm vir}$ as a function of halo mass for the isolated halos ($D > 10$) in a simulation with $\{\beta = 1.0, L = 1.0, z_{\rm SSB} = 0.5\}$ compared with the semianalytical results of Clampitt et al. (2012, Figure 3 (red)). The dashed black line shows the GR prediction $\overline{g}_{\rm vir} = 1$. The semianalytical results are for isolated halos and agree very well with the maximum $\overline{g}_{\rm vir}$ in our simulations. Note that the symmetron parameters used in Clampitt et al. (2012), $\{\beta = 1.0, L = 1.2, z_{\rm SSB} = 0.54\}$, are slightly different compared to our simulation, and also the definition $M = M_{300}$ was used for the virial mass as opposed to our $M = M_{340}$.

(A color version of this figure is available in the online journal.)

The results shown above are for halos at redshift $z = 0$. Another signature in the symmetron scenario is the redshift dependence of Δ_M. For halos at large redshifts, $z > z_{\rm SSB}$, we have $\Delta_M \approx 0$, independent of the environment and mass as the symmetry has not been broken at the background level and $\phi \sim 0$ almost everywhere in space, as demonstrated in Figures 7–10 in Davis et al. (2011a). If this signature is found in observations, then by dividing the observational samples into bins according to redshift one can probe the value of the symmetry-breaking redshift $z_{\rm SSB}$. The maximal strength of the deviation will again probe β, which can help to distinguish the symmetron from $f(R)$ gravity. If, for example, one finds $\Delta_M^{\rm Max} > (1/3)$ then $f(R)$ cannot account for the deviation.

6. COMPARISON WITH ANALYTICAL RESULTS

During the completion of this work a paper (Clampitt et al. 2012) came out with semianalytical halo scale predictions for the symmetron. In their analysis they assumed an NFW profile and calculated the symmetron fifth force for isolated halos. The quantity of interest is $\overline{g}_{\rm vir}$ (see Clampitt et al. 2012; Schmidt 2010 for details) which in our notation is given by

$$\overline{g}_{\rm vir} = 1 + \frac{\int r^3 \rho(r) F_N \Delta_M(r) dr}{\int r^3 \rho(r) F_N dr}, \qquad (35)$$

where F_N is the gravitational force and $\overline{g}_{\rm vir}$ is the average force to the average gravitational force over the halo. Since galaxies are spread around inside the halo, a measurement of the velocity dispersion of galaxies would therefore measure such an average. One of the cases shown in Clampitt et al. (2012) can be compared to our simulation results, and as a consistency check we perform this comparison.

In Figure 5, we show $\overline{g}_{\rm vir}$ together with the predictions from Clampitt et al. (2012). The results from their analysis seem to be in good agreement with our numerical results. It would be interesting to see if their analysis can be extended by taking the environment into account to obtain the simulation results we have presented here. This would allow for an easier comparison with future observations as N-body simulations are in general very time-consuming.

7. SUMMARY AND CONCLUSIONS

We have studied the environment dependence of the masses of dark matter halos in the symmetron modified gravity scenario. The potential governing the dynamics of the matter fields ($\Phi_- + \Phi_+$) can differ significantly from the lensing potential Φ_+ in this model, which leads to a clear difference between the mass of the halo as obtained from dynamical measurements and that obtained from gravitational lensing. Such an effect found in the symmetron model can be significantly stronger than in $f(R)$ gravity. This signature, which is unique to modified gravity, can in practice be measured by combining dynamical (e.g., velocity dispersion) and lensing mass measurements of clusters of galaxies or even single galaxies. We find that the environmental dependence is strongest for small halos as very large halos are sufficiently massive to be able to screen themselves. This implies that using dwarf galaxies (Jain & Vanderplas 2011) might prove the best way to probe this effect.

This feature of environmental dependence discovered also allows us, in principle, to distinguish between different modified gravity scenarios such as $f(R)$, more general chameleons, DGP, and the symmetron. In both DGP and $f(R)$, the maximum fractions of the fifth force to the Newtonian force in halos are around 30% while in chameleon/symmetron scenarios this fraction can be either smaller or larger, depending on the value of the coupling strength β. DGP differs from $f(R)$ and the symmetron in that there is basically no environmental dependence. There is also the possibility of measuring the redshift evolution of this effect by measuring clusters at high and low redshifts. As the symmetron force is negligible for $z > z_{\rm SSB}$ we will recover the GR predictions for all clusters, independent of mass and environment, at high redshifts.

Since different modified gravity theories can be highly degenerate with regard to both background cosmology and the growth rate of linear perturbations, it is crucial to identify new probes which can be used to separate them from each other. If one of these models is realized in nature then only a combination of many different probes will be able to pin down the correct theory. However, the first step would be to detect a deviation from GR, and a detection of the effect considered in this paper will be a smoking gun for modified gravity. It will therefore be very interesting to look for this effect using data from upcoming large-scale structure surveys.

The simulations used in this paper have been performed on TITAN, the computing facility at the University of Oslo in Norway. D.F.M. and H.A.W. thank the Research Council of Norway for FRINAT Grant 197251/V30. D.F.M. is also partially supported by project PTDC/FIS/111725/2009 and CERN/FP/116398/2010. B.L. is supported by Queens' College, the Department of Applied Mathematics and Theoretical Physics of University of Cambridge, and the Royal Astronomical Society. H.A.W. thanks S. K. Næss for many useful discussions.

REFERENCES

Adelberger, E. G. 2002, in CPT and Lorentz Symmetry, ed. V. A. Kostelecký (Singapore: World Scientific), 9

Arkani-Hamed, N., Georgi, H., & Schwartz, M. D. 2003, Ann. Phys., NY, 305, 96

Bertotti, B., Iess, L., & Tortora, P. 2003, Nature, 425, 374
Binetruy, P. 2006, Supersymmetry: Theory, Experiment, and Cosmology (Oxford: Oxford Univ. Press), 520
Brax, P., Burrage, C., & Davis, A.-C. 2011a, J. Cosmol. Astropart. Phys., JCAP09(2011)020
Brax, P., van de Bruck, C., Davis, A.-C., Khoury, J., & Weltman, A. 2004, Phys. Rev. D, 70, 123518
Brax, P., van de Bruck, C., Davis, A.-C., Li, B., & Shaw, D. J. 2011b, Phys. Rev. D, 83, 104026
Brax, P., van de Bruck, C., Davis, A.-C., & Shaw, D. 2010a, Phys. Rev. D, 82, 063519
Brax, P., van de Bruck, C., Davis, A.-C., et al. 2011c, Phys. Rev. D, 84, 123524
Brax, P., van de Bruck, C., Mota, D. F., Nunes, N. J., & Winther, H. A. 2010b, Phys. Rev. D, 82, 083503
Clampitt, J., Jain, B., & Khoury, J. 2012, J. Cosmol. Astropart. Phys., JCAP01(2012)030
Clifton, T., Mota, D. F., & Barrow, J. D. 2005, MNRAS, 358, 601
Davis, A.-C., Li, B., Mota, D. F., & Winther, H. A. 2011a, ApJ, 748, 61
Davis, A.-C., Lim, E. A., Sakstein, J., & Shaw, D. 2011b, Phys. Rev. D, 85, 123006
Decca, R. S., López, D., Fischbach, E., et al. 2007, Phys. Rev. D, 75, 077101
Deffayet, C., Dvali, G., Gabadadze, G., & Vainshtein, A. 2002, Phys. Rev. D, 65, 044026
de Rham, C. 2010, Phys. Lett. B, 688, 137
de Rham, C., Dvali, G., Hofmann, S., et al. 2008, Phys. Rev. Lett., 100, 251603
Dvali, G., Gabadadze, G., & Porrati, M. 2000, Phys. Lett. B, 485, 208
Fakhouri, O., & Ma, C.-P. 2009, MNRAS, 394, 1825
Fakhouri, O., & Ma, C. P. 2010, MNRAS, 401, 2245
Ferraro, S., Schmidt, F., & Hu, W. 2011, Phys. Rev. D, 83, 063503
Gabadadze, G. 2009, Phys. Lett. B, 681, 89
Gannouji, R., Moraes, B., Mota, D. F., et al. 2010, Phys. Rev. D, 82, 124006
Gill, S. P. D., Knebe, A., & Gibson, B. K. 2004, MNRAS, 351, 399
Haas, M. R., Schaye, J., & Jeeson-Daniel, A. 2011, MNRAS, 419, 2133
Hellwing, W. A., & Juszkiewicz, R. 2009, Phys. Rev. D, 80, 083522
Hinterbichler, K., & Khoury, J. 2010, Phys. Rev. Lett., 104, 231301
Hinterbichler, K., Khoury, J., Levy, A., & Matas, A. 2011, Phys. Rev. D, 84, 103521
Hinterbichler, K., Trodden, M., & Wesley, D. 2010, Phys. Rev. D, 82, 124018
Hoskins, J. K., Newman, R. D., Spero, R., & Schultz, J. 1985, Phys. Rev. D, 32, 3084
Jain, B., & Vanderplas, J. 2011, J. Cosmol. Astropart. Phys., JCAP10(2011)032
Khoury, J. 2010, arXiv:1011.5909
Khoury, J., & Weltman, A. 2004, Phys. Rev. D, 69, 044026
Knebe, A., Green, A., & Binney, J. 2001, MNRAS, 325, 845
Li, B., & Barrow, J. D. 2011, Phys. Rev. D, 83, 024007
Li, B., Mota, D. F., & Barrow, J. D. 2011, ApJ, 728, 109
Li, B., & Zhao, H. 2009, Phys. Rev. D, 80, 044027
Li, B., & Zhao, H. 2010, Phys. Rev. D, 81, 104047
Linde, A. 2008, in Inflationary Cosmology, ed. M. Lemoine, J. Martin, & P. Peter (Lecture Notes in Physics, Vol. 738; Berlin: Springer), 1
Mota, D. F., & Barrow, J. D. 2004a, MNRAS, 349, 291
Mota, D. F., & Barrow, J. D. 2004b, Phys. Lett. B, 581, 141
Mota, D. F., Sandstad, M., & Zlosnik, T. 2010, J. High Energy Phys., JHEP12(2010)051
Mota, D. F., & Shaw, D. J. 2007, Phys. Rev. D, 75, 063501
Nicolis, A., Rattazzi, R., & Trincherini, E. 2008, Phys. Rev. D, 79, 064036
Olive, K. A., & Pospelov, M. 2008, Phys. Rev. D, 77, 043524
Oyaizu, H., Lima, M., & Hu, W. 2008, Phys. Rev. D, 78, 123524
Schmidt, F. 2009, Phys. Rev. D, 80, 043001
Schmidt, F. 2010, Phys. Rev. D, 81, 103002
Vainshtein, A. I. 1972, Phys. Lett. B, 39, 393
Zhao, G.-B., Li, B., & Koyama, K. 2011a, Phys. Rev. D, 83, 044007
Zhao, G.-B., Li, B., & Koyama, K. 2011b, Phys. Rev. Lett., 107, 071303

Paper III

A Unified Description of Screened Modified Gravity
Philippe Brax, Anne-Christine Davis, Baojiu Li, Hans A. Winther
Physical Review D, vol. 86, Issue 4, (2012)

PHYSICAL REVIEW D **86,** 044015 (2012)

Unified description of screened modified gravity

Philippe Brax,[1,*] Anne-Christine Davis,[2,†] Baojiu Li,[3,‡] and Hans A. Winther[4,§]

[1]*Institut de Physique Theorique, CEA, IPhT, CNRS, URA 2306, F-91191Gif/Yvette Cedex, France*
[2]*DAMTP, Centre for Mathematical Sciences, University of Cambridge, Wilberforce Road, Cambridge CB3 0WA, United Kingdom*
[3]*ICC, Physics Department, University of Durham, South Road, Durham DH1 3LE, United Kingdom*
[4]*Institute of Theoretical Astrophysics, University of Oslo, 0315 Oslo, Norway*

(Received 2 April 2012; published 8 August 2012)

We consider modified gravity models driven by a scalar field whose effects are screened in high density regions due to the presence of nonlinearities in its interaction potential and/or its coupling to matter. Our approach covers chameleon, $f(R)$ gravity, dilaton and symmetron models and allows a unified description of all these theories. We find that the dynamics of modified gravity are entirely captured by the time variation of the scalar field mass and its coupling to matter evaluated at the cosmological minimum of its effective potential, where the scalar field has sat since an epoch prior to big bang nucleosynthesis. This new parametrization of modified gravity allows one to reconstruct the potential and coupling to matter and therefore to analyze the full dynamics of the models, from the scale dependent growth of structures at the linear level to nonlinear effects requiring N-body simulations. This procedure is illustrated with explicit examples of reconstruction for chameleon, dilaton, $f(R)$ and symmetron models.

DOI: 10.1103/PhysRevD.86.044015 PACS numbers: 04.50.Kd, 98.80.−k

I. INTRODUCTION

The discovery of the acceleration of the expansion of the Universe [1] has led to a reappraisal of some of the tenets of modern cosmology. In particular, the possibility of modifying the laws of gravity on short or large scales is taken more and more seriously [2].

In view of Weinberg's theorem stating that any Lorentz invariant field theory involving spin-2 fields must reduce to general relativity (GR) at low energy [3], any attempt to modify GR must involve extra degree(s) of freedom. The majority of known models involve scalar fields and can be separated into two broad classes, the ones involving nonlinearities in the kinetic terms and others with nonlinear interaction potentials. All these models have a coupling of the scalar field to matter and there could be an environmental dependence which would manifest itself in the screening behavior of the scalar field in high density regions [4,5]. Examples of such models abound: the dilatonic models [6,7] generalizing the Damour-Polyakov mechanism [8] where the coupling to gravity turns off in dense environments, the chameleon models [9–13] where a thin shell shielding the scalar field in dense bodies is present, and the symmetron models [14–20] where the scalar field has a symmetry breaking potential where the field is decoupled at high density.

Some models are essentially spin-offs of the previous ones like the $f(R)$ theories [21–31] (for recent reviews of the $f(R)$ gravity see [32,33]) which are only valid when they behave like chameleon theories with a thin shell mechanism in dense environments [31]. In all these examples, the large-scale properties on cosmological distances are intimately linked to the small-scale physics as probed in the solar system or laboratory tests of gravity. Stringent constraints on the possible modifications of gravity follow from the cosmology of these models too. In particular, they may lead to potentially lethal variations of particle masses or Newton's constant during big bang nucleosynthesis (BBN). This must be avoided at all costs as this may destroy the formation of elements, one of the big successes of the big bang model. Such a catastrophe can be avoided provided the scalar fields sit at the minimum of the density dependent effective potential prior to BBN. If this is the case, then the minimum of these models is stable enough to prevent large excursions of the scalar field and therefore of scalar masses/Newton's constant when the electron decouples during BBN. One of the most important consequences of this fact, which is common to chameleons, dilatons and symmetrons is that the cosmological background with the scalar field at the density dependent minimum of the effective potential behaves essentially like the Λ-cold dark matter (ΛCDM) model and is therefore almost indistinguishable from a cosmology comprising matter, radiation and a pure cosmological constant. This is a major drawback and would immediately render irrelevant the modified gravity/dark energy models with screening properties.

Fortunately, this is far from being the case as first anticipated in [10,34] where the equation governing the density contrast of CDM was first studied. Indeed, inside the Compton wavelength of the scalar field, the density contrast grows anomalously compared to its usual growth in the matter dominated era. If this discrepancy were large enough on astrophysical scales, this may be detectable by

*philippe.brax@cea.fr
†a.c.davis@damtp.cam.ac.uk
‡baojiu.li@durham.ac.uk
§h.a.winther@astro.uio.no

future galaxy surveys. It turns out that the perturbation equation at the linear level depends on the time evolution of the scalar field mass and the coupling strength to matter. With these two functions, all the time and space properties of the linear perturbations can be calculated.

In fact, these two time-dependent functions capture a lot more about the modified gravity models with screening properties: they allow one to reconstruct fully and uniquely the whole nonlinear dynamics of the models [5,35]. Hence given these two functions, not only can one compute linear perturbations, but one can study the gravitational properties of the models in the solar system and laboratory experiments. One can also analyze the cosmological behavior of the models with N-body simulations. This way of defining the models, a reversed engineering procedure from the mass and coupling functions to the nonlinear dynamics, is a lot more versatile than the usual direct route where a model is defined by its Lagrangian comprising the kinetic terms and an interacting potential. Indeed, all the usual models such as chameleons, $f(R)$, dilaton and symmetrons can be explicitly rediscovered by specifying the particular ways the mass and coupling functions behave in time. Moreover, one can design new families of models. At the linear level of cosmological perturbations, this approach is equivalent to a space and time dependent parametrization [36–45] in terms of the two Newtonian potentials obtained in the Jordan frame: the modified Poisson equation and the constitutive relation linking the two Newtonian potentials are directly and uniquely determined by the mass and coupling functions in the Einstein frame. For instance, we shall see below that one recovers the phenomenological description of $f(R)$ models which uses a space and time dependent parametrization [40] as a simple application of our formalism.

The paper is arranged as follows: in a first part we describe the modified gravity models with scalar fields and their cosmological background and gravitational properties. We only study models where gravity is modified due to nonlinearities in the potential and/or the coupling function of the scalar field to matter. Our analysis excludes the cases where the kinetic terms are not canonical and leading to the Vainshtein screening mechanism. We then describe the tomography of models with canonical kinetic terms, i.e. how to reconstruct their full dynamics using the time evolution of the mass and coupling functions. In Sec. IV, we focus on $f(R)$ models. In Sec. V we analyze the growth of structure. In Sec. VI, we consider the constraints on these models resulting from the variation of the fundamental constants. We conclude in Sec. VII.

Throughout this paper the metric convention is chosen as $(-,+,+,+)$; Greek indices $(\mu,\nu,\cdots)$ run over 0, 1, 2, 3 while Latin indices $(i,j,k,\cdots)$ run over 1, 2, 3. We shall adopt the unit $c=1$ and $m_{\rm Pl}$ denotes the Planck mass. Unless otherwise stated a subscript 0 will always mean the present-day value of a quantity.

II. MODIFIED GRAVITY

In this paper we propose a parametrization of a broad class of theories with a scalar degree of freedom, such as the chameleon, dilaton and symmetron theories, and $f(R)$ gravity. The success of these theories relies on mechanisms that suppress the fifth force in local, high-matter-density environments. We will find that the complete nonlinear Lagrangian comprising the kinetic terms and the interaction potential together with the coupling of the scalar field to matter can be reconstructed from the knowledge of the scalar field mass $m(a)$ and the coupling strength $\beta(a)$ as functions of time when the field sits at the minimum of the density dependent effective potential.

This mechanism relies on the fact that the scalar field must track that minimum since before BBN in order to preserve the constancy of particle masses at this epoch. In this section, we recall the setting of scalar field models and analyze their background evolution.

A. Modifying gravity with a scalar field

The action governing the dynamics of a scalar field ϕ in a scalar-tensor theory is of the general form

$$S=\int \mathrm{d}^4x\sqrt{-g}\left\{\frac{m_{\rm Pl}^2}{2}R-\frac{1}{2}(\nabla\phi)^2-V(\phi)\right\}+\int \mathrm{d}^4x\sqrt{-\tilde{g}}\mathcal{L}_m(\psi_m^{(i)},\tilde{g}_{\mu\nu}), \quad (1)$$

where g is the determinant of the metric $g_{\mu\nu}$, R is the Ricci scalar and $\psi_m^{(i)}$ are various matter fields labeled by i. A key ingredient of the model is the conformal coupling of ϕ with matter particles. More precisely, the excitations of each matter field $\psi_m^{(i)}$ couple to a metric $\tilde{g}_{\mu\nu}$ which is related to the Einstein-frame metric $g_{\mu\nu}$ by the conformal rescaling

$$\tilde{g}_{\mu\nu}=A^2(\phi)g_{\mu\nu}. \quad (2)$$

The metric $\tilde{g}_{\mu\nu}$ is the Jordan frame metric. We will analyze these models in the Einstein frame and come back to the Jordan frame picture later.

The fact that the scalar field couples to matter implies that the scalar field equation becomes density dependent. More precisely, the scalar field equation of motion (EOM) is modified due to the coupling of the scalar field ϕ to matter:

$$\Box\phi=-\beta T+\frac{\mathrm{d}V}{\mathrm{d}\phi}, \quad (3)$$

where T is the trace of the energy momentum tensor $T^{\mu\nu}$, $\Box\equiv\nabla^\mu\nabla_\mu$ and the coupling of ϕ to matter is defined by

$$\beta(\phi)\equiv m_{\rm Pl}\frac{\mathrm{d}\ln A}{\mathrm{d}\phi}. \quad (4)$$

This is equivalent to the usual scalar field EOM with the effective potential

$$V_{\rm eff}(\phi) = V(\phi) - [A(\phi) - 1]T. \quad (5)$$

The role of this effective potential $V_{\rm eff}(\phi)$ is crucial in all the modified gravity models we will consider. In essence, the effective potential is required to possess a unique matter dependent minimum in the presence of pressureless matter where $T = -\rho_m$. The resulting potential

$$V_{\rm eff}(\phi) = V(\phi) + [A(\phi) - 1]\rho_m \quad (6)$$

has a minimum $\phi_{\rm min}(\rho_m)$. The mass of the scalar field at the minimum

$$m^2 = \frac{{\rm d}^2 V_{\rm eff}}{{\rm d}\phi^2}\bigg|_{\phi_{\rm min}} \quad (7)$$

must be positive. In many cases (such as the generalized chameleon and dilaton models discussed below) $V(\phi)$ is a decreasing function and $\beta(\phi)$ is an increasing function as ϕ, though this is not the case for the generalized symmetron model.[1] This guarantees that the effective potential always has a minimum. In a cosmological setting we will also impose that $m^2 \gg H^2$ with H being the Hubble expansion rate. It can be shown easily that, depending on the shapes of $V(\phi)$ and $\beta(\phi)$, the chameleon, $f(R)$, dilaton and symmetron models are all described in a such a way.

When matter is described by a pressureless fluid with

$$T^{\mu\nu} = \rho_m u^\mu u^\nu \quad (8)$$

and $u^\mu \equiv {\rm d}x^\mu/{\rm d}\tau$ where τ is the proper time, the matter density ρ_m is conserved

$$\dot{\rho}_m + \theta\rho_m = 0 \quad (9)$$

where $\theta \equiv \nabla_\mu u^\mu$ and the trajectories are determined by the modified geodesics

$$\dot{u}^\mu + \beta\frac{\dot{\phi}}{m_{\rm Pl}}u^\mu = -\beta\frac{\partial^\mu\phi}{m_{\rm Pl}}. \quad (10)$$

In the weak-field limit with

$${\rm d}s^2 = -(1 + 2\Phi_N){\rm d}t^2 + (1 - 2\Phi_N){\rm d}x^i{\rm d}x_i, \quad (11)$$

and in the nonrelativistic case, this reduces to the modified geodesic equation for matter particles

$$\frac{{\rm d}^2 x^i}{{\rm d}t^2} = -\partial^i(\Phi_N + \ln A(\phi)). \quad (12)$$

This can be interpreted as the motion of a particle in the effective gravitational potential defined as

$$\Psi = \Phi_N + \ln A(\phi), \quad (13)$$

and is clearly a manifestation of the dynamics of modified gravity.

[1]For the generalized symmetron models, the potential is not monotonic but has the shape of a Mexican hat. However, in the part of the potential which will be of interest here, it is monotonically decreasing.

When a particle of mass M in a homogeneous background matter density is the source of gravity, the scalar field satisfies

$$(\nabla^2 + m^2)\phi = \beta\frac{M}{m_{\rm Pl}}\delta^{(3)}(r), \quad (14)$$

in which $\delta^{(3)}(r)$ is the three-dimensional Dirac δ function and m the scalar field mass in the background, implying that

$$\Psi = -(1 + 2\beta^2 e^{-mr})\frac{G_N M}{r}, \quad (15)$$

where $G_N = (8\pi)^{-1}m_{\rm Pl}^{-2}$ is the Newton constant. When $\beta \sim \mathcal{O}(1)$ and $m^{-1} \gg r$, this implies a substantial deviation from Newton's law. For bodies much bigger than a point particle following the modified geodesics, nonlinear effects imply that the effective coupling felt by the body is much smaller than β or the mass becomes much larger than the inverse of the typical size of the body ($m^{-1} \ll r$). This is what happens in the chameleon model and $f(R)$ gravity (the latter) and the dilaton and symmetron models (the former), and guarantees that solar system and laboratory tests of gravity are evaded.

B. Screening of modified gravity

In this section, we shall unify the description for the screening[2] mechanisms [4,5] involved in the chameleon, $f(R)$ gravity, dilaton and symmetron models. As we shall see, the screening of large and dense bodies can be expressed with a single criterion generalizing the thin-shell condition for the chameleon models. The constraints we find are typically stated in terms of the scalar field mass m_0 in the cosmological background today and the current Hubble scale H_0, making $\xi \equiv H_0/m_0$ a key quantity. Physically, ξ represents the range of the scalar fifth force to the Hubble radius and a particular value that will be recurrent is $m_0/H_0 \sim 10^3$ or $\xi \sim 10^{-3}$. This value means that the scalar field leaves its mark up to scales of the order of megaparsec, which again signals the transition where the modifications of gravity can be seen on linear perturbations or not.

1. Chameleons

The chameleon models (at least in their original form [9]—see [10–13,34] for other proposals) are characterized by a runaway potential and a nearly constant coupling β. Chameleons are screened deep inside a massive body, where the field settles at the minimum ϕ_c of $V_{\rm eff}(\phi)$ and stays constant up until a radius R_s close to the radius of the body, R. In this case, the field profile is given by

[2]To be clear, the "screening" of a body refers to the fact that the deviation from Newtonian gravity, i.e., the fifth force exerted by this body on a nearby test mass, is suppressed to evade local constraints—in analogy to the screening of the electric force from a charged particle.

$$\phi = \phi_c, \qquad R \leq R_s \tag{16}$$

The field varies sharply inside a thin shell according to

$$\frac{1}{r^2}\frac{\mathrm{d}}{\mathrm{d}r}\left[r^2\frac{\mathrm{d}\phi}{\mathrm{d}r}\right] = \beta\frac{\rho_m}{m_{\rm Pl}}, \qquad R_s \leq r \leq R \tag{17}$$

and decays outside

$$\phi = \phi_\infty - \frac{\beta}{4\pi m_{\rm Pl}}\left[1 - \frac{R_s^3}{R^3}\right]\frac{M}{r}\frac{e^{-m_\infty(r-R)}}{r} \tag{18}$$

where ϕ_∞ is the minimum of the effective potential outside the body and m_∞, M are respectively the masses of the scalar field and the body. At short distance compared to the large range m_∞^{-1}, the effective gravitational potential is

$$\Psi = \beta\frac{\phi_\infty}{m_{\rm Pl}} + \frac{G_N M}{r}\left[1 + 2\beta^2\left(1 - \frac{R_s^3}{R^3}\right)\right]. \tag{19}$$

Gravity is strongly modified by a factor $(1 + 2\beta^2)$ if there is no shell inside the body (i.e., $R_s = 0$) and one retrieves GR when R_s is close to R where

$$\frac{\Delta R}{R} = \frac{|\phi_\infty - \phi_c|}{6\beta m_{\rm Pl}\Phi_N}, \tag{20}$$

with $\Delta R \equiv R - R_s$ and $\Phi_N \equiv G_N M/R$ is the Newtonian potential at the surface of the body. The mass is screened when

$$|\phi_\infty - \phi_c| \ll 2\beta m_{\rm Pl}\Phi_N, \tag{21}$$

which is also the criterion to have a thin shell.

More precisely, this implies several very stringent experimental constraints on the chameleon models. The first one comes from the Lunar Ranging experiment [46] which measures the acceleration difference between Earth and the Moon in the gravitational field of the Sun

$$\eta = \frac{2(a_{\rm earth} - a_{\rm moon})}{a_{\rm earth} + a_{\rm moon}} \lesssim 10^{-13}. \tag{22}$$

For the chameleon model we have [9]

$$\eta \approx \beta^2\left(\frac{\Delta R_\oplus}{R_\oplus}\right)^2, \tag{23}$$

implying that

$$\beta\frac{\Delta R_\oplus}{R_\oplus} \lesssim 10^{-7}. \tag{24}$$

The Cassini experiment [47] imposes that the modification of the unscreened Cassini satellite in the vicinity of the Sun should be such that

$$\beta^2\frac{\Delta R_\odot}{R_\odot} \lesssim 10^{-5}. \tag{25}$$

Another type of constraint comes from cavity experiments where two small test bodies interact in a vacuum cavity [48]. This implies that

$$\beta\frac{\Delta R_{\rm cav}}{R_{\rm cav}} \lesssim 10^{-3}. \tag{26}$$

Finally, a loose bound must be imposed to guarantee that galaxies are not far off from being Newtonian [49]

$$\beta\frac{\Delta R_{\rm gal}}{R_{\rm gal}} \lesssim 1; \tag{27}$$

otherwise the modifications of gravity would have been seen by now in observations of galaxy clusters. These constraints strongly restrict the parameter space of the chameleon models.

2. Symmetrons

Symmetrons [16–20] are models with a Mexican hat potential, a local maximum at the origin and two global minima at $\pm\phi_\star$ like for example

$$V(\phi) = V_0 + \mu^2\phi_\star^2\left[-\frac{1}{2}\left(\frac{\phi}{\phi_\star}\right)^2 + \frac{1}{4}\left(\frac{\phi}{\phi_\star}\right)^4\right]. \tag{28}$$

In general the term $(\phi/\phi_\star)^4$ can be replaced by any even function which is bounded below, without changing the qualitative properties of the model.

Meanwhile, the coupling behaves like

$$A(\phi) = 1 + \frac{A_2}{2}\phi^2, \tag{29}$$

close to $\phi = 0$.

Let us consider a spherically dense body that is embedded in a homogeneous background. Inside this body the matter density ρ_m is constant and the scalar field profile is

$$\phi = C\frac{\sinh m_c r}{r}, \qquad r < R, \tag{30}$$

where the scalar field mass is given by $m^2 = A_2\rho_m - \mu^2$ and $-\mu^2$ is the negative curvature of the potential $V(\phi)$ at the origin. The field outside the body, on scales shorter than the large range m_∞^{-1} associated to the scalar field value ϕ_∞ which minimizes $V_{\rm eff}(\phi)$ outside, is

$$\phi = \phi_\infty + \frac{D}{r}, \qquad r > R, \tag{31}$$

where

$$\begin{aligned} C &= \frac{\phi_\infty}{m_c\cosh m_c R}, \\ D &= \frac{\sinh m_c R - m_c R\cosh m_c R}{m_c\cosh m_c R}\phi_\infty. \end{aligned} \tag{32}$$

If the body is dense enough, we have $m_c^2 \approx A_2\rho_m$ and $m_c R \gg 1$, implying that $D \approx -R\phi_\infty$. Identifying the coupling to matter $\beta_\infty = m_{\rm Pl}A_2\phi_\infty$, we find that the modified Newtonian potential outside the body is

$$\Psi = -\frac{G_N M}{r}\left[1 + \frac{A_2\phi_\infty^2}{\Phi_N}\right] + \mathcal{O}\left(\frac{R^2}{r^2}\right) = -\frac{G_N M}{r}\left[1 + \frac{\beta_\infty^2}{A_2 m_{\rm Pl}^2 \Phi_N}\right] + \mathcal{O}\left(\frac{R^2}{r^2}\right). \quad (33)$$

for r sufficiently large compared to R. For $R \ll r \ll m_\infty^{-1}$ the fifth force is screened provided

$$2A_2 m_{\rm Pl}^2 \Phi_N \gg 1, \quad (34)$$

which is equivalent to

$$|\phi_\infty - \phi_c| \ll 2m_{\rm Pl}\beta_\infty \Phi_N, \quad (35)$$

where $\phi_c = 0$. Note that this is the same screening criterion as in the chameleon case.

The screening in the symmetron model depends on A_2, Φ_N and the environment through the environmental field value ϕ_∞. Two test masses which are not screened when put in vacuum will be screened by a factor $(\phi_\infty/\phi_\star)^2$ if they are in a region of high matter density (which implies $\phi_\infty \ll \phi_\star$).

The transition of the minimum of $V_{\rm eff}(\phi)$ from $\phi = 0$ to $\phi = \phi_\star$ in the cosmological background happens in the recent past of the Universe provided

$$\mu^2 \sim A_2 \rho_{m0}, \quad (36)$$

where ρ_{m0} is the present matter density. For a polynomial potential $V(\phi)$, the mass-squared $m_\star^2$ at the minimum $\phi_\star$ is of order μ^2, implying that the mass of symmetrons in the present cosmological background satisfies

$$m_0^2 \sim A_2 m_{\rm Pl}^2 H_0^2, \quad (37)$$

One may see effects of modified gravity on astrophysical scales when $m_0/H_0 \lesssim 10^3$ which implies that $A_2 m_{\rm Pl}^2 \lesssim 10^6$.

Using the screening criterion we find that the Sun and the Milky Way with $\Phi_\odot \sim 10^{-6}$ are marginally screened whereas Earth with $\Phi_\oplus \sim 10^{-9}$ and the Moon with $\Phi_{\rm moon} \sim 10^{-11}$ are not screened. However, for the Solar System tests such as the Lunar Ranging experiment[3] and the Cassini satellite, what is more relevant is the value of the symmetron field $\phi_{\rm gal}$ in the Milky Way, which determines the strength $\beta(\phi_{\rm gal})$ of the modification of gravity.

This imposes

$$\frac{A_2\phi_{\rm gal}^2}{\Phi_\odot} \lesssim 10^{-5}. \quad (38)$$

For a generic symmetron potential we have[4] $\phi_{\rm gal}^2 \sim \frac{\rho_\infty}{\rho_{\rm gal}}\phi_\star^2$ where $\phi_\star$ is the minimum of $V_{\rm eff}(\phi)$ in the cosmological background with matter density ρ_∞. Using $\frac{\rho_\infty}{\rho_{\rm gal}} \sim 10^{-6}$, this leads to

$$10^{-6}\beta_\star^2 \frac{1}{2A_2 m_{\rm Pl}^2 \Phi_\odot} \sim \frac{10^{-6}}{\Phi_\odot}\frac{H_0^2}{m_0^2} \lesssim 10^{-5} \quad (39)$$

which is easily satisfied for $m_0/H_0 \sim 10^3$. Finally, in cavity experiments, the field ϕ inside the cavity is almost identical to the field in the bore, i.e., $\phi \sim 0$, implying no deviation from usual gravity in such experiments.

3. Dilaton

Dilatonic theories [6,7] are very similar to symmetrons inasmuch as they share the same type of coupling function,

$$A(\phi) = 1 + \frac{A_2}{2}(\phi - \phi_\star)^2, \quad (40)$$

but they differ as the dilaton potential $V(\phi)$ is a monotonically decreasing function of ϕ. All the dynamics can be analyzed in the vicinity of $\phi_\star$ as the minimum of the effective potential is close to $\phi_\star$ for large enough A_2.

The density dependent minimum of $V_{\rm eff}(\phi)$ is given by

$$\phi_{\rm min}(\rho_m) - \phi_\star = -\frac{V'(\phi_\star)}{A_2\rho_m}, \quad (41)$$

with the mass given by

$$m^2 = m_\star^2 + A_2\rho_m, \quad (42)$$

where $m_\star = m(\phi_\star)$ and the potential is chosen to be a quintessence potential such that $m_\star^2 \sim H_0^2$.

Let us consider a spherically dense body. Inside the body we have

$$\phi = \phi_c + C\frac{\sinh m_c r}{r}, \qquad r < R, \quad (43)$$

and outside

$$\phi = \phi_\infty + \frac{D}{r}, \quad (44)$$

for distances shorter than the range m_∞^{-1}. When $m_c R \gg 1$, we find that

$$D \approx -R(\phi_\infty - \phi_c), \quad (45)$$

and the effective Newtonian potential is

$$\Psi = -\frac{G_N M}{r}\left[1 + \frac{A_2(\phi_\infty - \phi_c)(\phi_\infty - \phi_\star)}{\Phi_N}\right] + \mathcal{O}\left(\frac{R^2}{r^2}\right), \quad (46)$$

for $R \ll r \ll m_\infty^{-1}$. Outside the body we have

$$\phi_\infty - \phi_\star = \frac{\beta_\infty}{A_2 m_{\rm Pl}} \quad (47)$$

with $\beta_\infty = \beta(\phi_\infty)$ and therefore

$$V'(\phi_\star) = -\beta_\infty \frac{\rho_\infty}{m_{\rm Pl}}, \quad (48)$$

from which we deduce that

[3]The Nordtvedt effect leads to a weak bound [16].
[4]See Eq. (19) in [16] for a more accurate expression.

$$\phi_\infty - \phi_c = \frac{\beta_\infty}{A_2 m_{\rm Pl}}\left(1 - \frac{\rho_\infty}{\rho_c}\right), \tag{49}$$

and finally

$$\Psi = -\frac{G_N M}{r}\left[1 + \frac{\beta_\infty^2}{A_2 m_{\rm Pl}^2 \Phi_N}\left(1 - \frac{\rho_\infty}{\rho_c}\right)\right] + \mathcal{O}\left(\frac{R^2}{r^2}\right). \tag{50}$$

for $R \ll r \ll m_\infty^{-1}$. The screening criterion is (almost) the same as in the symmetron case

$$2A_2 m_{\rm Pl}^2 \Phi_N \gg \left(1 - \frac{\rho_\infty}{\rho_c}\right), \tag{51}$$

or equivalently

$$|\phi_\infty - \phi_c| \ll 2\beta(\phi_\infty) m_{\rm Pl} \Phi_N, \tag{52}$$

which is the same as in the chameleon and dilaton cases.

The mass of the dilaton today in the cosmological background is

$$m_0^2 \approx A_2 \rho_{m0} = 3A_2 m_{\rm Pl}^2 \Omega_{m0} H_0^2, \tag{53}$$

in which Ω_{m0} is the present value of the fractional energy density of matter Ω_m, implying that $A_2 m_{\rm Pl}^2 \sim 10^6$ for models with $m_0/H_0 \sim 10^3$.

As in the symmetron case, this implies that both the Sun and the Milky Way are marginally screened when surrounded by the cosmological vacuum. But given that what matters for the magnitude of modified gravity is the dilaton value $\phi_\infty = \phi_{\rm gal}$ in the Milky Way, the Cassini bound can be written as

$$\frac{A_2(\phi_{\rm gal} - \phi_c)(\phi_{\rm gal} - \phi_\star)}{\Phi_N} \lesssim 10^{-5}, \tag{54}$$

which leads to

$$\frac{1}{A_2 m_{\rm Pl}^2 \Phi_\odot}\frac{\rho_\infty}{\rho_{\rm gal}} \lesssim 10^{-5}. \tag{55}$$

Using $\frac{\rho_\infty}{\rho_{\rm gal}} \sim 10^{-6}$, we see that the Cassini bound is satisfied for dilatons.

4. The screening criterion

We have seen that all the models of the chameleon, dilaton and symmetron types lead to a screening mechanism provided that

$$|\phi_\infty - \phi_c| \ll 2\beta(\phi_\infty) m_{\rm Pl} \Phi_N, \tag{56}$$

where ϕ_c is the value inside the body assumed to be at the minimum of the effective potential, ϕ_∞ is the minimum value outside the body and Φ_N is Newton's potential at the surface of the body. This is a universal criterion which is *independent* of the details of the model. In fact, it depends only on the values of the scalar field which minimizes the effective potential $V_{\rm eff}(\phi)$ inside and outside the body. If this criterion is satisfied, then the value inside the body does not deviate much from the minimum value there.

Phenomenologically, we have just recalled that stringent local constraints on modified gravity can be expressed in terms of the screening condition. In the following we shall *assume that the Milky Way satisfies the screening criterion*. When this is the case, local tests of gravity in the Solar System and in the laboratory can be easily analyzed as $\phi_{\rm gal}$ can be determined analytically. In the chameleon, dilaton and symmetron cases, this allows one to determine bounds on the ratio m_0/H_0 which essentially dictates if modified gravity has effects on astrophysical scales. The screening condition for the Milky Way may be relaxed slightly for some model parameters because it is itself in a cluster with higher density than the background. In this case, full numerical simulations are required to determine $\phi_{\rm gal}$ and see if local tests of gravity are satisfied. This may enlarge the allowed parameter space of the models slightly and lead to interesting effects. Numerical simulations are left for future work.

One of the advantages of the screening condition is that it only depends on the minimum values of the scalar field in different matter densities. In the following section, we will find an explicit formula for $\phi_c - \phi_\infty$ which depends only on the time variation of the mass $m(a)$ and coupling $\beta(a)$ in a cosmological background. This may seem surprising as the behavior of the scalar field may appear to be loosely connected to the scalar field dynamics in a static environment. In fact, the relation between both regimes of modified gravity, cosmological and static, follows from the fact that the scalar field sits at the minimum of its effective potential $V_{\rm eff}(\phi)$ since before BBN. As it evolves from BBN through the dark ages and then the present epoch, the cosmological values of the scalar field experience all the possible minima of $V_{\rm eff}(\phi)$. Hence realizing a tomography of the cosmological behavior of the scalar field, i.e., just knowing its mass and coupling to matter as a function of time since before BBN, will allow us to analyze the gravitational properties of the models.

5. The reason for a universal screening condition

As we have seen in the examples above, we get the same screening condition for all known models. Below we argue why this is the case for a whole range of models satisfying only some simple assumptions.

We start with the most general model for the behavior of the scalar field in matter

$$\nabla^2 \phi = V_{{\rm eff},\phi} = V_{,\phi} + \frac{\beta(\phi)\rho_m}{m_{\rm Pl}} \tag{57}$$

and we will analyze the standard setup (a spherical body of density ρ_c and radius R embedded in a background of density ρ_∞) under the following assumptions:

(1) The effective potential has a matter dependent minimum $\phi(\rho)$.
(2) For any (physical) solution to the field equation, the mass of the field at $r = 0$, $m_S = m(\phi_S, \rho_c)$, is a

positive monotonically increasing function of the density ρ_c and satisfies[5] $\lim_{\rho_c\to\infty} m(\phi_S(\rho_c), \rho_c) = \infty$.

(3) Outside the body, where $\rho_\infty \ll \rho_c$, and within the Compton wavelength of the field m_∞^{-1} the solution to the field equation is well approximated by $\phi = \phi_\infty + \frac{D}{r}$. This means that a first order Taylor expansion around ϕ_∞ holds outside the body.

Now we can look at the solutions to the field equation under the previous assumptions. The field starts out at some field value $\phi = \phi_S$ inside the body, and close to $r = 0$ the solution can therefore be written

$$\phi = \phi_S + B\left(\frac{\sinh(m_S r)}{m_S r} - 1\right) \tag{58}$$

for some constant B. We can for our purposes, without loss of generality, assume that $B > 0$. Because of our assumption on m_S, for a large enough ρ_c the field must start off very close to the minimum $\phi = \phi_c$ inside the body where the driving force $V_{\text{eff},\phi}$ vanishes. Otherwise the solution ($\sim e^{m_S r}/r$) grows too fast inside the body and overshoots the exterior solution. For a sufficiently large ρ_c the field stays close to ϕ_c almost all the way to[6] $r = R$. It follows from a second order Taylor expansion around ϕ_S that this is guaranteed to be the case as long as

$$\frac{V_{\text{eff},\phi\phi\phi}(\phi_S, \rho_c)(\phi_\infty - \phi_S)}{V_{\text{eff},\phi\phi}(\phi_S, \rho_c) m_S R} \ll 1. \tag{59}$$

When all these conditions are satisfied, there exists a critical solution in the limit $\rho_c \to \infty$ which reads

$$\phi = \phi_c \qquad r < R, \tag{60}$$

$$\phi = \phi_\infty + \frac{(\phi_c - \phi_\infty)R}{r} \qquad r > R, \tag{61}$$

which, apart from the numerical values of ϕ_∞ and ϕ_c, is completely model independent. This critical solution and its implications, for the case of power-law chameleon theories, was discussed in [9]. Another regime which can be described by exact solutions without having to solve model dependent equations is realized when $\phi_\infty \gg \beta_\infty m_{\text{Pl}} \Phi_N$. In this regime the theory is effectively linear and the solution reads

$$\phi = \phi_\infty + \frac{\beta_\infty \rho_c R^2}{6 m_{\text{Pl}}}\left(\frac{r^2}{R^2} - 3\right) \qquad r < R, \tag{62}$$

$$\phi = \phi_\infty - \frac{\beta_\infty \rho_c R^3}{3 m_{\text{Pl}} r} \qquad r > R, \tag{63}$$

where $\beta_\infty = \beta(\phi_\infty)$. This is the same type of solution as found in Newtonian gravity, and the fifth force to gravity ratio on a test mass outside the body is

$$\frac{F_\phi}{F_G} = 2\beta_\infty^2, \tag{64}$$

while for the critical solution we find

$$\frac{F_\phi}{F_G} = 2\beta_\infty^2\left(\frac{|\phi_\infty - \phi_c|}{2\beta_\infty m_{\text{Pl}} \Phi_N}\right). \tag{65}$$

Comparing the two cases we see that the critical solution corresponds to a screened fifth force given that

$$|\phi_\infty - \phi_c| \ll 2\beta_\infty m_{\text{Pl}} \Phi_N, \tag{66}$$

which is exactly the screening condition we have found for chameleons, symmetrons and dilatons by solving the field equation explicitly. It is easy to show that the assumptions we started with do hold for these models. The critical solution, which formally only holds in the limit $\rho_c \to \infty$, will be a good approximation for the case of finite ρ_c as long as the screening condition holds by a good margin. As current local gravity experiments give very tight constraints, if one wants to have cosmological signatures i.e. $\beta_\infty = \mathcal{O}(1)$, then this will be true in most cases.

For the case where $|\phi_\infty - \phi_c| \sim 2 m_{\text{Pl}} \beta_\infty \Phi_N$ we would have to solve the model dependent equation to get accurate solutions. These solutions will interpolate between the two regimes found above, see e.g. [50] for a thorough derivation of chameleon equations in all possible regimes.

C. Cosmological scalar field dynamics

Here we consider the cosmological evolution of the scalar field ϕ in modified gravity models with a minimum of $V_{\text{eff}}(\phi)$ at which the scalar field mass m satisfies $m^2 \gg H^2$. The cosmology of the scalar field is tightly constrained by BBN physics due to the coupling of the scalar field to matter particles. The fact that the scalar field evolves along the minimum of $V_{\text{eff}}(\phi)$ implies that the masses of fundamental particles

$$m_\psi = A(\phi) m_{\text{bare}}, \tag{67}$$

in which m_{bare} is the bare mass appearing in the matter Lagrangian, evolve too. In practice, tight constraints on the time variation of masses since the time of BBN

$$\frac{\Delta m_\psi}{m_\psi} = \beta \frac{\Delta\phi}{m_{\text{Pl}}}, \tag{68}$$

where $\Delta\phi$ is the total variation of the field since BBN, impose that $\Delta m_\psi / m_\psi$ must be less than $\sim 10\%$. At a

[5] As $\rho_c \to \infty$ we have $\phi_S \to \phi_c$; the minimum for the matter density is ρ_c. The reason we explicitly write the limit here instead of taking $\phi_S = \phi_c$ directly is to account for models where $\lim_{\phi\to\phi_c} V_{\text{eff},\phi\phi} = 0$, but where $\lim_{\rho_c\to\infty} V_{\text{eff},\phi\phi}(\phi_S(\rho_c), \rho_c) = \infty$ as can be the case for generalized symmetron models as we shall see later on. Loosely speaking we can state this condition as follows: the mass at the minimum inside the body is increasing with ρ_c.

[6] For chameleons the solution only grows in a thin-shell close to the surface, but for large enough densities the field hardly moves at all.

redshift of order $z_e \approx 10^9$, electrons decouple and give a "kick" [10] to the scalar field which would lead to a large violation of the BBN bound. To avoid this, the field must be close to the minimum of $V_{\rm eff}(\phi)$ before z_e and simply follow the time evolution of the minimum given by

$$\left.\frac{{\rm d}V}{{\rm d}\phi}\right|_{\phi_{\rm min}} = -\beta\frac{\rho_m}{m_{\rm Pl}}. \tag{69}$$

Moreover, the total excursion of the scalar field following the minimum must be small enough. In practice, we will always assume that $|\phi/m_{\rm Pl}| \ll 1$ along the minimum trajectory, implying that the BBN bound for the time dependent minimum is always satisfied. The models are then valid provided the electron kick does not perturb the minimum too much. We analyze this now.

The background evolution of the scalar field is governed by the homogeneous scalar field equation

$$\ddot{\phi} + 3H\dot{\phi} + \frac{{\rm d}V_{\rm eff}}{{\rm d}\phi} = 0. \tag{70}$$

We assume that the contribution of the scalar field to the Hubble rate in the Friedmann equation is negligible until the acceleration of the Universe sets in

$$H^2 = \frac{\rho_{\rm rad} + \rho_m + \rho_\phi}{3m_{\rm Pl}^2}, \tag{71}$$

where

$$\rho_\phi = \frac{1}{2}\dot{\phi}^2 + [A(\phi) - 1]\rho_m + V(\phi). \tag{72}$$

The models that we consider here have a dynamical minimum located at $\phi_{\rm min}(t)$ such that

$$\left.\frac{{\rm d}V_{\rm eff}}{{\rm d}\phi}\right|_{\phi_{\rm min}} = 0. \tag{73}$$

Defining $\delta\phi \equiv \phi - \phi_{\rm min}$, we have for linear perturbations around the minimum

$$\ddot{\delta}\phi + 3H\dot{\delta}\phi + m^2\delta\phi = F, \tag{74}$$

where

$$F = -\frac{1}{a^3}\frac{\rm d}{{\rm d}t}\left[a^3\frac{{\rm d}\phi_{\rm min}}{{\rm d}t}\right]. \tag{75}$$

Using the minimum equation, we find that

$$\dot{\phi}_{\rm min} = \frac{3H}{m^2}\beta A\frac{\rho_m}{m_{\rm Pl}}, \tag{76}$$

and the forcing term is then

$$F = -\frac{3\rho_{m0}a^{-3}}{m_{\rm Pl}}\frac{\rm d}{{\rm d}t}\left[\frac{A\beta H}{m^2}\right]. \tag{77}$$

We must also take into account the kicks that the field receives every time a relativistic species decouples. These kicks correspond to the abrupt variation of the trace of the energy momentum tensor of a decoupling species at the transition between the relativistic and nonrelativistic regimes. The abrupt change of T^μ_μ for the decoupling species happens on a time scale much smaller than one Hubble time and can be modeled out using an "instantaneous kick" approximation [10] where the contribution to the scalar field equation is a δ function. For kicks at the decoupling times t_j, the source term becomes

$$F = -\frac{3\rho_0}{m_{\rm Pl}a^3}\frac{\rm d}{{\rm d}t}\left[\frac{A\beta H}{m^2}\right] - A\beta\sum_j \kappa_j H_j m_{\rm Pl}\delta(t - t_j), \tag{78}$$

where $\kappa_j \approx g_i/g_\star(m_j) \lesssim 1$ depends on the number of relativistic species $g_\star(m_j)$ at time t_j and the number of degrees of freedom of the decoupling species g_j.

Let us now go through the different cosmological eras. During inflation, the Hubble rate is nearly constant and the field is nearly constant.[7] Indeed, the trace of the energy momentum tensor is

$$T \approx -12H^2m_{\rm Pl}^2, \tag{79}$$

in which $\rho_m = -p_m = 3H^2m_{\rm Pl}^2$ is nearly constant in the slow roll approximation. As a result, the source term in the perturbed scalar field equation vanishes, and averaging over the oscillations with the fast period $1/m \ll 1/H$ we have

$$\langle\delta\phi^2\rangle \propto a^{-3}, \tag{80}$$

implying that the field reaches the minimum of the effective potential very rapidly during inflation.

Assuming that reheating is instantaneous and that the field is not displaced during reheating, the field starts in the radiation era at the minimum of the effective potential during inflation. As the minimum has moved to larger values, the field rolls down towards the new minimum, overshooting and then stopping at a value

$$\phi_{\rm overshoot} \approx \phi_{\rm inflation} + \sqrt{6\Omega^i_\phi}m_{\rm Pl}, \tag{81}$$

depending on the initial density fraction Ω^i_ϕ in the scalar field [10]. After this the field is in an undershoot situation where the field is essentially moved according to the kicks

$$\ddot{\phi} + 3H\dot{\phi} = -A\beta\sum_j \kappa_j H_j m_{\rm Pl}\delta(t - t_j). \tag{82}$$

Each kick brings the field to smaller values, with a variation

$$\Delta\phi_j = -\beta_j A_j \kappa_j m_{\rm Pl}, \tag{83}$$

[7]Note the parametrization $m(a) = m_0a^{-r}$ to be introduced below only applies when the scalar field is sourced by the pressureless matter, and does not apply to the inflationary era, in which ϕ remains nearly constant simply because the density of the inflaton does so.

in the radiation era [10]. Although the details depend on the kicks and the initial energy density of the field, we can assume that after all the kicks before BBN, the field is close to the minimum of $V_{\rm eff}(\phi)$. We will assume that this is the case by $z_{\rm ini} \approx 10^{10}$ where the matter density is equivalent to the one in dense bodies on Earth today. If this were not the case then the field would move by

$$\Delta\phi_e = -\beta_e A_e \kappa_e m_{\rm Pl}, \tag{84}$$

when the electron decouples during BBN, and the masses of particles would vary too much during BBN. Note that for the rest of this subsection a subscript e will be used to denote the value of a quantity at the electron decoupling.

Hence viable models must be such that the scalar field remains in the neighborhood of the minimum since well before BBN. In this case, the deviation of the field from the minimum can be easily obtained from

$$\ddot{\delta\phi} + 3H\dot{\delta\phi} + m^2\delta\phi = -\frac{3\rho_{m0}a^{-3}}{m_{\rm Pl}}\frac{\rm d}{{\rm d}t}\left[\frac{A\beta H}{m^2}\right] - A_e\beta_e\kappa_e H_e m_{\rm Pl}\delta(t-t_e), \tag{85}$$

where we only take into account the electron kick. Defining $\delta\phi = a^{-3/2}\psi$, we find that

$$\ddot{\psi} + \left[m^2 + \frac{9w}{4}H^2\right]\psi = -\frac{3\rho_{m0}a^{-3/2}}{m_{\rm Pl}}\frac{\rm d}{{\rm d}t}\left[\frac{A\beta H}{m^2}\right] - A_e\beta_e\kappa_e H_e a_e^{3/2} m_{\rm Pl}\delta(t-t_e). \tag{86}$$

As $m^2 \gg H^2$, the solution is obtained using the WKBapproximation and reads

$$\frac{\delta\phi}{m_{\rm Pl}} = -\frac{9\Omega_{m0}H_0^2}{a^3m^2}\frac{\rm d}{{\rm d}t}\left[\frac{A\beta H}{m^2}\right] - \Theta(t-t_e)A_e\beta_e\kappa_e\frac{H_e}{\sqrt{m_e m}}\frac{a_e^{3/2}}{a^{3/2}}\sin\int_{t_e}^{t} m(t'){\rm d}t', \tag{87}$$

in which the second term is only present when $t > t_e$, Θ being the Heaviside function. We will always assume that β and m vary over cosmological times; hence we have

$$\frac{\rm d}{{\rm d}t}\left[\frac{A\beta H}{m^2}\right] = g(t)\frac{A\beta H^2}{m^2}, \tag{88}$$

in which $g(t)$ is a slowly varying function of time whose value is of order unity. Averaging over the rapid oscillations, we have

$$\frac{\langle\delta\phi^2\rangle}{m_{\rm Pl}^2} = \frac{81\Omega_{m0}^2 g^2 A^2\beta^2}{a^6}\frac{H_0^4}{m_0^4}\frac{m_0^4}{m^4}\frac{H^4}{m^4} + \frac{A_e^2\beta_e^2\kappa_e^2}{2}\frac{a_e^3}{a^3}\frac{H_e^2}{m_e^2}\frac{m_e}{m}. \tag{89}$$

The first term is of order $\beta_0^2 H_0^8/m_0^8 \ll 1$ now, implying that it has a negligible influence on the particle masses. This guarantees that the minimum is indeed a solution of the equations of motion. The second term corresponds to the response of the scalar field to a kick. It is initially very small as suppressed by $H_e^2/m_e^2 \ll 1$, implying a tiny variation of the fermion masses during BBN. Its influence increases with time as $1/ma^3$ and we must impose that this never compensates for the fact that H_e^2/m_e^2 is extremely small.

Consider an interesting example with $m(a) = m_0 a^{-r}$ which will reappear later. In such a case the second term in the above equation can be rewritten as

$$\frac{A_e^2\beta_e^2\kappa_e^2}{2}\frac{a_e^3}{a^3}\frac{H_e^2}{m_e^2}\frac{m_e}{m} \sim \frac{H_0^2}{m_0^2}\frac{\Omega_{r0}}{\Omega_{m0}}a_e^{r-1}a^{r-3}, \tag{90}$$

where we have assumed $A_e^2\beta_e^2\kappa_e^2 \sim \mathcal{O}(1)$ and $\Omega_{r0} \ll \Omega_{m0}$ is the fractional energy density for radiation (photons and massless neutrinos) at present. From this formula we can easily see that

(1) when $r < 3$ the minimum of $V_{\rm eff}$ given by the minimum equation is an attractor, because the magnitude of the oscillation decreases in time;
(2) assuming that $H_0 \sim 10^{-3}m_0$ (see below) and $\Omega_{m0} \sim 10^3\Omega_{r0}$, then today we have $\langle\delta\phi^2\rangle/m_{\rm Pl}^2 \sim 10^{-9}a_e^{r-1}$ which is of order one if $r = 0$. Clearly, for $r \lesssim 2$ the amplitude of oscillation can be too big ($\sqrt{\langle\delta\phi^2\rangle} \gg \phi_{\rm min}$) at early times;
(3) if $r \geq 3$ which is the case for $f(R)$ gravity models in which $f(R) \sim R + R_0 - R_1(R_\star/R)^n$, $\sqrt{\langle\delta\phi^2\rangle}/m_{\rm Pl}$ increases with time but never becomes significantly large. For example, if $r = 3$ then $\sqrt{\langle\delta\phi^2\rangle}/m_{\rm Pl} \sim 10^{-15}$ today, which means that, although the minimum of $V_{\rm eff}(\phi)$ is not strictly speaking an attractor, it is extremely stable to kicks and governs the background dynamics of the model.

D. The equation of state

We have described how the cosmological constraint from BBN imposes that the scalar field must be at the minimum of the effective potential since BBN. As such the minimum of the effective potential acts as a slowly varying cosmological constant. We have also seen that when $m^2 \gg H^2$, a large class of models are such that the minimum is stable. In this case, the dynamics are completely determined by the minimum equation

$$\left.\frac{{\rm d}V}{{\rm d}\phi}\right|_{\phi_{\rm min}} = -\beta A\frac{\rho_m}{m_{\rm Pl}}. \tag{91}$$

In fact, the knowledge of the time evolution of the mass m and the coupling β is enough to determine the time evolution of the field. Indeed, the mass at the minimum of $V_{\rm eff}$,

$$m^2 \equiv \left.\frac{{\rm d}^2V_{\rm eff}(\phi)}{{\rm d}\phi^2}\right|_{\phi_{\rm min}}, \tag{92}$$

and the minimum relation leads to

$$V'' \equiv \frac{\mathrm{d}^2V}{\mathrm{d}\phi^2} = m^2(a) - \beta^2 A(\phi)\frac{\rho_m}{m_{\rm Pl}^2} - \frac{\mathrm{d}\beta}{\mathrm{d}\phi}A(\phi)\frac{\rho_m}{m_{\rm Pl}}, \tag{93}$$

where the couplings to matter β can be field dependent. Using the minimum equation, we deduce that the field evolves according to

$$\frac{\mathrm{d}\phi}{\mathrm{d}t} = \frac{3H}{m^2}\beta A\frac{\rho_m}{m_{\rm Pl}}. \tag{94}$$

This is the time evolution of the scalar field at the background level since the instant when the field starts being at the minimum of the effective potential. In particular, we have

$$\frac{1}{2}\left(\frac{\mathrm{d}\phi}{\mathrm{d}t}\right)^2 = \frac{27}{2}\Omega_m\beta^2A^2\left(\frac{H}{m}\right)^4\rho_m \tag{95}$$

which is tiny compared to ρ_m.

Because of the interaction between the scalar field and matter, the energy momentum tensor of the scalar field is not conserved. Only the total energy momentum

$$\dot{\rho}_{\rm tot} = -3H(\rho_{\rm tot} + p_{\rm tot}) \tag{96}$$

is conserved, where the total energy density is

$$\rho_{\rm tot} \equiv \rho_m + \rho_\phi \tag{97}$$

with

$$\rho_\phi = \frac{\dot{\phi}^2}{2} + V_{\rm eff}(\phi), \tag{98}$$

$$p_{\rm tot} \equiv p_\phi = \frac{\dot{\phi}^2}{2} - V(\phi), \tag{99}$$

and where we have neglected the radiation component in the matter era. It is crucial to notice that the energy density of the scalar field involves the effective potential $V_{\rm eff}$ while the pressure only involves V. This is a crucial feature of scalar-tensor theories.

We can define the effective equation of state of the dark energy fluid as

$$w_\phi = \frac{p_\phi}{\rho_\phi}. \tag{100}$$

Using the Friedmann equation we find the Raychaudhuri equation involving the effective equation of state w_ϕ as

$$\frac{\ddot{a}}{a} = -\frac{1}{6m_{\rm Pl}^2}[\rho_m + (1+3w_\phi)\rho_\phi] \equiv -\frac{1}{6m_{\rm Pl}^2}(1+3w_{\rm tot})\rho_{\rm tot} \tag{101}$$

where we have defined the total equation of state

$$w_{\rm tot} = \frac{p_{\rm tot}}{\rho_{\rm tot}}. \tag{102}$$

The Universe is accelerating provided $\ddot{a} \geq 0$ which leads to

$$w_{\rm tot} \leq -\frac{1}{3} \tag{103}$$

as expected, which is equivalent to

$$w_\phi \leq -\frac{1}{3}\left(1 + \frac{\rho_m}{\rho_\phi}\right). \tag{104}$$

The situation of the modified gravity models can be easily analyzed as

$$w_\phi + 1 = \frac{\dot{\phi}^2 + (A-1)\rho_m}{\frac{\dot{\phi}^2}{2} + V(\phi) + (A-1)\rho_m}, \tag{105}$$

which can be approximated as

$$w_\phi + 1 \approx \frac{\dot{\phi}^2}{V(\phi)} + (A-1)\frac{\Omega_m}{\Omega_\phi}. \tag{106}$$

The first term corresponds to the usual quintessence contribution and the second term can be approximated as $\frac{\beta\phi}{m_{\rm Pl}}\frac{\Omega_m}{\Omega_\phi} \sim -\frac{\beta}{m_{\rm Pl}}\frac{V_{,\phi}}{V_{,\phi\phi}}\frac{\Omega_m}{\Omega_\phi} = 3\beta^2\Omega_m\frac{H^2}{m^2}\frac{\Omega_m}{\Omega_\phi}$. This implies that

$$w_\phi + 1 \approx (A-1)\frac{\Omega_m}{\Omega_\phi} \approx 3\Omega_m\beta^2\left(\frac{H}{m}\right)^2\frac{\Omega_m}{\Omega_\phi}. \tag{107}$$

In the recent past of the Universe where Ω_m and Ω_ϕ have been of the same order of magnitude, this implies that the background scalar field acts as a cosmological constant due to the large H^2/m^2 suppression. In the past, the background cosmology deviates from a ΛCDM model only if Ω_ϕ becomes so small that it compensates for m^2/H^2. We will not consider this situation in the following.

III. MODIFIED GRAVITY TOMOGRAPHY

A. Reconstruction of the dynamics

We have seen that when $m^2 \gg H^2$ a large class of models are such that the minimum of the effective potential is stable or quasistable, and in these cases the dynamics are completely determined by the minimum equation

$$\left.\frac{\mathrm{d}V}{\mathrm{d}\phi}\right|_{\phi_{\rm min}} = -\beta A\frac{\rho_m}{m_{\rm Pl}}. \tag{108}$$

In fact, the knowledge of the time evolution of the mass m and the coupling β is enough to determine the bare potential $V(\phi)$ and the coupling function $A(\phi)$ completely. To see this, integrating Eq. (94) once, we find

$$\phi(a) = \frac{3}{m_{\rm Pl}}\int_{a_{\rm ini}}^{a}\frac{\beta(a)}{am^2(a)}\rho_m(a)\mathrm{d}a + \phi_c, \tag{109}$$

where ϕ_c is the initial value of the scalar field at $a_{\rm ini} < a_{\rm BBN}$ and we have taken $A(\phi) \approx 1$, as the temporal variation of fermion masses must be very weak. If the

coupling β is expressed in terms of the field ϕ and not the scale factor a, this is also equivalent to

$$\int_{\phi_c}^{\phi} \frac{\mathrm{d}\phi}{\beta(\phi)} = \frac{3}{m_{\rm Pl}} \int_{a_{\rm ini}}^{a} \frac{1}{am^2(a)} \rho_m(a) \mathrm{d}a. \tag{110}$$

Similarly the minimum equation implies that the potential can be reconstructed as a function of time

$$V = V_0 - \frac{3}{m_{\rm Pl}^2} \int_{a_{\rm ini}}^{a} \frac{\beta^2(a)}{am^2(a)} \rho_m^2(a) \mathrm{d}a, \tag{111}$$

where V_0 is the initial value of the potential at $a = a_{\rm ini}$. This defines the bare scalar field potential $V(\phi)$ parametrically when $\beta(a)$ and $m(a)$ are given. Hence we have found that the full nonlinear dynamics of the theory can be recovered from the knowledge of the *time* evolutions of the mass and the coupling to matter since before BBN.

B. Tomography

The previous reconstruction mapping gives a one-to-one correspondence between the scale factor a and the value of the field $\phi(a)$ in the cosmic background. As the scale factor is in a one-to-one correspondence with the matter energy density $\rho_m(a)$, we have obtained a mapping $\rho_m \rightarrow \phi(\rho_m)$ defined using the time evolution of $m(a)$ and $\beta(a)$ only. Given these evolutions, one can reconstruct the dynamics of the scalar field for densities ranging from cosmological to Solar System values using Eqs. (109) and (111). By the same token, the interaction potential can be reconstructed for all values of ϕ (and ρ_m) of interest, from the Solar System and Earth to the cosmological background now: a tomography of modified gravity.

In particular, we can now state the screening condition of modified gravity models as

$$\int_{a_{\rm in}}^{a_{\rm out}} \frac{\beta(a)}{am^2(a)} \rho_m(a) \mathrm{d}a \ll \beta_{\rm out} m_{\rm Pl}^2 \Phi_N, \tag{112}$$

with constant matter densities $\rho_{\rm in,out} = \rho_m(a = a_{\rm in,out})$ inside and outside the body respectively, and where we have defined $\beta_{\rm out} \equiv \beta(a = a_{\rm out})$. It is remarkable that the gravitational properties of the screened models are captured by the cosmological mass and coupling functions only.

C. Dilatons

Let us consider a first example: the dilaton models in which the coupling function $\beta(\phi)$ vanishes for a certain value $\phi_\star$ of the scalar field ϕ. On the other hand, we assume that the potential is positive definite and is of runaway type. It is enough to study the dynamics in the vicinity of the field $\phi_\star$, where

$$\beta(\phi) \approx A_2 m_{\rm Pl}(\phi - \phi_\star), \tag{113}$$

from which we deduce that

$$\ln \left| \frac{\phi - \phi_\star}{\phi_c - \phi_\star} \right| = 9A_2 m_{\rm Pl}^2 \Omega_{m0} H_0^2 \int_{a_{\rm ini}}^{a} \frac{\mathrm{d}a}{a^4 m^2(a)}, \tag{114}$$

and therefore

$$|\beta(\phi)| = |\beta(\phi_c)| \exp\left[9A_2 m_{\rm Pl}^2 \Omega_{m0} H_0^2 \int_{a_{\rm ini}}^{a} \frac{\mathrm{d}a}{a^4 m^2(a)} \right]. \tag{115}$$

In particular, we find the relation between the coupling at the initial time and other cosmological times.

The initial coupling (taken at $a_{\rm ini} < a_{\rm BBN}$) is the same as in dense matter on Earth, *as long as* the field minimizes its effective potential in a dense environment, and it is related to the cosmological value of β today, $\beta(\phi_0)$, by

$$|\beta(\phi_0)| = |\beta(\phi_c)| \exp\left[9A_2 m_{\rm Pl}^2 \Omega_{m0} H_0^2 \int_{a_{\rm ini}}^{1} \frac{\mathrm{d}a}{a^4 m^2(a)} \right]. \tag{116}$$

It is possible to have a very small coupling in dense matter $|\beta(\phi_c)| \ll 1$ for any value of the coupling on cosmological scales $|\beta(\phi_0)|$ provided that $A_2 > 0$ and that the time variation of $m(a)$ is slow and does not compensate for the $1/a^4$ divergence in the integrand. In this situation, the coupling function β converges exponentially fast towards zero: this is the Damour-Polyakov mechanism [8]. The fact that $A_2 > 0$ guarantees that the minimum of the coupling function is stable and becomes the minimum of the effective potential which attracts the scalar field in the long time regime. If $A_2 < 0$, the effect of the coupling is destabilizing and implies that ϕ diverges exponentially fast away from $\phi_\star$.

Alternatively, a smooth variation of the coupling function to matter in the cosmological background and therefore interesting consequences for the large-scale structure can be achieved when the evolution of the mass of the scalar field compensates for the $1/a^4$ factor in the radiation era and evolves in the matter era. This is obtained for models with

$$m^2(a) = 3A_2 H^2(a) m_{\rm Pl}^2. \tag{117}$$

Indeed, $H(a) \sim a^{-2}$ in the radiation era, which implies that the time variation of β between BBN and matter-radiation equality is

$$\beta(\phi) = \beta(\phi_c) \exp\left[3 \frac{\Omega_{m0}}{\Omega_{r0}} (a - a_{\rm ini}) \right], \tag{118}$$

and in the matter dominated era

$$\beta(\phi) = \beta(\phi_{\rm eq}) \left(\frac{a}{a_{\rm eq}} \right)^3 = \beta(\phi_{\rm eq}) \frac{\rho_m(a_{\rm eq})}{\rho_m(a)}, \tag{119}$$

where a subscript eq denotes the value of a quantity at the matter-radiation equality. This is the behavior of the dilaton models we have already analyzed gravitationally in § II B 2.

D. Symmetron

In the symmetron models the coupling to matter vanishes identically in dense regions or at redshifts $z > z_\star$, while a larger coupling is obtained after a transition at a redshift $z_\star$ and in the low-matter-density regions. This can be obtained by choosing

$$\beta(a) = \beta_\star \sqrt{1 - \left(\frac{a_\star}{a}\right)^3}, \tag{120}$$

for $z < z_\star$ and $\beta = 0$, $z > z_\star$. Similarly we choose

$$m(a) = m_\star \sqrt{1 - \left(\frac{a_\star}{a}\right)^3}. \tag{121}$$

Using the reconstruction mapping, it is straightforward to find that

$$\phi(a) = \phi_\star \sqrt{1 - \left(\frac{a_\star}{a}\right)^3}, \tag{122}$$

for $z < z_\star$ and $\phi = 0$ before. The potential for $z < z_\star$ as a function of a can then be reconstructed, using the technique introduced above, as

$$V(a) = V_0 + \frac{\beta_\star^2 \rho_\star^2}{2 m_\star^2 m_{\rm Pl}^2}\left[\left(\frac{a_\star}{a}\right)^6 - 1\right], \tag{123}$$

where

$$\rho_\star = \frac{\rho_{m0}}{a_\star^3}, \tag{124}$$

is the matter density at the transition between $\phi(a) = 0$ and $\phi(a) > 0$. The potential as a function of ϕ is then

$$V(\phi) = V_0 + \frac{\lambda}{4}\phi^4 - \frac{\mu^2}{2}\phi^2, \tag{125}$$

where

$$\phi_\star = \frac{2\beta_\star \rho_\star}{m_\star^2 m_{\rm Pl}}, \tag{126}$$

and

$$m_\star = \sqrt{2}\mu, \qquad \lambda = \frac{\mu^2}{\phi_\star^2}, \tag{127}$$

together with

$$\beta(\phi) = \frac{\beta_\star}{\phi_\star}\phi. \tag{128}$$

This completes the reconstruction of the particular symmetron model presented in [16] from $m(a)$ and $\beta(a)$.

E. Generalized symmetrons

With the parametrization developed in this paper it is easy to create new models (in a more intuitive way than starting with the Lagrangian) by changing the mass and coupling functions. Here we give a simple example by generalizing the symmetron models.

We start by generalizing the coupling function Eq. (120)

$$\beta(a) = \beta_\star\left[1 - \left(\frac{a_\star}{a}\right)^3\right]^{1/q}, \tag{129}$$

for $z < z_\star$ and $\beta = 0$ for $z > z_\star$. Similarly we choose

$$m(a) = m_\star\left[1 - \left(\frac{a_\star}{a}\right)^3\right]^{1/p}, \tag{130}$$

where the field evolves as

$$\phi(a) = \phi_\star\left[1 - \left(\frac{a_\star}{a}\right)^3\right]^{1/(m-n)}, \tag{131}$$

where we have defined

$$m = \frac{2(p - q + pq)}{p - 2q + pq}, \qquad n = \frac{2p - 2q + pq}{p - 2q + pq}, \tag{132}$$

and where

$$\phi_\star = \frac{(m - n)\beta_\star \rho_\star}{m_\star^2 m_{\rm Pl}}. \tag{133}$$

Eventually we find

$$V(\phi) = V_0 + \frac{(m - n)\beta_\star^2 \rho_\star^2}{m_\star^2 m_{\rm Pl}^2}\left[\frac{1}{m}\left(\frac{\phi}{\phi_*}\right)^m - \frac{1}{n}\left(\frac{\phi}{\phi_*}\right)^n\right] \tag{134}$$

and

$$\beta(\phi) = \beta_\star\left(\frac{\phi}{\phi_\star}\right)^{n-1}. \tag{135}$$

The indices m and n should be taken to be even integers to keep the potential symmetric around $\phi = 0$. The standard symmetron corresponds to the choice $m/2 = n = 2$.

We can now show explicitly that this generalized symmetron model has the screening property as we did for the original symmetron model in § II B 2. Let us consider a spherically dense body of density ρ_c and radius R embedded in a homogeneous background. The field profile inside the body is

$$\phi = \phi_S \frac{\sinh m_S r}{m_S r}, \qquad r < R \tag{136}$$

where

$$m_S^2 \simeq \left(\frac{d\beta(\phi)}{d\phi}\right)_S \frac{\rho_c}{m_{\rm Pl}} = m_\star^2 \frac{n - 1}{m - n}\frac{\rho_c}{\rho_\star}\left(\frac{\phi_S}{\phi_\star}\right)^{n-2} \tag{137}$$

is the scalar field mass at $r = 0$, ϕ_S the corresponding field value and $\rho_\star$ is as in the symmetron model the critical matter density when the transition of the minimum of $V_{\rm eff}(\phi)$ from $\phi = 0$ to $\phi = \pm\phi_\star$ takes place in the cosmological background.

The field outside the body, on scales shorter than the large range $m_\star^{-1}$, is

$$\phi = \phi_* + \frac{D}{r}, \qquad r > R \tag{138}$$

Matching at $r = R$ gives us the solution

$$\phi_S \cosh(m_S R) = \phi_\star \tag{139}$$

$$D = \phi_\star R\left(\frac{\tanh(m_S R)}{m_S R} - 1\right) \tag{140}$$

The first condition, which determines ϕ_S, can be written

$$\frac{\phi_S}{\phi_\star}\cosh\left[\sqrt{\alpha}\left(\frac{\phi_S}{\phi_\star}\right)^{n/2-1}\right] = 1 \tag{141}$$

where $\alpha = \frac{n-1}{m-n}\frac{\rho_c}{\rho_\star}(m_\star R)^2$. We can change it into a simple equation for $m_S R$

$$(m_S R)^2 \cosh^{n-2}(m_S R) = \alpha \tag{142}$$

From these equations we see that when $\alpha \gg 1$ we get $\phi_S \approx 0$, $m_S R \gg 1$ and therefore $D \approx -\phi_\star R$. Note that if $n > 2$ the mass vanishes at $\phi = 0$; however, this is not a problem for the screening mechanism. Even though a large α pushes the field down towards $\phi = 0$, m_S is still an increasing function of α according to Eq. (142).

The fifth force on a test mass outside the body is found to be screened as long as

$$|\phi_c - \phi_\infty| \ll 2 m_{\rm Pl}\beta_* \Phi_N \tag{143}$$

where $\phi_c = \phi_S \approx 0$ and $\phi_\infty = \phi_\star$. This condition is equivalent to $\alpha \gg 1$ and shows that the screening property is present in this model.

Comparing the case $n = 2$ with $n > 2$ we find that even though $\phi_S/\phi_\star$ is larger in the latter case, the coupling $\beta(\phi_S)$ is smaller as long as we have screening. This means that the force between two test masses in a dense environment is more screened for larger n. Local constraints for the generalized symmetrons are therefore satisfied for (at least) the same range as the standard symmetron: $m_0/H_0 \gtrsim 10^3$.

IV. RECONSTRUCTING $f(R)$ MODELS

A. Gravity tests and chameleons

Consider now the important case of a nonvanishing coupling function $\beta(a)$. Defining $\beta(a) = \beta_0 g(a)$ and $m = m_0 f(a)$, we find that

$$\frac{\phi - \phi_c}{m_{\rm Pl}} = 9\beta_0\Omega_{m0}\frac{H_0^2}{m_0^2}\int_{a_{\rm ini}}^{a} {\rm d}a\,\frac{g(a)}{a^4 f^2(a)}, \tag{144}$$

which allows one to test the screening properties of these models.

Let us first consider the Solar System tests. Evaluating Eq. (144) in the Galactic background, we find that[8]

$$\frac{\phi_{\rm gal} - \phi_c}{m_{\rm Pl}} = 9\beta_0\Omega_{m0}\frac{H_0^2}{m_0^2}\int_{a_{\rm ini}}^{a_{\rm gal}} {\rm d}a\,\frac{g(a)}{a^4 f^2(a)}, \tag{145}$$

where $a_{\rm gal} \approx 10^{-2}$ is the scale factor when the matter density in the cosmological background equals the Galactic density $\rho_{\rm gal} \approx 10^6 \rho_c$. Defining

$$\frac{\Delta R}{R} = \frac{\phi_{\rm gal} - \phi_c}{6 m_{\rm Pl}\beta_c \Phi_\odot}, \tag{146}$$

where R is the radius of a spherical body, the modification of gravity in the Solar System has a strength

$$2\beta_{\rm gal}\beta_c\frac{3\Delta R_\odot}{R_\odot}. \tag{147}$$

In this expression $\beta_{\rm gal}$ is the value of the coupling function $\beta(\phi)$ in the Galactic background, $\Phi_\odot$ is the value of the Solar Newtonian potential ($\Phi_\odot \sim 10^{-6}$) and β_c is the coupling inside a dense body. The magnitude should be less than 10^{-5} to comply with the Cassini bound in the Solar System [47]. This condition is independent of β_c and reads

$$\beta_0\beta_{\rm gal}\int_{a_{\rm ini}}^{a_{\rm gal}} {\rm d}a\,\frac{g(a)}{a^4 f^2(a)} \lesssim 10^{-5}\frac{m_0^2}{9\Omega_{m0}H_0^2}\Phi_\odot. \tag{148}$$

The integral

$$I \equiv \int_{a_{\rm ini}}^{a_{\rm gal}} {\rm d}a\,\frac{g(a)}{a^4 f^2(a)}, \tag{149}$$

is potentially divergent for small values of $a_{\rm ini} \sim 10^{-10}$. Hence we must impose that $f(a)^2/g(a)$ compensates the $1/a^4$ divergence in the integrand. As mentioned above, we have assumed that galaxies are screened to minimize the disruption of their dynamics, although the necessity of this condition should be ascertained using N-body simulations [30]. Enforcing the screening condition imposes

$$|\phi_{\rm gal} - \phi_0| \lesssim 6\beta_0 m_{\rm Pl}\Phi_{\rm gal}, \tag{150}$$

in which the Galactic Newtonian potential is $\Phi_{\rm gal} \sim 10^{-6}$ and

$$\frac{\phi_0 - \phi_{\rm gal}}{m_{\rm Pl}} = 9\beta_0\Omega_{m0}\frac{H_0^2}{m_0^2}\int_{a_{\rm gal}}^{1} {\rm d}a\,\frac{g(a)}{a^4 f^2(a)}. \tag{151}$$

A slightly stronger bound is obtained from the Lunar Ranging experiment [46] with the 10^{-5} on the right-hand side of Eq. (148) replaced by 10^{-7}.

Strong constraints can also be obtained from laboratory experiments. Using the fact that the initial matter density at $z_{\rm ini} \sim 10^{10}$ is roughly the same as that in a typical test mass in the laboratory, gravity is not modified provided test bodies are screened, i.e.,

$$|\phi_{\rm lab} - \phi_c| \lesssim 2\beta_c m_{\rm Pl}\Phi_{\rm lab}, \tag{152}$$

where $\Phi_{\rm lab} \sim 10^{-27}$ for typical test bodies in cavity experiments of size L, and $\phi_{\rm lab} = \phi(a_{\rm lab})$ is determined by $m(a_{\rm lab}) \sim 1/L$ (see the Appendix for more details).

[8]Again, here for simplicity we have assumed that the scalar field minimizes $V_{\rm eff}(\phi)$ in the Galactic background. While this is true for a certain parameter space, in general it should be tested against numerical simulations.

B. $f(R)$ Gravity reconstruction

Viable $f(R)$ models are nothing but chameleons [31] with a constant value of the coupling function $\beta(\phi) = 1/\sqrt{6}$. We have already described the background dynamics of these models. Here we shall derive the mapping between the evolution of the scalar field mass $m(a)$ and the function $f(R)$ for curvature values ranging from the ones in dense bodies to cosmological ones. These models are equivalent to chameleon models where the potential is given by[9]

$$V(\phi) = m_{\rm Pl}^2 \frac{Rf_R - f}{2f_R^2} \tag{153}$$

in which $f_R = {\rm d}f/{\rm d}R$. The mapping between R and ϕ is given by

$$f_R = \exp\left(-2\beta\frac{\phi}{m_{\rm Pl}}\right). \tag{154}$$

Given the mass function $m(a)$, we have

$$\phi(a) = 9\beta\Omega_{m0}H_0^2 m_{\rm Pl}\int_{a_{\rm ini}}^{a}\frac{{\rm d}a}{a^4 m^2(a)} + \phi_c, \tag{155}$$

and

$$V = V_0 - 3\int_{a_{\rm ini}}^{a}\frac{\beta^2}{am^2(a)}\frac{\rho_m^2(a)}{m_{\rm Pl}^2}\,{\rm d}a. \tag{156}$$

We can reconstruct $R(a)$ using the fact that

$$R(\phi) = -e^{(2\beta(\phi/m_{\rm Pl}))}\frac{1}{\beta m_{\rm Pl}}\frac{\rm d}{{\rm d}\phi}[e^{(-4\beta(\phi/m_{\rm Pl}))}V(\phi)], \tag{157}$$

and $f(R)$ using

$$f(R) = R(\phi)e^{(-2\beta(\phi/m_{\rm Pl}))} - \frac{2}{m_{\rm Pl}^2}e^{(-4\beta(\phi/m_{\rm Pl}))}V(\phi), \tag{158}$$

which is equivalent to

$$f(R) = \frac{2}{m_{\rm Pl}^2}e^{(-4\beta(\phi/m_{\rm Pl}))}V(\phi) - \frac{1}{\beta m_{\rm Pl}}e^{(-4\beta(\phi/m_{\rm Pl}))}\frac{{\rm d}V}{{\rm d}\phi}, \tag{159}$$

once we have obtained $V(\phi)$ from the above implicit parametrization.

When $\beta\phi/m_{\rm Pl} \ll 1$ as required from the BBN constraints, the above equations can be simplified and read

$$f(R) = R - 2\frac{V(\phi)}{m_{\rm Pl}^2} \tag{160}$$

where

$$R(\phi) = -\frac{1}{\beta m_{\rm Pl}}\frac{{\rm d}V}{{\rm d}\phi} + \frac{4}{m_{\rm Pl}^2}V(\phi). \tag{161}$$

This is the parametric reconstruction mapping of $f(R)$ models.

C. Large curvature $f(R)$ models

We can apply these results to the case with $m = m_0 a^{-r}$ leading to models where

$$\frac{\phi - \phi_c}{m_{\rm Pl}} = \frac{9\Omega_{m0}\beta H_0^2}{(2r-3)m_0^2}a_{\rm ini}^{2r-3}\left[\left(\frac{a}{a_{\rm ini}}\right)^{2r-3} - 1\right], \tag{162}$$

which reduces to

$$\frac{\phi - \phi_c}{m_{\rm Pl}} = \frac{9\Omega_{m0}\beta H_0^2}{(2r-3)m_0^2}a^{2r-3} \tag{163}$$

at late times. Similarly we have

$$V(a) = V_0 - \frac{3\beta^2\rho_{m0}^2}{2(r-3)m_{\rm Pl}^2 m_0^2}(a^{2r-6} - a_{\rm ini}^{2r-6}). \tag{164}$$

Now for late enough times we have

$$V = V_0 - C\left[\frac{\phi - \phi_c}{m_{\rm Pl}}\right]^{(2(r-3)/(2r-3))} \tag{165}$$

for a constant C. Notice that for $3/2 < r < 3$, these models are chameleons with an inverse power-law potential $V(\phi) \sim \phi^{-n}$ with

$$n = 2\frac{3-r}{3-2r}. \tag{166}$$

We can equivalently find that

$$R(\phi) \approx \frac{2C}{\beta m_{\rm Pl}^2}\frac{r-3}{2r-3}\left[\frac{\phi - \phi_c}{m_{\rm Pl}}\right]^{-(3/(2r-3))} + 4\frac{V_0}{m_{\rm Pl}^2}. \tag{167}$$

Finally we find that

$$f(R) = R - \frac{2}{m_{\rm Pl}^2}\left[V_0 + C\left(\frac{R - 4\frac{V_0}{m_{\rm Pl}^2}}{R_\star}\right)^{-n}\right], \tag{168}$$

where $R_\star = 2(r-3)C/[(2r-3)\beta m_{\rm Pl}^2]$ and

$$n = \frac{2}{3}(r-3). \tag{169}$$

Large curvature models are defined for $r > 3$ here. This completes, in this particular example, the reconstruction of the $f(R)$ models from the knowledge of the function $m(a)$.

The gravitational constraints for these models have been fully analyzed in [5]. We have summarized these constraints in Fig. 1 where we see that the strongest constraints on the range of the scalar interaction arise for $r \lesssim 3$, i.e., for inverse power-law chameleon models. For $r \gtrsim 3$, i.e., for large curvature $f(R)$ models, the screening of the

[9] In the discussion of $f(R)$ gravity we shall use R to denote the Ricci scalar.

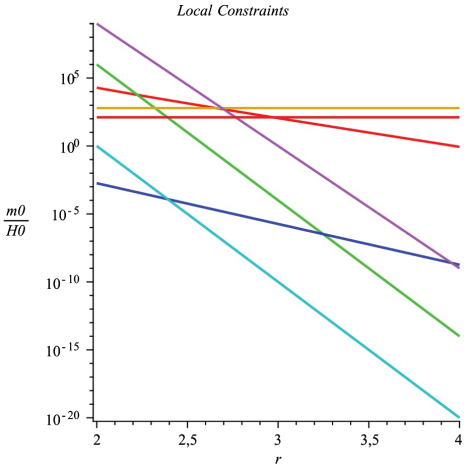

FIG. 1 (color online). The constraints on m_0/H_0 as a function of r for $\beta_0 = 1/\sqrt{6}$ and $s = 0$. Valid models must be above the (listed from top to bottom at $r = 2$) mauve (cavity), green ($m > H$), red (solar system), brown (galaxy), light red ($\dot{\mu}$), and cyan ($mL \gtrsim 1$) lines. The blue line (bottom line at $r = 2$) gives the detectability of effects on the CMB by the Planck satellite. The strongest constraints are the cavity and galactic bounds for small and large r respectively. Models with $r \gtrsim 3$ satisfy the constraints and can lead to a modified gravity regime on large scales.

Milky Way is a loose constraint which needs to be further analyzed with N-body simulations.

D. Comparison with the B parametrization

The $f(R)$ theories are generally parametrized using [28]

$$B = \frac{f_{RR}}{f_R} H \frac{\mathrm{d}R}{\mathrm{d}H}, \tag{170}$$

and $f_R - 1$ now. As $\phi/m_{\rm Pl} \ll 1$ we have that

$$f_R - 1 = -2\beta \frac{\phi}{m_{\rm Pl}}, \tag{171}$$

allowing one to reconstruct the field history entirely:

$$f_R - f_{R0} = 18\beta^2 \Omega_{m0} H_0^2 \int_a^1 \frac{1}{a^4 m^2(a)}\, \mathrm{d}a, \tag{172}$$

which depends on the mass evolution uniquely. This can be rewritten using the B function. In fact, using

$$\frac{\mathrm{d}H}{H} = -\frac{3}{2}(1+w) H \mathrm{d}t, \tag{173}$$

in an era dominated by a fluid of equation of state w, we find that

$$B = -\frac{f_{RR}}{f_R} \frac{2}{3(1+w)} \frac{\dot{R}}{H}. \tag{174}$$

With $f_R = e^{(-2\beta(\phi/m_{\rm Pl}))}$ we have

$$f_{RR} \frac{\mathrm{d}R}{\mathrm{d}t} = -2\beta \frac{f_R}{m_{\rm Pl}} \frac{\mathrm{d}\phi}{\mathrm{d}t} \tag{175}$$

and therefore

$$B = \frac{4\beta}{3(1+w) m_{\rm Pl}} \frac{\mathrm{d}\phi}{H \mathrm{d}t}, \tag{176}$$

and using the minimum equation we get

$$B = \frac{6\beta^2}{1+w} \Omega_m \frac{H^2}{m^2}. \tag{177}$$

Because $\beta = 1/\sqrt{6}$, in the matter dominated era this gives

$$B = \Omega_m \frac{H^2}{m^2}, \tag{178}$$

which is completely determined by $m(a)$. Hence we find that

$$f_R - f_{R0} = 3 \int_a^1 \frac{B(a)}{a}\, \mathrm{d}a. \tag{179}$$

The knowledge of $B(a)$ and f_{R0} determines the background evolution in the $f(R)$ gravity models in a completely equivalent way to the $m(a)$ parametrization.

V. GROWTH OF LARGE-SCALE STRUCTURE

We have shown that the nonlinear structure of the screened models can be reconstructed from the knowledge of the mass and coupling functions. These functions are *time dependent* only. In particular, we have seen that this allows one to *fully* analyze the gravitational tests and the cosmological background evolution. Moreover we have shown that the cosmological dynamics typically is indistinguishable from a ΛCDM model at the background level. Here we will find that this is not the case at the perturbative level and that the mass and coupling function allow a full description of the linear and nonlinear regimes.

A. Linear structure growth

The linear perturbation equations for a scalar field coupled to matter particles are listed in [51] in the covariant and gauge invariant formalism. Denoting by Δ_m the density contrast of the pressureless matter, v_m its velocity and $\delta\phi$ the perturbation[10] in the scalar field, their evolution equations are as follows:

$$\Delta_m'' + \frac{a'}{a}\Delta_m' - \frac{1}{2}\frac{\rho_m}{m_{\rm Pl}^2} a^2 \Delta_m + k\beta(a) m_{\rm Pl}^{-1} (k\delta\phi - \phi' v_m) = 0, \tag{180}$$

[10]Note that this is different from above, where we used $\delta\phi$ to denote the oscillation of the background ϕ around $\phi_{\rm min}(t)$.

$$v_m' + \frac{a'}{a} v_m + \beta(a) m_{\rm Pl}^{-1} (\phi' v_m - k\delta\phi) = 0, \qquad (181)$$

$$\delta\phi'' + 2\frac{a'}{a}\delta\phi' + [k^2 + a^2 m^2(a)]\delta\phi + \beta(a)\frac{\rho_m}{m_{\rm Pl}} a^2 \Delta_m + k\phi' \mathcal{Z} = 0, \qquad (182)$$

where a prime denotes the derivative with respect to the conformal time, $k\mathcal{Z} = \Psi'$ in the Newtonian gauge is a variable of the curvature perturbation which is irrelevant for our discussion since it is multiplied by $\phi'/m_{\rm Pl} \ll \mathcal{H} = a'/a$, and we have neglected contribution from radiation as we are focusing on late times.

Neglecting the terms proportional to ϕ' in the above equations we get the following equation [10]

$$\Delta_m'' + \frac{a'}{a}\Delta_m - \frac{1}{2}\frac{\rho_m}{m_{\rm Pl}^2} a^2 \Delta_m \left[1 + \frac{2\beta^2(a)}{1 + \frac{a^2 m^2(a)}{k^2}}\right] = 0, \qquad (183)$$

where we have used the fact that, given that in Eq. (182) the term $k^2 + a^2 m^2 \gg \mathcal{H}^2$, $\delta\phi$ follows the solution

$$\delta\phi \approx -\frac{\beta(a)}{k^2 + a^2 m^2(a)} \frac{\rho_m}{m_{\rm Pl}} a^2 \Delta_m, \qquad (184)$$

and rapidly oscillates around it (see more details below).

On very large scales, $k \ll am(a)$, we can see that Eq. (183) reduces to

$$\Delta_m'' + \frac{a'}{a}\Delta_m - \frac{1}{2}\frac{\rho_m}{m_{\rm Pl}^2} a^2 \Delta_m = 0, \qquad (185)$$

which governs the growth of matter density perturbation in the ΛCDM model. The effect of modified gravity is incorporated in the second term in the brackets of Eq. (183) and becomes significant when $am(a)/k \lesssim 1$, namely for a light scalar field mass $m(a)$ or on small length scales. For all models shown here the cosmic microwave background (CMB) radiation spectrum is the same as the ΛCDM prediction, because the scales relevant for the CMB are very large and therefore not affected by the modified gravity.

In order to illustrate these considerations, we have computed the linear matter power spectra $P(k)$ for a number of generalized chameleon (Fig. 2) and symmetron (Fig. 3) models.

For the generalized chameleon models, we have used

$$m = m_0 a^{-r}, \qquad \beta = \beta_0 a^{-s} \qquad (186)$$

The impact of gravity tests for $\beta = 1/\sqrt{6}$, $s = 0$ have been given in Fig. 1. There we can see that values of $r \gtrsim 3$ are favored by the local gravity tests. We have varied the four parameters in the parametrization of $\beta(a)$ and $m(a)$: β_0, r, s and m_0. Because m_0 is not dimensionless, we have defined a new variable $\xi \equiv H_0/m_0$ instead. We find the following results, all as expected:

(1) increasing the coupling β_0 strengthens the modification of gravity, which causes more matter clustering, resulting in a higher matter power spectrum;
(2) r characterizes how fast the scalar field mass decreases in time: the higher r the faster it decays. Given that m_0 is fixed, a higher value of r means that the Compton wavelength (essentially the range of the modification to gravity) decreases faster in the past, and therefore the modification of gravity starts to take effect later—this would mean less matter clustering;
(3) s specifies how fast the coupling function changes in time: $s = 0$ implies $\beta(a)$ remains constant, while $s > 0$ ($s < 0$) means $\beta(a)$ decreases (increases) in time. If β_0 is fixed, the larger s is, the larger $\beta(a)$ becomes at high redshifts—this would mean a stronger modification to gravity and stronger matter clustering;
(4) ξ specifies how heavy the scalar field is, or equivalently the range of the modification of gravity: smaller ξ means shorter Compton length of the scalar field, and therefore weaker matter clustering.

The potential of the generalized symmetron models has been given in Eqs. (132) and (134), but one should be careful that the parameters p, q (or equivalent n, m) cannot take arbitrary values. For example, ϕ^n might not be well defined if $\phi < 0$. Here let us consider the special case with $p = 2$ ($n = 2$, $m = 2 + q$), in which the potential becomes

$$V(\phi) = V_0 + \frac{q\beta_\star^2 \rho_\star^2}{m_\star^2 m_{\rm Pl}^2}\left[\frac{1}{2+q}\left[\frac{\phi}{\phi_*}\right]^{2+q} - \frac{1}{2}\left[\frac{\phi}{\phi_*}\right]^2\right] \qquad (187)$$

and this avoids the situation in which the scalar field becomes massless at $\phi = 0$. Furthermore, choosing $q = 2, 4, 6, \cdots$ not only ensures that ϕ^{2+q} is well defined for any value of ϕ, but also makes the potential symmetric about $\phi = 0$, as in the original symmetron model. Finally, with $p = 2$ another property of the original symmetron model, that $\beta(\phi) \propto \phi$, is preserved as well.

Again, the results in Fig. 3 are as expected:

(1) increasing $a_\star$ implies that the modification of gravity starts to take effect at a later time, and this will weaken the matter clustering;
(2) increasing $\beta_\star$ increases the coupling strength overall, and leads to stronger matter clustering;
(3) increasing q increases $\beta(a)$ for $a > a_\star$ and causes stronger structure growth;
(4) decreasing ξ, as in the chameleon case, decreases the range of the modification of gravity, and therefore leads to less matter clustering.

Before we finish this subsection, let us come back to the evolution of the scalar field perturbation $\delta\phi$. As explained above, an analytic approximation to this can be obtained in Eq. (184). However, as for the background evolution,

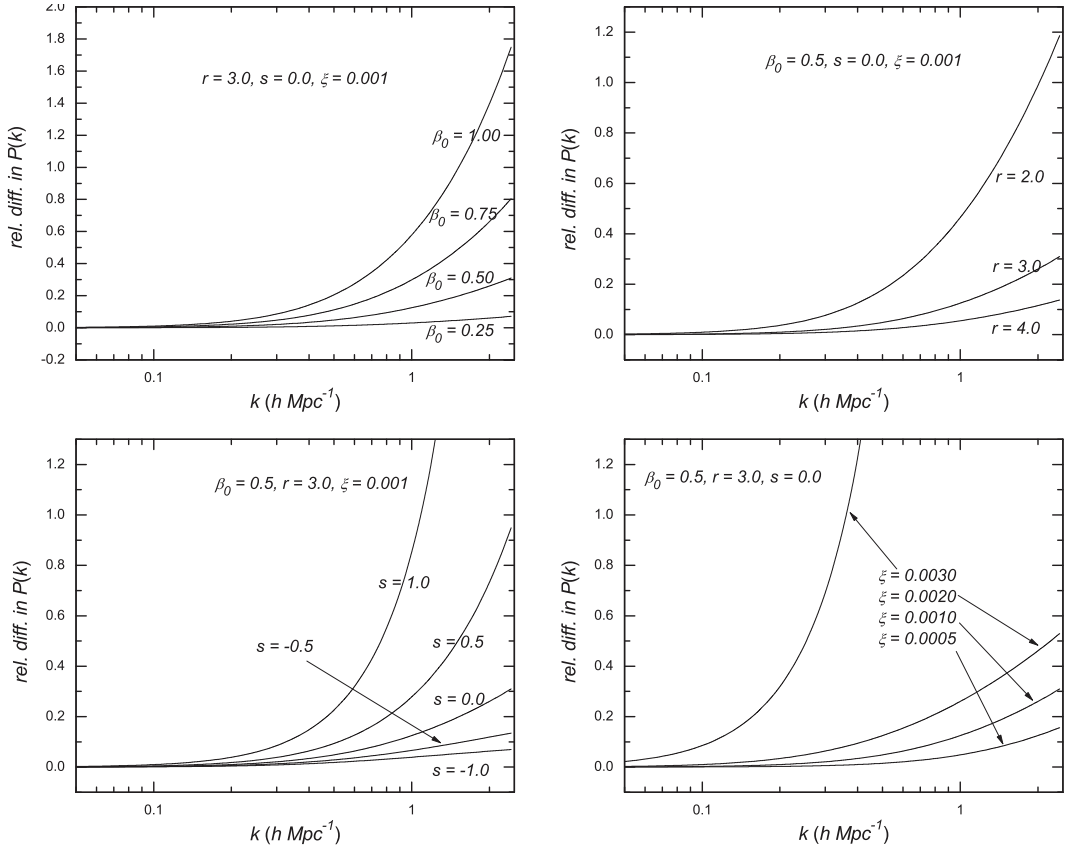

FIG. 2. The relative difference of the matter power spectrum $P(k)$ in the chameleon model from that in the ΛCDM model with exactly the same background expansion history, initial conditions and physical parameters. Upper left panel: The dependence of the result on the modified gravity parameter β_0. Upper right panel: The dependence of the result on the parameter r. Lower left panel: The dependence of the result on the parameter s. Lower right panel: The dependence of the result on the parameter $\xi \equiv H_0/m_0$.

where ϕ oscillates quickly around $\phi_{\rm min}(t)$, we may expect that the true value of $\delta\phi$ oscillates around the analytic solution as well. This is confirmed in Fig. 4.

In the model shown in Fig. 4 we have chosen $r = 3.0$. Obviously, the larger r is, the larger the scalar field mass $m(a)$ becomes at early times. A rapid decrease of $m(a)$ would mean that the effective potential for $\delta\phi$ changes its steepness very quickly. Suppose the oscillation of $\delta\phi$ has some initial kinetic energy, then as the effective potential becomes less steep the amplitude of the oscillations increases since the kinetic energy does not disappear quickly. Consequently, if we increase r further we get even stronger oscillations and if, in contrast, we decrease r then the oscillations become weaker. We have checked explicitly that for $r = 1.0$ there is essentially no oscillation.

At late times $H_0/m_0 = \xi \sim 10^{-3}$, which implies that the period of the oscillation is roughly 10^{-3} the Hubble time, and is much longer than the typical time scales for human observations. As a result, one cannot average $\delta\phi$ over several periods to get $\langle\delta\phi\rangle$. Indeed, as the amplitude of oscillation in Fig. 4 is bigger than the analytic solution of $\delta\phi$ in Eq. (184), the value of $\delta\phi$ one observes at a given time is rather random and could be far from the one given in Eq. (184). This is the case for the $f(R)$ gravity model in [30], where $r = 4.5$.

Whilst this seems to be a problem, this is not really the case. Indeed in the Solar System the matter density is so high that the oscillation is faster than it is in the cosmological background, and we actually observe the averaged value $\langle\delta\phi\rangle$. On linear scales, as $\delta\phi$ oscillates, overshooting and undershooting the value given in Eq. (184), we have checked by replacing the numerical solution of $\delta\phi$ by the analytical formula given in Eq. (184) that we obtain identical power spectra $P(k)$ in the two approaches.

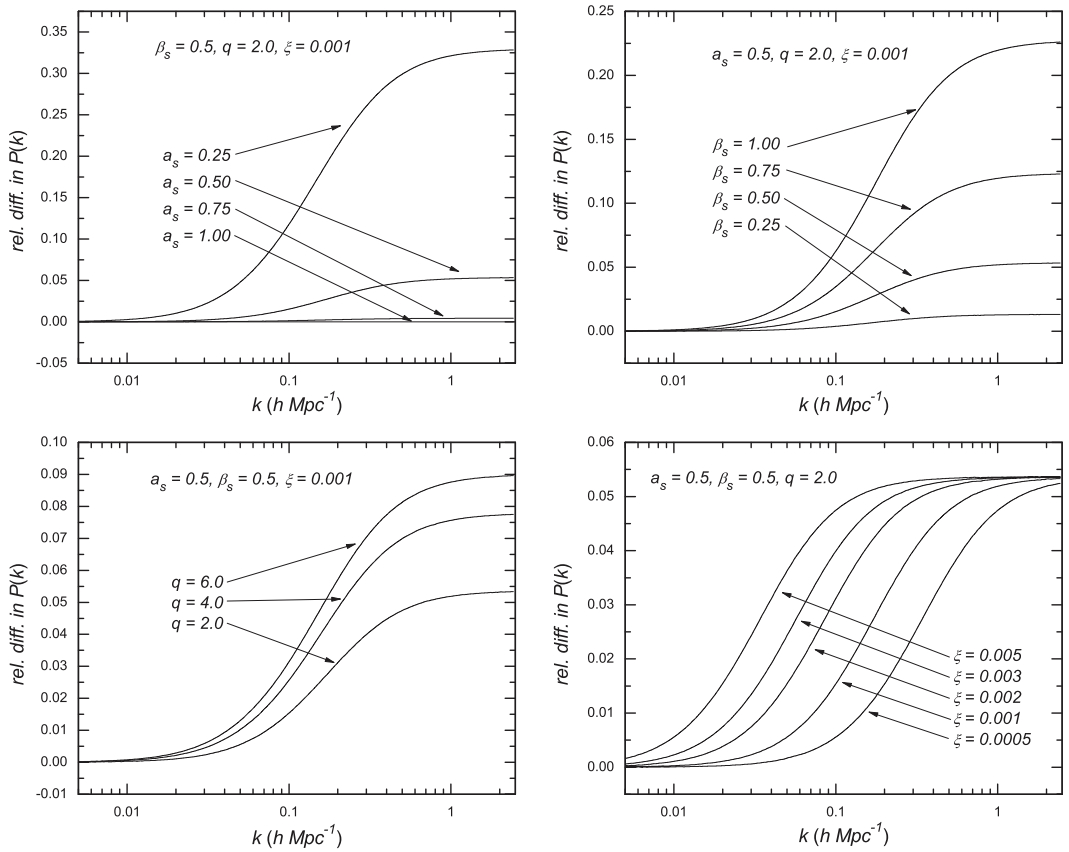

FIG. 3. The relative difference of the matter power spectrum $P(k)$ in generalized symmetron models from that in the ΛCDM model with exactly the same background expansion history, initial conditions and physical parameters. Upper left panel: The dependence of the result on the parameter $a_\star$ (the scale factor value at which the symmetry breaking of the effective potential happens). Upper right panel: The dependence of the result on the modified gravity parameter $\beta_\star$. Lower left panel: The dependence of the result on the parameter q. Lower right panel: The dependence of the result on the parameter $\xi \equiv H_0/m_\star$. As an example we have chosen $p = 2$.

Hence the mean value solution Eq. (184) gives a very good description of the statistical properties of linear perturbations.

B. The Jordan frame picture

In this section we compare our results with a simple and effective way of parametrizing linear perturbations which has been used in the literature in the past few years [38–45] (other interesting and more general approaches for the linear regime include the parametrized post-Friedmann framework of [36,37] and the fully covariant parametrization of [52–54]). Such a way of parametrizing any modification of gravity utilizes two arbitrary functions $\mu(k, a)$ and $\gamma(k, a)$ through the (modified) Poisson equation

$$-k^2\Psi = 4\pi\mu(k, a)G_N a^2\delta\rho_m, \tag{188}$$

and the slip relation

$$\Phi = \gamma(k, a)\Psi. \tag{189}$$

Here G_N is the bare Newton constant, and Ψ and Φ are the two gravitational potentials in the Newtonian gauge:

$$\mathrm{d}\tilde{s}^2 = -a^2(1 + 2\Psi)\mathrm{d}\eta^2 + a^2(1 - 2\Phi)\mathrm{d}x^2, \tag{190}$$

in which (η, x) are the conformal time and comoving coordinates.

So far we have focused on the Einstein frame. In the Jordan frame as described by the line element above, the perturbative dynamics can be described using two Newtonian potentials where we have the relation

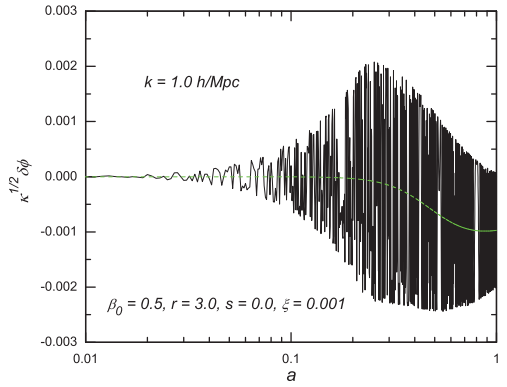

FIG. 4 (color online). An illustration of the time evolution of the scalar field perturbation $\delta\phi$. The black solid curve is the numerical solution while the green dashed curve is the analytical approximation given in Eq. (184). The results here are for $k = 1\ h\mathrm{Mpc}^{-1}$ but the qualitative feature remains for other values of k. The modified gravity parameters are shown beside the curves.

$$\mathrm{d}\tilde{s}^2 = A^2(\phi)\mathrm{d}s^2, \tag{191}$$

and ds^2 is the line element in the Einstein frame expressed in the Newtonian gauge. Expanding in perturbation around a background value with $A[\phi(t)] \approx 1$, we can relate these two potentials to the Einstein frame Newton potential

$$\Psi = \Phi_N + \beta\frac{\delta\phi}{m_{\rm Pl}}, \qquad \Phi = \Phi_N - \beta\frac{\delta\phi}{m_{\rm Pl}}. \tag{192}$$

Hence we see that in the Jordan frame the two Newtonian potentials are not equal, a fact which can be interpreted as resulting from the existence of a nonanisotropic stress contribution coming from the scalar field. It is useful to define

$$\epsilon(k, a) = \frac{2\beta^2}{1 + \frac{m^2a^2}{k^2}}. \tag{193}$$

Using the definitions in Eq. (192), the analytical approximation for $\delta\phi$ in Eq. (184) and the Poisson equation

$$-k^2\Phi_N = \frac{1}{2}\frac{\rho_m}{m_{\rm Pl}^2}a^2\Delta_m, \tag{194}$$

it can be derived easily that

$$\gamma(k, a) \equiv \frac{\Phi}{\Psi} = \frac{1 - \epsilon(k, a)}{1 + \epsilon(k, a)}, \qquad \mu(k, a) = 1 + \epsilon(k, a). \tag{195}$$

These results are valid for all the models which can be described by a field tracking the minimum of the effective potential since before BBN. More precisely we find that

$$\mu(k, a) = \frac{(1 + 2\beta^2)k^2 + m^2a^2}{k^2 + m^2a^2}, \qquad \gamma(k, a) = \frac{(1 - 2\beta^2)k^2 + m^2a^2}{(1 + 2\beta^2)k^2 + m^2a^2}. \tag{196}$$

These are closely related to the popular parametrization of modified gravity used in the literature. Here they are valid for any model of modified gravity at the linear level of cosmological perturbations as long as the background cosmology is described by a scalar field slowly evolving in time and following the time dependent minimum of the effective potential where $m^2 \gg H^2$.

As a numerical illustration, in Fig. 5 we have compared the function $\gamma(a, k)$ calculated using three different methods: (1) the full numerical solution as shown by the black solid curve, (2) the value obtained by using the definitions in Eq. (192), the analytical approximation for $\delta\phi$ in Eq. (184) and Φ_N solved from the Poisson equation numerically (the red dashed curve) and (3) Eq. (196) as shown by the blue dotted curve. We can see that the latter two agree with each other very well, showing that the parametrization given in Eq. (196) works very well in practice and describes the statistical properties of linear perturbations.

The full numerical solution, however, again shows the oscillating behavior, but the oscillation always centers around the averaged value defined by the previous formulas. As discussed earlier, over many oscillations there will be a cancellation and the net effect on a statistical observable today is the same for all three curves.

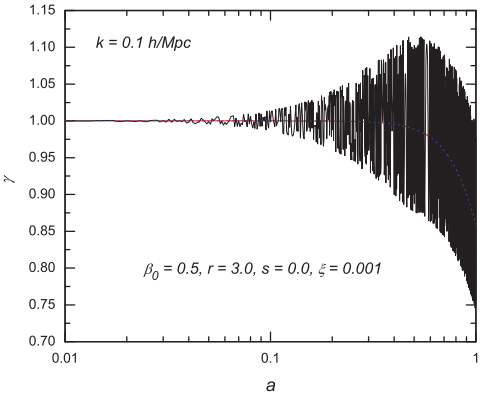

FIG. 5 (color online). The time evolution of $\gamma(k, a)$ for a chosen value of $k = 0.1\ h\mathrm{Mpc}^{-1}$ as an illustration. The black solid is the full numerical solution, the red dashed curve is obtained using the numerical value of Φ_N using the analytical solution of $\delta\phi$ given in Eq. (184), while the blue solid curve is Eq. (196). The modified gravity parameters are shown beside the curves.

C. $f(R)$ gravity in the Jordan frame

Let us concentrate now on the case of $f(R)$ gravity. The perturbations are then determined by

$$\mu(k,a) = \frac{\frac{4}{3}k^2 + m^2a^2}{k^2 + m^2a^2}, \qquad \gamma(k,a) = \frac{\frac{2}{3}k^2 + m^2a^2}{\frac{4}{3}k^2 + m^2a^2}. \tag{197}$$

For large curvature models with $m = m_0 a^{-r}$, this becomes

$$\mu(k,a) = \frac{\frac{4}{3}\frac{k^2}{m_0^2}a^{3n+4} + 1}{\frac{k^2}{m_0^2}a^{3n+4} + 1}, \qquad \gamma(k,a) = \frac{\frac{2}{3}\frac{k^2}{m_0^2}a^{3n+4} + 1}{\frac{4}{3}\frac{k^2}{m_0^2}a^{3n+4} + 1}. \tag{198}$$

When $n = \frac{2}{3}(r-3) \ll 1$, we retrieve the phenomenological parametrization [40]

$$\mu(k,a) \approx \frac{\frac{4}{3}\frac{k^2}{m_0^2}a^4 + 1}{\frac{k^2}{m_0^2}a^4 + 1}, \qquad \gamma(k,a) = \frac{\frac{2}{3}\frac{k^2}{m_0^2}a^4 + 1}{\frac{4}{3}\frac{k^2}{m_0^2}a^4 + 1}. \tag{199}$$

Our parametrization in Eq. (196) covers all the possible $f(R)$ models.

D. Nonlinear effects

Matter clustering on galactic and cluster scales is an important probe of modified gravity. The nonlinearity in both the structure formation process and the dynamics of the scalar field for scales $k \gtrsim 0.1\ h\mathrm{Mpc}^{-1}$ require full numerical simulations [55,56].

The $\beta(a)$, $m(a)$ parametrization can completely specify the nonlinear dynamics of ϕ with two temporal functions. Indeed, as we have seen above, one can reconstruct the potential $V(\phi)$ and the coupling function together with the background evolution $\phi(a)$. Then one can study the nonlinear evolution of the scalar field perturbation which, in the quasistatic limit, is governed by

$$\nabla^2\phi = \left[\beta(\phi)\frac{\rho_m}{m_{\rm Pl}} - \beta(\bar{\phi})\frac{\bar{\rho}_m}{m_{\rm Pl}}\right] + \frac{\mathrm{d}V(\phi)}{\mathrm{d}\phi} - \frac{\mathrm{d}V(\bar{\phi})}{\mathrm{d}\phi}, \tag{200}$$

where the overbar means the background value.

One can easily obtain $\mathrm{d}V(\phi)/\mathrm{d}\phi$ analytically or numerically, and this can be used to solve the quasistatic dynamics numerically. An advantage is that *temporal* functions $m(a)$, $\beta(a)$ completely specify the dynamics of ϕ, in particular its *spatial* configuration, and there is no need for a k-space parametrization.

On linear scales, this is equivalent to the Jordan-frame description with the two spatially dependent functions $\mu(k,a)$ and $\gamma(k,a)$ being defined by $\epsilon(k,a)$ which depends on the two functions $m(a)$ and $\beta(a)$, as given in Eq. (196). But in practice, working with two temporal functions is much more direct. Furthermore, the parametrization described in Eq. (196) fails to faithfully describe the nonlinear effects or the environmental dependence. In essence, by going from $m(a)$ and $\beta(a)$ to $\mu(k,a)$ and $\gamma(k,a)$, one not only introduces spatial dependence but also loses the ability to describe nonlinear structure formation: in this sense, we may describe the approach using $\mu(k,a)$ and $\gamma(k,a)$ as the *linear parametrization* of structure formation while $m(a)$ and $\beta(a)$ provide a *fully nonlinear parametrization* of modified gravity.[11]

Past experience has shown that in modified gravity [e.g., chameleon and $f(R)$] models, nonlinear effects become important as soon as the linear perturbation result deviates from the corresponding ΛCDM prediction. This emphasizes the importance of using full numerical simulations in the study of these models. However, the full numerical simulations are generally very time and resource-consuming, and are therefore left for future work.

VI. VARIATION OF CONSTANTS

We have seen that the background evolution of the scalar field is specified by the time dependent mass and coupling functions. As the scalar field evolves, the particle masses and the gauge coupling constants change in time too. The time variation of masses and gauge couplings is tightly constrained by laboratory experiments [57]. In this section, we analyze the time drift of the fine structure constant and the electron to proton mass ratio.

A. The fine structure constant

The scalar field also has an effect on gauge couplings and particle masses. The fermion masses are given by

$$m_F(\phi) = A(\phi)m_{\rm bare}, \tag{201}$$

where $m_{\rm bare}$ is the bare mass in the Lagrangian. Meanwhile, quantum effects such as the presence of heavy fermions lead to the potential coupling of ϕ to photons [58]

$$S_{\rm gauge} = -\frac{1}{4g_{\rm bare}^2}\int \mathrm{d}^4x\sqrt{-g}B_F(\phi)F_{\mu\nu}F^{\mu\nu}, \tag{202}$$

where $g_{\rm bare}$ is the bare coupling constant and

$$B_F(\phi) = 1 + \beta_\gamma\frac{\phi}{m_{\rm Pl}} + \ldots. \tag{203}$$

The scalar coupling to the electromagnetic field would lead to a dependence of the fine structure constant on ϕ as

[11] Our parametrization also provides a clear characterization of the class of physical models (namely a scalar field coupled to matter) considered here, which is important in parametrizing modified gravity [54], and not automatically incorporated in the (μ, γ) parametrization.

$$\frac{1}{\alpha} = \frac{1}{\alpha_{\rm bare}} B_F(\phi), \tag{204}$$

implying that

$$\frac{\dot\alpha}{\alpha} \approx -\beta_\gamma \frac{\dot\phi}{m_{\rm Pl}} \tag{205}$$

where we have assumed that $\beta_\gamma \phi/m_{\rm Pl} \ll 1$. Using the evolution equation we find that

$$\frac{\dot\alpha}{H\alpha} \approx -9\beta_\gamma \beta \Omega_m \frac{H^2}{m^2}. \tag{206}$$

Hence the negative variation of the fine structure constant in one Hubble time is related to the small ratio $H/m \ll 1$ and the couplings of ϕ to matter and photons. The best experimental bound on the variation of α now comes from aluminum and mercury single-ion clocks [59]: $\frac{\dot\alpha}{\alpha}|_0 = (-1.6 \pm 2.3) \cdot 10^{-17}\ {\rm yr}^{-1}$. Taking $H_0^{-1} \sim 1.5 \cdot 10^{10}$ yr, we get the conservative bound $|\frac{\dot\alpha}{H\alpha}|_0 \lesssim 2 \cdot 10^{-7}$. As a result, the experimental bounds on the time variation of α lead to constraints on $\beta_0\beta_{\gamma 0}$ as $\beta_0\beta_{\gamma 0} \lesssim 0.8 \cdot 10^{-7} \frac{m_0^2}{H_0^2}$. For models with $\beta_0 = \mathcal{O}(1)$, $\Omega_{m0} \sim 0.25$ and $m_0/H_0 \approx 10^3$ where effects on large-scale structure are present, $\beta_{\gamma 0} \lesssim 0.1$, which is a much tighter bound than present experimental ones $\beta_{\gamma 0} \lesssim 10^{11}$ [60].

The time evolution in the past is also particularly interesting. For symmetron models, we find that the time variation of α is

$$\frac{\dot\alpha}{H\alpha} \approx -9\beta_\star\beta_\gamma\Omega_{m0}\left(\frac{H_0}{m_\star}\right)^2 \frac{1}{a^3\sqrt{1-(\frac{a_\star}{a})^3}}. \tag{207}$$

Here, the time variation of α increases as one reaches the transition $a_\star$. This is a large variation which may happen in the recent past of the Universe and may have observable consequences in the emission lines of distant objects.

It should however be noted that even though $\dot\alpha/\alpha$ can be very large, the relative difference of α between Earth and some other sparser place in the Universe is constrained to be less than

$$\left|\frac{\Delta\alpha}{\alpha}\right| < \frac{\phi_\star\beta_\gamma}{m_{\rm Pl}} = 3\beta_\star\beta_\gamma\Omega_{m0}\left(\frac{H_0}{m_\star}\right)^2\frac{\rho_\star}{\rho_{m0}} \tag{208}$$

If we instead consider a quadratic coupling to photons, $B_F(\phi) = 1 + \frac{A_2^\gamma}{2}\phi^2$, we find

$$\left|\frac{\Delta\alpha}{\alpha}\right| < A_2^\gamma \frac{\phi_\star^2}{2} = 3\beta_\star\beta_\gamma\Omega_{m0}\left(\frac{H_0}{m_\star}\right)^2\frac{\rho_\star}{\rho_{m0}} \tag{209}$$

where $\beta_\gamma = \beta A_2^\gamma/A_2 = \phi_\star m_{\rm Pl} A_2^\gamma$.

Interestingly, for both cases and for our fiducial parameter values $m_\star \sim 10^3 H_0$, $\rho_\star \sim \rho_{m0}$ and $\beta \sim \beta_\gamma = \mathcal{O}(1)$ this term is of the same order as the claimed variation of α reported in [61].

B. The variation of masses

Fundamental fermions such as the electrons have a universal mass dependence $m_F = A(\phi)m_{\rm bare}$, implying that

$$\frac{\dot m_F}{H m_F} = 9\beta^2\Omega_m\frac{H^2}{m^2}. \tag{210}$$

Nucleons such as the proton have a mass given by the phenomenological formula

$$m_p = C_{\rm QCD}\Lambda_{\rm QCD} + b_u m_u + b_d m_d + C_p\alpha, \tag{211}$$

where $\Lambda_{\rm QCD} \sim 217$ MeV is the QCD scale, $b_u + b_d \sim 6$, $b_u - b_d \sim 0.5$, $C_{\rm QCD} \sim 5.2$, $m_u^{\rm bare} \sim 5\,{\rm MeV}$, $m_d^{\rm bare} \sim 10\,{\rm MeV}$ and $C_p\alpha_{\rm bare} \sim 0.62$ MeV. Assuming conservatively that $\Lambda_{\rm QCD}$ is scalar independent, we get

$$\frac{\dot m_p}{H m_p} \approx 9\Omega_m\beta\frac{H^2}{m^2}\left(\frac{b_u m_u^{\rm bare} + b_d m_d^{\rm bare}}{m_p}\beta - \frac{C_p\alpha_{\rm bare}}{m_p}\beta_\gamma\right). \tag{212}$$

It is particularly important to study the variation of

$$\nu = \frac{m_e}{m_p} \tag{213}$$

from which we find that its time variation is positive for modified gravity models:

$$\frac{\dot\nu}{\nu} \approx 9\Omega_m\beta\frac{H^2}{m^2}\left(\beta + \frac{C_p\alpha_{\rm bare}}{m_p}\beta_\gamma\right). \tag{214}$$

The current experimental constraint is $\frac{\dot\nu}{\nu}|_0 = (-3.8 \pm 5.6)10^{-14}\ {\rm yr}^{-1}$ which yields the upper bound on β_0: $\beta_0^2 \lesssim 10^{-5}\frac{m_0^2}{H_0^2}$. For $\beta_0 = \mathcal{O}(1)$, this entails that $m_0/H_0 \gtrsim 10^{2.5}$. Again for symmetron models, the electron to proton mass ratio would vary rapidly in time around the transition time $a_\star$. It would be interesting to study if such a variation could have relevant effects on the physics of distant objects.

VII. CONCLUSION

We have developed a novel parametrization of modified gravity models first presented in [5]. Starting with the time-evolution of the mass and the matter coupling of a scalar field in the cosmological background, we have been able to reverse engineer the complete dynamics of these models in a simple way.

We have applied these results to well-known modified gravity models: chameleons, $f(R)$ gravity, dilatons and symmetrons. In each case, we have explicitly given the mapping and the full reconstruction. We have also shown how one can apply local constraints using this formalism and then use it to make predictions for linear cosmological perturbations.

New classes of models can be engineered in a more intuitive way than starting from a Lagrangian. The

Lagrangian itself can be completely reconstructed. One only needs to specify two functions whose physical meaning is easily grasped: namely the mass (the inverse range of the fifth force) and the coupling to matter.

The real strength of this approach compared to existing parametrizations in the literature is that we can reconstruct the whole theory at the linear and nonlinear levels and be sure that it corresponds to a concrete physical model defined via a Lagrangian. This effectively supersedes existing parametrizations of modified gravity with a screening mechanism by being able to make predictions for nonlinear clustering of matter via N-body simulations. This will be the subject of future work.

ACKNOWLEDGMENTS

A. C. D. is supported in part by STFC. B. L. is supported by the Royal Astronomical Society and Durham University. H. A. W. thanks the Research Council of Norway FRINAT Grant No. 197251/V30. P. B. and H. A. W. thank DAMPT at Cambridge University and H. A. W. thanks IPhT CEA Saclay for hospitality where part of this work was carried out.

APPENDIX: THE CAVITY CONSTRAINT

In this Appendix, we will explicitly develop the calculation leading to the cavity constraint for chameleon and $f(R)$ models.

Consider a cavity of radius L with a residual density $\rho_{\rm cav} \ll \rho_c$ where ρ_c is the density of the bore surrounding the cavity. The field inside the cavity is $\phi_{\rm cav}$ and deviates slightly from this value across the cavity. Expanding the effective potential around $\phi_{\rm cav}$ and putting $\delta\phi = \phi - \phi_{\rm cav}$, we have

$$\frac{1}{r^2}\frac{\mathrm{d}}{\mathrm{d}r}\left(r^2\frac{\mathrm{d}}{\mathrm{d}r}\delta\phi\right) - m_{\rm cav}^2\delta\phi = V_{{\rm eff},\phi}(\phi_{\rm cav}) \tag{A1}$$

where $m_{\rm cav}$ is the scalar field mass inside the cavity and $V_{{\rm eff},\phi} \equiv \mathrm{d}V_{\rm eff}(\phi)/\mathrm{d}\phi$ is nonzero unless $\phi_{\rm cav}$ minimizes the effective potential. Inside the cavity the solution is

$$\delta\phi = A\frac{\sinh(m_{\rm cav}r)}{r} - \frac{V_{{\rm eff},\phi}(\phi_{\rm cav})}{m_{\rm cav}^2}; \tag{A2}$$

outside the cavity we have

$$\phi = \phi_c + B\frac{e^{-m_c r}}{r}, \tag{A3}$$

where A, B are constants of integral, ϕ_c is the minimum of the effective potential outside the cavity and m_c the mass at that minimum. Matching at $r = L$, we find that

$$B = \frac{e^{m_c L}}{1 + m_c L}[\sinh(m_{\rm cav}L) - m_{\rm cav}L]A, \tag{A4}$$

and

$$A\left[\frac{m_c}{1 + m_c L}\sinh(m_{\rm cav}L) + \frac{m_{\rm cav}}{1 + m_c L}\right] = \phi_c - \phi_{\rm cav} + \frac{V_{{\rm eff},\phi}(\phi_{\rm cav})}{m_{\rm cav}^2}. \tag{A5}$$

Evaluating the solution at the origin and putting $\delta\phi(r = 0) = 0$ we have

$$A = \frac{V_{{\rm eff},\phi}(\phi_{\rm cav})}{m_{\rm cav}^3}. \tag{A6}$$

This leads to

$$1 + \frac{\sinh(m_{\rm cav}L)}{m_{\rm cav}L} = -\frac{\phi_{\rm cav}m_{\rm cav}^2}{V_{{\rm eff},\phi}(\phi_{\rm cav})}, \tag{A7}$$

where we have used $m_c L \gg 1$.

For potentials $V \sim 1/\phi^n$ and as long as $\phi_{\rm cav}$ is much less than the effective minimum in the cavity we have

$$\frac{\sinh(m_{\rm cav}L)}{m_{\rm cav}L} = n, \tag{A8}$$

which implies that

$$m_{\rm cav}L = \mathcal{O}(1), \tag{A9}$$

where $m_{\rm cav}$ is dominated by the potential term.

[1] E. J. Copeland, M. Sami, and S. Tsujikawa, Int. J. Mod. Phys. D **15**, 1753 (2006).
[2] T. Clifton, P. G. Ferreira, A. Padilla, and C. Skordis, Phys. Rep. **513**, 1 (2012).
[3] S. Weinberg and E. Witten, Phys. Lett. **96B**, 59 (1980).
[4] J. Khoury, arXiv:1011.5909.
[5] P. Brax, A.-C. Davis, and B. Li, arXiv:1111.6613.
[6] P. Brax, C. van de Bruck, A. C. Davis, and D. J. Shaw, Phys. Rev. D **82**, 063519 (2010).
[7] P. Brax, C. van de Bruck, A.-C. Davis, B. Li, and D. J. Shaw, Phys. Rev. D **83**, 104026 (2011).
[8] T. Damour and A. M. Polyakov, Nucl. Phys. **B423**, 532 (1994).
[9] J. Khoury and A. Weltman, Phys. Rev. D **69**, 044206 (2004); D. F. Mota and D. J. Shaw, *ibid.* **75**, 063501 (2007).
[10] P. Brax, C. van de Bruck, A.-C. Davis, J. Khoury, and A. Weltman, Phys. Rev. D **70**, 123518 (2004).
[11] P. Brax, C. van de Bruck, and A. C. Davis, J. Cosmol. Astropart. Phys. 11 (2004) 004.
[12] P. Brax, C. van de Bruck, D. F. Mota, N. J. Nunes, and H. A. Winther, Phys. Rev. D **82**, 083503 (2010).

[13] R. Gannouji, B. Moraes, D. F. Mota, D. Polarski, S. Tsujikawa, and H. A. Winther, Phys. Rev. D **82**, 124006 (2010).
[14] M. Pietroni, Phys. Rev. D **72**, 043535 (2005).
[15] K. A. Olive and M. Pospelov, Phys. Rev. D **77**, 043524 (2008).
[16] K. Hinterbichler and J. Khoury, Phys. Rev. Lett. **104**, 231301 (2010).
[17] K. Hinterbichler, J. Khoury, A. Levy, and A. Matas, Phys. Rev. D **84**, 103521 (2011).
[18] P. Brax, C. van de Bruck, A.-C. Davis, B. Li, B. Schmauch, and D. J. Shaw, Phys. Rev. D **84**, 123524 (2011).
[19] A.-C. Davis, B. Li, D. F. Mota, and H. A. Winther, Astrophys. J. **748**, 61 (2012).
[20] J. Clampitt, B. Jain, and J. Khoury, J. Cosmol. Astropart. Phys. 01 (2012) 030.
[21] A. A. Starobinsky, Phys. Lett. **91B**, 99 (1980).
[22] S. M. Carroll, V. Duvvuri, M. Trodden, and M. S. Turner, Phys. Rev. D **70**, 043528 (2004).
[23] S. M. Carroll, A. de Felice, V. Duvvuri, D. A. Easson, M. Trodden, and M. S. Turner, Phys. Rev. D **71**, 063513 (2005).
[24] T. Faulkner, M. Tegmark, E. F. Bunn, and Y. Mao, Phys. Rev. D **76**, 063505 (2007).
[25] I. Navarro and K. Van Acoleyen, J. Cosmol. Astropart. Phys. 02 (2007) 022.
[26] L. Amendola, R. Gannouji, D. Polarski, and S. Tsujikawa, Phys. Rev. D **75**, 083504 (2007).
[27] S. Carloni, A. Troisi, and P. K. S. Dunsby, Gen. Relativ. Gravit. **41**, 1757 (2009).
[28] Y.-S. Song, W. Hu, and I. Sawicki, Phys. Rev. D **75**, 044004 (2007).
[29] B. Li and J. D. Barrow, Phys. Rev. D **75**, 084010 (2007).
[30] W. Hu and I. Sawicki, Phys. Rev. D **76**, 064004 (2007).
[31] P. Brax, C. van de Bruck, A. C. Davis, and D. J. Shaw, Phys. Rev. D **78**, 104021 (2008).
[32] T. P. Sotiriou and V. Faraoni, Rev. Mod. Phys. **82**, 451 (2010).
[33] A. De Felice and S. Tsujikawa, Living Rev. Relativity **13**, 3 (2010).
[34] P. Brax, C. van de Bruck, A.-C. Davis, and A. M. Green, Phys. Lett. B **633**, 441 (2006).
[35] P. Brax and A.-C. Davis, Phys. Rev. D **85**, 023513 (2012).
[36] E. Bertschinger, Astrophys. J. **648**, 797 (2006).
[37] W. Hu and I. Sawicki, Phys. Rev. D **76**, 104043 (2007).
[38] B. Jain and P. Zhang, Phys. Rev. D **78**, 063503 (2008).
[39] L. Amendola, M. Kunz, and D. Sapone, J. Cosmol. Astropart. Phys. 04 (2008) 013.
[40] E. Bertschinger and P. Zukin, Phys. Rev. D **78**, 024015 (2008).
[41] Y.-S. Song and K. Koyama, J. Cosmol. Astropart. Phys. 01 (2009) 048.
[42] R. Bean and M. Tangmatitham, Phys. Rev. D **81**, 083534 (2010).
[43] S. F. Daniel, E. V. Linder, T. L. Smith, R. R. Caldwell, A. Cooray, A. Leauthaud, and L. Lombriser, Phys. Rev. D **81**, 123508 (2010).
[44] L. Pogosian, A. Silvestri, K. Koyama, and G. Zhao, Phys. Rev. D **81**, 104023 (2010).
[45] G. Zhao, H. Li, E. V. Linder, K. Koyama, D. J. Bacon, and X. Zhang, Phys. Rev. D **85**, 123546 (2012).
[46] J. G. Williams, S. G. Turyshev, and D. Boggs, arXiv:1203.2150.
[47] B. Bertotti, L. Iess, and P. Tortora, Nature (London) **425**, 374 (2003).
[48] E. G. Adelberger (EOT-WASH Group Collaboration), arXiv:hep-ex/0202008.
[49] R. Pourhasan, N. Afshordi, R. B. Mann, and A. C. Davis, J. Cosmol. Astropart. Phys. 12 (2011) 005.
[50] T. Tamaki and S. Tsujikawa, Phys. Rev. D **78**, 084028 (2008).
[51] B. Li and H. Zhao, Phys. Rev. D **80**, 044027 (2009).
[52] C. Skordis, Phys. Rev. D **79**, 123527 (2009).
[53] P. G. Ferreira and C. Skordis, Phys. Rev. D **81**, 104020 (2010).
[54] J. Zuntz, T. Baker, P. G. Ferreira, and C. Skordis, arXiv:1110.3830.
[55] B. Li and J. D. Barrow, Phys. Rev. D **83**, 024007 (2011).
[56] B. Li, G. B. Zhao, R. Teyssier, and K. Koyama, J. Cosmol. Astropart. Phys. 01 (2012) 051.
[57] F. Luo, K. A. Olive, and J.-P. Uzan, Phys. Rev. D **84**, 096004 (2011).
[58] P. Brax, C. Burrage, A.-C. Davis, D. Seery, and A. Weltman, Phys. Lett. B **699**, 5 (2011).
[59] J.-P. Uzan, Living Rev. Relativity **14**, 2 (2011).
[60] J. H. Steffen, A. Upadhye, A. Baumbaugh, A. S. Chou, P. O. Mazur, R. Tomlin, A. Weltman, and W. Wester, Phys. Rev. Lett. **105**, 261803 (2010).
[61] J. K. Webb, V. V. Flambaum, C. W. Churchill, M. J. Drinkwater, and J. D. Barrow, Phys. Rev. Lett. **82**, 884 (1999).

Paper IV

Systematic simulations of modified gravity: symmetron and dilaton models
Philippe Brax, Anne-Christine Davis, Baojiu Li, Hans A. Winther, Gong-Bo Zhao
Journal of Cosmology and Astroparticle Physics, Issue 10, (2012)

Paper V

Systematic simulations of modified gravity: chameleon models

Philippe Brax, Anne-Christine Davis, Baojiu Li, Hans A. Winther, Gong-Bo Zhao

Journal of Cosmology and Astroparticle Physics, Issue 4, (2013)

Paper VI

Cosmological Supersymmetric Model of Dark Energy
Philippe Brax, Anne-Christine Davis, Hans A. Winther
Physical Review D, vol. 85, Issue 8, (2012)

PHYSICAL REVIEW D **85,** 083512 (2012)

Cosmological supersymmetric model of dark energy

Philippe Brax,[1,*] Anne-Christine Davis,[2,†] and Hans A. Winther[3,‡]

[1]*Institut de Physique Theorique, CEA, IPhT, CNRS, URA 2306, F-91191Gif/Yvette Cedex, France*
[2]*DAMPT, Cambridge University, United Kingdom*
[3]*Institute of Theoretical Astrophysics, University of Oslo, 0315 Oslo, Norway*

(Received 4 January 2012; published 18 April 2012)

Recently, a supersymmetric model of dark energy coupled to cold dark matter, the supersymmetron, has been proposed. In the absence of cold dark matter, the supersymmetron field converges to a supersymmetric minimum with a vanishing cosmological constant. When cold dark matter is present, the supersymmetron evolves to a matter-dependent minimum where its energy density does not vanish and could lead to the present acceleration of the Universe. The supersymmetron generates a short-ranged fifth force which evades gravitational tests. It could lead to observable signatures on structure formation due to a very strong coupling to dark matter. We investigate the cosmological evolution of the field, focusing on the linear perturbations and the spherical collapse and find that observable modifications in structure formation can indeed exist. Unfortunately, we find that when the growth rate of perturbations is in agreement with observations, an additional cosmological constant is required to account for dark energy. In this case, effects on large-scale structures are still present at the nonlinear level which are investigated using the spherical collapse approach.

DOI: 10.1103/PhysRevD.85.083512 PACS numbers: 95.36.+x, 04.50.Kd, 98.80.Cq

I. INTRODUCTION

Dark energy, the component responsible for the late time acceleration of our Universe, is currently well described by a cosmological constant in the lambda cold dark matter (ΛCDM) concordance model. ΛCDM has been very successful in explaining a large range of observations probing a vast range in length scales, but from a theoretical point of view the model suffers from the fine-tuning problem and the coincidence problem [1]. This has led to more general models for dark energy. Scalar field models have been particularly popular over the last decade, and are predicted to exist in many theories of high energy physics, like string theory and supergravity (see e.g. [2,3] and references therein).

However, many of the dark energy models that have been constructed so far suffer from problems akin to the ones they are trying to solve or introduce new issues themselves. At best, they can be treated as low energy field theories valid well below the electron mass, corresponding to the very late phase of the Universe. Hence, these models need to be embedded in a better defined theory whose ultraviolet behavior is under control. So far, no such complete scenario has been constructed. Dark energy models also seem to require the existence of a very light scalar field whose coupling to matter leads to a long-ranged fifth force whose presence is at odds with current gravitational tests. Screening mechanisms [4–10] have been invoked in order to alleviate this problem. Axionlike particles with derivative couplings to matter are also possible candidates [11].

On the other hand, it could well be that the dark sector of the Universe, composed of the still undiscovered cold dark matter and dark energy (DE), could be described by a globally supersymmetric theory [12–14]. In such a case, the vanishingly small amount of dark energy which is necessary to generate the acceleration of the Universe could result from a small cosmological breaking of supersymmetry due to the nonzero CDM energy density. Such a scenario would naturally lead to a close relationship between the dark energy and the CDM energy densities. Of course, one should also ensure that corrections to the globally supersymmetric scalar potential coming from the soft supersymmetry breaking in the minimal supersymmetric standard model sector do not spoil the CDM-DE correspondence and the properties of the scalar potential in the late time Universe.

Recently [15], such a supersymmetric model of dark energy coupled to cold dark matter, the supersymmetron, was proposed by two of us. In the absence of cold dark matter, the supersymmetron converges to a supersymmetric minimum with a vanishing cosmological constant. When cold dark matter is present, the supersymmetron evolves to a matter-dependent minimum where its energy density does not vanish and can contribute to the dark energy budget of the Universe.

The supersymmetron generates a short-ranged fifth force between the CDM and the DE which evades gravitational tests, but could lead to observable signatures on structure formation as found in similar modified gravity theories [16–23].

In this paper, we analyze the cosmological evolution of the supersymmetron at the background level and the evolution of dark matter perturbations in the linear and

*philippe.brax@cea.fr
†a.c.davis@damtp.cam.ac.uk
‡h.a.winther@astro.uio.no

nonlinear regime. The nonlinear regime is studied by using spherical collapse. Because of the highly nonlinear behavior of the field during the spherical collapse, we are able to extract constraints on the model parameters, which are then used to constrain the background cosmology. The spherical collapse model has been previously used in models with a simple Yukawa-type modification of gravity, in the so-called $f(R)$/chameleon models [24–27], in brane-world cosmologies [28], and in models which allow for dark energy fluctuations [29–40]. We find that a cosmological constant (CC) must be included in the model and that linear perturbations do not deviate from their ΛCDM counterparts. On the other hand, nonlinear effects are significant on astrophysical scales.

The outline of this paper is as follows. In Sec. II, we present the supersymmetric formulation of the model, in Sec. III we derive static solutions to the field equation, and then in Sec. IV we study the cosmological evolution of the supersymmetron including the cosmological background evolution, linear perturbations, and the spherical collapse. In Sec. V, we revisit the original mass scales of the model before summarizing and concluding in Sec. VI.

II. THE SUPERSYMMETRON

A. Supersymmetric formulation

In globally supersymmetric models of the scalar sector, models are specified by their Kahler potential and the superpotential. With these two functions, we can construct the scalar potential and the kinetic term for the fields. For the supersymmetron, we have

$$K(\phi, \bar{\phi}, \phi_\pm, \bar{\phi}_\pm) = |\phi_+|^2 + |\phi_-|^2 + \frac{\Lambda_1^2}{2}\left|\frac{\phi}{\Lambda_1}\right|^{2\beta}, \quad (1)$$

$$W(\phi, \phi_\pm) = m\left(1 + \frac{g\phi}{m}\right)\phi_+\phi_-, \quad (2)$$

$$+ \frac{\Lambda_0^3\beta}{\sqrt{2}\alpha}\left(\frac{\phi}{\Lambda_0}\right)^\alpha + \frac{\Lambda_2^3}{\sqrt{2}}\left(\frac{\phi}{\Lambda_2}\right)^\beta, \quad (3)$$

where ϕ is the dark energy superfield, $\phi_\pm$ is the CDM particles, and Λ_i are some (for now) unspecified mass scales.

The kinetic term follows from

$$\mathcal{L}_{\rm kin} = K_{\phi\bar{\phi}}(\partial\phi)^2 = \frac{\kappa(\phi)^2}{2}(\partial\phi)^2, \quad (4)$$

$$\kappa(\phi) = \beta\left(\frac{\phi}{\Lambda_1}\right)^{\beta-1}, \quad (5)$$

and the scalar potential is given by the F-term

$$V_F = K^{\phi\bar{\phi}}|\partial_\phi W|^2 = \left|\Lambda^2 + \frac{M^{2+n/2}}{\phi^{n/2}}\right|^2, \quad (6)$$

where $n = 2(\beta - \alpha)$ and the mass scales M and Λ are given by

$$\Lambda^4 = \left(\frac{\Lambda_1}{\Lambda_2}\right)^{2\beta-2}\Lambda_2^4, \quad (7)$$

$$M^{n+4} = \left(\frac{\Lambda_1}{\Lambda_0}\right)^{2\beta-2}\Lambda_0^{n+4}. \quad (8)$$

Taking $\phi = |\phi|e^{i\theta}$, the scalar potential is seen to be minimized for $e^{(in\theta/2)} = -1$. The angular field θ is stabilized at this minimum with a mass which is always much greater than the gravitino mass [15] implying that

$$V_F = \left(\Lambda^2 - \frac{M^{2+n/2}}{\phi^{n/2}}\right)^2. \quad (9)$$

In the rest of this paper, we will write ϕ instead of $|\phi|$ for simplicity. The potential is minimized, with vanishing potential energy, for $\phi = \phi_{\rm min}$ where

$$\phi_{\rm min} = \left(\frac{M}{\Lambda}\right)^{(4/n)}M. \quad (10)$$

Because of the coupling between ϕ and $\phi_\pm$ in the superpotential, the fermionic CDM particles acquire a scalar field dependent mass

$$m_f(\phi) = m\left(1 + \frac{g\phi}{m}\right). \quad (11)$$

When the fermionic CDM develops a nonvanishing number density $n_{\rm CDM} = \langle\psi_+\psi_-\rangle$ in the early Universe, we get a new contribution to the scalar potential

$$V_{\rm eff} = V_F + \frac{g\phi}{m}\rho_{\rm CDM}, \qquad \rho_{\rm CDM} = mn_{\rm CDM} \quad (12)$$

which lifts the supersymmetric minimum and produces a nonzero dark energy component which can lead to the acceleration of our Universe.

B. Effective four-dimensional model

The effective theory for the sypersymmetron can be viewed as a scalar-tensor theory where CDM particles follow geodesics of the rescaled metric $\tilde{g}_{\mu\nu} = g_{\mu\nu}A(\phi)$ where

$$A(\phi) = 1 + \frac{g\phi}{m}. \quad (13)$$

The effective four-dimensional action describing the dynamics of the supersymmetron is given by

$$S_{\rm eff} = \int d^4x\sqrt{-g}\left[\frac{R}{2}M_{\rm pl}^2 - \frac{\kappa(\phi)^2}{2}(\partial\phi)^2 - V_F(\phi)\right] + S_{\rm CDM}(A^2(\phi)g_{\mu\nu}; \psi), \quad (14)$$

where g is the determinant of the metric $g_{\mu\nu}$, $M_{\rm pl}^2 \equiv \frac{1}{8\pi G}$ is the reduced Planck mass, and $S_{\rm CDM}$ is the dark matter

action. If a coupling to baryons is included, the large mass of the supersymmetron field will ensure that this field would be practically invisible in local experiments.

C. Reparametrization of the model parameters

In this subsection, we rewrite the original mass scales of the model in terms of some more intuitive physical quantities which will simplify our analysis.

The coupling of the supersymmetron to dark matter $A(\phi)$ can be written

$$A(\phi) = 1 + x\left(\frac{\phi}{\phi_{\rm min}}\right), \tag{15}$$

where

$$x \equiv \frac{g\phi_{\rm min}}{m} \tag{16}$$

is a dimensionless parameter which parametrizes the coupling strength of the supersymmetron to matter.

We further introduce the density

$$\rho_\infty \equiv \frac{n\Lambda^4}{x} \tag{17}$$

and

$$\rho_\infty \equiv \rho^0_{\rm CDM}(1 + z_\infty)^3 \tag{18}$$

which is the CDM density (and the corresponding redshift) when the field ϕ reaches the vicinity of the supersymmetric minimum $\phi_{\rm min}$.

When studying the cosmological dynamics of the model, it is convenient to introduce the canonically normalized field φ via

$$d\varphi = \kappa(\phi)d\phi \rightarrow \varphi(\phi) = \Lambda_1\left(\frac{\phi}{\Lambda_1}\right)^\beta. \tag{19}$$

In terms of φ, the potential and coupling becomes

$$V_F(\varphi) = \Lambda^4\left(1 - \left(\frac{\varphi_{\rm min}}{\varphi}\right)^{(n/2\beta)}\right)^2, \tag{20}$$

$$A(\varphi) = 1 + x\left(\frac{\varphi}{\varphi_{\rm min}}\right)^{(1/\beta)}, \tag{21}$$

where $\varphi_{\rm min} = \varphi(\phi_{\rm min})$. The mass of the supersymmetron after having converged to the supersymmetric minimum is given by

$$m^2_\infty = \frac{\rho_\infty x n}{2\beta^2\varphi^2_{\rm min}}. \tag{22}$$

A constraint on m_∞ can be obtained by requiring that the effects of supergravity corrections to the potential of the supersymmetron are irrelevant. Let us assume that supersymmetry is broken at the supergravity level in a spontaneous way. There are two main sources of corrections to the scalar potential coming from

$$e^{K/m^2_{\rm Pl}}m^2_{3/2}m^2_{\rm Pl} \supset Km^2_{3/2} \tag{23}$$

and

$$K^{\phi\bar\phi}|D_\phi W|^2 \supset \frac{|K_\phi|^2 m^2_{3/2}}{\kappa^2(\phi)}. \tag{24}$$

These corrections lead to a contribution to the scalar potential

$$\delta V \sim m^2_{3/2}\varphi^2. \tag{25}$$

This contribution to the scalar potential increases with ϕ and does not modify the cosmological dynamics provided it is much smaller than the matter term in the effective potential $\delta V(\phi_{\rm min}) \ll x\rho_\infty$ which leads to

$$\varphi^2_{\rm min} \ll \frac{x\rho_\infty}{m^2_{3/2}}. \tag{26}$$

Using (22), we find that the mass in the late time Universe is constrained by

$$m_\infty \gg m_{3/2}, \tag{27}$$

where $m_{3/2}$ is the gravitino mass and is typically much larger than 1 eV [41]. We will therefore require

$$m_\infty \gg \mathcal{O}(1)\ {\rm eV} \tag{28}$$

which is our first constraint. Of course, supersymmetry breaking in the observable sector of the standard model, i.e. amongst the standard model particles, leads to a cosmological constant which is independent of the supersymmetron sector. In the following, we will see that a small cosmological constant is required in the supersymmetron scenario whose origin may come from, in part, the supersymmetry breaking scale in the observable sector. The three physical parameters $\{\rho_\infty, x, m_\infty\}$ together with the two indices $\{n, \beta\}$ completely characterize the effective model. In the end, we will go back and compare our results with the original mass scales.

D. Supersymmetron dynamics

The field equation for φ follows from a variation of Eq. (14) with respect to φ and reads

$$\Box\varphi = V_{{\rm eff},\varphi}, \tag{29}$$

where the effective potential is given by

$$V_{\rm eff}(\varphi) = V_F(\varphi) + (A(\varphi) - 1)\rho_{\rm CDM}. \tag{30}$$

The minimum φ_ρ of the effective potential is determined by

$$\left(\frac{\varphi_{\rm min}}{\varphi_\rho}\right)^{(n+1)/\beta} - \left(\frac{\varphi_{\rm min}}{\varphi_\rho}\right)^{(n+2)/2\beta} = \frac{\rho_{\rm CDM}}{\rho_\infty} \tag{31}$$

and has the approximate solution

$$\frac{\varphi_\rho}{\varphi_{\min}} \simeq \begin{cases} 1 & \rho_{\rm CDM} \lesssim \rho_\infty \\ \left(\frac{\rho_\infty}{\rho_{\rm CDM}}\right)^{\beta/(n+1)} & \rho_{\rm CDM} \gg \rho_\infty. \end{cases} \quad (32)$$

A nonzero dark matter condensate is seen to lower the minimum from the supersymmetric minimum. The energy density associated with the supersymmetron is

$$V_{\rm eff}(\varphi_\rho) \simeq \begin{cases} \frac{x\rho_{\rm CDM}(1+n)}{n}\left(\frac{\rho_\infty}{\rho_{\rm CDM}}\right)^{1/(n+1)} & \rho_{\rm CDM} \gg \rho_\infty \\ x\rho_{\rm CDM} & \rho_{\rm CDM} \lesssim \rho_\infty \end{cases} \quad (33)$$

which for small n and $\rho_{\rm CDM} \gg \rho_\infty$ behaves like a cosmological constant, but evolves as CDM after the field has converged to the supersymmetric minimum. This means that if the supersymmetron accounted for all dark energy, then acceleration would be a transient phenomenon.

The mass of the field, $m_\varphi^2 \equiv V_{{\rm eff},\varphi\varphi}$, is given by

$$m_\varphi^2 = m_\infty^2\left[\frac{2(n+\beta)}{n}\left(\frac{\varphi_{\min}}{\varphi_\rho}\right)^{(n/\beta)+2} - \frac{(n+2\beta)}{n}\left(\frac{\varphi_{\min}}{\varphi_\rho}\right)^{(n/2\beta)+2} + \frac{2(1-\beta)}{n}\frac{\rho_{\rm CDM}}{\rho_\infty}\left(\frac{\varphi_{\min}}{\varphi_\rho}\right)^{2-(1/\beta)}\right]. \quad (34)$$

When the field follows the minimum of the effective potential, this expression simplifies to

$$\frac{m_\rho^2}{m_\infty^2} \simeq \begin{cases} 1 & \rho_{\rm CDM} \lesssim \rho_\infty \\ \frac{2(n+1)}{n}\left(\frac{\rho_{\rm CDM}}{\rho_\infty}\right)^{(n+2\beta)/(n+1)} & \rho_{\rm CDM} \gg \rho_\infty. \end{cases} \quad (35)$$

We see that the mass is always greater than the value at the supersymmetric minimum and from the constraint Eq. (28) the mass is therefore always greater than a few eV's.

The conformal coupling Eq. (15) leads to a fifth force (see e.g. [42,43]) between dark matter particles, which in the nonrelativistic limit (and per unit mass) is given by

$$\vec{F}_\varphi = \frac{d\log A(\varphi)}{d\varphi}\vec{\nabla}\varphi. \quad (36)$$

This fifth force will have an impact on structure formation which is investigated in the following sections.

III. STATIC CONFIGURATIONS

In this section, we derive the static spherical symmetric solutions for the supersymmetron, which we then use later on when studying the spherical collapse.

In a static spherical symmetric metric with weak gravitational fields, the field equation Eq. (29) reads

$$\frac{d^2\varphi}{dr^2} + \frac{2}{r}\frac{d\varphi}{dr} = V_{F,\varphi} + A_{,\varphi}\rho. \quad (37)$$

We consider a spherical body of dark matter (a halo) with radius R and a top-hat density profile

$$\rho = \begin{cases} \rho_c & r < R \\ \rho_b & r > R \end{cases} \quad (38)$$

and impose the standard boundary conditions

$$\frac{d\varphi(r\to 0)}{dr} = \frac{d\varphi(r\to\infty)}{dr} = 0, \quad (39)$$

$$\varphi(r\to\infty) = \varphi_b = \varphi_\rho(\rho_b). \quad (40)$$

The mass at the minimum inside (outside) the body is denoted by m_c (m_b).

Outside the halo, we can linearize the field equation around the background value φ_b with the solution

$$\varphi(r) = \varphi_b - \frac{BR}{r}e^{-m_b(r-R)} \qquad r > R \quad (41)$$

and where the constant B is determined by matching to the interior solution. The interior solutions are calculated below for several different cases.

A. Point-particle solutions

We first look at the point-particle solution, which can be found by first deriving the solution for fixed R and then taking the limit $R \to 0$ with $M = \frac{4\pi}{3}R^3\rho_c$ fixed.

In this limit, we expect the solution inside the body to be a very small perturbation of the background solution and we can assume $m_b R \ll 1$. A second-order Taylor expansion in r gives us the solution

$$\varphi = \varphi(0) + \frac{A_{,\varphi_b}\rho_c r^2}{6} \qquad r < R. \quad (42)$$

Matching to the exterior solution at $r = R$ gives

$$\varphi(0) = \varphi_b - \frac{A_{,\varphi_b}\rho_c R^2}{2}, \quad (43)$$

$$BR = \frac{A_{,\varphi_b}M}{4\pi}. \quad (44)$$

Taking the limit $R \to 0$ and using Eq. (36), we find that the gravity plus fifth-force potential is given by

$$V(r) = \frac{GM}{r}(1 + 2(A_{,\varphi_b}M_{\rm pl})^2 e^{-m_\varphi r}) \quad (45)$$

which is the same as the prediction from linear perturbation theory[1] as we will see later on. Contrary to chameleons where this type of solution holds at linear scales, here the

[1]By taking the Fourier transform of Eq. (69), we recover Eq. (45), see e.g. [44].

large mass of the supersymmetron means that this solution only applies for microscopic bodies.

B. Small overdensity

Now, we turn to the case where the size of the overdensity has to be taken into account. Note that we cannot make the approximation $m_b R \ll 1$ as the mass of the supersymmetron is generally very large

$$\frac{1}{m_b} < \frac{1}{m_\infty} \ll \frac{1}{\text{eV}} \sim 10^{-6}\ \text{m}. \tag{46}$$

Since we are interested in astrophysical-sized overdensities, $R = \mathcal{O}(\text{Mpc})$, we will always have $m_b R \gg 1$.

We take $\varphi = \varphi_0 + \delta\varphi$ and Taylor expand the field equation inside the body around $\varphi_0 \equiv \varphi(r = 0)$:

$$\frac{d^2\delta\varphi}{dr^2} + \frac{2}{r}\frac{d\delta\varphi}{dr} = V^{\text{eff}}_{,\varphi_0} + m_0^2\delta\varphi, \qquad m_0^2 \equiv V^{\text{eff}}_{,\varphi\varphi_0} \tag{47}$$

which gives the solution

$$\varphi = \varphi_0 + \frac{V^{\text{eff}}_{,\varphi_0}}{m_0^2}\left(\frac{\sinh(m_0 r)}{m_0 r} - 1\right) \qquad r < R. \tag{48}$$

Matching at $r = R$ and using $m_0 R$, $m_b R \gg 1$ to simplify the analysis, we find

$$\varphi_0 \simeq \varphi_b - \frac{V^{\text{eff}}_{,\varphi_0}}{m_0^2}\left(\frac{\sinh(m_0 R)}{m_0 R} + \frac{\cosh(m_0 R)}{m_b R}\right), \tag{49}$$

$$B \simeq \frac{\varphi_b - \varphi_0}{1 + \frac{m_b}{m_c}} \simeq \frac{\varphi_b - \varphi_0}{2}. \tag{50}$$

We assume that φ_0 is just a small perturbation in the background: $\varphi_0 = \varphi_b - \delta\varphi$, and expand the above expression to first order in $\delta\varphi$. This leads to

$$\delta\varphi \simeq \frac{(\rho_c - \rho_b)A_{,\varphi_b}}{m_b^2} \tag{51}$$

and

$$B = \frac{(\rho_c - \rho_b)A_{,\varphi_b}}{2m_b^2}. \tag{52}$$

This gives a total force, $F = \frac{G_{\text{eff}}\Delta M}{R^2}$ on a shell close to the edge of the overdensity where

$$\left(\frac{G_{\text{eff}}}{G}\right) = 1 + \frac{6(A_{,\varphi_b}M_{\text{pl}})^2}{(m_b R)} \tag{53}$$

which is suppressed compared to the point-particle solution. This solution is only valid when

$$\delta\varphi \simeq \frac{(\rho_c - \rho_b)A_{,\varphi_b}}{m_b^2} \ll \varphi_b. \tag{54}$$

Putting $\rho_c = (1 + \Delta)\rho_b$ and using $\frac{\rho_b A_{,\varphi_b}}{\varphi_b} \sim m_b^2$, we see that this condition reduces to

$$\Delta \ll 1 \tag{55}$$

i.e. a very small overdensity.

C. Large overdensity

For large overdensities, we expect screening and we therefore look for chameleonlike solutions [9,10,42,45–48]. That is, we assume that the field is very close to the minimum, $\varphi_c = \varphi_\rho(\rho_c)$, of the effective potential inside the body and the only variations of the field are in a thin shell close to the surface. Linearizing the field equation about φ_c leads to the solution

$$\varphi(r) = \varphi_c + C\frac{\sinh(m_c r)}{m_c r} \qquad r < R. \tag{56}$$

Because of the form of the field equation for general $\beta \neq 1$, we cannot solve the equation in the thin shell, but we will assume that this solution is valid all the way to $r = R$. This will be the case if the shell is very thin as found in chameleon theories [43,47,48], and as we will see below this is the case for the supersymmetron when the density contrast of our overdensity is large. In fact, we find that the supersymmetron is very similar in behavior to strongly coupled chameleons as studied in [47].

Matching the two solutions at $r = R$, we obtain

$$B \simeq (\varphi_b - \varphi_c) \tag{57}$$

i.e. the solution found is the critical solution where the field almost does not change inside the body. We can rewrite this equation in the standard chameleon form by introducing the equivalent thin-shell factor

$$\frac{\Delta R}{R} \equiv \frac{(\varphi_b - \varphi_c)}{6\beta_{\varphi_c}\Phi_c M_{\text{pl}}^2}, \qquad \beta_{\varphi_c} = A_{,\varphi_c}M_{\text{pl}}, \tag{58}$$

where $\Phi_c = \frac{G\Delta M}{R} = \frac{(\rho_c - \rho_b)R^2}{6M_{\text{pl}}^2}$ is the Newtonian potential of the overdensity. The total force on a spherical shell close to the surface is now $F = \frac{G_{\text{eff}}\Delta M}{R^2}$ where

$$\left(\frac{G_{\text{eff}}}{G}\right) = 1 + 2\beta_{\varphi_c}^2\left(\frac{3\Delta R}{R}\right) \times (1 + m_b R). \tag{59}$$

This solution is valid as long as the quadratic term in the Taylor expansion of $V_{\text{eff},\varphi}$ around φ_c is suppressed compared to the linear term at $r = R$. This condition turns into

$$\frac{m_b}{m_c}\left(\frac{\varphi_b}{\varphi_c}\right) \ll 1 \rightarrow \Delta \gg 1. \tag{60}$$

We have not found an explicit solution for $\Delta \sim 1$, but if we take $\Delta \rightarrow 0$ in Eq. (59) we recover Eq. (53). Thus, the two approximations agree for $\Delta \sim 1$ and we will therefore use equation Eq. (59) as an approximation for the fifth force for all Δ.

For a body of fixed size R, the effective gravitational constant is seen to decrease with increasing ρ_c demonstrating the chameleonlike behavior and thus we recover the Newtonian regime for virialized halos, see Fig. 4.

IV. COSMOLOGICAL SUPERSYMMETRON

In this section, we discuss the cosmological evolution of the supersymmetron at the background level, the linear perturbations, and the spherical collapse.

A. Background cosmology

The background evolution of the supersymmetron in a flat Friedmann-Lemaitre-Robertson-Walker metric

$$ds^2 = -dt^2 + a(t)^2(dx^2 + dy^2 + dz^2) \tag{61}$$

is determined by the Friedman equation which in the late Universe reads

$$3M_{\rm pl}^2H^2 = \rho_b + \rho_{\rm CDM} + \rho_{\rm DE}, \tag{62}$$

where ρ_b is the baryon density, $\rho_{\rm CDM}$ the dark matter density, and $\rho_{\rm DE}$ is the dark energy density. In the following, we will ignore the baryons and treat all matter as CDM. The CDM energy density is conserved implying that

$$\dot{\rho}_{\rm CDM} + 3H\rho_{\rm CDM} = 0. \tag{63}$$

The DE density is given by the sum of the energy density in the supersymmetron and a CC

$$\rho_{\rm DE} = \rho_{\rm CC} + \rho_\varphi, \tag{64}$$

where $\rho_\varphi = \frac{\dot{\varphi}^2}{2} + V_F + (A(\varphi) - 1)\rho_{\rm CDM}$. We will later see that a nonzero CC is required to have a viable cosmology. This CC may come from supersymmetry breaking [15].

The field equation Eq. (29) in the Friedmann-Lemaitre-Robertson-Walker metric Eq. (61) becomes

$$\ddot{\varphi} + 3H\dot{\varphi} + V_{{\rm eff},\varphi} = 0. \tag{65}$$

The mass of the field is constrained by Eq. (28) which means that $m_\varphi \gg H$ in the late Universe. The minimum φ_ρ is therefore an attractor which the field follows. Along this attractor, the kinetic term is negligible as $\frac{\dot{\varphi}^2}{2V_{\rm eff}} \sim \left(\frac{H}{m_\varphi}\right)^2 \ll 1$. In Fig. 1, we show the cosmological evolution of φ_ρ and m_φ with redshift.

When the supersymmetron follows the attractor, we have

$$\rho_\varphi \simeq \begin{cases} x\rho_{\rm CDM}\frac{(n+1)}{n}\left(\frac{\rho_\infty}{\rho_{\rm CDM}}\right)^{1/(n+1)} & \rho_{\rm CDM} \gg \rho_\infty \\ x\rho_{\rm CDM} & \rho_{\rm CDM} \lesssim \rho_\infty. \end{cases} \tag{66}$$

The equation of state along the attractor is given by

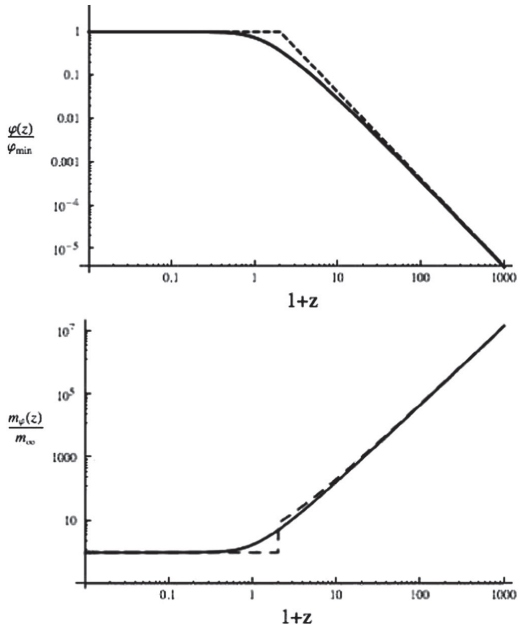

FIG. 1. The cosmological evolution of φ_ρ (above) and m_φ (below) as function of redshift. The dashed line shows the analytical approximation Eq. (32) (above) and Eq. (35) (below). The supersymmetron parameters are $z_\infty = 1.0$, $\beta = 1$, and $n = 0.5$. x and m_∞ do not have any influence on the evolution of the minimum and do therefore not need to be specified here.

$$\omega_\varphi = \frac{p_\varphi}{\rho_\varphi} \simeq -\frac{V_F}{V_{\rm eff}} \simeq \begin{cases} -\frac{1}{n+1} & \rho_{\rm CDM} \gg \rho_\infty \\ 0 & \rho_{\rm CDM} \ll \rho_\infty. \end{cases} \tag{67}$$

To have acceleration of the Universe without a CC, we need to impose $z_\infty > 0$ and $n < 2$. When the field converges to the supersymmetric minimum, $p_\varphi \simeq -V_F \to 0$ and the acceleration stops. To have agreement with observations, we need a nonzero CC, as was pointed out in [15]. With the inclusion of a CC, the dark energy equation of state is modified

$$\omega_{\rm DE} = \frac{p_\varphi - \rho_{\rm CC}}{\rho_\varphi + \rho_{\rm CC}} \simeq \begin{cases} \omega_\varphi & \rho_\varphi \gg \rho_{\rm CC} \\ -1 & \rho_\varphi \ll \rho_{\rm CC}. \end{cases} \tag{68}$$

In Fig. 2, we show the dark energy equation of state as function of redshift and $f \equiv \frac{\Omega_\varphi}{\Omega_\varphi + \Omega_{\rm CC}}$: the fraction of dark energy in the supersymmetron to the total dark energy density today.

To find out how large a contribution the supersymmetron we can have in the energy budget of our Universe, we will first look at the linear perturbations to get a constraint on the model parameters and then apply these constraints to the background cosmology.

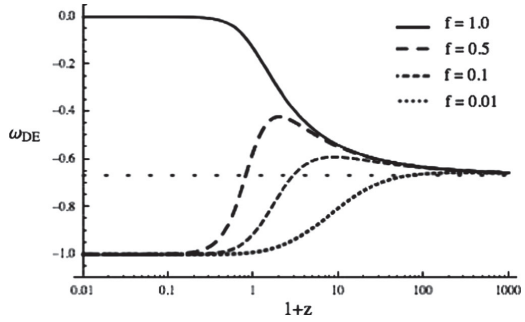

FIG. 2. The equation of state for the supersymmetron as function of redshift for four different values of $f = \frac{\Omega_\varphi}{\Omega_\varphi + \Omega_{CC}}$: the fraction of dark energy in the supersymmetron to the total dark energy density today. The horizontal dotted line shows the analytical approximation $\omega_\varphi = -\frac{1}{n+1}$. The supersymmetron parameters are $z_\infty = 1.0$, $\beta = 1$, $n = 0.5$ and x is fixed to give the desired f in each case.

B. Linear perturbations

The coupling of the supersymmetron Eq. (15) to dark matter leads to a fifth force which will influence the growth of the linear perturbations and structure formation in general. The similarity of the model with chameleons yields that in high-density regions the fifth force will be screened as shown in Sec. III.

The growth of the dark matter perturbations $\delta = \frac{\delta\rho_{CDM}}{\rho_{CDM}}$ for subhorizon scales are determined by (see e.g. [45,49–51])

$$\ddot{\delta} + 2H\dot{\delta} = \frac{3}{2}H^2\Omega_{CDM}(a)\delta\left(\frac{G_{eff}(k)}{G}\right)_{lin}, \qquad (69)$$

where the effective gravitational constant is given by

$$\left(\frac{G_{eff}(k)}{G}\right)_{lin} = 1 + \frac{2((\log A)_{,\varphi}M_{pl})^2}{1 + \frac{a^2m_\varphi^2}{k^2}} \approx 1 + \frac{2(A_{,\varphi}M_{pl})^2}{m_\varphi^2}\frac{k^2}{a^2}, \qquad (70)$$

where the last equality comes from the fact that the supersymmetron is very heavy compared to astrophysical scales and where we have assumed $A(\varphi) - 1 \ll 1$ [see Eq. (73)].

In order to have signatures on the linear perturbations, we need the coupling strength to satisfy $2(A_{,\varphi}M_{pl})^2 \gg 1$, i.e. the supersymmetron must be very strongly coupled. It has been argued [52,53] that an adiabatic instability exists in the regime, a point we will return to when discussing the nonlinear evolution in the next section.

At early times, $\rho_{CDM} \gg \rho_\infty$, we find

$$\left(\frac{G_{eff}(k)}{G}\right)_{lin} \approx 1 + \left(\frac{6}{(n+1)\Omega^0_{CDM}}\right) \times x10^4\left(\frac{k/a}{0.1h\ \mathrm{Mpc}^{-1}}\right)^2 \times \left(\frac{1+z_\infty}{1+z}\right)^{3/(n+1)} \qquad (71)$$

and as the field converges to the supersymmetric minimum we obtain

$$\left(\frac{G_{eff}(k)}{G}\right)_{lin} \approx 1 + \left(\frac{12}{n\Omega^0_{CDM}}\right) \times \frac{x10^4}{(1+z_\infty)^3}\left(\frac{k/a}{0.1h\ \mathrm{Mpc}^{-1}}\right)^2. \qquad (72)$$

In both cases, we see that a comoving scale of $k/a = \mathcal{O}(0.1h\ \mathrm{Mpc}^{-1})$ (a linear scale in general relativity) will experience a very large correction if $x \ll 1$ is not satisfied. With $x \ll 1$, we also have

$$A(\varphi) - 1 = x\left(\frac{\varphi}{\varphi_{min}}\right)^{(1/\beta)} < x \ll 1 \qquad (73)$$

justifying our claim.

To get a constraint on the model parameters, we define k_{mod} via

$$\left(\frac{G_{eff}(k_{mod}, z=0) - G}{G}\right)_{lin} \equiv 1 \qquad (74)$$

and impose $k_{mod} > 0.1h\ \mathrm{Mpc}^{-1}$ in order for the growth of perturbations to be in agreement with ΛCDM at large scales. With this definition, we can get a constraint on the energy density in the supersymmetron to the total dark energy today. By using Eqs. (74) and (66), we find

$$\frac{\Omega_\varphi}{\Omega_\varphi + \Omega_{CC}} = \begin{cases} \frac{(n+1)^2\Omega^2_{CDM}10^{-4}}{6(1-\Omega_{CDM})}\left(\frac{0.1h/\mathrm{Mpc}}{k_{mod}}\right)^2 & \rho^0_{CDM} \gg \rho_\infty \\ \frac{n\Omega^2_{CDM}10^{-4}(1+z_\infty)^3}{12(1-\Omega_{CDM})}\left(\frac{0.1h/\mathrm{Mpc}}{k_{mod}}\right)^2 & \rho^0_{CDM} \lesssim \rho_\infty. \end{cases} \qquad (75)$$

If $\rho^0_{CDM} \gg \rho_\infty$, the energy density in the supersymmetron today is negligible compared to the CC. In the other regime $\rho^0_{CDM} \lesssim \rho_\infty$, we find

$$\frac{\Omega_\varphi}{\Omega_\varphi + \Omega_{CC}} < 10^{-4}(1+z_\infty)^3 \qquad (76)$$

and we must require $z_\infty > 10$ if the supersymmetron is to account for a significant part of the dark energy budget. However, the dominating contribution to dark energy must be the CC as otherwise the equation of state Eq. (68) reads $\omega_{DE} \approx 0$ today and hence no acceleration. Thus, is both cases we find that a pure CC is required to account for dark energy.

Returning to the linear perturbations, we see that the linear effective gravitational constant is increasing as we

go to smaller scales (large k). For $k > k_{\rm mod}$, the supersymmetron fifth force is dominating over gravity at the linear level and to have a viable theory we need a large $k_{\rm mod}$. At nonlinear scales, we expect a chameleonlike effect to kick in and screen the fifth force. We will study the nonlinear effects by looking at the spherical collapse.

C. Spherical collapse

In this section, we look at the collapse of a spherical top-hat overdensity taking the supersymmetron fifth force into account. This will allow us to extract constraints on the model parameters by requiring the model to agree with ΛCDM on large scales.

The equation of motion of a spherical shell at the edge of the top-hat overdensity in a scalar-tensor theory with a fifth force was derived in [24]. The final form of the equation can be understood from a simple Newtonian argument. In the derivation below, we neglect the CC energy density because the Newtonian picture does not assign any energy density to pressure and therefore a Newtonian derivation cannot yield the correct contribution (which involves contributions from pressure) from the CC without some *ad hoc* assumptions.

The total energy of a collapsing spherical shell of matter is given by

$$\frac{E}{m_{\rm shell}} = \frac{1}{2}\dot{r}^2 - \frac{GM_{<r}}{r} + V(\varphi), \tag{77}$$

where $V(\varphi)$ is the fifth-force potential. Neglecting shell crossing so that the total energy is conserved and using $\dot{E} = 0$, we get Newton's law for the shell

$$m_{\rm shell}\ddot{r} = -(F_{\rm gravity}(r) + F_{\varphi}(r)) \tag{78}$$

which can be written

$$\frac{\ddot{r}(t)}{r(t)} = -\frac{1}{6}\frac{\rho_{\rm CDM}}{M_{\rm pl}^2}\left(1 + \frac{F_{\varphi}(r)}{F_{\rm gravity}(r)}\right) = -\frac{1}{6}\frac{\rho_{\rm CDM}}{M_{\rm pl}^2}\left(\frac{G_{\rm eff}(r)}{G}\right)_{\rm sph}. \tag{79}$$

The term on the right-hand side of Eq. (79) agrees with the matter term found from a full derivation including pressure and gives the result

$$\frac{\ddot{r}(t)}{r(t)} = \frac{1}{3}\frac{\rho_{\rm DE}}{M_{\rm pl}^2} - \frac{1}{6}\frac{\rho_{\rm CDM}}{M_{\rm pl}^2}\left(\frac{G_{\rm eff}(r)}{G}\right)_{\rm sph}. \tag{80}$$

In the following, the DE density is taken to be a pure CC and the effective gravitational constant is derived in Sec. III, see Eq. (59). For a small overdensity of size r, we can write Eq. (53) as

$$\left(\frac{G_{\rm eff}(r)}{G}\right)_{\rm sph} \approx 1 + \left(\frac{4}{n\Omega^0_{\rm CDM}}\right)\times\frac{x10^{36}}{(1+z_\infty)^3}\left(\frac{\rm Mpc/h}{r}\right)\times\left(\frac{m_\infty}{\rm eV}\right)\times\left(\frac{\rho_\infty}{\rho_{\rm CDM}}\right)^{(2-2\beta)/(n+1)} \tag{81}$$

when $\rho_{\rm CDM} \lesssim \rho_\infty$ and

$$\left(\frac{G_{\rm eff}(r)}{G}\right)_{\rm sph} \approx 1 + \left(\frac{4}{\sqrt{2n(n+1)}\Omega^0_{\rm CDM}}\right)\times\frac{x10^{36}}{(1+z_\infty)^3}\times\left(\frac{\rm Mpc/h}{r}\right)\times\left(\frac{m_\infty}{\rm eV}\right)\times\left(\frac{\rho_\infty}{\rho_{\rm CDM}}\right)^{(4-2\beta+n)/2(n+1)} \tag{82}$$

for $\rho_{\rm CDM} \gg \rho_\infty$. Note that the effective gravitational constant in the spherical collapse is much larger than the corresponding linear value. For a large-scale overdensity today, $\rm Mpc/h \lesssim r$, to agree with ΛCDM we must require

$$x \lesssim 10^{-36}\left(\frac{\rm eV}{m_\infty}\right) \ll 10^{-36}. \tag{83}$$

For such a small value of x, by looking at Eqs. (71) and (72) we see that the linear perturbations will be indistinguishable from ΛCDM. This also means that the adiabatic instability that might exist in these models is avoided at the linear level.

By changing coordinates to $y = \frac{r}{aR}$ where $R = \frac{r_i}{a_i}$, we can write Eq. (80) in the form

$$y'' + \left(2 - \frac{3}{2}\Omega_m(N)\right)y' + \frac{\Omega_m(N)}{2}(y^{-3} - 1)y\left(\frac{G_{\rm eff}(aRy)}{G}\right)_{\rm sph} = 0, \tag{84}$$

where a prime denotes a derivative with respect to $N = \log(a)$.

The density contrast $\Delta = \frac{\rho_{\rm CDM}}{\bar{\rho}_{\rm CDM}} - 1$ of the collapsing sphere can be obtained from $\Delta = y^{-3} - 1$ and the mass from $M \approx \frac{4\pi R^3}{3}\bar{\rho}^0_{\rm CDM}$. Early on, we have $y \approx 1 - \frac{\Delta}{3}$ as the overdensity follows the expansion, and by linearizing this equation we obtain the equation for the linear evolution of the density contrast

$$\Delta'' + \left(2 - \frac{3}{2}\Omega_m(N)\right)\Delta' - \frac{3}{2}\Omega_m(N)\Delta\left(\frac{G_{\rm eff}(r)}{G}\right)_{\rm lin} = 0, \tag{85}$$

where

$$\left(\frac{G_{\rm eff}(r)}{G}\right)_{\rm lin} = 1 + 2(A_{,\varphi}M_{\rm pl})^2(1 + m_b r)e^{-m_b r} \tag{86}$$

which is the same equation as for the linear perturbations Eq. (69) in real space. As mentioned before,

$$\left(\frac{G_{\rm eff}(r)-G}{G}\right)_{\rm lin} \ll \left(\frac{G_{\rm eff}(r)-G}{G}\right)_{\rm sph} \lesssim \mathcal{O}(1) \qquad (87)$$

on linear scales and the linear equation reduces to that of ΛCDM. This also shows that nonlinear effects are very dominant in this model.

The initial conditions for the numerical implementation are taken to be the same as for ΛCDM:

$$y_i = 1 - \frac{\Delta_i}{3}, \qquad y_i' = \frac{\Delta_i}{3}, \qquad \Delta_i' = \Delta_i. \qquad (88)$$

In Fig. 3, we show the evolution of the radius of an overdensity at different scales. Smaller overdensities collapse earlier as the fifth force is more dominant.

In Fig. 4, we plot the evolution of the effective gravitational constant for the same case as Fig. 3. As the density contrast of the collapsing sphere increases, the chameleon mechanism kicks in and effectively shields the fifth force.

Too see more clearly the effect of the fifth force on the formation of halos, we calculate the linearly extrapolated density contrast for collapse today as function of the virial mass of the halo compared to the ΛCDM prediction $\delta_c \approx 1.67$, see Fig. 5. Low-mass halos are seen to require a smaller linear density contrast than that of ΛCDM in order to collapse due to the fifth force.

With the linear collapse threshold δ_c, we can predict the halo mass function. In the standard Press-Schechter approach, one assumes that all regions with $\delta > \delta_c$ in the linear extrapolated density field collapse to form halos. The fraction of mass within halos with a given mass is determined by the variance of the linear density field smoothed over that scale. We adopt the Sheth-Tormen (ST) prescription [54] for the halo mass function. The ST description for the comoving number density of halos per logarithmic mass interval in the virial mass M is given by

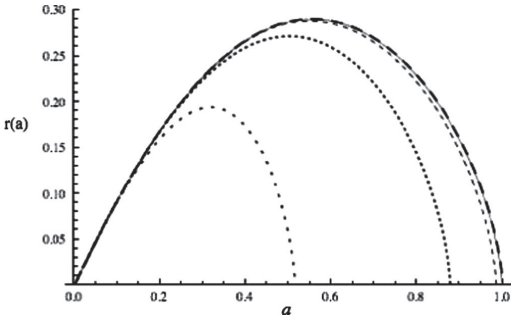

FIG. 3. $r(a)$ as a function of the scale factor a for $R = \frac{r_i}{a_i} = 0.1, 1, 10, 100$ Mpc$/h$ (from left to right) compared with the behavior for r in usual ΛCDM (solid line). The initial density contrast is the same in all runs and is fixed such as to give collapse today for ΛCDM. The supersymmetron parameters are $z_\infty = 0.0$, $\beta = n = 1$, $x = 10^{-43}$, and $m_\infty = 10^5$ eV.

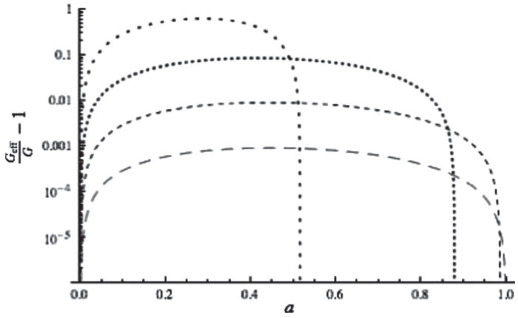

FIG. 4. The strength of the fifth force at the surface of the spherical overdensity during the collapse as a function of the scale factor a for $R = \frac{r_i}{a_i} = 0.1, 1, 10, 100$ Mpc$/h$ (from top to bottom). The parameters are the same as in Fig. 1.

$$n_{\log M} = \frac{dn}{d\log M} = \frac{\bar\rho}{M} f(\nu) \frac{d\nu}{d\log M}, \qquad (89)$$

where the peak threshold

$$\nu = \frac{\delta_c(M)}{\sigma(M)} \qquad (90)$$

and

$$\nu f(\nu) = C\sqrt{\frac{2}{\pi} a\nu^2}\left(1 + \frac{1}{(a\nu^2)^p}\right) e^{-(a\nu^2/2)}. \qquad (91)$$

We adopt the standard parameters $a = 0.75$ and $p = 0.3$ in the following for which $C = 0.322$. $\sigma(M)$ is the variance of the linear density field convolved with a top-hat of radius R ($M = \frac{4\pi}{3}\bar\rho R^3$),

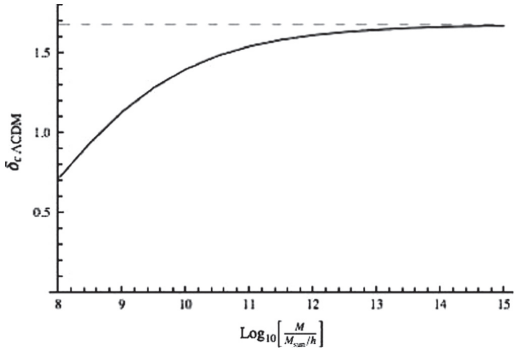

FIG. 5. The ΛCDM-lineary-extrapolated critical density contrast for collapse for the supersymmetron as a function of the halo mass. The dashed line shows the ΛCDM prediction $\delta_c \approx 1.67$. The supersymmetron parameters are $z_\infty = 0.0$, $\beta = n = 1$, $x = 10^{-43}$, and $m_\infty = 10^5$ eV.

$$\sigma(R)^2 = \int \frac{k^3}{2\pi^2} P_L(k)|W(kR)|^2 \frac{dk}{k}, \tag{92}$$

where $P_L(k)$ is the linear power spectrum, which for the supersymmetron is that of ΛCDM, and $W(x) = \frac{3}{x^3} \times (\sin(x) - x\cos(x))$ is the Fourier transform of the top-hat window function. The power-spectrum is normalized to $\sigma_8 \equiv \sigma(R = 8\ \mathrm{Mpc}/h)$. We have chosen $\sigma_8 = 0.8$ in our analysis.

The virial theorem gives us the condition for virialization of a halo. This condition reads $2T + W = 0$, where $T = \frac{3}{10} M\dot{R}^2$ is the kinetic energy and $W = -\int d^3x \rho_m(x)\vec{x}\cdot\vec{\nabla}\Psi$ is the potential energy. In the presence of a fifth force, the potential $\Psi = \Phi_N + A(\varphi\rho_m)$ is the sum of the gravitational potential and the fifth-force potential. In the spherical symmetric case, we have

$$W = W_N - \int_0^R 4\pi r^3 \rho_m \frac{dA(\varphi)}{dr} dr, \tag{93}$$

where $W_N = -\frac{3}{5}\frac{GM^2}{R}$ is the gravitational potential energy. Performing the integration on the right-hand side using integration by parts, we find

$$\left| \int_0^R 4\pi r^3 \rho_m \frac{dA(\varphi)}{dr} \right| \leq 4\pi R^3 \rho_m (A(\varphi(R)) - 1). \tag{94}$$

Note that this term is usually much smaller than the gravitational potential energy. This can be understood from the chameleon thin-shell analogue: the fifth force is only felt in a thin shell close to the surface of the body and therefore the potential energy associated with the fifth force for the whole halo is small.

In Fig. 6, we show the ST mass function of the supersymmetron relative to that of ΛCDM. Because the supersymmetron fifth force is increasing with decreasing scale, we recover ΛCDM on large scales, but see an enhancement in the mass function for low-mass halos.

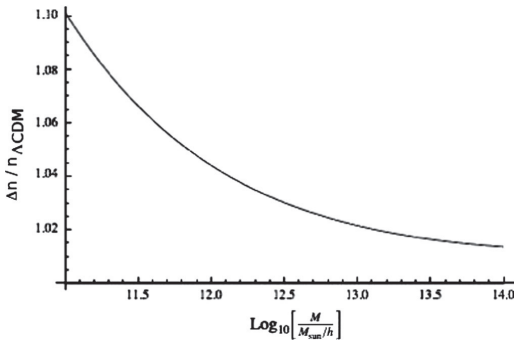

FIG. 6. The fractional difference in the supersymmetron mass function compared to ΛCDM at $z = 0$. The symmetron parameters are $m_\infty = 10^5$ eV, $z_\infty = 0.0$, $x = 10^{-43}$, and $\beta = n = 1$. The supersymmetron converges to ΛCDM for large halo masses.

V. MASS SCALES

Having found a range for our model parameters which gives predictions that are in agreement with current observations, we will now analyze how these constraints affect the original mass scales Λ_i, of the model.

We start by defining $x' = 10^{40}x$, $m' = \frac{m}{g\ \mathrm{TeV}}$, and $z' = (1 + z_\infty)^3$. We can now rewrite Eq. (16) as

$$\frac{\phi_{\min}}{H_0} \approx 10^5 m' x' \tag{95}$$

and Eq. (17) as

$$\left(\frac{\Lambda}{M_{\mathrm{pl}}}\right)^4 \approx 10^{-160} x' z'. \tag{96}$$

From Eq. (10), we find

$$\left(\frac{M}{M_{\mathrm{pl}}}\right)^{n+4} \approx 10^{-160-55n} x'^{n+1} m'^n z'. \tag{97}$$

By using Eq. (7), we get

$$\left(\frac{\Lambda_1}{\Lambda_0}\right)^{2\beta-2}\left(\frac{\Lambda_0}{M_{\mathrm{pl}}}\right)^{n+4} \approx 10^{-160-55n} x'^{n+1} m'^n z', \tag{98}$$

$$\left(\frac{\Lambda_1}{\Lambda_2}\right)^{2\beta-2}\left(\frac{\Lambda_2}{M_{\mathrm{pl}}}\right)^{4} \approx 10^{-160} x' z' \tag{99}$$

from which we find

$$\left(\frac{\Lambda_2}{\Lambda_0}\right)^{2+2\beta}\left(\frac{\Lambda_0}{10^5 H_0}\frac{1}{x'm'}\right)^n \approx 1. \tag{100}$$

The simplest case to analyze is $\beta = 1$ for which the scale Λ_1 vanishes from the theory. We find

$$\Lambda_2 \approx 10^{20}(x'z')^{1/4} H_0 \tag{101}$$

i.e. Λ_2 needs to be between the current Hubble scale and the dark energy scale. This scale can be elevated by increasing the redshift $z_\infty \gg 1$, but we typically need a redshift in the very early Universe to reach super-TeV scales. For Λ_0, we find

$$\Lambda_0 \approx 10^{20}\left(\frac{z'}{(x'm')^n}\right)^{(1/4)} H_0. \tag{102}$$

In the general case $\beta \neq 1$, we see from Eq. (98) that taking $\beta < 1$ together with $\Lambda_1 \gg \Lambda_0$, Λ_2 can serve to increase the other two scales. For example, $\beta = \frac{1}{2}$ and $\Lambda_1 \approx M_{\mathrm{pl}}$ gives

$$\Lambda_2 \approx \Lambda_0 \approx 10^{28}(x'z')^{(1/5)} H_0 \tag{103}$$

which is around the dark energy scale. There seems to be no unfine-tuned way of bringing these mass scales up to typical particle physics scales if we want the cosmological symmetry breaking to be close to the present era. For

example, to have $\Lambda_2 \sim$ TeV when $\beta = 1$ and $x' \approx 1$ then Eq. (98) shows that we need $z' \approx 10^{100}$ which translates to $\rho_\infty \approx (10^{13}\ \mathrm{GeV})^4$.

Finally, and from a field theoretic point of view, the scale Λ_1 has a different status from $\Lambda_{0,2}$. The former appears in the Kähler potential as a suppression of scales for higher-dimensional operators and signals the typical scales above which the effective field theory description breaks down. On the contrary, $\Lambda_{0,2}$ appear in the superpotential and are protected by nonrenormalization theorems. Hence, we expect that Λ_1 should be sensitive to high-energy physics and represents the effective cutoff of the theory. On the other hand, $\Lambda_{0,2}$ may be already present at very high energy even if these scales are very low. Of course, this does not provide an explanation for the discrepancy of scales between Λ_1 and $\Lambda_{0,2}$ which is not natural.

VI. DISCUSSION AND CONCLUSION

We have studied the cosmological evolution of the supersymmetron and its possible effects on structure formation. Requiring that linear perturbations are in agreement with ΛCDM on large scales, we find that the energy density in the supersymmetron is negligible compared to the dark matter density and a pure cosmological constant must be introduced to play the role of dark energy.

The nonlinear evolution of the model was also investigated by using the spherical collapse model. Spherically symmetric solutions to the field equation have been derived and used to predict the fifth-force effects on a collapsing halo. The effective gravitational constant at the edge of a spherical overdensity has been found to be much larger than the linear prediction due to the highly nonlinear properties of the model. The model parameter must be tuned such that the spherical collapse is under control on large scales. This implies that linear perturbations reduce to that of ΛCDM. On nonlinear scales, the model then predicts a faster collapse than that of ΛCDM. In particular, we find that the supersymmetron predicts an excess of small mass halos compared to ΛCDM. However, for this to be the case, one or more of the mass scales in the theory must be fine-tuned.

On very small scales, i.e. galaxy scales, the matter density is large enough to effectively screen the fifth force via the chameleon mechanism. This nonlinear regime could in principle be probed using N-body simulations. However, due to the enormous mass of the field this poses a severe challenge for existing methods.

ACKNOWLEDGMENTS

A. C. D. is supported in part by STFC. H. A. W. thanks the Research Council of Norway FRINAT Grant No. 197251/V30. H. A. W. thanks DAMPT at Cambridge University and IPhT CEA Saclay for the hospitality where a part of this work was carried out.

[1] E. J. Copeland, M. Sami, and S. Tsujikawa, Int. J. Mod. Phys. D **15**, 1753 (2006).
[2] P. Binetruy, *Supersymmetry* (Oxford University, New York, 2006).
[3] A. D. Linde, Lect. Notes Phys. **738**, 1 (2008).
[4] A. I. Vainshtein, Phys. Lett. **39B**, 393 (1972).
[5] C. Deffayet, G. R. Dvali, G. Gabadadze, and A. I. Vainshtein, Phys. Rev. D **65**, 044026 (2002).
[6] N. Arkani-Hamed, H. Georgi, and M. D. Schwartz, Ann. Phys. (N.Y.) **305**, 96 (2003).
[7] K. Hinterbichler and J. Khoury, Phys. Rev. Lett. **104**, 231301 (2010).
[8] J. Khoury, arXiv:1011.5909.
[9] J. Khoury and A. Weltman, Phys. Rev. Lett. **93**, 171104 (2004).
[10] J. Khoury and A. Weltman, Phys. Rev. D **69**, 044026 (2004).
[11] K. Choi, Phys. Rev. D **62**, 043509 (2000).
[12] E. J. Copeland, N. J. Nunes, and F. Rosati, Phys. Rev. D **62**, 123503 (2000).
[13] P. Brax and J. Martin, Phys. Lett. B **468**, 40 (1999).
[14] P. Brax and J. Martin, Phys. Rev. D **61**, 103502 (2000).
[15] P. Brax and A.-C. Davis, Phys. Lett. B **707**, 1 (2012).
[16] A. C. Davis, B. Li, D. F. Mota, and H. A. Winther, Astrophys. J. **748**, 61 (2012).
[17] P. Brax, C. van de Bruck, A.-C. Davis, B. Li, and D. J. Shaw, Phys. Rev. D **83**, 104026 (2011).
[18] G.-B. Zhao, B. Li, and K. Koyama, Phys. Rev. D **83**, 044007 (2011).
[19] B. Li, D. F. Mota, and J. D. Barrow, Astrophys. J. **728**, 109 (2011).
[20] B. Li and H. Zhao, Phys. Rev. D **80**, 044027 (2009).
[21] M. Baldi, Nucl. Phys. B, Proc. Suppl. **194**, 178 (2009).
[22] H. Oyaizu, Phys. Rev. D **78**, 123523 (2008).
[23] H. Oyaizu, M. Lima, and W. Hu, Phys. Rev. D **78**, 123524 (2008).
[24] P. Brax, R. Rosenfeld, and D. A. Steer, J. Cosmol. Astropart. Phys. 08 (2010) 033.
[25] P. Brax, C. van de Bruck, A.-C. Davis, and A. M. Green, Phys. Lett. B **633**, 441 (2006).
[26] F. Schmidt, M. V. Lima, H. Oyaizu, and W. Hu, Phys. Rev. D **79**, 083518 (2009).
[27] B. Li and G. Efstathiou, arXiv:1110.6440.
[28] F. Schmidt, W. Hu, and M. Lima, Phys. Rev. D **81**, 063005 (2010).
[29] D. F. Mota and C. van de Bruck, Astron. Astrophys. **421**, 71 (2004).
[30] N. J. Nunes and D. F. Mota, Mon. Not. R. Astron. Soc. **368**, 751 (2006).

[31] N. J. Nunes, A. C. da Silva, and N. Aghanim, Astron. Astrophys. **450**, 899 (2006).
[32] C. Horellou and J. Berge, Mon. Not. R. Astron. Soc. **360**, 1393 (2005).
[33] M. Manera and D. F. Mota, Mon. Not. R. Astron. Soc. **371**, 1373 (2006).
[34] L. R. Abramo, R. C. Batista, L. Liberato, and R. Rosenfeld, J. Cosmol. Astropart. Phys. 11 (2007) 012.
[35] L. R. Abramo, R. C. Batista, L. Liberato, and R. Rosenfeld, Phys. Rev. D **79**, 023516 (2009).
[36] S. Basilakos, J. C. Bueno Sanchez, and L. Perivolaropoulos, Phys. Rev. D **80**, 043530 (2009).
[37] F. Pace, J.-C. Waizmann, and M. Bartelmann, arXiv: 1005.0233 [Mon. Not. R. Astron. Soc. (to be published)].
[38] P. Creminelli, G. D'Amico, J. Norena, L. Senatore, and F. Vernizzi, J. Cosmol. Astropart. Phys. 03 (2010) 027.
[39] P. Valageas, Astron. Astrophys. **525**, A98 (2010).
[40] L. Amendola, M. Gasperini, D. Tocchini-Valentini, and C. Ungarelli, Phys. Rev. D **67**, 043512 (2003).
[41] H. P. Nilles, Phys. Rep. **110**, 1 (1984).
[42] D. F. Mota and D. J. Shaw, Phys. Rev. D **75**, 063501 (2007).
[43] P. Brax, C. van de Bruck, D. F. Mota, N. J. Nunes, and H. A. Winther, Phys. Rev. D **82**, 083503 (2010).
[44] L. Amendola and S. Tsujikawa, *Dark Energy—Theory and Observations* (Cambridge University Press, Cambridge, England, 2010).
[45] P. Brax, C. van de Bruck, A.-C. Davis, J. Khoury, and A. Weltman, Phys. Rev. D **70**, 123518 (2004).
[46] P. Brax, C. van de Bruck, A. C. Davis, J. Khoury, and A. Weltman, in *Phi in the Sky: Workshop on the Quest for Cosmological Scalar Fields*, AIP Conf. Proc. No. 736 (AIP, New York, 2005).
[47] D. F. Mota and D. J. Shaw, arXiv:0805.3430.
[48] T. Tamaki and S. Tsujikawa, Phys. Rev. D **78**, 084028 (2008).
[49] L. Amendola, Phys. Rev. D **69**, 103524 (2004).
[50] D. F. Mota and H. A. Winther, Astrophys. J. **733**, 7 (2011).
[51] R. Gannouji, B. Moraes, D. F. Mota, D. Polarski, S. Tsujikawa, and H. A. Winther, Phys. Rev. D **82**, 124006 (2010).
[52] R. Bean, E. E. Flanagan, and M. Trodden, New J. Phys. **10**, 033006 (2008).
[53] R. Bean, E. E. Flanagan, and M. Trodden, Phys. Rev. D **78**, 023009 (2008).
[54] R. K. Sheth and G. Tormen, Mon. Not. R. Astron. Soc. **308**, 119 (1999).

Paper VII

ISIS: a new N-body cosmological code with scalar fields based on RAMSES
Claudio Llinares, David F. Mota, Hans A. Winther
Submitted to A&A July (2013)

Paper VIII

The Layzer-Irvine Equation for Scalar-Tensor Theories
Hans A. Winther
Submitted to PRD June (2013)

The Layzer-Irvine Equation for Scalar-Tensor Theories: A Test of Modified Gravity N-body Simulations

Hans A. Winther[1,*]

[1] *Institute of Theoretical Astrophysics, University of Oslo, 0315 Oslo, Norway*

(Dated: June 11, 2013)

The Layzer-Irvine equation describes energy conservation for a pressure less fluid interacting though quasi-Newtonian gravity in an expanding Universe. We derive the Layzer-Irvine equation for scalar field theories where the scalar field interacts with the matter fields and show applications of this equation by applying it to N-body simulations of modified gravity theories where it can be used as a dynamical test of the accuracy and the implementation when solving the equations of motion.

I. INTRODUCTION

The apparent accelerated expansion of the Universe [1, 2] is one of the biggest puzzles in modern cosmology. There exist several theoretical explanations for it and these generally goes under the broad term dark energy [3].

Dark energy in the form of a cosmological constant is currently the best fit to observations, but it has several theoretical problems like the fine-tuning and the coincidence problem. Some of these problems can be elevated if the energy density of the cosmological constant becomes dynamical. This approach leads to dark energy models where the accelerated expansion is due to some new dynamical field [4]. The dark energy field(s) evolves on cosmological time scales, and therefore if dark energy has interactions with ordinary baryonic matter then a cosmologically long range fifth-force will be the result [5].

Gravity is very well tested in the solar system and the results agree perfectly with the predictions of General Relativity [6]. A gravitational interaction that differ from General Relativity are at odds with local gravity experiments and in models where the dark energy is coupled to dark matter (like coupled quintessence [7]) it is therefore generally assumed that there is no coupling to baryons. If a coupling to baryons do exist (we call this scenario modified gravity) then a screening mechanism [8] is needed to evade local experiments and at the same time give rise to interesting dynamics on cosmological scales.

In the last decade several modified gravity models with a screening mechanism, most based on a single scalar degree of freedom, have been put forward. Models following from works on massive gravity such as DGP [9] and the Galileon [10, 11] are well known examples. Another class of models are the chameleon-like models such as the chameleon/$f(R)$ [12–15], symmetron [16, 17] and environmental dependent dilaton [18].

For this last class of models it has been shown that the background cosmology is generally very close to that of ΛCDM. However, even though the background cosmology is the same, the growth of linear perturbations is modified and alters structure formation. One can also show quite generally that the results of local gravity experiments implies a interaction range in the cosmological background today in the sub megaparsec region [19]. This is in the range where perturbations in the fiducial ΛCDM model goes from being well described by linear theory to where one needs more elaborated methods like N-body simulations to make accurate predictions of the theory.

N-body simulations for modified gravity theories requires one to fully solve for the 3D distribution of the scalar field just as one normally does for the gravitational potential. The highly non-linear form of the field-equation makes this computationally challenging. Recently, several different N-body codes have been created that does this job [20–25], and studies of structure formation in the non-linear regime have been performed for many different modified gravity models like for example the chameleon/$f(R)$ gravity [26–28], the symmetron [29, 30], the environmental dependent dilaton [31], the DGP model [32, 33] and phenomenological fifth-force models [34]. For a review of N-body simulations for non-standard scenarios see [35].

One important lesson learned from these studies is that one needs simulations to make accurate predictions: linear perturbation theory gives inaccurate results for almost all scales where the matter power-spectra differs from ΛCDM [28, 30].

Before performing such simulations the scalar field solver needs to be properly tested for both static and dynamical cases where analytical or semi-analytical solutions exist. For the static case several tests already exist (see e.g. [20]), while for the time evolution of the cosmological simulations so far the only real test is to compare the results with that of other codes.

There is however one other test based on energy conservation, that so far has been ignored for modified gravity simulations, which can be used for this purpose. For collision less N-body simulation (i.e. dark matter only simulations) a Newtonian energy conservation equation, taking into account the expanding background, exist and is known as the Layzer-Irvine equation [36, 37]. This equation gives a relation between the kinetic energy and the gravitational potential energy of dark matter particles and is valid throughout the process of structure formation. The Layzer-Irvine equation also has other applications including the determination of the density, mass and size of galaxy clusters [38–40].

In this paper, we derive the Layzer-Irvine equation for a quite general class of modified gravity models and the methods we use can easily be generalized to get the equation for any scalar field model of interest. We implement the resulting

*Email address: h.a.winther@astro.uio.no

equation in an N-body code and show that it can be used as a new dynamical test for N-body codes of modified gravity.

The setup of this paper is as follows. We begin by briefly reviewing scalar-tensor theories of modified gravity in Sec. (II) and the Layzer-Irvine equation for standard gravity in Sec. (III). The modified Layzer-Irvine equation is derived in Sec. (IV) and we discuss how to implement this equation in an N-body code in Sec. (VI). In Sec. (VII) we present the results from tests on N-body simulations of modified gravity before we summarize and conclude in Sec. (VIII).

Throughout this paper we use units of $c = \hbar = 1$ and the metric signature $(-,+,+,+)$.

II. SCALAR-TENSOR THEORIES OF MODIFIED GRAVITY

In this section be briefly review scalar-tensor modified gravity theories. We are in this paper mainly interested in scalar-tensor theories defined by the action

$$S = \int d^4x\sqrt{-g}\left[\frac{R}{16\pi G} + f(X,\phi)\right] + S_m(A^2(\phi)g_{\mu\nu};\psi_m) \quad (1)$$

where R is the Ricci scalar, G is the bare gravitational constant, g is the determinant of the metric $g_{\mu\nu}$, ϕ the scalar field, $X = -\frac{1}{2}g^{\mu\nu}\phi_{,\mu}\phi_{,\nu}$ and ψ_m represents the different matter-fields which are coupled to the scalar field ϕ via the conformal rescaled metric $\tilde{g}_{\mu\nu} = A^2(\phi)g_{\mu\nu}$.

The Einstein equations follows from a variation of the action with respect to $g_{\mu\nu}$ and reads

$$R_{\mu\nu} - \frac{1}{2}Rg_{\mu\nu} = 8\pi G\left[A(\phi)T^m_{\mu\nu} + T^\phi_{\mu\nu}\right] \quad (2)$$

where $T^m_{\mu\nu}$ is the energy-momentum tensor for the matter fields and

$$T^\phi_{\mu\nu} = f_X\phi_{,\mu}\phi_{,\nu} + g_{\mu\nu}f, \qquad f_X \equiv \frac{\partial f}{\partial X} \quad (3)$$

is the energy-momentum tensor for the scalar field.

The Klein-Gordon equation for ϕ follows from a variation of the action with respect to ϕ and reads

$$\nabla_\mu(f_X\nabla^\mu\phi) = -f_{,\phi} - A_{,\phi}T_m \quad (4)$$

where $T_m = g^{\mu\nu}T^m_{\mu\nu}$ is the trace of the energy-momentum tensor of the matter field(s). In the rest of this paper we will only consider a single dust like matter component for which $T^m = -\rho_m$. The conformal coupling of ϕ to matter gives rise to a fifth-force which in the non relativistic limit and per unit mass is given by

$$\vec{F}_\phi = -\vec{\nabla}\log A = -\frac{\beta(\phi)}{M_{\rm Pl}}\vec{\nabla}\phi, \qquad \beta(\phi) \equiv \frac{d\log A(\phi)}{d\phi} \quad (5)$$

The Bianchi identity and the field equations implies the following conservation equations

$$\nabla_\mu T^{\mu\nu}_\phi = +\frac{\partial\log A}{\partial\phi}A(\phi)T^{\mu\nu}_m\nabla_\mu\phi \quad (6)$$

$$\nabla_\mu(A(\phi)T^{\mu\nu}_m) = -\frac{\partial\log A}{\partial\phi}A(\phi)T^{\mu\nu}_m\nabla_\mu\phi \quad (7)$$

$$\nabla_\mu T^{\mu\nu}_m = 0 \quad (8)$$

The equations presented above are the only one we need to derive the modified Layzer-Irvine equation. For a more thorough review of scalar tensor modified gravity theories see [41].

III. THE LAYZER-IRVINE EQUATION FOR GENERAL RELATIVITY

In this section we re-derive the Layzer-Irvine equation for the case of a collision less fluid interacting with gravity in an expanding background. This equation was first derived by Layzer [36] and Irvine [37] in the early 1960s and our derivation below will be close up to that of [36].

We will here only consider a flat spacetime. However, the results we derive below also applies for curved spacetimes as long as we only apply them to regions smaller than the radius of curvature [36]. The background metric of a flat homogenous and isotropic Universe is the Friedmann-Lemaître-Robertson-Walker metric

$$ds^2 = -dt^2 + dr^2 = -dt^2 + a^2(t)(dx^2 + dy^2 + dz^2) \quad (9)$$

In the following $\vec{x}$ will denote the comoving coordinate and $\vec{r} = a\vec{x}$ the physical coordinate. For a collection of collision less particles the energy momentum tensor is given by

$$T^{\mu\nu}_m(\vec{x'}) = \sum_i \frac{m_i\delta(\vec{x'} - \vec{x_i})u^\mu_i u^\nu_i}{\sqrt{-g}} \quad (10)$$

where u^μ_i is the four velocity of particle i. If we treat the collection of particles as a fluid then we can define

$$T^{\mu\nu}_m = \rho_m u^\mu u^\nu \quad (11)$$

where u^μ is the four-velocity of the fluid. We let $\rho_m(r,t) = \overline{\rho}_m(t) + \delta\rho_m(r,t)$ denote the matter density field and $\vec{v} = a\dot{\vec{x}}$ the peculiar velocity field. An overbar will always denote a quantity defined in the background cosmology, e.g. $\overline{\rho}_m(t)$ is the homogenous and isotropic component of the matter field.

The continuity equation for the energy-momentum tensor reads

$$\nabla_\mu T^{0\mu}_m = 0 \quad \rightarrow \quad \nabla_\mu(\rho_m u^\mu) = 0 \quad (12)$$

By writing out the components and subtracting off the background equation, $\dot{\overline{\rho}}_m + 3H\overline{\rho}_m = 0$, we get it on a convenient form

$$(a^3\dot{\delta}\rho_m) + a^3\vec{\nabla}_r(\rho_m\vec{v}) = 0 \quad (13)$$

In the real Universe the metric is perturbed due to the presence of matter perturbations and this equation will have additional contributions like terms containing the time derivative of the Newtonian potential Φ_N. These terms can generally be neglected as long as the weak-field approximation $\Phi_N \ll 1$ holds (which is the case for most cosmological and astrophysical applications).

The equation describing the motion of the particles (fluid) is the geodesic (Euler) equation,

$$\frac{du^i}{d\tau} + \Gamma^i_{\mu\nu} u^\mu u^\nu = 0, \qquad u^i = \frac{dx^i}{d\tau} \tag{14}$$

If we take the energy-momentum tensor of matter to be that of particles then this equation follows directly from the Bianchi identity. Writing out the geodesic equation and neglecting small terms, we get an equation of motion very similar to the Newtonian result generalized to an expanding background

$$\ddot{\vec{x}} + 2H\dot{\vec{x}} = -\frac{1}{a}\vec{\nabla}_r \Phi_N \tag{15}$$

or equivalently

$$\frac{\partial(a\vec{v})}{\partial t} = -\vec{\nabla}_r(a\Phi_N) \qquad v^i = a\dot{x}^i \tag{16}$$

The Newtonian gravitational potential is determined by the Poisson equation

$$\nabla_r^2 \Phi_N = 4\pi G \delta\rho_m \tag{17}$$

and the solution can also be written explicitly as

$$\Phi_N(r,t) = -G\int \frac{\delta\rho_m(r',t)d^3r'}{|r-r'|} \tag{18}$$

where the integration is over the whole space. The system of equation

$$\ddot{\vec{x}} + 2H\dot{\vec{x}} = -\frac{1}{a}\vec{\nabla}_r \Phi_N \tag{19}$$

$$\nabla_r^2 \Phi_N = 4\pi G \delta\rho_m \tag{20}$$

forms the basis of N-body simulations for collision less matter.

To form the Layzer-Irvine equation we need to integrate the equation of motion Eq. (16) over space. In the following we will consider a very large, but finite, volume to be able to neglect surface terms arising from integration by parts and to avoid convergence problems. It is also possible to consider, as is the case for N-body simulations, a finite volume with periodic boundary conditions. We will in the next section discuss how to handle the case of going to an infinite volume, which turns out to be pretty straight forward and does not change the form of the final equations.

To form the Layzer-Irvine equation we contract Eq. (16) with $\vec{v}a\rho_m d^3r = \vec{v}a^4\rho_m d^3x$ and integrate over the distribution of particles with the result

$$\frac{\partial T}{\partial t} + 2HT = -\int d^3r(\rho_m\vec{v})\cdot(\vec{\nabla}_r\Phi_N) \tag{21}$$

where

$$T = \int \frac{1}{2}v^2\rho_m d^3r = \sum_{i=1}^{N_{\rm particles}} \frac{1}{2}m_i v_i^2 \tag{22}$$

denotes the total kinetic energy associated with the peculiar motion. Using integration by parts and applying the continuity equation Eq. (13) we can rewrite the right hand side of Eq. (21) as

$$\begin{aligned} -\int(\vec{\nabla}_r\Phi_N)\cdot\vec{v}\rho_m d^3r &= \int \Phi_N\vec{\nabla}_r(\vec{v}\rho_m)d^3r \\ &= -\int \Phi_N\frac{\partial}{\partial t}(\delta\rho_m d^3r) \end{aligned} \tag{23}$$

which can be rewritten once again using the Poisson equation as

$$-\int \Phi_N\frac{\partial}{\partial t}(\delta\rho_m d^3r) = -\left(\frac{\partial U_N}{\partial t} + HU_N\right) \tag{24}$$

where

$$\begin{aligned} U_N &= \int \frac{1}{2}\Phi_N\delta\rho_m d^3r \\ &= -\frac{G}{2}\int\int \frac{\delta\rho_m(r,t)\delta\rho_m(r',t)d^3rd^3r'}{|r-r'|} \end{aligned} \tag{25}$$

is the gravitational potential energy. Collecting results we are left with

$$\frac{\partial}{\partial t}(T+U_N) + H(2T+U_N) = 0 \tag{26}$$

which is the Layzer-Irvine equation.

If the total energy $E = T + U_N$ is conserved we recover the well known virial relation $2T + U_N = 0$.

By making the definitions (the justifications for these definitions in terms of statistical physics of fluids have been given by Irvine [37])

$$\epsilon_m = \frac{T+U_N}{\mathcal{V}} \tag{27}$$

$$3p_m = \frac{2T+U_N}{\mathcal{V}} \tag{28}$$

where[1] $\mathcal{V} = \int d^3r$ we have that Eq. (26) can be written on the more familiar form

$$\frac{\partial}{\partial t}\epsilon_m + 3H(\epsilon_m + p_m) = 0 \tag{29}$$

which a cosmological continuity equation.

[1] For an infinite volume this is to be understood as a limiting procedure.

IV. LAYZER-IRVINE EQUATION FOR SCALAR-TENSOR THEORIES

In this section we derive the Layzer-Irvine equation for the class of scalar-tensor (modified gravity) theories given by the action Eq. (1). We will just state the equations describing our system without derivation, as a complete derivation of the equations below can be found in e.g. [31].

As we did in the previous section we take the energy-momentum tensor of the matter to be that of particles. Note that we use the definition of $T^{\mu\nu}_m$ depicted in Eq. (2) so that the density ρ_m satisfies the usually continuity equation Eq. (13), but as we will see below the Newtonian potential is sourced by the density $\rho_J = A(\phi)\rho_m$. The continuity equation in terms of this density reads

$$\frac{(a^3\dot{\delta\rho_J})}{a^3} + \vec{\nabla}_r(\rho_J\vec{v}) - \rho_J\vec{v}\vec{\nabla}_r\log A - \dot{\log A}\delta\rho_J - \overline{\rho}_J\frac{\partial}{\partial t}\log\frac{A}{\overline{A}} = 0 \tag{30}$$

where $\rho_J = A(\phi)\rho_m$ and $\delta\rho_J = A(\phi)\rho_m - A(\overline{\phi})\overline{\rho}_m$.

The geodesic equation describing the motion of the fluid is modified due to the presence of the coupling of ϕ to matter

$$\frac{du^i}{d\tau} + \Gamma^i_{\mu\nu}u^\mu u^\nu = -\frac{d\log A}{d\phi}\left(\phi^{,i} + u^\mu\phi_{,\mu}u^i\right) \tag{31}$$

which in the non-relativistic limit becomes

$$\frac{\partial}{\partial t}(a\vec{v}) + (a\vec{v})\frac{\partial\log A}{\partial t} = -a\vec{\nabla}_r(\Phi_N + \log A) \tag{32}$$

The Poisson equation is also modified due to the presence of the scalar field and reads

$$\nabla^2_r\Phi_N = 4\pi G\delta\rho_J + 4\pi G\delta S_\phi \equiv 4\pi G\delta S_{\rm tot} \tag{33}$$

where the source coming from the scalar field is

$$\delta S_\phi = \delta\rho_\phi + 3\delta p_\phi \tag{34}$$

with $\delta\rho_\phi = \rho_\phi - \overline{\rho}_\phi$ and likewise for δp_ϕ. The energy density and pressure of the scalar field are defined as $\rho_\phi = T^0_{\phi\,0}$ and $p_\phi = \frac{1}{3}T^i_{\phi\,i}$ respectively.

Contracting Eq. (32) with $a\vec{v}\rho_J d^3r = a^4\vec{v}\rho_J d^3x$ and integrating up we find

$$\dot{T} + 2H(T+\delta T) = -\int\vec{\nabla}_r(\Phi_N + \log A)\rho_J\vec{v}d^3r \tag{35}$$

where

$$T = \int d^3r\frac{1}{2}v^2\rho_J \tag{36}$$

$$\delta T = \int d^3r\frac{1}{2}v^2\rho_J\left(\frac{\partial\log A}{\partial\log a}\right) \tag{37}$$

Using the continuity equation Eq. (30) we can remove the velocity term in Eq. (35) by integration by parts to find

$$\int\vec{\nabla}_r(\Phi_N + \log A)\vec{v}\rho_J d^3r = \tag{38}$$

$$+\int\Phi_N\left(\frac{\partial}{\partial t}(\delta S_{\rm tot}d^3r)\right) \tag{39}$$

$$-\int\Phi_N\left(\frac{\partial}{\partial t}(\delta S_\phi d^3r)\right) \tag{40}$$

$$+\int\log A\left(\frac{\partial}{\partial t}(\delta\rho_J d^3r)\right) \tag{41}$$

$$-\int d^3r(\Phi_N + \log A)\delta S_{\rm tot}\frac{\partial\log A}{\partial t} \tag{42}$$

$$+\int d^3r(\Phi_N + \log A)\delta S_\phi\frac{\partial\log A}{\partial t} \tag{43}$$

$$-\int d^3r(\Phi_N + \log A)\overline{\rho}_J\frac{\partial}{\partial t}\log\frac{A}{\overline{A}} \tag{44}$$

$$-\int d^3r(\Phi_N + \log A)(\vec{\nabla}_r\log A)\rho_J\vec{v} \tag{45}$$

We will now go through the different terms one by one.

The first term Eq. (39) can be integrated by parts with the result

$$\int\Phi_N\left(\frac{\partial}{\partial t}(\delta S_{\rm tot}d^3r)\right) = \dot{U}_N + HU_N \tag{46}$$

$$U_N = \int\frac{\Phi_N}{2}\delta S_{\rm tot}d^3r = -\frac{1}{8\pi G}\int d^3r(\vec{\nabla}_r\Phi_N)^2 \tag{47}$$

This last form of U_N follows from the Poisson equation and integration by parts and is identical to that of standard gravity except here the Newtonian potential is also sourced by the scalar field.

The term Eq. (40) is of order $\dot{U}_{S_\phi}$ where

$$U_{S_\phi} = \int\frac{\Phi_N}{2}\delta S_\phi d^3r \tag{48}$$

This term cannot be written on a form that does not include time-derivatives of the Newtonian potential[2]. We will therefore assume $|U_{S_\phi}| \ll |U_N|$ so that we can neglect this term and the term in Eq. (43). For known modified gravity theories this assumption is usually satisfied (see e.g. [29]).

The term Eq. (42) becomes $-H(2\delta U_N + \delta U_{\log A})$ where

$$\delta U_N = \int d^3r\frac{\Phi_N}{2}\delta S_{\rm tot}\frac{\partial\log A}{\partial\log a} \tag{49}$$

$$\delta U_{\log A} = \int d^3r\Phi_N\delta S_{\rm tot}\frac{\partial\log A}{\partial\log a} \tag{50}$$

[2] This is crucial when we later will implement these equations in an N-body code as time-derivatives of the gravitational potential is in most codes not known.

In the following all terms δU_x will mean U_x with the inclusion of a factor $\frac{\partial \log A}{\partial \log a}$ in the integrand. We have, for example,

$$U_N + \delta U_N = \int d^3r \frac{\Phi_N}{2} \delta S_{\rm tot} \left(1 + \frac{\partial \log A}{\partial \log a}\right) \tag{51}$$

and similar for all other terms U_x so that all the terms δU_x can be neglected when $\left|\frac{\partial \log A}{\partial \log a}\right| \ll 1$.

The term Eq. (44) can be neglected as its is a factor $|\Phi_N + \log A| \ll 1$ smaller than a term coming from Eq. (42) as we will show below.

The term Eq. (45) can also be neglected. To see this, take the worst case scenario of a scalar fifth-force which is proportional to gravity everywhere with some constant strength β. In this case this term is of order

$$2\beta^2(1+2\beta^2)\frac{\partial}{\partial t}\int d^3r \frac{\Phi_N^2}{2}\delta S_{\rm tot} \tag{52}$$

and the integrand is a factor $2\beta^2(1+2\beta^2)\Phi_N \ll 1$ smaller than the integrand of U_N for the interesting case $\beta \lesssim \mathcal{O}(1)$.

The only term left to evaluate is Eq. (41). The equation needed to rewrite this term can be found by either using the field equation or more directly by using the conservation equation for the energy-momentum tensor of the scalar field Eq. (3). For the first approach we start with the field equation

$$\begin{aligned}\mathcal{L}_\phi \equiv & \frac{1}{a^3}\frac{\partial}{\partial t}\left(a^3 f_X \dot{\phi}\right) - \vec{\nabla}_r \cdot \left(f_X \vec{\nabla}_r \phi\right) \\ & - f_{,\phi} + \log A_{,\phi}\rho_J = 0\end{aligned} \tag{53}$$

At the background level this equation simplifies to

$$\mathcal{L}_{\overline{\phi}} \equiv \frac{1}{a^3}\frac{\partial}{\partial t}\left(a^3 f_X \dot{\overline{\phi}}\right) - f_{,\phi} + \log A_{,\phi}\rho_J = 0 \tag{54}$$

The two equations above (trivially) implies

$$\int d^3r (\mathcal{L}_\phi \dot{\phi} - \mathcal{L}_{\overline{\phi}} \dot{\overline{\phi}}) = 0 \tag{55}$$

which can be written out and integrated by parts to get it on a convenient form. This procedure applies for any scalar field theory.

The second approach is to start directly from the conservation equation for the scalar field Eq. (6) and integrate it over space to get

$$\begin{aligned}&\frac{\partial}{\partial t}\int d^3r \left(T_\phi{}^0_0 - \overline{T}_\phi{}^0_0\right) + H\int d^3r (T_\phi{}^i_i - \overline{T}_\phi{}^i_i) \\ &= \int d^3r \left(A(\phi)T_m \frac{\partial \log A}{\partial t} - A(\overline{\phi})\overline{T}_m \frac{\partial \log \overline{A}}{\partial t}\right)\end{aligned} \tag{56}$$

where an overbar as usual denotes a background quantity. This expression is valid for any scalar-field theory in which $f = f(\phi, \partial\phi, \partial\partial\phi, ...)$ and not just for our particular $f = f(X, \phi)$. However, if we have a theory where the coupling to the matter sector is not conformal, then the right hand side of this equation needs to be modified.

When we specialize to theories given by the action Eq. (1) we find

$$\begin{aligned}&\left(\dot{U}_{\nabla\phi} - HU_{\nabla\phi}\right) + \left(\dot{U}_{\dot\phi} + 3HU_{\dot\phi}\right) + (U_f - 3HU_f) \\ &+ (\dot{U}_A - H\delta U_A) + \dot{U}_{\log A} = \int \log A \frac{\partial}{\partial t}\left(\delta\rho_J d^3r\right)\end{aligned} \tag{57}$$

where

$$U_{\nabla\phi} = \int d^3r f_X \frac{1}{2}(\nabla_r\phi)^2 \tag{58}$$

$$U_{\dot\phi} = \int d^3r f_X \frac{1}{2}\left(\dot\phi^2 - \dot{\overline{\phi}}^2\right) \tag{59}$$

$$U_f = \int d^3r \left(g(X,\phi) - g(\overline{X},\overline{\phi})\right) \tag{60}$$

$$U_A = \int d^3r \left(\log A(\phi) - \log A(\overline{\phi})\right)\overline{\rho}_J \tag{61}$$

$$\delta U_A = \int d^3r \left(\log A(\phi) - \log A(\overline{\phi})\right)\overline{\rho}_J \left(\frac{\partial \log \overline{A}}{\partial \log a}\right) \tag{62}$$

The g function is defined as $g(X,\phi) \equiv f_X(X,\phi)X - f(X,\phi)$ and

$$\begin{aligned}U_{\log A} &= \int d^3r \log A \delta S_{\rm tot} \\ &= -\frac{1}{4\pi G}\int d^3r \left(\vec{\nabla}_r\Phi_N\right)\cdot(\vec{\nabla}_r \log A)\end{aligned} \tag{63}$$

We can now combine all the results above to get the modified Layzer-Irvine equation

$$\begin{aligned}&\frac{\partial}{\partial t}\left(T + U_N + U_{\log A} + U_A + U_{\nabla\phi} + U_f + U_{\dot\phi}\right) \\ &+ H\left(2T + U_N - U_{\nabla\phi} - 3U_f + 3U_{\dot\phi}\right) \\ &+ H\left(2\delta T - 2\delta U_N - \delta U_{\log A} - \delta U_A\right) = 0\end{aligned} \tag{64}$$

The derivation above assumed a finite volume or a box with periodic boundary conditions. If the volume is infinite we reformulate the equation in terms of

$$W_i = \frac{U_i}{\mathcal{V}} \tag{65}$$

where $\mathcal{V} = \int d^3r = a^3\int d^3x$. The final equation are then to be read as first integrating over a finite volume $\mathcal{V}$ and then taking the limit $\lim_{\mathcal{V}\to\infty} W_i$. This procedure leaves the equation invariant.

To understand the final equation better we can rewrite it slightly. We start with the space averaged energy density and pressure of the scalar field (the space integral of the T_0^0 and T_i^i components)

$$\epsilon_\phi = \frac{U_{\dot\phi} + U_{\nabla\phi} + U_f}{\mathcal{V}} \tag{66}$$

$$3p_\phi = \frac{3U_{\dot\phi} - U_{\nabla\phi} - 3U_f}{\mathcal{V}} \tag{67}$$

where $\mathcal{V} = \int d^3r = a^3 \int d^3x$ is the volume of the Universe or region in question. For the case where the integration is over an infinite region of space then the equations above are to be read as first integrating over a finite volume $\mathcal{V}$ and then taking the limit $\lim_{\mathcal{V}\to\infty}$. We now associate, as we did for standard gravity,

$$\epsilon_m = \frac{T + U_N}{\mathcal{V}} \tag{68}$$

$$3p_m = \frac{2T + U_N}{\mathcal{V}} \tag{69}$$

with the internal energy and the cosmic pressure for the matter (due to gravity) and $\epsilon_{\phi m} = \frac{U_{\log A}}{\mathcal{V}}$ with the potential energy associated with the matter-scalar interaction.

Inserting all this in the modified Layzer-Irvine equation, neglecting the (typically) small terms δU_x, we can write it on the form

$$\frac{\partial}{\partial t}(\epsilon_\phi + \epsilon_m + \epsilon_{m\phi}) + 3H(\epsilon_\phi + \epsilon_m + \epsilon_{m\phi} + p_\phi + p_m) \simeq 0 \tag{70}$$

which is a continuity equation. The total energy density is seen to be just the sum of the expected matter, scalar and interaction energy density and the pressure likewise.

There is one last, but very handy, relation we can derive in the case where the time-derivatives of the scalar field can be neglected in the Klein-Gordon equation. Starting from $U_{\nabla\phi}$ and using integration by parts we find

$$\begin{aligned} U_{\nabla\phi} &= -\frac{1}{2}\int d^3r \phi \nabla(f_X \nabla\phi) \\ &= -\frac{1}{2}\int d^3r \phi \left(f_{,\overline{\phi}} - f_{,\phi} + \frac{\beta(\phi)\rho_m}{M_{\rm Pl}} - \frac{\beta(\overline{\phi})\overline{\rho}_m}{M_{\rm Pl}} \right) \end{aligned} \tag{71}$$

Now if β is a constant then this equation reduces to

$$U_{\nabla\phi} + \frac{1}{2}U_{\log A} = -\frac{1}{2}\int d^3r \phi \left(f_{,\overline{\phi}} - f_{,\phi} \right) \tag{72}$$

which can be used separately from the Layzer-Irvine equation as a consistency relation or together with the Layzer-Irvine equation itself to remove e.g. the term $U_{\nabla\phi}$. The advantage of using Eq. (72) is that it does not depend on time-derivatives and can also be used for a static configuration.

V. SPECIFIC MODELS

In this section we go through specific models and conditions where additional approximations and simplifications can be made. The simplifications we make are those that apply when doing N-body simulations and are not always applicable in general. We start by checking that the equation we have derived gives predictions that agree with our expectations.

A. Enhanced Gravity

Lets, as a consistency check, start with the case where we have a fifth-force that has an infinite Compton wavelength and a constant coupling β. This is achieved by taking $f(X,\phi) = X$ and $A(\phi) = e^{\frac{\beta\phi}{M_{\rm Pl}}}$. This case corresponds to standard gravity, but where Newtons constant G is a factor $1 + 2\beta^2$ larger. Under the assumption that we can neglect time-derivatives in the Klein-Gordon equation for the scalar field we find

$$\log A = \frac{\beta\phi}{M_{\rm Pl}} = 2\beta^2\Phi_N \tag{73}$$

giving

$$U_{\log A} = 4\beta^2 U_N, \quad U_{\nabla\phi} = -2\beta^2 U_N \tag{74}$$

Since $\frac{\beta\phi}{M_{\rm Pl}} = 2\beta^2\Phi_N \ll 1$ we can safely put $A = 1$. This means we can also take $U_A = 0$ and $U_{\dot\phi}$ is negligible as this is second order in the time-derivative of the gravitational potential. The term $U_f \equiv 0$ as $g - \overline{g} \equiv 0$ and this also holds if we add a constant potential (a cosmological constant) to the scalar field. This leaves us with the equation

$$\frac{\partial}{\partial t}\left(T + U_{\rm tot}\right) + H\left(2T + U_{\rm tot}\right) = 0 \tag{75}$$

where $U_{\rm tot} = U_N(1+2\beta^2)$. This is exactly the same result we would get if the gravitational constant is enhanced by a factor $(1 + 2\beta^2)$, i.e. $G_{\rm eff} = G(1 + 2\beta^2)$.

B. Yukawa interaction

The next simplest case is a linear scalar field coupled to matter. This case leads to a total gravitational force between two masses of the Yukawa type

$$\vec{F} = -\frac{GM_1M_2}{r^2}\left(1 + 2\beta^2(1 + mr)e^{-mr}\right)\frac{\vec{r}}{r} \tag{76}$$

where $2\beta^2$ is the strength and m^{-1} is the range of the matter-scalar interaction.

This scenario is achieved by taking $f(X,\phi) = X - V(\phi)$ where $V(\phi) = \frac{1}{2}m^2\phi^2$ and $A(\phi) = e^{\frac{\beta\phi}{M_{\rm Pl}}}$.

As for the case above we can neglect U_A and $U_{\dot\phi}$, but now the term U_f is non-zero

$$U_f = \int d^3r \frac{1}{2}m^2\left(\phi^2 - \overline{\phi}\right)^2 \tag{77}$$

and represents the potential energy of the scalar field itself. From equation Eq. (72) we get the very simple relation

$$U_{\nabla\phi} + \frac{1}{2}U_{\log A} + U_f = 0 \tag{78}$$

which gives the Layzer-Irvine equation

$$\frac{\partial}{\partial t}(T + U_{\rm tot}) + 2H(2T + U_{\rm tot} - 2U_f) = 0 \tag{79}$$

where $U_{\rm tot} = U_N + \frac{1}{2}U_{\log A}$. We can now check that we get the correct value for $U_{\rm tot}$.

If we assume the time-derivatives can be neglected then we can Fourier transform the Klein-Gordon equation with the result

$$\mathcal{F}(\phi) = \frac{\beta \mathcal{F}(\delta\rho_m)}{M_{\rm Pl}} \frac{k^2}{k^2+m^2} \tag{80}$$

Taking the inverse Fourier transform and using the convolution theorem together with $\mathcal{F}^{-1}\left(\frac{4\pi}{m^2+k^2}\right) = \frac{1}{r}e^{-mr}$ we can write down an explicit solution for the scalar field

$$\frac{\beta\phi}{M_{\rm Pl}} = -2\beta^2 G \int \frac{\delta\rho(r_1) d^3 r_1}{|\vec{r}-\vec{r_1}|} e^{-m|\vec{r}-\vec{r_1}|} \tag{81}$$

From this it follows that

$$\begin{aligned} U_{\rm tot} &= U_N + \frac{1}{2}U_{\rm logA} \\ &= -\frac{G}{2}\int\int \frac{\delta\rho(r_1,t)\delta\rho(r_2,t) d^3r_1 d^3 r_2}{|\vec{r_1}-\vec{r_2}|} \times \\ &\quad \times (1+2\beta^2 e^{-m|\vec{r_1}-\vec{r_2}|}) \end{aligned} \tag{82}$$

which is the correct potential energy for a Yukawa interaction combined with gravity. In the limit $m \to 0$ we recover the case discussed above.

C. Non-clustering scalar field

In theories where the scalar field does not cluster significantly the factor $\frac{\partial \log A}{\partial \log a}$ can be taken to be equal to the background value giving $\delta U_x = \frac{\partial \log \overline{A}}{\partial \log a} U_x$.

For quintessence models $f = X - V$ and the coupling to matter is zero ($\beta \equiv 0$) giving the same equation as for standard gravity. The modifications from standard gravity are only implicit in the evolution of $H(t)$. This is also expected as the quintessence field only affects the background cosmology.

Coupled quintessence [7] is a class of models where dark matter and dark energy (given by the scalar field ϕ) have interactions. General models in this class have a time-varying coupling $\beta(\phi) \simeq \beta(\overline{\phi}) \equiv \beta(a)$. The interaction range in these models, when explaining dark energy, are of the order of the Hubble radius giving $\log A \simeq 2\beta^2(a)\Phi_N$ and the Layzer-Irvine equation simplifies greatly to

$$\frac{\partial}{\partial t}(T + U_{\rm tot}) + H(2T + U_{\rm tot}) + 2\frac{\beta(a)\dot{\overline{\phi}}}{M_{\rm Pl}}(T - U_{\rm tot}) = 0 \tag{83}$$

where $U_{\rm tot} = (1+2\beta^2(a))U_N$ is the total potential energy.

D. Chameleon-like theories

Chameleon-like modified gravity theories refers to models given by the action Eq. (1) with $f = X - V(\phi)$. Examples of such model are the $f(R)$/chameleon [12], the symmetron [16] and the environmental dependent dilaton [18]. In these models local gravity constraints forces $\frac{\partial \log A}{\partial \log a} \ll 1$ [19] and all the terms δU_x can be neglected. This also generally implies that $|\dot{\phi}| \ll |\vec{\nabla}\phi|$ implying $U_{\dot{\phi}} \ll U_{\nabla\phi}$, an approximation often refereed to as the quasi-static approximation [29] and is the reason why N-body simulation of these theories can neglect the time-derivatives in the Klein-Gordon equation[3]. This leaves us with the simplified equation

$$\begin{aligned} &\frac{\partial}{\partial t}(T + U_N + U_{\log A} + U_{\nabla\phi} + U_f + U_A) \\ &+ H(2T + U_N - U_{\nabla\phi} - 3U_f) = 0 \end{aligned} \tag{84}$$

VI. IMPLEMENTATION IN N-BODY CODES

In this section we discuss how to numerically implement the modified Layzer-Irvine equation in an N-body code and how we can monitor the level of which it is satisfied.

For standard gravity the kinetic energy of the dark matter particles are calculated from

$$T = \int d^3 r \frac{1}{2} v^2 \rho_m = \sum_{i=1}^{N_{\rm part}} \frac{1}{2} m_i v_i^2 \tag{85}$$

where m_i is the mass of each N-body particle with $m_i = \frac{\rho_{m0} B_0^3}{N_{\rm part}}$ when all particles have the same mass. B_0 denotes the boxsize and $N_{\rm part}$ the number of particles in the simulation.

Using the Poisson equation and integration by parts, the gravitational potential energy can be written

$$U_N = \int d^3 r \frac{1}{2}\Phi_N \delta\rho_m = \frac{1}{4\pi G}\int d^3 r \frac{1}{2}\Phi_N \nabla_r^2 \Phi_N \tag{86}$$

$$= -\frac{1}{8\pi G}\int d^3 r (\vec{\nabla}_r \Phi_N)^2 \tag{87}$$

In an N-body code we can approximate this potential (here for a grid based code) by

$$U_N \simeq -\frac{1}{8\pi G}\sum_{i=0}^{N_{\rm cell}} dx^3_{\rm cell\ i} (\vec{F}_N)_i^2 \tag{88}$$

where the sum is over all the cells of the grid structure, $(\vec{F}_N)_i = -(\vec{\nabla}_r \Phi_N)_i$ is the force field and $dx^3_{\rm cell\ i}$ is the volume of grid-cell i.

In modified gravity, the kinetic energy is modified compared to standard gravity as the mass of the particles are now ϕ dependent

$$T = \sum_{i=1}^{N_{\rm part}} \frac{1}{2} m_i(\phi) v_i^2 \tag{89}$$

[3] Recently, a new code came out where the full Klein-Gordon equation is solved for the first time in an N-body code [25]. Solving the full equation does not seem to have an impact on observables like the power-spectrum and mass-function, but can have large effects in low-density environments.

where $m_i(\phi) = A(\phi)m_i$ and where $\sum_i m_i = \rho_{m0}B_0^3$. As for standard gravity we have

$$U_N \simeq -\frac{1}{8\pi G}\sum_{i=0}^{N_{\rm cell}} dx^3_{{\rm cell}\ i}(\vec{F}_N)_i^2 \tag{90}$$

The fifth-force potential can be rewritten using the Poisson equation and integration by parts to give

$$U_{\log A} = -\frac{1}{8\pi G}\int d^3r\ 2(\vec{\nabla}_r\Phi_N)\cdot(\vec{\nabla}_r \log A) \tag{91}$$

which can be evaluated as

$$U_{\log A} \simeq -\frac{1}{8\pi G}\sum_{i=0}^{N_{\rm cell}} dx^3_{{\rm cell}\ i} 2(\vec{F}_N)_i\cdot(\vec{F}_\phi)_i \tag{92}$$

where $(\vec{F}_N)_i = -\left(\frac{\beta(\phi)}{M_{\rm Pl}}\vec{\nabla}_r\phi\right)_i$ is the fifth-force in grid cell i. The other potentials are trivial to calculate, for example

$$U_A \simeq \sum_{i=0}^{N_{\rm cell}} dx^3_{{\rm cell}\ i}(A(\phi_i) - A(\overline{\phi})) \tag{93}$$

There is also a further simplification for theories with constant coupling β (i.e. $\log A \equiv \frac{\beta\phi}{M_{\rm Pl}}$) where we can write the term $U_{\nabla\phi}$ as

$$U_{\nabla\phi} \simeq +\frac{(2\beta^2)^{-1}}{8\pi G}\sum_{i=0}^{N_{\rm cell}} dx^3_{{\rm cell}\ i}(\vec{F}_\phi)_i^2 \tag{94}$$

When implementing the Layzer-Irvine equation in an N-body code it is convenient to work with the normalized potentials

$$E_i \equiv \frac{a^2U_i}{(H_0B_0)^2\rho_{m0}B_0^3} \tag{95}$$

In this form the potentials are dimensionless and also the kinetic friction term $2HT$ is removed from the equation. This is also the definition used in `RAMSES` [43], for which the N-body code `ISIS` [21] we have used to implement these equations, is based on.

To define the deviation from the modified Layzer-Irvine equation we first start by writing it as

$$\sum_i\left(\alpha_i\frac{\partial}{\partial t} + \gamma_i H\right)E_i = 0 \tag{96}$$

where $\alpha_i > 0$ and γ_i are constants or functions of the background cosmology only. In order to evaluate this equation numerically, it is more convenient to rephrase it as the integral equation

$$\sum_i \alpha_i\left(E_i(a_j) - E_i(a_0)\right) + \int_{a_0}^{a_j}\sum_i(\gamma_iE_i)\frac{da}{a} = 0 \tag{97}$$

We denote the left hand side of the equation above as σ_j. To have something to compare σ_j against we define

$$\Sigma_j \equiv \sum_i \alpha_i\left(|E_i(a_j)| - |E_i(a_0)|\right) + |\int_{a_0}^{a_j}\sum_i(\gamma_iE_i)\frac{da}{a}| \tag{98}$$

We can now define the error, or deviation, from the Layzer-Irvine equation at time-step j by

$$\epsilon_j \equiv \frac{\sigma_j}{\Sigma_j} \tag{99}$$

The function $\epsilon(a)$ will be referred to as the Layzer-Irvine constant.

It only remains to define how we calculate the integral in Eq. (97). In an N-body code we only have the potentials $E_i(a_j)$ at each discrete time-step j and must therefore use some approximation for the integral. We start by writing the integral in Eq. (97) as

$$I_j = \int_{a_0}^{a_j}\sum_i(\gamma_iE_i)\frac{da}{a} = \sum_{k=1}^{j}\int_{a_{k-1}}^{a_k}\sum_i(\gamma_iE_i)\frac{da}{a} \tag{100}$$

so that $I_j = I_{j-1} + \delta I_j$ where

$$\delta I_j = \int_{a_{j-1}}^{a_j}\sum_i(\gamma_iE_i)\frac{da}{a} \tag{101}$$

This integral is approximated by the mean value of the discrete integrand and an exact integration of $\int da/a$ giving

$$\delta I_j \simeq \frac{\left[\sum_i(\gamma_iE_i)\right]_{a=a_{j-1}} + \left[\sum_i(\gamma_iE_i)\right]_{a=a_j}}{2}\log\left(\frac{a_j}{a_{j-1}}\right) \tag{102}$$

VII. TESTS ON N-BODY SIMULATIONS

We have run N-body simulations of modified gravity theories to see whether the Layzer-Irvine equation developed here is satisfied and also to see what level of violation we would get if a mistake is made in the implementation. For all the modified gravity models we present tests of here we have beforehand tested the code against static configurations where known analytic solutions exist and found a good agreement. We will therefore assume that the implementation of the (static) Klein-Gordon equation is correct and the tests we perform will tell us if the code is able to accurately solve for the time-integration of these models.

The N-body simulations performed in this paper is done with the `ISIS` code [21] which is based on the public available code `RAMSES` [43].

A. Enhanced gravity and the Yukawa interaction

We have implemented the Yukawa interaction model described in Sec. (V B) in the N-body code ISIS [21]. We ran

simulations in a box of $B_0 = 200\ \mathrm{Mpc}/h$ with $N = 128^3$ particles and a standard WMAP7 cosmology starting from $z = 20$. The model parameters used in this test are $m^{-1} = \{1, 5, \infty\}\ \mathrm{Mpc}/h$ together with $2\beta^2 = \{0.01, 0.1, 0.5\}$. The $m^{-1} = \infty$ run is equivalent to standard gravity with an enhanced gravitational constant $G \to G(1 + 2\beta^2)$ and serves as a benchmark for the modified gravity models we will look at below.

In Fig. (1) we show the Layzer-Irvine constant ϵ for the enhanced gravity model ($m^{-1} = \infty$) with $1 + 2\beta^2 = 1.5$, $1 + 2\beta^2 = 1.1$, $1 + 2\beta^2 = 1.01$ and standard gravity $\beta = 0$. All the simulations use the same initial conditions and the same background cosmology. We find that $\epsilon \lesssim 0.01$ during the whole evolution for all runs which is also what we get for the standard gravity simulation. This test tells us that even when gravity is enhanced the code is still able to accurately solve the N-body equations.

The dotted line in Fig. (1) shows the Layzer-Irvine constant calculated using the Layzer-Irvine equation for standard gravity Eq. (26). These results are equivalent to what we would get if we made a mistake in the numerical implementation consisting of taking the pre-factor in the geodesic equation to be a factor $1 + 2\beta^2$ larger than the correct value. The huge deviation we see, even for $1 + 2\beta^2 = 1.1$, demonstrates the usefulness of the Layzer-Irvine equation: a small mistake in the numerical implementation of the geodesic equation will show up as a clear violation in the Layzer-Irvine constant.

In Fig. (2) we show the Layzer-Irvine constant for the Yukawa model with $2\beta^2 = 0.1$ and $m^{-1} = \{1, 5, \infty\}$ Mpc/h together with an enhanced gravity simulation with the same strength. The Layzer-Irvine constant is just as well satisfied for the Yukawa simulations as for the pure gravity simulation.

For the Yukawa interaction we also test the consistency relation Eq. (72). This relation does not involve time evolution so the results in one time-step is independent of the previous time-steps and this allow us to use it to test the code for a realistic[4] static configuration where no analytical solutions can be found. The results are shown in Fig. (3). The deviation from this relation (measured against the sum of the absolute values of the three terms) for the most extreme model are found to be less than 0.2% during the whole evolution.

In all cases we see that the Layzer-Irvine constant for the Yukawa interaction is small and the deviation we find is roughly the same as for the enhanced gravity simulation with the same β.

We note that the (small) violation of the Layzer-Irvine equation is closely related to the creation of new refinements in the code. The relative fraction of new refinements being created in the simulations peaks during the period $0.2 \lesssim a \lesssim 0.5$ which agrees with the time when we see the largest deviation. This happens because when new refinement are created we automatically increase the accuracy in the calculation of the potentials while leaving the kinetic energy (which comes from the particles) untouched. We also note that the evolution of the Layzer-Irvine constant for any model, standard gravity included, depends sensitively on the refinement criterion, the number of particles and the time-stepping criterion used in the simulation. A complete study of all these effects are beyond the scope of this paper.

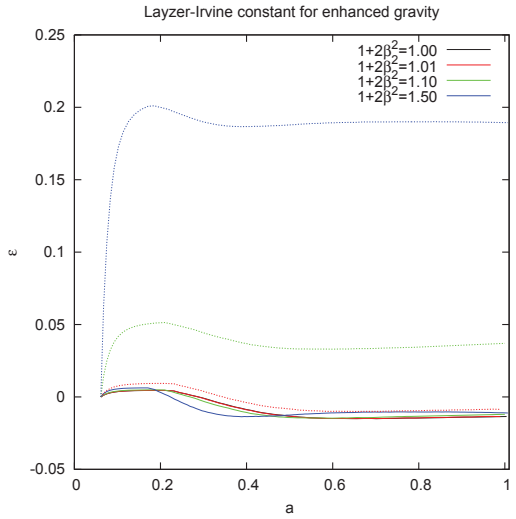

FIG. 1. The Layzer-Irvine constant as function of scale factor for the enhanced gravity model (solid lines) $G_{\mathrm{eff}} = G(1+2\beta^2)$. The dotted lines show the corresponding Layzer-Irvine constant calculated using the pure GR equation Eq. (26), i.e. when not taking the potential energies of the scalar field ($U_{\nabla\phi}$ and $U_{\log A}$) into account.

B. $f(R)$ gravity

An $f(R)$ model can be always be written as a scalar tensor theory where $A(\phi) = e^{\frac{\beta\phi}{M_{\mathrm{Pl}}}}$ with $\beta = 1/\sqrt{6} \approx 0.408$ and for some model specific potential $V(\phi)$ [44].

The particular Hu-Sawicky $f(R)$ model [42] has been implemented in ISIS. The implementation has been properly tested against analytical (static) configurations and against results from the literature. The code was found to work accurately.

For the simulations performed in [21] we have calculated the Layzer-Irvine constant[5]. These simulations all have $N = 512^3$ particles in a box $B_0 = 256\ \mathrm{Mpc}/h$ using a standard WMAP7 cosmology. See [21] for more details.

In Fig. (4) we show the Layzer-Irvine constant for the three simulations with $f(R)$ model parameters $|f_{R0}| = \{10^{-4}, 10^{-5}, 10^{-6}\}$ compared to a ΛCDM simulation using

[4] With realistic we mean a density distribution similar to what we have when making cosmological equations

[5] When calculating the Layzer-Irvine constant we have used Eq. (84) which is consistent with the approximations used in the simulation.

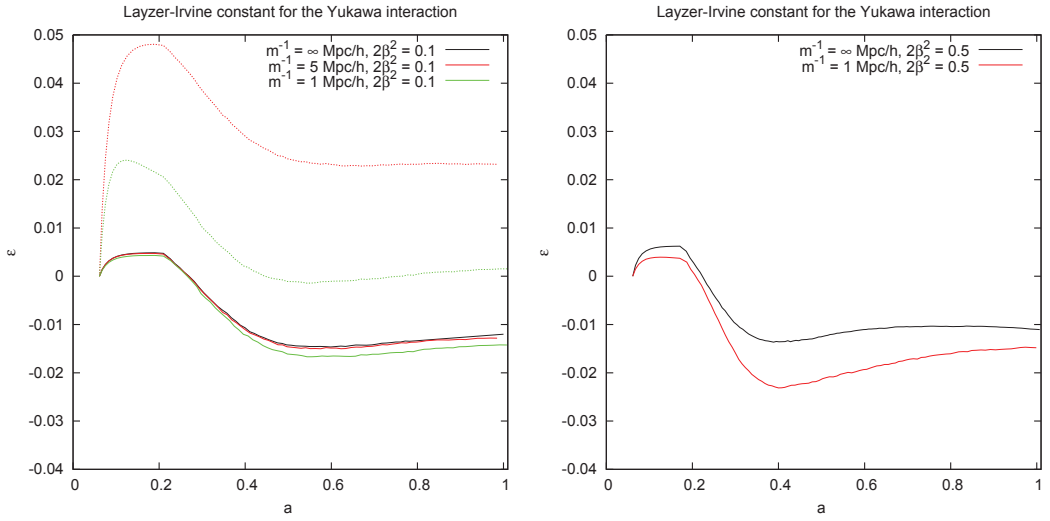

FIG. 2. The Layzer-Irvine constant as function of scale factor for Yukawa interaction model (solid lines) with coupling strength $2\beta^2 = 0.1$ (left) and $2\beta^2 = 0.5$ (right). The dotted lines show the corresponding Layzer-Irvine constant calculated using the pure GR equation Eq. (26).

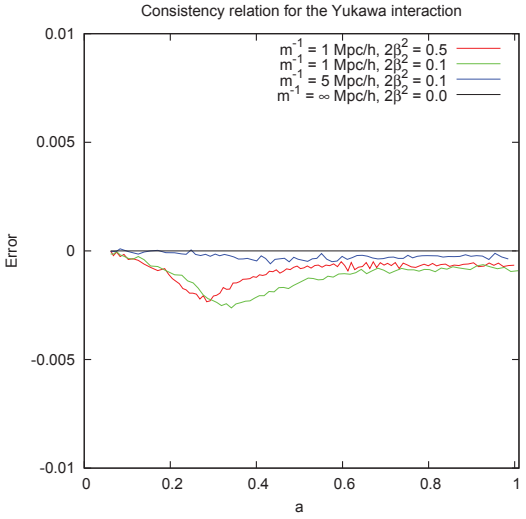

FIG. 3. Test of the consistency relation $U_{\nabla\phi} + \frac{1}{2}U_{\log A} + U_f \equiv 0$ for the Yukawa interaction model. The error is defined as $(U_{\nabla\phi} + \frac{1}{2}U_{\log A} + U_f)/(|U_{\nabla\phi}| + \frac{1}{2}|U_{\log A}| + |U_f|)$.

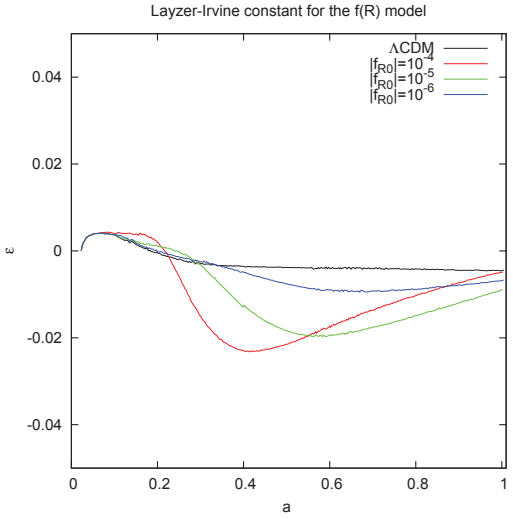

FIG. 4. The Layzer-Irvine constant as function of scale factor for the $f(R)$ simulations of [21].

the same initial conditions. For a description of the model and the meaning of the parameters see e.g. [27, 42].

We find that the Layzer-Irvine constant has a maximum deviation of $\sim 2\%$ which is comparable with the evolution of the Yukawa interaction with $\beta = 0.5$ presented above.

VIII. CONCLUSIONS

We have derived the Layzer-Irvine equation, describing quasi-Newtonian energy conservation for a collision less fluid in an expanding background, for a large class of scalar-tensor modified gravity theories. The equation derived have been tested in N-body simulations of modified gravity theories.

Monitoring the Layzer-Irvine equation is one of the few

tests that directly probes the time-evolution of a simulation.

We demonstrated that a mistake made in the implementation of a modified gravity theory, consisting of a wrong prefactor in the geodesic equation off by no more than a few percent from the correct one, will lead to a huge violation of the Layzer-Irvine equation. Such a mistake will also give effects on the matter power-spectrum, but these can be degenerate with cosmic variance.

As a test, the Layzer-Irvine equation can be used in several different ways. When implementing new models in an N-body code one often make several approximations to simplify the equations of motion. One way to apply it is to take the actual equation we put into the code, derive the corresponding Layzer-Irvine equation and run the simulation. The results from this equation will tell us how good the code solves the equations we actually try to solve, i.e. how good is the accuracy and the methods used. Secondly, we can take the full Layzer-Irvine equation and test it. The results from this equation can tell us something about how good the approximations we have used are. Lastly, for models with constant coupling we can use the relation Eq. (72) as a new static test which can be applied to any density distribution where no analytic or semi-analytic solution of the Klein-Gordon can be found.

There are scalar-tensor theories that are not covered by our analysis, like for example the Galileon, however the same methods we used here can easily be applied to any scalar field theory of interest.

ACKNOWLEDGEMENTS

The author is supported by the Research Council of Norway FRINAT grant 197251/V30. I would like to thank D. F. Mota for many useful discussions about this topic.

[1] Riess, A. G., Filippenko, A. V., Challis, P., et al. 1998, AJ, 116, 1009
[2] Perlmutter, S., Aldering, G., Goldhaber, G., et al. 1999, ApJ, 517, 565
[3] E. J. Copeland, M. Sami and S. Tsujikawa, Int. J. Mod. Phys. D, **15**, 1753 (2006).
[4] C. Wetterich, Astron. Astrophys. **301** (1995) 321 [hep-th/9408025].
[5] S. M. Carroll, Phys. Rev. Lett. **81** (1998) 3067 [astro-ph/9806099].
[6] Will, C. M. "Theory and experiment in gravitational physics." Cambridge University Press (1981).
[7] L. Amendola, Phys. Rev. D **62** (2000) 043511 [astro-ph/9908023].
[8] J. Khoury, arXiv:1011.5909 [astro-ph.CO].
[9] G. R. Dvali, G. Gabadadze and M. Porrati, Phys. Lett. B **485** (2000) 208 [hep-th/0005016].
[10] A. Nicolis, R. Rattazzi and E. Trincherini, Phys. Rev. D **79** (2009) 064036 [arXiv:0811.2197 [hep-th]].
[11] C. Deffayet, G. Esposito-Farese and A. Vikman, Phys. Rev. D **79** (2009) 084003 [arXiv:0901.1314 [hep-th]].
[12] J. Khoury and A. Weltman, Phys. Rev. D **69** (2004) 044026 [astro-ph/0309411].
[13] D. F. Mota and D. J. Shaw, Phys. Rev. D **75** (2007) 063501 [hep-ph/0608078].
[14] P. Brax, C. van de Bruck, A. -C. Davis, J. Khoury and A. Weltman, Phys. Rev. D **70** (2004) 123518 [astro-ph/0408415].
[15] P. Brax, C. van de Bruck, D. F. Mota, N. J. Nunes and H. A. Winther, Phys. Rev. D **82** (2010) 083503 [arXiv:1006.2796 [astro-ph.CO]].
[16] K. Hinterbichler and J. Khoury, Phys. Rev. Lett. **104** (2010) 231301 [arXiv:1001.4525 [hep-th]].
[17] K. A. Olive and M. Pospelov, Phys. Rev. D **77** (2008) 043524 [arXiv:0709.3825 [hep-ph]].
[18] P. Brax, C. van de Bruck, A. -C. Davis and D. Shaw, Phys. Rev. D **82** (2010) 063519 [arXiv:1005.3735 [astro-ph.CO]].
[19] P. Brax, A. -C. Davis, B. Li and H. A. Winther, Phys. Rev. D **86** (2012) 044015 [arXiv:1203.4812 [astro-ph.CO]].
[20] B. Li, G. -B. Zhao, R. Teyssier and K. Koyama, JCAP **1201** (2012) 051 [arXiv:1110.1379 [astro-ph.CO]].
[21] Lineares, C. . Mota, D. F. , Winther, H. A. To appear.
[22] E. Puchwein, M. Baldi and V. Springel, arXiv:1305.2418 [astro-ph.CO].
[23] H. Oyaizu, Phys. Rev. D **78** (2008) 123523 [arXiv:0807.2449 [astro-ph]].
[24] B. Li and J. D. Barrow, Phys. Rev. D **83** (2011) 024007 [arXiv:1005.4231 [astro-ph.CO]].
[25] C. Llinares and D. Mota, arXiv:1302.1774 [astro-ph.CO].
[26] H. Oyaizu, M. Lima and W. Hu, Phys. Rev. D **78** (2008) 123524 [arXiv:0807.2462 [astro-ph]].
[27] G. -B. Zhao, B. Li and K. Koyama, Phys. Rev. D **83** (2011) 044007 [arXiv:1011.1257 [astro-ph.CO]].
[28] P. Brax, A. -C. Davis, B. Li, H. A. Winther and G. -B. Zhao, JCAP **1304** (2013) 029 [arXiv:1303.0007 [astro-ph.CO]].
[29] A. -C. Davis, B. Li, D. F. Mota and H. A. Winther, Astrophys. J. **748** (2012) 61 [arXiv:1108.3081 [astro-ph.CO]].
[30] P. Brax, A. -C. Davis, B. Li, H. A. Winther and G. -B. Zhao, JCAP **1210** (2012) 002 [arXiv:1206.3568 [astro-ph.CO]].
[31] P. Brax, C. van de Bruck, A. -C. Davis, B. Li and D. J. Shaw, Phys. Rev. D **83** (2011) 104026 [arXiv:1102.3692 [astro-ph.CO]].
[32] F. Schmidt, Phys. Rev. D **80** (2009) 043001 [arXiv:0905.0858 [astro-ph.CO]].
[33] B. Li, G. -B. Zhao and K. Koyama, JCAP **1305** (2013) 023 [arXiv:1303.0008 [astro-ph.CO]].
[34] W. A. Hellwing and R. Juszkiewicz, Phys. Rev. D **80** (2009) 083522 [arXiv:0809.1976 [astro-ph]].
[35] M. Baldi, Phys. Dark Univ. **1** (2012) 162 [arXiv:1210.6650 [astro-ph.CO]].
[36] Layzer, D. 1963, Astrophys. J. , 138, 174
[37] Irvine, W. M. 1961, Ph.D. Thesis,
[38] P. P. Avelino and A. Barreira, Phys. Rev. D **85** (2012) 063504 [arXiv:1112.0417 [astro-ph.CO]].
[39] P. P. Avelino and C. F. V. Gomes, arXiv:1305.6064 [astro-ph.CO].
[40] A. C. Balfagon, R. Ramirez-Satorras and A. R. Martinez, arXiv:1006.0110 [astro-ph.CO].
[41] T. Clifton, P. G. Ferreira, A. Padilla and C. Skordis, Phys. Rept. **513** (2012) 1 [arXiv:1106.2476 [astro-ph.CO]].

[42] W. Hu and I. Sawicki, Phys. Rev. D **76** (2007) 064004 [arXiv:0705.1158 [astro-ph]].
[43] Teyssier, R. 2002, AAP, 385, 337
[44] P. Brax, C. van de Bruck, A. -C. Davis and D. J. Shaw, Phys. Rev. D **78** (2008) 104021 [arXiv:0806.3415 [astro-ph]].